# Characterising the structural brain changes in Huntington's disease using translational neuroimaging

*This dissertation is submitted for the degree of Doctor of Philosophy at Cardiff University*

**Jessica Steventon**

November 2014

# Thesis Summary

This thesis examined the *macro*-structural and *micro*-structural changes in Huntington's disease (HD) in order to improve understanding of the temporal and spatial patterns of neurodegeneration, and the functional relevance of these changes. Translational techniques were employed using genetic mouse models of HD in combination with a patient cohort to examine grey and white matter changes with a particular focus on white matter microstructure.

In the patient cohort, the cognitive profile was examined using a cognitive battery not before applied in HD. Specific deficits were found in set-shifting and flexibility, verbal reasoning, working memory and paired associate learning, along with subtle differences in response inhibition that were sensitive to disease burden. A composite cognitive score was produced to examine the relationship between cognitive function and brain structure. A multi-modal examination of white matter tract-specific microstructural measurements revealed abnormalities in the corpus callosum and cingulum bundle that were sensitive to disease burden (chapter 4). In chapter 5, multiple analysis techniques converged to reveal tissue macrostructure abnormalities that were also sensitive to disease burden in HD. Cortical changes were less consistent, and unlike the microstructure findings, white matter macrostructural abnormalities were not related to disease burden.

In chapters 6 and 7, genetic mouse models of HD were used to examine changes across the disease course, and to pilot an interventional design. In vivo diffusion MRI and $T_2$-weighted MRI sequences were acquired at 2 different time points in the HdhQ150 knock-in model of HD and imaging data is presented alongside behavioural results and immunohistochemistry. In chapter 7, an environmental modification regime was tested in the YAC128 mouse model using in vivo MRI. Environmental intervention reduced the degree of disease-related atrophy, altered tissue microstructure and improve motor but not cognitive performance in YAC128 mice.

# Declaration

This work has not previously been accepted in substance for any degree and is not concurrently submitted in candidature for any degree.

Signed ………………………………………. (candidate) Date……………………….

## STATEMENT 1

This thesis is being submitted in partial fulfilment of the requirements for the degree of PhD.

Signed ………………………………………. (candidate) Date……………………….

## STATEMENT 2

This thesis is the result of my own independent work/investigation, except where otherwise stated.

Other sources are acknowledged by explicit references.

Signed ………………………………………. (candidate) Date……………………….

## STATEMENT 3

I hereby give consent for my thesis, if accepted, to be available for photocopying and for inter-library loan, and for the title and summary to be made available to outside organisations.

Signed ………………………………………. (candidate) Date……………………….

## STATEMENT 4: PREVIOUSLY APPROVED BAR ON ACCESS

I hereby give consent for my thesis, if accepted, to be available online in the University's Open Access repository and for inter-library loans after expiry of a bar on access previously approved by the Academic Standards & Quality Committee.

Signed ……………………… (candidate) Date …………………………

# Acknowledgments

I would like to express my gratitude to the persons below for supporting and advising me throughout the course of this PhD.

**Firstly I would like to express my special appreciation and thanks to my supervisors, Derek Jones, Anne Rosser and Becky Trueman.**

Derek, you have been incredibly supportive to me throughout my PhD and I have learnt a huge amount from you which has helped me to grow as a research scientist. Thank you for your patience, constant encouragement and (most of) your advice!

Anne and the rest of the team at Cardiff Huntington's Disease Centre, thank you for your help, support and advice in making this work possible. A special thanks to Candace Farman and Kathy Price for your help with patient recruitment.

Becky, your positivity, words of encouragement and advice on all aspects of my project has been very gratefully received. I would especially like to thank you for your support during my period of illness and for stepping in and saving the experiment!

**Secondly, I would like to thank my friends and colleagues in the Brain Repair Group, CUBRIC, and EMRIC for all of your help, advice and support over the past 4 years.**

Thank you to all at the Brain Repair Group, with special thanks to David Harrison, Emma Yhnell and Yat Pateel for your help and advice with this work, it has been pretty eventful at times but I made it! Huge thanks to Jane Heath for her never-ending histology knowledge.

Andrew Stewart, the one-man band in EMRIC. Thank you for helping and encouraging me to try out my many ideas, and for your support and good company during the *many many* hours spent in the basement.

Fellow diffusion'ers, Mark Drakesmith, Greg Parker, Sonya Bells, Claudia Metzler-Baddeley, and Silvia De Santis, for answering my many 'just a quick question' questions and emails with patience and good will!

I wish to thank the Wellcome Trust for their financial support and excellent training programme without which this thesis would not have been possible.

A very special thank you to my parents: thank you for your love, support, inspiration and encouragement and for teaching me to always work hard, persevere, and pursue my dreams. Finally, I wish to express my deepest thanks to Adam who supported me and this work in so many ways; for patiently allowing me to pilot all of my cognitive tests, for listening to countless presentations, for being my late-night taxi to and from the lab, and for your perpetual encouragement.

**Finally, I would like to thank the HD community and their families who so generously gave their time and support to this project.**

# Glossary of abbreviations

| | |
|---|---|
| ANOVA | analysis of variance |
| CAG | cytosine, adenine and guanine DNA base |
| CHARMED | composite hindered and restricted model of diffusion |
| CSD | constrained spherical deconvolution |
| CSF | cerebrospinal fluid |
| DRL | damped Richardson Lucy |
| FA | fractional anisotropy |
| EM | environmental modifiers |
| EPI | echo planar imaging |
| FOV | field of view |
| FWF | free water fraction |
| HARDI | high angular resolution diffusion imaging |
| HD | Huntington’s disease |
| HTT | human huntingtin |
| htt | mouse huntingtin |
| ISCED | International Standard Classification of Education |
| mcDESPOT | multi-component analysis of T1 and T2 relaxation |
| MD | mean diffusivity |
| MSN | medium spiny neurons |
| MRI | magnetic resonance imaging |
| MWF | myelin water fraction |
| PCA | principal component analysis |
| RESTORE | robust estimation of tensors by outlier rejection |
| ROI | region of interest |
| RVF | restricted volume fraction |
| SD | spherical deconvolution |
| SNR | signal to noise ratio |
| TE | echo time |
| TR | repetition time |
| UHDRS | Unified Huntington’s Disease Rating Scale |
| VBM | voxel-based morphometry |
| YAC | yeast artificial chromosome |

# List of Figures and Tables

Figure 1.1 Direct and indirect pathways of the basal ganglia. ......................................13
Figure 1.2. Proposed basal ganglia-thalamocortical loops . ........................................14
Figure 1.3 Candidate white matter pathways affected in HD .....................................17
Figure 1.4 An example of an operant chamber. ........................................................27
Table 1.1 Genetic Profile of Mouse Models of Huntington's disease. ..........................30
Table 1.2 Phenotype of Mouse Models of HD ...........................................................31
Table 1.3 Neuropathology of HD mouse models .......................................................32

Figure 2.1 Training procedure for the Rotarod test. . ..................................................55
Figure 2.2 The Unified Huntington's Disease Rating Scale (UHDRS) .............................63
Figure 2.3 Educational attainment for HD and healthy control participants.. .............65
Figure 2.4 The three different trial types on the colour-word Stroop task.. .................67
Figure 2.5 Example trials from four different cognitive tasks. .....................................69
Figure 2.6 Spatial Planning Task. .............................................................................73
Table 2.1 Comparison of mouse and patient MRI parameters. ...................................53
Table 2.2 Demographic information for participants. ................................................65
Table 2.3 Reward contingencies and win/loss frequency in the Gambling Task. ..........72
Table 2.4 Diffusion parameters for the twice-refocused spin echo (TRSE) sequences. . 75
Table 2.5 CHARMED Gradient Orientations Scheme ...................................................76

Figure 3.1 Stages of the Intra-dimensional /Extra-dimensional (ID/ED) Task. .............91
Figure 3.2 Descriptive statistics for cognitive test performance.. ................................98
Table 3.1 Cognitive tasks and the correlation with finger tap speed. ...........................94
Table 3.2 Principal Component Analysis (PCA) of cognitive performance. .................101

Figure 4.1 Analysis pipeline for low and high b-value diffusion MRI images.. ............119
Figure 4.2 Schematic of corpus callosum parcellation.. ............................................121
Figure 4.3 Parcellation of the Corticospinal Tract. ...................................................122
Figure 4.4 Segmentation of the cingulum bundle. ....................................................123
Figure 4.5 Effect of tracking algorithm on FA estimates in the corpus callosum.125
Figure 4.6 Tensor metrics in segments of the corpus callosum ……………………..128
Figure 4.7 Results from the Corticospinal Tract reconstruction. ................................134
Figure 4.8 . Group differences in the cingulum bundle and its subdivisions ...............138
Table 4.1 Corpus Callosum descriptive statistics for the non-tensor based metrics....131

Figure 5.1 Schematic of analysis pipeline for shape analysis ....................................156

Figure 5.2 Results of VBM Analysis. .......... 161
Figure 5.3 Total grey matter, white matter, whole brain volume and intracranial volume in HD patients and healthy controls.. .......... 162
Figure 5.4 Percentage magnitude of sub-cortical atrophy .......... 164
Figure 5.5 Correlation between cortical thickness and disease burden .......... 171
Figure 5.6 Shape analysis for sub-cortical regions. .......... 174
Figure 5.7 Summary of results in relation to basal-ganglia-cortical circuity ..... 174
Table 5.1 Group differences in sub-cortical volume based on segmentation software .......... 162
Table 5.2 Descriptive statistics for raw volume measures (mm$^3$) .......... 164
Table 5.3 Correlation coefficients between volume and disease burden .......... 168

Figure 6.1 Demonstration of crossing fibers in the mouse brain .......... 187
Figure 6.2 Experimental design from birth to 20 months. .......... 188
Figure 6.3 Preprocessing steps of diffusion MR data .......... 190
Figure 6.4 Atlas Based Segmentation of the HdhQ150 mouse brain. .......... 192
Figure 6.5 Deterministic tractography of the corpus callosum.. .......... 194
Figure 6.6 Bregma positions for measures of cortical thickness . .......... 196
Figure 6.7 Left: Survival rates and weights of animals . .......... 199
Figure 6.8 Behavioural Assessment at 19 months old. .......... 201
Figure 6.9 Results of the VBA analysis at 7 months of age .......... 202
Figure 6.10 Absolute results of Atlas-Based Segmentation .......... 206
Figure 6.11 Cortical thickness measures .......... 209
Figure 6.12 Tensor-based values for tract reconstructions of the corpus callosum . .. 211
Table 6.1 Relationship between whole brain volume and regions of interest volume .......... 204

Figure 7.1 Cognitive enrichment performance at 18-months old. .......... 226
Figure 7.2 Behavioural Outcome Measures.. .......... 233
Figure 7.3 Manual segmentation of ROI's and mean raw volume .......... 236
Figure 7.4. Reconstructed pathways and statistics in the corpus callosum .......... 240
Table 7.1 Multiple regression analysis for behavioural measures. .......... 234
Table 7.2 Multiple regression analysis for macrostructural measures .......... 237
Table 7.3 Multiple regression analysis for microstructural measures .......... 241

Table Appendix 3.1 Relationship between age and volume.. .......... 265
Table Appendix 3.2 Relationship between cognitive tests and age. .......... 266
Table Appendix 3.4 Box's test of equality of covariance for tensor metrics .......... 273
Figure Appendix 4.1 Preliminary electron microscopy results .......... 274

# Contents

Thesis Summary ........................................................................................ i
Declaration ........................................................................................ iii
Acknowledgments ........................................................................................ v
Glossary of abbreviations ........................................................................................ vi
List of Figures and Tables ........................................................................................ vii

1. **General Introduction** ........................................................................ 1

1.1 *What is Huntington's Disease?* ........................................................ 1

*Trinucleotide repeats* ........................................................................ 2

*Huntingtin (HTT) protein expression and localisation* ........................................ 4

*Cognitive profile* ........................................................................ 6

*Psychiatric profile* ........................................................................ 8

*Motor profile* ........................................................................ 10

*Grey matter pathology* ........................................................................ 11

*White matter pathology* ........................................................................ 15

*Candidate white matter pathways in HD* .............................................. 16

*Inflammation in HD and Gliosis* ........................................................ 21

*Animal models of Huntington's disease*..........................................................22.

*Lesion models* ........................................................................ 22

*Genetic models* ........................................................................ 23

*Behavioural phenotyping in animal models of HD* ................................ 25

*Treatment options in Huntington's disease*.............................................. 33

*Symptomatic treatments* ........................................................................ 33

*Cell-based therapies* ........................................................................ 33

*Gene-based therapies* ........................................................................ 35

*Environmental enrichment* ........................................................................ 36

*Exercise* ........................................................................ 36

1.2 *Magnetic resonance imaging to study HD neuropathology* ................37

*$T_1$- and $T_2$- weighted MRI in HD* ..........................................................40

*Diffusion MRI to probe tissue microstructure* ...... ................................43

*Tensor-based models and metrics* .......................................................43

*Non-tensor based approaches* ............................................................44

*Diffusion Tractography* .........................................................................45

*Diffusion MRI in HD* ..............................................................................47

*Pre-clinical experimental MRI as a translational tool to study HD*..........48

Aims of this thesis ..................................................................................50

2. **Methods to characterise Huntington's disease** .....................................51

*2.1 Pre-clinical Methods* ..........................................................................51

*Ethical statement* ..................................................................................51

*Breeding* ................................................................................................52

*Genotyping* ............................................................................................52

*Housing* .................................................................................................52

*Behaviour Assessment* ..........................................................................52

*MRI Acquisition* .....................................................................................55

*MRI Image Processing* ...........................................................................57

*Perfusion* ...............................................................................................57

*Ex vivo MRI tissue preparation* ...............................................................57

*Immunohistochemistry* ..........................................................................58

*2.2 Human Methods* ................................................................................59

*Inclusion criteria* ....................................................................................60

*Exclusion criteria* ...................................................................................60

*Cognitive tests* .......................................................................................66

*MRI Acqusition* ......................................................................................75

*MRI Image Processing* ............................................................................78

Statistical analysis ........................................................................................81

3. Cognitive Characterisation of Huntington's disease ..............................83

Chapter Summary ........................................................................................83
Introduction ..................................................................................................83
Methods .......................................................................................................88
Results..........................................................................................................93
Discussion...................................................................................................101

4. Higher-order deterministic tractography of white matter pathways in HD ........................................................................................ 109

Chapter summary.......................................................................................109
Introduction ................................................................................................110
Methods .....................................................................................................117
Results........................................................................................................125
Discussion...................................................................................................139

5. Moving beyond volume: Macrostructural changes in HD ..................149

Chapter Summary .......................................................................................149
Introduction ................................................................................................149
Methods .....................................................................................................153
Results ........................................................................................................160
Discussion...................................................................................................175

6. Longitudinal structural imaging of the HdhQ150 mouse model of Huntington's disease .......................................................................183

Chapter Summary .......................................................................................183
Introduction ................................................................................................183
Methods .....................................................................................................188
Results.........................................................................................................198

Discussion.......................................................................................... 212

7. **In vivo MRI evidence that neuropathology is attenuated by environmental modifiers in the YAC128 HD mouse model** ................................................ 221

Chapter Summary ............................................................................... 221

Introduction ......................................................................................... 222

Methods ............................................................................................... 223

Results ................................................................................................. 231

Discussion............................................................................................ 241

Acknowledgment of financial support ........................................................ 245

8. **General Discussion** ........................................................................ 246

Appendix 1 Solutions ............................................................................ 258
Appendix 2 ISCED scale ......................................................................... 262
Appendix 3 Statistical assumptions ........................................................... 264
Appendix 4 Preliminary electron microscopy in the HdhQ150 mouse model . 274

References............................................................................................ 276

# 1. General Introduction

## 1.1 What is Huntington's disease?

Despite reports suggesting the existence of Huntington's disease from as early as the 17th century (Lanska, 2000), Huntington's disease (HD), or hereditary chorea as it was originally termed, was first succinctly described in 1872 by an American physician, George Huntington (Huntington, 1967). Chorea, Latin for dance, describes the dance-like, rhythmic movements that characterise the motor component of HD, distinguishable from other chorea disorders by its late onset of symptoms and hereditary nature (Lanska, 2000).

Today, HD is recognised as a genetically-inherited progressive and fatal neurodegenerative disease with an estimated prevalence of 5-10 cases per 100,000 in the Caucasian population in North America and Western Europe (Gil & Rego, 2008; Harper, 1992), with the prevalence varying by ethnic origin and different predisposing genetic profiles in each population (Agostinho, Santos, Alvarenga, & Paiva, 2013). In the United Kingdom, more recent estimates suggest that the prevalence of diagnosed HD is substantially higher than previously estimated, with 12.3 cases in every 100,000 in 2010 (Evans et al., 2013).

The disease is caused by a dominant mutation on an autosomal chromosome, meaning that men and women are at equal risk of inheriting the disease and one inherited copy of the mutated gene is necessary to produce the disease. There is currently no cure and the disease is fatal approximately 20 years after the onset of motor symptoms (Rinaldi et al., 2012).

## *The HD gene - Huntingtin*

In the human body, we possess approximately 30,000 genes. The devastating effects of HD are caused by a mutation in just one of these genes – the Huntingtin, or *HTT* gene. In 1993, the Huntington's Disease Collaborative Research team (Group, 1993) discovered the genetic cause of HD, a mutation triggered by an expansion in the number of trinucleotide repeats in an unstable DNA region of the *HTT* gene, located on the short arm of chromosome 4 (4p16.3). This discovery has allowed predictive genetic testing to identify gene-positive individuals prior to the onset of symptoms.

### *Trinucleotide repeats*

In the normal HTT gene, the three DNA bases cytosine, adenine and guanine (CAG) form a trinucleotide which codes for glutamine. The HTT gene codes for the Huntingtin (HTT) protein, with each trinucleotide producing a glutamine unit, thus forming a polyglutamine tract. Whereas in the normal HTT gene, the CAG trinucleotide is repeated less than 36 times, in the mutant HTT gene, this section of trinucleotide repeats is pathologically expanded above a threshold which alters the form of the protein (Nance, Mathias-Hagen, Breningstall, Wick, & McGlennen, 1999) and results in an elongated stretch of glutamine near the N-terminal tail of the protein (Zuccato, Valenza, & Cattaneo, 2010).

The threshold for complete penetrance and the cause of the HD phenotype is around 37-39 CAG repeats. Individuals with "intermediate" CAG repeats ranging from 27-35 tend to have a normal phenotype, however the expanded CAG repeat is somatically unstable, undergoing progressive length increases over time (De Rooij, De Koning Gans, Roos, Van Ommen, & Den Dunnen, 1995; V. Wheeler et al., 2007; V. C. Wheeler et al., 1999) thus "intermediate" CAG repeats are at an increased risk of expanding into the pathological range when transmitted to offspring, usually upon paternal transmission (Pearson, 2003; V. Wheeler, et al., 2007). Somatic instability is tissue-specific, with particularly high levels found in the striatum and cortex (Kennedy et al., 2003; V. Wheeler, et al., 1999) and occurs in post-mitotic neurons (Gonitel et al., 2008; Shelbourne et al., 2007).

The number of CAG repeats is inversely related to the age of symptom onset and despite being the strongest determining factor (Persichetti et al., 1996; Wexler et al., 2004), additional environmental and genetic factors also affect the age of onset (Wexler, et al., 2004). Juvenile-onset HD is a rarer more severe form of the disease, associated with >50 CAG repeats, earlier disease onset and quicker disease progression (Persichetti, et al., 1996).

In order to understand the pathological mechanism of the mutant HTT protein, the physiological function of the wild-type HTT protein must first be understood. Several functions of wild-type HTT have been suggested and a number of molecular and cellular abnormalities associated with mutant HTT elucidated, although the relative roles, interactions and timings remain under active investigation (Zuccato, et al., 2010). A number of studies have suggested that wild-type HTT may be a scaffold protein involved in the coordination of other proteins for intracellular transport and signalling processes (S. H. Li & Li, 2004). The wild-type *HTT* gene has a pro-survival role; in the absence of normal Huntingtin, there is a reduction in the survival and phenotypic stability of neural cells (O'Kusky, Nasir, Cicchetti, Parent, & Hayden, 1999; Rigamonti et al., 2000).

Abnormal cellular and molecular mechanisms in HD include mitochondrial dysfunction and impaired calcium signalling due to the accumulation of polyglutamine tract fragments in the cell cytoplasm (Damiano et al., 2013; Napoli et al., 2013; Rosenstock et al., 2010; Yano et al., 2014; Zhang et al., 2008), abnormal protein-protein interaction, impaired gene transcription, intranuclear inclusions due to the translocation of mutant HTT fragments to the nucleus, altered vesicular transport and recycling (Cui et al., 2006; DiFiglia et al., 1997; R. Smith et al., 2009; Zuccato, et al., 2010), altered NMDA receptor activity (Heng, Detloff, Wang, Tsien, & Albin, 2009;

Tallaksen-Greene, Janiszewska, Benton, Ruprecht, & Albin, 2010; Young et al., 1988), and defective glutamatergic and dopaminergic neurotransmitter systems (Crook & Housman, 2012; B. R. Miller & Bezprozvanny, 2010; Mittal & Eddy, 2013). It is known that some of these abnormalities are driven by the presence of the mutant protein and a toxic gain of function (Imarisio et al., 2008; Sipione & Cattaneo, 2001), for example, mutant but not wild-type huntingtin directly causes defects in mitochondria activity (Panov et al., 2002), however the loss of the normal HTT protein also contributes to HD neuropathology through a toxic loss of function (Schulte & Littleton, 2011).

### *Huntingtin (HTT) protein expression and localisation*

HTT is ubiquitously expressed throughout the central nervous system, in peripheral tissues and during embryonic development (Strong et al., 1993), and in human tissue, expression is at the highest level in the brain (T. Group, 1993). HTT is also expressed in non-human mammalian tissue (Aronin et al., 1995; Sharp et al., 1995) and has been detected throughout all stages of embryonic and postnatal mouse development as well as throughout the adult mouse brain. HTT protein is located in many subcellular compartments and organelles, including in cell bodies, dendrites and nerve terminals, the Golgi body, endoplasmic reticulum, synaptic vesicles, microtubules and mitochondria (DiFiglia et al., 1995; C. Gutekunst et al., 1995; C Gutekunst et al., 1999; Sharp, et al., 1995; Trottier et al., 1995). Such diversity in localisation impedes the ability to define the proteins function.

Studies of HTT expression in the human brain are able to directly compare normal and mutant protein expression in the same person because of the dominant nature of HD. Most people with the mutation are heterozygotes, carrying the mutant HTT protein on one allele and a normal HTT protein on the non-affected allele. Western blot analyses of cultured cells and tissue from HD patients have shown differential expression between the mutant and normal alleles. A relative reduction in mutant HTT expression has been shown in the cerebral cortex, frontal cortex and cerebellum in most studies (Ide, Nukina, Masuda, Goto, & Kanazawa, 1995; Persichetti et al., 1995; Persichetti, et al., 1996; Trottier, et al., 1995) although other studies report no difference in expression (Schilling et al., 1995). Evidence suggests the length of the pathological CAG repeat is related to both the degree of reduced expression (Gutekunst, et al., 1995; Persichetti, et al., 1996) and the localisation of expression changes, with longer CAG repeats associated with a more diffuse reduction in expression.

Along with western blot analyses, RNA in situ hybridization has been used to measure and localise RNA expression. HTT-messenger-RNA (mRNA) contains the information for just the HTT protein, following transcription of the *HTT* gene in a DNA strand. Normal HTT mRNA expression has been shown in both the human and rat brain predominantly in neurons, with glial expression present but to a lesser degree (Landwehrmeyer et al., 1995; Strong, et al., 1993). Similarly, immunohistochemical studies in human, monkey, and rat brain suggest that HTT is localized throughout the neuronal cytoplasm and is enriched in some nerve endings (DiFiglia, et al., 1995; C. Gutekunst, et al., 1995; Sharp, et al., 1995). Regional differences in the density of mRNA staining have been shown in both the rat and human brain, with the highest mutant mRNA expression found in dentate gyrus cells, hippocampal pyramidal cells, and cerebellar Purkinje and granular cells (Strong, et al., 1993).

Mutant HTT also interferes with the transcriptional machinery at different levels (Martin et al., 2011). Non-coding micro-RNAs act as post-transcriptional regulators of gene expression and play an important role in neuronal development and differentiation as well as maintaining the function of mature neurons. Lee et al. (2011) showed a reduction of total miRNA levels in two different mouse models of HD at symptomatic time points, suggesting miRNA expression or processing may be affected in HD. The mutant HTT gene also interferes with the activities of DNA-binding transcription factors by forming intracellular aggregates, leading to insoluble inclusion bodies which bind and sequester additional proteins, impairing the functioning of numerous transcription factors (Davies et al., 1997; DiFiglia, et al., 1997; Kazantsev, Preisinger, Dranovsky, Goldgaber, & Housman, 1999; Kazantsev et al., 2002; Steffan et al., 2000).

## *Symptoms of Huntington's disease*

Huntington's chorea was re-named Huntington's disease in the 1980's based on the recognition that symptoms were more widespread than purely chorea and included non-motor symptoms (Roos, 2010). Although the formal diagnosis of manifest HD is based on the presence of motor abnormalities, deficits in other domains are frequently present prior to this point, known as the pre-symptomatic or prodromal stage of HD. The non-motor symptoms of HD have been shown to be more highly associated with functional decline and increased burden for the families of individuals affected (Hamilton et al., 2003; Paulsen, 2011; Paulsen et al., 2010; Peavy et al., 2010). In all symptom domains, the profile of deficits changes with disease progression.

### *Cognitive profile*

As early as 15 years prior to the onset of a motor deficit, subtle emotion recognition deficits and poorer cognitive performance are observed compared to gene-negative controls (Stout et al., 2011). Pre-symptomatic gene-carriers are impaired at recognising facial expressions, with a particular deficit in recognising disgust, shown to be related to decreased insula activation (Hennenlotter et al., 2004).

Moving closer to disease onset, impairments in visuomotor performance, working memory and executive function start to emerge (Kirkwood et al., 2000; Papp, Kaplan, & Snyder, 2011). Nearly 40% of pre-symptomatic participants were found to meet criteria for mild cognitive impairment, the transitional stage between normal cognition and dementia (Duff et al., 2010). Processing speed is affected, with slowed cognitive processing becoming progressively worse closer to disease onset, with evidence suggesting underlying caudate nucleus and prefrontal cortical involvement (Ho et al., 2003; Rothlind, Brandt, Zee, Codori, & Folstein, 1993; Snowden, Craufurd, Thompson, & Neary, 2002; Sánchez-Pernaute et al., 2000). Slowed processing is also a feature of HD in the motor (bradykinesia) and psychiatric (depression, apathy) domain, and shown to have a similar or overlapping neural basis (Hickie et al., 1999; Zamboni, Huey, Krueger, Nichelli, & Grafman, 2008).

More pronounced memory deficits are not commonly observed until the advanced disease stage (Bamford, Caine, Kido, Cox, & Shoulson, 1995; Snowden, et al., 2002), and thought to be driven by deficits in memory retrieval as opposed to storage (Rohrer, Salmon, Wixted, & Paulsen, 1999). The prevalence of dementia in HD is difficult to estimate, because it is heavily dependent on the criteria used. There is currently no universally accepted criterion for diagnosing dementia in HD (Paulsen, 2011), with most criteria focused on dementia features in Alzheimer's Disease (Peavy, et al., 2010), and thus not correctly reflecting the unique set of deficits in HD. Unlike in Alzheimer's Disease, where the profile of deficits is thought to be more cortical in nature, in manifest HD, the cognitive deficit profile is regarded as 'subcortical' at least in the earlier stages, with deficits in the attentional domain, immediate memory domain, executive functioning, and visuospatial domain (Butters, Wolfe, Martone, Granholm, & Cermak, 1985; Ho, et al., 2003) whereas semantic memory and delayed recall memory are less affected (Ho, et al., 2003; Kirkwood, et al., 2000). Psychomotor skill in particular was found to decline in early and moderate HD (Ho, et al., 2003; Taylor & Hansotia, 1983).

Executive dysfunction are a feature of both pre- and symptomatic HD and appear to be specific, with deficits seen in pre- and early HD on the Stroop test (Holl, Wilkinson, Tabrizi, Painold, & Jahanshahi, 2013; Tabrizi et al., 2013), which measures inhibition of pre-potent responses, whereas performance on the Iowa Gambling task which measures risky decision-making, did not differ compared to controls (Holl, et al., 2013). This specific pattern of executive deficits may reflect the difference in neural substrate; both executive functioning and inhibitory processes used in the Stroop task are mediated by striatal-cortical connections, both shown to be dysfunctional in early HD. In contrast, risky decision-making involves the ventromedial caudate and its cortical connections, known to be spared in early HD (Holl, et al., 2013). Manifest HD participants have been shown to have deficits in tests of verbal fluency (Ho, et al., 2003; Holl, et al., 2013), which measure internally guided word search and production and require the person to both suppress the retrieval and production of inappropriate words and monitor their output accordingly. The decline in verbal fluency over time is less marked compared to other executive function tasks, such as the Stroop (Ho, et al., 2003), however this could be due to floor effects. Moreover, when considering the multiple neurocognitive impairments that are evident in HD, evidence for a selective executive deficit should be in excess of the average performance deficit across a range of other cognitive tasks that do not impose heavy executive demands (Laws, 1999; E. Miller, 1984). A meta-analysis of 30 studies found that the verbal fluency deficits were not differentially larger in magnitude than the deficits in verbal intelligence or speed, suggesting that fluency deficits in HD may stem not primarily from executive dysfunction but slowed cognitive processing speed and/or a deficit in verbal ability (Henry, Crawford, & Phillips, 2005).

### *Psychiatric profile*

The Europe-wide REGISTRY study containing patients at all disease stages found that 20% of patients had severe psychiatric problems (Orth et al., 2011). Psychiatric symptoms have been shown to be related to reduced functional capacity in cross-sectional and longitudinal studies alike (Duijn, Reedeker, Giltay, Roos, & Mast, 2010; Epping et al., 2013; Tabrizi, et al., 2013), and of the three symptom domains, represent the most distressing aspect of HD for patients and their families (Hamilton, et al., 2003).

In the pre-symptomatic stage, increased apathy, anxiety, depression, perseveration, irritability and suicidal ideation have all been observed (Duff et al., 2007; Epping, et al., 2013; Fiedorowicz, Mills, Ruggle, Langbehn, & Paulsen, 2011; Tabrizi et al., 2009; Tabrizi, et al., 2013). Depression symptoms in the pre-symptomatic stage did not increase with proximity to formal HD diagnosis (Epping, et al., 2013), unlike the majority of cognitive symptoms. This dissociation suggests that although some of the neuropsychiatric symptoms in HD are related to cognitive deficits (M. Smith, Mills, Epping, Westervelt, & Paulsen, 2012), an independent mechanism may underlie the neuropsychiatric phenotype.

Apathy, a symptom of both pre- and symptomatic HD, includes a loss of initiation, spontaneity, motivation, interest and concern about self-care. The prevalence of apathy as well as other loss-of-affect psychiatric symptoms in HD is likely to be underestimated due to sampling bias, as participants experiencing such symptoms are less likely to participate in a study. Unlike depression, the prevalence and severity of apathy is known to increase with disease progression (Duijn, et al., 2010; Kingma, van Duijn, Timman, van der Mast, & Roos, 2008; Tabrizi, et al., 2013). Prevalence rates vary between 34-76% for apathy and 33-69% for depression, depending on disease stage and measurement criteria (Craufurd, Thompson, & Snowden, 2001; Kulisevsky et al., 2001; Leroi & Michalon, 1998; Murgod et al., 2001; Paulsen et al., 2005; Paulsen, Ready, Hamilton, Mega, & Cummings, 2001; van Duijn, Kingma, & van der Mast, 2007). Apathy has also shown to be highly related to worse global and executive functioning and medication use, especially neuroleptics and benzodiazepines (Duijn, et al., 2010). There are inconsistent findings on the relationship between depression and apathy in HD (Duijn, et al., 2010; Levy et al., 1998; Paulsen, et al., 2001).

Irritability is a prominent symptom of both pre- and symptomatic HD with an estimated prevalence of between 38-73% across different studies (Craufurd, et al., 2001; Kulisevsky, et al., 2001; Murgod, et al., 2001; J. Paulsen, et al., 2001) and has been shown to be associated with impulsivity and aggression, presumed to be driven by an underlying disruption to emotional processing circuitry between the amygdala and medial orbitofrontal cortex (Klöppel et al., 2010). Anxiety is also a prominent symptom, with prevalence estimated between 34% and 61% depending on the sample and rating scale used (Craufurd, et al., 2001; Kulisevsky, et al., 2001; Murgod, et al., 2001; Paulsen, et al., 2005;  Paulsen, et al., 2001). Less commonly experienced psychiatric symptoms include psychosis, delusions, hallucinations (Craufurd & Snowden, 2002; Paulsen, et al., 2001) and obsessive and compulsive symptoms, with obsessive symptoms being twice as prevalent as compulsive symptoms (Anderson, Louis, Stern, & Marder, 2001). Suicidal ideation has been shown to be co-morbid with, and predicted by depression, anxiety and irritability (Wetzel et al., 2011), as well as by alcohol and drug abuse. In a large study of symptomatic HD patients, 19% reported current suicidal ideation (Wetzel, et al., 2011).

### *Motor profile*

Even before the clinical onset of a motor deficit, subtle motor symptoms are detectable, including oculomotor deficits, reduced force when protruding the tongue, slowed movement speed and reaction time, and abnormalities in muscle stretch (Kirkwood, et al., 2000; Penney et al., 1990; M. A. Smith, Brandt, & Shadmehr, 2000). This suggests that the sensitivity of the measures determines the clinical definition of onset, and supports the search for biomarkers to more accurately define different disease stages.

Formal diagnosis of adult-onset onset HD is commonly made after the onset of a profile of motor symptoms, which frequently includes chorea (Folstein, 1989; Snell, MacMillan, Cheadle, & Fenton, 1993). In addition to chorea, motor symptoms in early HD commonly include coordination deficits, reduced control over handwriting, oculomotor dysfunction and rigidity (Phillips, Bradshaw, & Chiu, 1994; Tabrizi, et al., 2009). In contrast, in the middle stage of HD, involuntary movements are often more pronounced, dystonia, chorea and parkinsonism are present, and difficulties with balance, speech, gait, swallowing and manual dexterity are experienced, along with a slowing in the production of voluntary movements (Girotti, Marano, Soliveri, &

Geminiani, 1988; Young, Shoulson, & Penney, 1986). In the more advanced stages of HD, assistance with self-care is required as the disease renders the individual unable to walk and speak due to a combination of deficits including rigidity and bradykinesia. Serious weight loss is often observed, along with loss of bladder and bowel control and problems with swallowing are evident due to loss of control of the throat muscles (Folstein, 1989; Kirkwood, Su, Conneally, & Foroud, 2001; Young, et al., 1986). Rigidity and bradykinesia can be present from the onset of symptoms in juvenile -onset HD and also in some cases of adult onset disease (Hayden, 1980; Quarrell, 2014).

## *Neuropathology in Huntington's disease*

### *Grey matter pathology*

Despite the ubiquitous pattern of HTT protein expression, at the cellular level, mutant HTT results in the loss of specific neuronal populations in the striatum and cerebral cortex, and insoluble HTT protein aggregates form specifically in the nucleus, cytoplasm, and neuronal processes (DiFiglia, et al., 1997; C Gutekunst, et al., 1999). The protein aggregates have been found to occur in higher concentrations in the cortex than in the striatum (Gutekunst, et al., 1999) whilst the precise role of these aggregates in HD is still under debate (e.g. Arrasate & Finkbeiner, 2012). More recent work suggests that HTT aggregates may be an adaptive cellular response rather than play a causative role in HD pathology. The formation of neuronal inclusions (HTT aggregates) was found to reduce both the level of diffuse mutant HTT and the risk of striatal neuronal death, with the risk of neuronal death becoming independent of the level of mutant HTT only after the formation of inclusions, compared to a highly correlated relationship prior to inclusion formation (Arrasate, Mitra, Schweitzer, Segal, & Finkbeiner, 2004). Taken together, this suggests that neuronal inclusions may signal a new adapted neuronal state (Arrasate, et al., 2004; J. Miller et al., 2010), although further research is required to unpick the specific responses in different neuronal subsets.

Atrophy is most severe in the striatum, comprised of the caudate nucleus and the putamen, with postmortem studies reporting a mean volume decrease of 58% in the striatum in HD brains (Lange, Thörner, Hopf, & Schröder, 1976; J. P. Vonsattel & DiFiglia, 1998). Post-mortem studies also report atrophy elsewhere in the basal ganglia, in the globus pallidus as well as in the thalamus and in the cerebral cortex (de la Monte, Vonsattel, & Richardson, 1988; J. Vonsattel et al., 1985), suggesting that striato-thalamo-cortical circuity is particularly vulnerable in HD. In the striatum, approximately 95% of the neurons are γ-aminobutyric acid (GABA)-ergic projection medium spiny neurons (MSN's), whilst approximately 5% are interneurons. In HD, pathology occurs specifically in the MSN's whereas striatal interneurons are typically unaffected or only mildly affected at late stages of the disease (Reiner et al., 1988). Specific sub-types of MSN's in the striatum are also differentially vulnerable in HD, depending on their projection targets and neurochemical content. There are two different output projection pathways of the striatum: a "direct" pathway, which projects axons mono-synaptically to the internal segment of the globus pallidus or to the substantia nigra, and an "indirect" pathway, which projects axons poly-synaptically to the external segment of the globus pallidus, as shown simplistically in Figure 1.1. In HD, the enkephalin containing MSN's which project along the indirect pathway to the external globus pallidus die in the early stages of the disease (Deng et al., 2004), causing disinhibition of the external globus pallidus, which in turn causes inhibition in the subthalamic nucleus (STN), altering the excitation in the globus pallidus internal (GPi) and from there the firing rate of the thalamus. An increase in thalamic firing to neurons in the motor cortex produces the motor symptoms which define the clinical onset of the disease. In contrast, the MSN's that contain substance P and are involved in the direct pathways projecting to the GPi are affected later in the disease course (Albin, Qin, Young, Penney, & Chesselet, 1991; Albin et al., 1992; Albin et al., 1990). Nevertheless, morphometric changes to the dendritic trees of surviving MSN's have also been found, with evidence of both regenerative and degenerative changes such as re-curving terminal dendritic branches, abnormal growth and formation of new collaterals, and local increase or decrease in spine density, suggesting dendritic

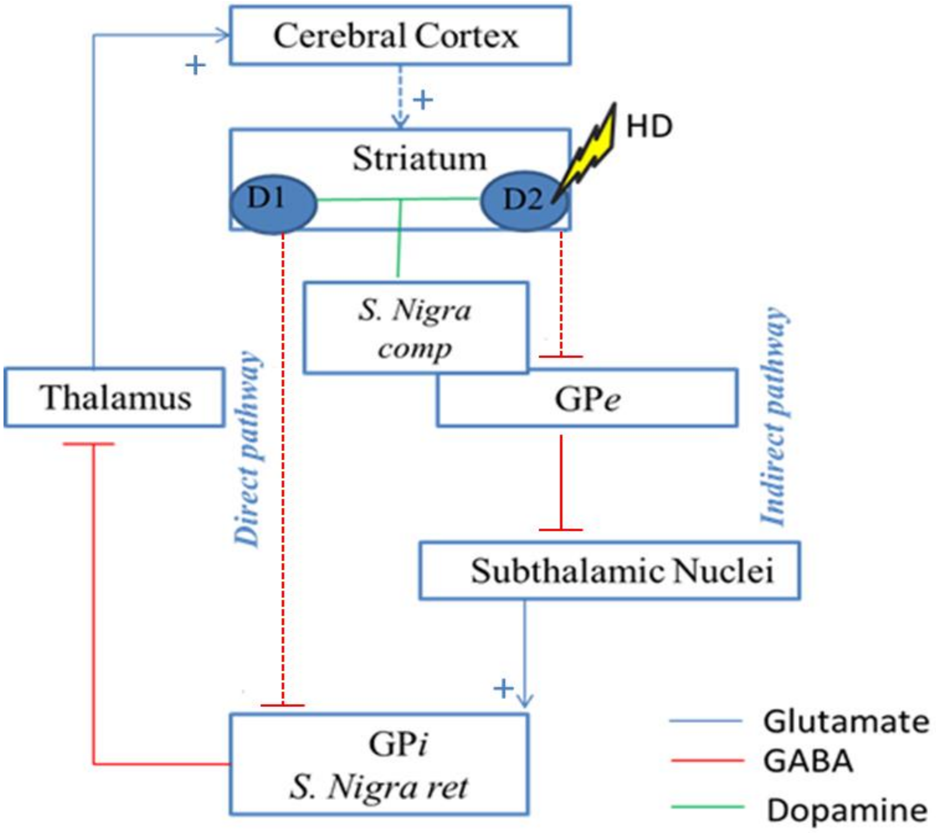
Cerebral Cortex
+
+
HD
Striatum
D1
D2
S. Nigra comp
Thalamus
GPe
Direct pathway
Indirect pathway
Subthalamic Nuclei
+
GPi
S. Nigra ret
Glutamate
GABA
Dopamine

Figure 1.1 Direct and indirect pathways of the basal ganglia. (Adapted from Alexander & Crutcher (1990). Dashed lines represent pathways affected in HD. Abbreviations: GPe : external segment of the globus pallidus, GPi: internal segment of the globus pallidus, S. Nigra ret : substantia nigra reticulate, S. Nigra comp: substantia nigra compacta.

pathology may be biphasic (Graveland, Williams, & DiFiglia, 1985).

The basal ganglia is not purely a motor system as once thought (Evarts & Thach, 1969), but is also involved in learning and memory, and many of the cognitive symptoms in HD may also be due to the altered circuitry between the basal ganglia and frontal cortex. For example, lesioning the caudate causes cognitive deficits in primate models (Divac, Rosvold, & Szwarcbart, 1967).

A number of functionally distinct cortico-striatal loops (Figure 1.2) have been proposed (G. E. Alexander, et al., 1990), which fit with subsequent work showing the somato-topic organisation of the basal ganglia (Miyachi et al., 2006; Nambu, 2011) and may explain the heterogeneity of symptoms experienced in HD. The proposed core

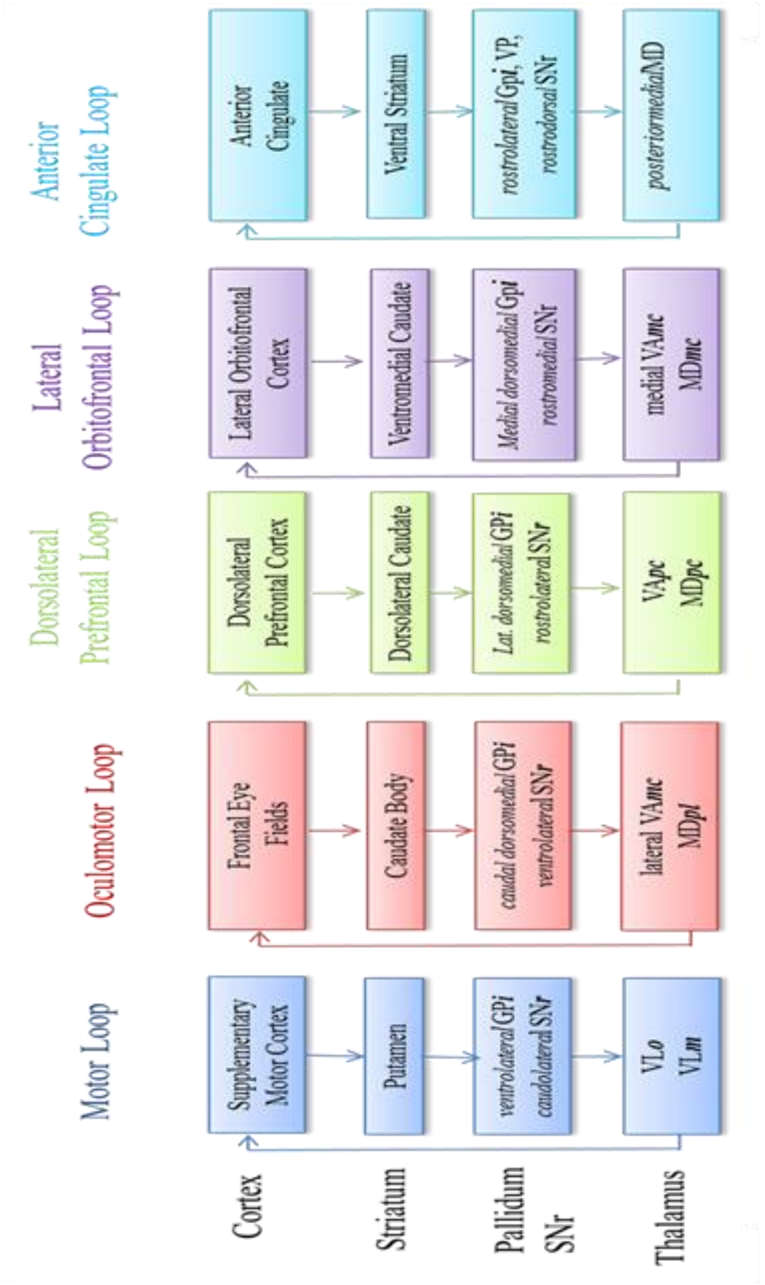
Motor Loop
Oculomotor Loop
Dorsolateral Prefrontal Loop
Lateral Orbitofrontal Loop
Anterior Cingulate Loop
Cortex
Striatum
Pallidum SNr
Thalamus
Supplementary Motor Cortex
Putamen
ventrolateral GPi caudolateral SNr
VLo VLm
Frontal Eye Fields
Caudate Body
caudal dorsomedial GPi ventrolateral SNr
lateral VAmc MDpl
Dorsolateral Prefrontal Cortex
Dorsolateral Caudate
Lat. dorsomedial GPi rostrolateral SNr
VApc MDpc
Lateral Orbitofrontal Cortex
Ventromedial Caudate
Medial dorsomedial Gpi rostromedial SNr
medial VAmc MDmc
Anterior Cingulate
Ventral Striatum
rostrolateral Gpi, VP, rostrodorsal SNr
posteriormedial MD

Figure 1.2. Proposed basal ganglia-thalamocortical loops (Adapted from (G. E. Alexander, et al., 1990). Abbreviations: GPi, internal segment of the globus pallidus; SNr, substantia nigra pars reticular; VP, ventral pallidum; Lat, lateral; MD, Medial Dorsal nucleus of thalamus (MDmc, medial dorsal pars magnocellularis; pm-MD, paramedian portion of the MDmc; MDpc, medial dorsa pars parvocellularis; MDpl, medial dorsal pars paralamellaris), VA; Ventral Anterior nucleus (VAmc, ventralis anterior pars magnocellularis; VApc, ventralis anterior pars parvocellularis), VL, Ventral Lateral nucleus (VLm, ventralis lateralis pars medialis; VLo, ventralis lateralis pars oralis).

circuits arise from different cortical areas and project topographically to the striatum, and then onto the globus pallidum/substantia nigra, before being projected to specific thalamic nuclei and back to the frontal cortex.

Degeneration in the cerebral cortex also contributes to disease pathology with volumetric loss of up to 29% found post-mortem (de la Monte, et al., 1988) and may be more involved in the cognitive and psychiatric symptoms experienced. Pyramidal neurons have been found to be particularly vulnerable in layers III and V (J. Vonsattel, et al., 1985) whereas overall neuronal loss is most prominent in layers V and VI (Selemon, Rajkowska, & Goldman-Rakic, 2004) and associated with a decrease in dorsolateral prefrontal cortical thickness and an increase in glial cell density in layer VI (Selemon, et al., 2004). The neuronal loss in layer VI is important because layer VI neurons do not project to the striatum, thus suggesting that cortical pathology is not a secondary effect of Wallerian degeneration of axon terminals from the striatum but is instead an independent primary process (Ramaswamy & Kordower, 2012).

### *White matter pathology*

White matter atrophy and a reduction in ferritin iron levels in white matter have been found even at the pre-symptomatic stage of HD (Bartzokis & Tishler, 2000; Ciarmiello et al., 2006; J. Paulsen, et al., 2010). There is now an increasing body of research showing white matter abnormalities are a feature of HD independent of neuronal loss (Beglinger et al., 2005; Fennema-Notestine et al., 2004; Stefan Klöppel et al., 2008; Mario Mascalchi et al., 2004; Myers et al., 1991; Nopoulos, Epping, Wassink, Schlaggar, & Perlmutter, 2011; Paulsen et al., 2008; Reading et al., 2005; H. Rosas et al., 2010; Tabrizi, et al., 2009; Weaver et al., 2009). Despite volumetric white matter loss of 29–34% being reported in post-mortem HD brains over 20 years ago (de la Monte, et al., 1988), the precise role of white matter in the disease pathology remains unclear. White matter is composed of axons, which carry the electrical impulses from one neuron to another, as well as myelin, which is a fatty layer which when wrapped around axons increases neural signal conduction velocity by allowing for the saltatory conduction of action potentials. It is unclear in HD whether axons, myelin, or both are affected, and how white matter changes contribute to neuropathology. One possibility is that a single event triggers a cascade of cellular alterations, including changes to white matter, whereas an alternative scenario is that white matter degeneration may independently contribute to HD pathology. Changes in white matter can occur due to a number of factors, including degeneration and loss of axons, degeneration of myelin, a direct effect of loss of grey matter volume in the form of Wallerian degeneration, or a combination of some or all of these.

In HD, it is known that mutant HTT aggregates localise in the axons as well as in neurons (H. Li, Li, Yu, Shelbourne, & Li, 2001; X. J. Li, 1999; Sinadinos et al., 2009). The presence of HTT aggregates in the axon may physically interfere with normal axonal trafficking of proteins and membrane bound organelles, and there is now a substantial body of research showing disrupted axonal transport in HD (H. Li, et al., 2001; J. Y. Li & Conforti, 2013; X. J. Li, 1999; Sinadinos, et al., 2009). In addition to axonal changes, there is also evidence suggesting that myelin breakdown contributes to white matter atrophy in HD (Bartzokis, Lu, Tishler, & Fong, 2007). There are a number of research findings which indirectly implicate myelin; it is known that cholesterol is needed for myelin formation during development (Dietschy & Turley, 2004; Saher et al., 2005) and cholesterol metabolism impairments have been associated with several neurodegenerative disorders, including HD (Valenza et al., 2007; Valenza & Cattaneo, 2010, 2011; Valenza et al., 2005). In addition, thinner myelin sheaths and decreased expression of myelin based protein have been found in mouse models of HD (Xiang et al., 2011).

### *Candidate white matter pathways in HD*

The impact of the HTT mutant gene on specific white matter pathways is not known, and likewise, the specific contribution any white matter abnormality makes to the clinical features of the disease is not understood. There are a number of candidate white matter pathways that require investigation.

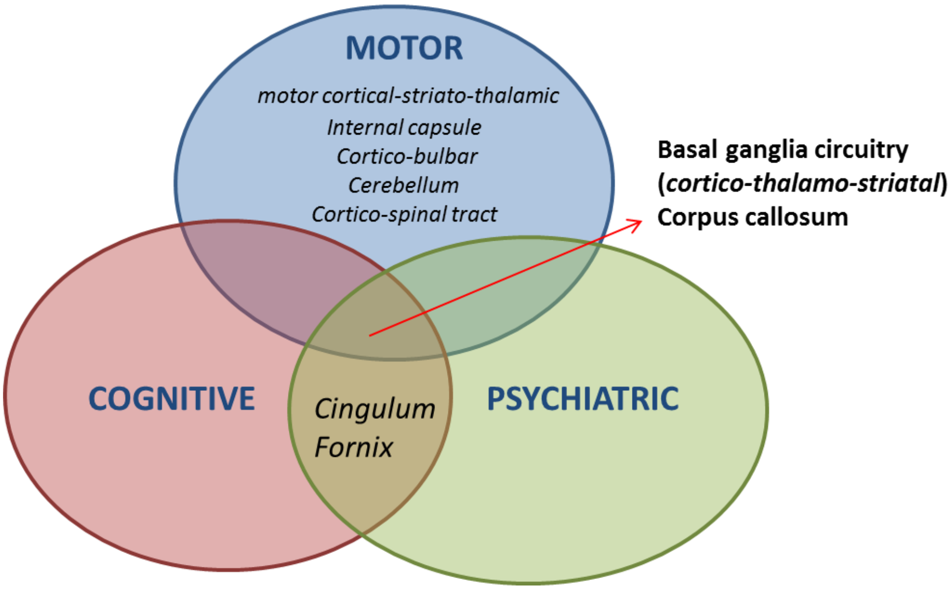
MOTOR
motor cortical-striato-thalamic
Internal capsule
Cortico-bulbar
Cerebellum
Cortico-spinal tract
Basal ganglia circuitry
(cortico-thalamo-striatal)
Corpus callosum
COGNITIVE
Cingulum
Fornix
PSYCHIATRIC

Figure 1.3 Candidate white matter pathways affected in HD, showing the white matter tracts in relation to the three symptom domains. Many tracts are likely to play a role in multiple domains.

***Motor Pathways*** HD is clinically defined by the onset of motor symptoms; therefore the motor pathways in the brain are hypothesised to be affected. In the human brain, the thalamus, basal ganglia, cerebellum, and brain stem are all involved in movement, thus it is hypothesised that the white matter pathways between these areas may be altered in HD. A recent diffusion MRI study supports this, with symptomatic HD patients found to have altered tensor based metrics (see section 2.3) in the caudate-paracentral and putamen-motor tracts (Poudel et al., 2014). The motor cortex includes the primary motor cortex, premotor cortex and supplementary motor area, all of which are somatotopically organized, and through various cortical afferent and efferent pathways controls motor coordination, planning, initiation and performance. The different cortical areas play different roles in motor function. The primary motor cortex is involved in the execution of movement, the premotor cortex is involved in motor control, including movement preparation and sensory and spatial guidance, whereas the supplementary motor area (SMA), made up of the pre-SMA and SMA proper (Y. Matsuzaka, Aizawa, & Tanji, 1992) is involved in motor task sequencing and movement initiation (Passingham, 1994). The SMA proper has efferent and afferent projections to the primary motor cortex and is involved in movement execution, whereas the pre-SMA, receiving inputs from the prefrontal cortex and the cingulate motor areas, is involved in movement decision-making. The motor cortex contains both pyramidal cells and other projection neurons, with a different proportion of the two neuronal classes depending on the cortical layer. The anterior and anterior-mid body of the corpus callosum contains fibers which connect the motor, premotor and supplementary motor areas in each hemisphere (Hofer & Frahm, 2006), thus the corpus callosum is also a candidate motor pathway affected in HD. Previous work has found altered diffusion tensor metrics in the corpus callosum in both pre- symptomatic and symptomatic HD patients compared to controls and importantly a correlation between these metrics and motor scores (Dumas et al., 2012).

The pyramidal motor pathways are involved in the voluntary control of movements and include the corticobulbar and corticospinal pathways. These long axons originate in the motor cortex and travel via the internal capsule through the midbrain to the cerebellar peduncle. Volume loss in the internal capsule of HD patients has previously been reported (Della Nave et al., 2010), with the degree of atrophy found to correlate with motor impairment (Jech et al., 2007). Recent work using diffusion MRI has found differences in tensor based metrics bilaterally in the corticospinal tract in symptomatic HD patients, whereas pre-symptomatic patients were found to have elevated iron in the left corticospinal tract specifically between the brain stem and thalamus, but no differences in terms of diffusion MR metrics. Importantly, the tensor based metrics in the corticospinal tract correlated with motor function score in both groups of patients, suggesting that abnormalities in the corticospinal tract may have functional significance in HD (Phillips et al., 2014).

The cerebellum is involved in coordinating muscle activity, equilibrium and tone and although previously overlooked, a handful of recent studies suggest the cerebellum and its connections may play a role in the neuropathology of HD (Dougherty, Reeves, Lesort, Detloff, & Cowell, 2013; Georgiou-Karistianis, Stout, et al., 2013). The major cerebellar tracts are the *spino-cerebellar*, connecting the spinal cord and the cerebellum, the *vestibulo-spinal,* connecting the vestibular system and the cerebellum, *cortico-ponto-cerebellar*, connecting the cortex, pons and cerebellum and the *dentato-rubro-thalamic* connecting the dentate nucleus of the cerebellum, the red nucleus and the thalamus.

***Cognitive pathways*** The basal ganglia are involved in many functional pathways affecting emotional, motivational, associative and cognitive processing along with motor function. Atrophy to basal ganglia structures is a pathological feature of HD, explaining the myriad of cognitive, emotional and motor symptoms experienced. Planning and problem-solving ability as well as working memory performance were found to be associated with frontal white matter volume and striatal volume in pre-symptomatic HD patients (Papp et al., 2013). Similarly, reduced BOLD activity was found in both pre-symptomatic and manifest HD participants relative to controls in the thalamus as well as the anterior cingulate gyrus during a spatial working memory task, (Georgiou-Karistianis, Poudel, et al., 2013), suggesting that frontocortical-striatal connections may be involved in the cognitive symptoms experienced in HD.

The fornix is a major white matter bundle projecting from the hippocampus to other brain structures, including some of the structures known to be affected in HD, such as the thalamus and nucleus accumbens, and is one of the most important anatomical structures related to memory. Given the memory deficits observed in HD (Bamford, et al., 1995; Dumas, van den Bogaard, Middelkoop, & Roos, 2013), it is plausible that fornix microstructure may be affected. In line with this, tensor based metrics in the fornix were found to be altered in HD participants compared to controls in a whole-brain diffusion MRI analysis (Della Nave, et al., 2010) although it has yet to be established whether fornix microstructure is related to cognitive deficits in HD.

The cingulum connects the cingulate cortex with the prefrontal cortex, premotor regions, cortical association areas in the parietal and occipital lobes, parahippocampal cortex and the thalamus (Mufson & Pandya, 1984) and has been implicated in Alzheimer's disease and mild cognitive impairment (Y. L. Chang et al., 2014). Given that atrophy has been observed in the thalamus and in the cerebral cortex in HD (de la Monte, et al., 1988; J. Vonsattel, et al., 1985), and that there are phenotypic overlaps between HD and Alzheimer's disease, the cingulum deserves attention as a potential candidate white matter tract affected in HD. Despite this, the cingulum has not been examined in a tract-specific analysis in HD before, and is reconstructed for the first time in HD participants in chapter 4.

Finally, along with being involved in motor function, the corpus callosum also contains fibers involved in cognitive function. Thinning of the corpus callosum has been found in post-mortem HD brains (Vonsattel, et al., 1985) and in vivo abnormalities found with MRI (see 2.2 and 2.3), and in early stage HD, cognitive scores were found to correlate with tensor based metrics obtained in the corpus callosum (Dumas, et al., 2012). In chapters 4, 6 and 7, corpus callosum microstructure is explored in patients and mouse models respectively.

**Pathways related to emotional / psychiatric symptoms.** It is less clear which pathways may relate to the psychiatric symptoms in HD specifically, simply because this area has received less research attention. However, limbic system circuitry has been found to be associated with psychiatric symptoms in the non-HD population. The fornix and cingulum bundles are the most prominent white matter fiber tracts within the limbic system and measures of volume and tissue microstructure in the cingulum have been found to be associated with psychiatric disorders including depression, obsessive compulsive disorder and schizophrenia (Fitzsimmons, Schneiderman, et al., 2014; Keedwell et al., 2012; Szeszko et al., 2005), Similarly, fornix microstructure has been found to be altered in a number of psychiatric conditions (Fitzsimmons, Hamoda, et al., 2014; Via et al., 2014).

Prefrontal cortical connections are also likely to be involved in psychiatric symptoms. A functional BOLD study observed that reduced activity in the prefrontal cortices in symptomatic HD patients was associated with increased neuropsychiatric disturbance within the domains of executive dysfunction, pathological impulses, disinhibition, and depression (Gray et al., 2013). A separate BOLD study found that emotion-related dysfunctions were associated with a disruption in the striatal-thalamo-cortical loop (Dogan et al., 2014).

### *Inflammation in HD and Gliosis*

There is mounting evidence that various inflammatory processes may mediate neuropathology in HD (Kaushik & Basu, 2013; Sapp et al., 2001; Silajdžić et al., 2013). A normal inflammatory response in the brain begins with the activation of microglia, which are immune cells which when activated have a protection and repair role, acting as phagocytes to remove pathogens and cellular debris and signalling the release of inflammatory mediators (cytokines and chemokines). If this neuroinflammatory response is an acute response, the release of inflammatory mediates may trigger oxidative and nitrosative stress, however, the short-lived nature of the responses does not have a detrimental effect on neuronal health long-term. In contrast, a chronic and self-perpetuating immune response with chronic microglia activation and sustained inflammatory mediator release results in increased oxidative and nitrosative stress and subsequent neuronal cell death and disease advancement. Chronic neuroinflammation has been associated with a range of neurodegenerative disease including HD, with elevated levels of inflammatory cytokines and chemokines found in the plasma of patients with HD as well as in pre-symptomatic HD gene-carriers (Björkqvist et al., 2008; Wild et al., 2011). Mutant huntingtin has been shown to be expressed in microglia (Shin et al., 2005) and in vivo imaging, in vitro and postmortem studies converge in showing that microglia are activated in both pre-symptomatic and symptomatic HD (Sapp, et al., 2001; Tai et al., 2007a, 2007b). Huntingtin-induced immune activation is not confined to the CNS, with peripheral immune system dysfunction also reported in HD (Björkqvist, et al., 2008; Dalrymple et al., 2007). Thus, it is evident that inflammation plays a role in HD, although the precise details and the interaction between CNS and PNS pathology have yet to be established.

## *Animal models of Huntington's disease*

### Lesion models

In the broadest terms, animal models of HD are either non-genetic or genetic models. Prior to the discovery of the HD gene in 1993, HD research was reliant on non-genetic models, where cell death was induced to model the neuropathology seen in HD. Cell death can be induced either by the delivery of excitotoxins or metabolic toxins which disrupt mitochondria functioning. Whereas metabolic toxins provide a higher level of neuropathological validity compared to excitotoxic lesions, selecting affecting medium spiny neurons in a progressive manner (Borlongan, Koutouzis, & Sanberg, 1997; Brouillet et al., 1993), the inter-animal variability and the incidence of gross non-specific striatal damage are higher (Dunnett & Rosser, 2004). The most commonly used excitotoxic agents are quinolinic acid, a NMDA-selective glutamate agonist, and kainic acid, a non-NMDA glutamate agonist, which induce cell death by binding to their cognate receptors on striatal neurons. Quinolinic acid is currently the most widely used neurotoxin in HD animal models because it causes preferential degeneration of GABA-ergic neurons, the same class of neurons affected in HD, whilst sparing other cells such as cholinergic interneurons (Schwarcz, Whetsell, & Mangano, 1983). The degree of cell loss is preferential for transplantation studies, however the main limitation of excitotoxic models is the lack of association with the genetic cause of HD; lesions do not produce mutant HTT, mice do not develop neuronal inclusions, and cell death is sudden and not progressive.

### Genetic models

Genetic models of HD incorporate a similar genetic defect to that seen in patients, allowing for the study of early pathological, cellular and molecular alterations caused by the mutation, which is not possible in patients in vivo. Genetic models do not suffer the same degree of variance in terms of disease stage and number of CAG repeats as in human studies, allowing for more experimental control. The majority of genetic models of HD are in mice, however, transgenic rat models (von Hörsten et al., 2003), primate models (Yang et al., 2008), and genetically modified models in C. elegans (Faber, Voisine, King, Bates, & Hart, 2002), drosophila melanogaster (Warrick et al., 1998), zebrafish (Schiffer et al., 2007) and sheep (Jacobsen et al., 2010) have been created.

Genetic animal models can take one of three forms. Knock-out models were the first to be developed (Duyao et al., 1995; Nasir et al., 1995; Zeitlin, Liu, Chapman, Papaioannou, & Efstratiadis, 1995) whereby the HTT gene was removed from the genome entirely. A knock-out model was useful in determining the function of the HTT gene, with knock-out animals not surviving embryonic development, demonstrating the crucial role HTT plays in embryogenesis (Duyao et al., 1995; Nasir et al., 1995; Zeitlin, Liu, Chapman, Papaioannou, & Efstratiadis, 1995. More recently, conditional knock-out models have been developed, where the Huntingtin gene can be eliminated from the specific organ being studied as opposed to every organ where Huntingtin is expressed, and inducible knock-out models allow the gene to be knocked at a specific time, such as after development.

Whereas knock-out models are useful for understanding the function of the gene, transgenic and knock-in models are more suitable as models of HD, where questions about disease progression and intervention outcomes can be assessed. In transgenic models, the mutant gene is inserted randomly into the animal genome in addition to the two normal copies of endogenous huntingtin (*Htt*) (Barnes et al., 1994). Transgenic models have tended to produce an acute, and fast-acting phenotype (see

Table 1.2) although more recently, transgenic models have been generated which express longer fragments, or the full-length human mutant *HTT* gene, such as the yeast artificial chromosome (YAC) (Hodgson et al., 1999a; Slow et al., 2003a) and bacterial artificial chromosome (BAC) models (Gray et al., 2008), which produce a more progressive phenotype.

Knock-in models have the CAG repeat mutation inserted into the endogenous animal Huntingtin *(Htt*) gene via homologous recombination (Lin et al., 2001) or the animal exon 1 is replaced with the pathologically expanded human exon 1 (Ishiguro et al., 2001; Wheeler et al., 2000). The gene is not over-expressed as there is no change in the number of copies of the gene, and the use of the endogenous *Hdh* promoter means that these models should produce a similar expression profile to that seen in the human condition and allow expression of the complete mutant gene. Knock-in mice can be homozygous or heterozygous for the mutation and produce a very mild phenotype and protracted time course to disease onset, as shown in Table 1.1 and Table 1.2.

This thesis includes work on mouse models of HD (chapters 6 and 7). Tables 1.2 and 1.3 show the different animal models of HD and the associated phenotype and neuropathology. There is a wide range in time course in the development of neuropathological and behavioural deficits as well as a range in the phenotype displayed in various transgenic and knock-in lines. The two mouse lines used in this thesis are outlined in bold, and are well characterised lines. The R61/2 mouse models have been the most studied (Mangiarini et al., 1996). These mice have a severe phenotype and neuropathology occurs early in life, with a relatively quick progression of symptoms and reduced lifespan, making the model less appropriate for long-term studies, such as those evaluating the long-term effects of therapeutic interventions. An alternative transgenic HD mouse model is the yeast artificial chromosome (YAC) mouse model, which was created by cloning an artificial yeast vector that contained an expanded polyglutamine repeat into the mouse genome (Hodgson, et al., 1999a). The transgenic YAC128 mouse model expresses the entire human huntingtin gene with 120

CAG repeats (Slow et al., 2003b) and recapitulates many of the features of human HD including a progressive phenotype, motor abnormalities from 3 months of age, striatal atrophy at 8 months old, and cortical atrophy seen at 12 months old (Slow, et al., 2003b). The YAC128 mouse model was developed specifically with the testing of therapeutics in mind; the HD-related phenotypes of the YAC128 mice show phenotypic uniformity with low inter-animal variability (Slow, et al., 2003b), age-dependent striatal neurodegeneration, and a longer lifespan compared to the commonly used R6/1 and R6/2 mouse lines. The HdhQ150 mouse model (Lin, et al., 2001), which is characterised in chapter 6, is a knock-in model that expresses full length mutant Htt, and contains a 150 CAG repeat insertion. $\text{Hdh}^{Q150/Q150}$ mice display a progressive motor deficit which manifest at approximately 100 weeks old on the rotarod test, balance beam, and activity measures, with an abnormal gait and clasping phenotype also evident (Heng, Tallaksen-Greene, Detloff, & Albin, 2007). Cognitive deficits appear prior to motor deficits, as is the case in the human disease (Brooks, Betteridge, Trueman, Jones, & Dunnett, 2006). Neuropathological changes include striatal cell loss (M. Heng, et al., 2007), nuclear aggregates in the dorsal striatum, nucleus accumbens and piriform cortex, with fewer aggregates in the cortex, cerebellum and hippocampus (Lin, et al., 2001).

### *Behavioural phenotyping in animal models of HD*

Behavioural testing is necessary to characterise the phenotype of different mouse models of HD, and can be used as an outcome measure to assess disease progression and the effect of therapeutic interventions. Different tests can be used to assess different symptoms of HD (Brooks & Dunnett, 2009) including motor, cognitive and emotional functioning. In the motor and cognitive domain, the majority of tests require a training period to acclimatise the mouse to the new environment and ensure anxiety-related behaviour is not being measured.

In the motor domain, the rotarod test (B. Jones & Roberts, 1968) and balance beam (Perry et al., 1995) are both commonly used to assess motor coordination and balance. The rotarod test involves placing the animal on a rotating beam either at a fixed or accelerating speed, and measuring the latency to fall from the rod over a number of trials and is used to assess motor coordination, motor learning, balance and endurance (Alvarez-Fischer et al., 2008; Schallert, Fleming, Leasure, Tillerson, & Bland, 2000). The balance beam involves placing the animal on a beam of varying diameters, with the ability to traverse it considered to be an indicator of balance; the number of paw slips and time taken to traverse the beam are measured over a given time period. Locomotor activity can be assessed in a number of ways and for varying periods of time. 24-hour monitoring allows activity to be examined across the circadian cycle, whereas shorter monitoring times are also sensitive to anxiety-related behaviours. A variety of circular (de Visser, van den Bos, Kuurman, Kas, & Spruijt, 2006) and square (L. Menalled et al., 2009) open-field tests measure general activity levels in an open arena using different tracking methods, either by manual recording, or more recently, using automated methods such as infrared beams, and video-tracking, with differing degrees of sensitivity. When first placed in the centre of the arena, a healthy non-mutant mouse will typically run to the walled edges of the arena and explore the perimeter of the arena. Over time with habituation, anxiety levels will reduce and the mouse will explore more central regions of the arena. Gait is commonly assessed by painting the feet of animals and examining the pattern of footprints; transgenic HD mice have been shown to display irregularly spaced shorter strides and an uneven left–right step pattern compared with the evenly spaced and accurately positioned footprints of wild-type mice (Carter et al., 1999). Limb clasping behaviour, where the fore and hindlimbs are clasped together when the mouse is suspended by the tail, is also commonly seen in HD mice and although the precise neurological reason for this response is not known, it is a sign of neurological and motor abnormality. Grip strength can be measured either by assessing the ability of a mouse to remain clinging to an inverted grid, or hanging on a wire with its forepaws for a period of time (Brooks, Higgs, Jones, & Dunnett, 2012), or by measuring the force required to loosen the mouse's grip on a bar. Other observational measures such as the presence of a tremor, abnormal limb displacements, and righting reflex are also used.

Cognitive tasks are commonly delivered using either operant chambers (see Figure 1.4) or some form of maze. Cognition is more challenging to assess as tests often require a long period of training for the mouse to be able to learn the task. Operant learning paradigms are commonly run in operant boxes, or 'Skinner boxes', such as the nine-hole box, where an array of 9-holes is used as the response location, and mice must learn to poke their nose into the holes in response to a light inside the hole. Depending on the task, reinforcements can be provided in the chambers based on the mouse's response. Various different operant paradigms have been designed for the operant boxes, such as the five-choice serial reaction time (5-CSRT) test, which is a test of attentional function (Humby, Laird, Davies, & Wilkinson, 1999) and requires the mouse to respond rapidly to stimuli appearing at random in one of five holes in the array, with reaction time and accuracy as outcome measures. This is of interest in HD models as various facets of attention have been reported to be affected in individuals with HD (Hart et al., 2012; Hart et al., 2013; Thompson et al., 2010).

Sequence learning tasks are an extension of the choice reaction time task, where the mouse now needs to respond to a sequence of stimuli, rather than just one. Sequence learning is of interest in HD because research has shown the ability to acquire and act upon serial order information depends on the basal ganglia (Kermadi & Joseph, 1995; Mushiake & Strick, 1993, 1995).

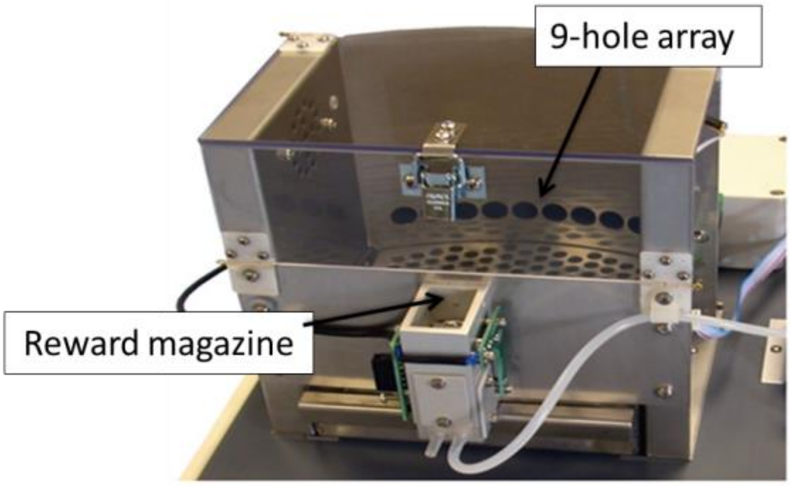

Figure 1.4 An example of an operant chamber. In this example, there are 9-holes with LED's behind each.

The serial implicit learning task (Trueman, Brooks, & Dunnett, 2005) is one such task, where the majority of sequences are random, but embedded within the task is a predictable task, where the location of the second stimuli can be fully predicted from the specific location of the first stimuli. Aside from the time required to train the mice to achieve a baseline score, a second disadvantage with using operant chambers is the necessity for food restriction during training/testing periods, which may have varying effects within a cohort depending on differences in genotype, sex, strain, or metabolism (Trueman, Dunnett, & Brooks, 2012).

The Morris water maze (Morris, Garrud, Rawlins, & O'Keefe, 1982) is the classic test for assessing spatial memory and involves releasing the mouse into a pool containing opaque water and the mouse must learn to find a hidden platform to escape (Lipp and Wolfer, 1998). Healthy, wild-type mice learn to quickly find the platform, and once the platform is removed, continue to search in the same quadrant in which the platform was previously location, suggesting spatial retention and defined as spatial reference memory. Performance on the Morris water maze is well established as being dependent on hippocampal function (Bannerman et al., 1999; Morris, et al., 1982; Whishaw, 1995).

The spatial alternation T-maze task is commonly used to assess discrimination learning and working memory (Deacon & Rawlins, 2006). The apparatus is in the form of a T placed horizontally, and animals are placed at the base of the T and allowed to choose one of the goal arms adjoining the other end of the stem. If two trials are performed in quick succession, on the second trial the rodent tends to choose the arm not visited before without reinforcement, reflecting memory of the first choice and termed 'spontaneous alternation' (Dember & Richman, 1989) which has been found to be sensitive to dysfunction of the hippocampus, cerebellum, thalamus and substantia innominata (Lalonde, 2002). Variants of the task include a ‘forced choice alternation’ where entry to the alternate arm is prevented on the first run, and reinforcement is presented at the end of the arm (Deacon & Rawlins, 2006).

The water T-maze apparatus has been used to design a set-shifting task in which the rodent must learn a rule and then switch to a different rule, which is dependent on the prefrontal cortex (Birrell & Brown, 2000). Set-shifting deficits are observed in HD patients (Lawrence, Sahakian, Rogers, Hodge, & Robbins, 1999), and YAC128 mice were found to show set-shifting deficits on the adapted T-maze protocol (Brooks et al., 2012). Other cognitive tests, such as the radial arm maze (8 arms in a radial configuration around a central starting point) have the advantage that working and reference memory can be assessed simultaneously (Olton, 1979; Olton & Papas, 1979).

The psychiatric and emotional features of HD are most challenging to characterise in animal models, as internal symptoms such as delusions, hallucinations and suicidal ideation cannot be assessed. There are however a number of tests which are thought to measure more overt symptoms, such as depression, anxiety and anhedonia. The Porsolt forced swim test is a commonly used paradigm to assess depression-like behaviour and antidepressant action in rodents (Porsolt, Bertin, & Jalfre, 1978) and involves measuring the degree of mobility of mice when forced to swim in a restricted space with no escape option. Increased immobility is interpreted as a marker for reduced motivation, and a depressive state. Nevertheless, the motor deficit and weight loss seen in HD mice may affect the validity of this test specifically in HD mice. The sucrose intake test is a test of anhedonia, or the inability to experience pleasure. A reduction in sucrose consumption and preference compared to healthy control mice is interpreted as a reduction in reward sensitivity (Willner, Towell, Sampson, Sophokleous, & Muscat, 1987). Anxiety can also be inferred from freezing behaviour in the open-field test previously described, and from behaviour on the elevated plus maze, in which rodents are placed at the junction of the four arms of the maze, facing an open arm, and entries/duration in each arm are recorded (Walf & Frye, 2007).

Table 1.1 Genetic Profile of Mouse Models of Huntington's disease. *Htt* = mouse Huntingtin gene; *HTT* = human Huntingtin gene; BAC: bacterial artificial chromosome; YAC: yeast artificial chromosome. ↑= Increase in; ↓= Decrease in; outlined rows reflect the mouse models used in this thesis. References reflect the first instance of an observed effect.

| GENETIC PROFILE | | | | | |
|---|---|---|---|---|---|
| **Model** | **Genetic insertion and promoter** | **Background** | **CAG repeat length** | **Mutant protein expression level** | **References** |
| ***Transgenic models*** | | | | | |
| R61 | Randomly inserted, human HTT promoter | CBA/C57Bl6 | 115 | 31% of endogenous levels | Mangiarini, et al., 1996 |
| R62 | Randomly inserted, *Exon 1 of human gene and first 262 bp of intron 1* | CBA/C57Bl6 | 144 | 75% of endogenous levels | Mangiarini, et al., 1996 |
| **YAC 72, 128** | **Several copies of entire mutant human protein expressed** | **FVB/N** | **72 /128** | **75- 200% of endogenous levels** | **Hodgson et al., 1999, Slow et al, 2003** |
| N171-82Q | N-terminal fragment of human HTT, HTT expression in neurons driven by mouse prion protein promoter | C3H/HEJ x C57Bl/6J | 82 | 10- 20% of endogenous | Schilling et al., 1999, 2001 |
| BAC-HD | full length human *HTT* with modified exon 1 | FVB/NJ | 97 mixed CAA-CAG repeats | 300% of endogenous | Gray et al., 2008 |
| ***Knock-in models*** | | | | | |
| HdhQ50 | chimeric HD/Htt exon 1 | 129/CD1 | 48 | Endogenous levels | White et al., 1997 |
| HdhQ92 | chimeric HD/Htt exon 1 | 129/CD1 | 90 | Endogenous levels | Wheeler at al., 2000 |
| HdhQ111 | chimeric HD/Htt exon 1 | 129/CD1 | 109 | Endogenous levels | Wheeler at al., 2000, 2003 |
| **HdhQ150** | **Htt exon 1** | **129/C57BL/6** | **150** | **Endogenous levels** | **Lin et al 2001** |
| Hdh94 | chimeric HD/Htt exon 1 | | 94 / 140 | Endogenous levels | Levine et al., 1999 |
| Hdh 6/72; Hdh 4/80 | Htt exon 1 | 129/C57BL/6 | 72 /80 | ~50% ↓in expression of mutant allele | Shelbourne et al., 1999 |
| Hdh (CAG)140 | chimeric HD/Htt exon 1 | C57BL/6 | 140 | Endogenous levels | Menalled, Sison, Dragatsis, Zeitlin, & Chesselet, 2003 |

Table 1.2 Phenotype of Mouse Models of HD. *Hdh* = mouse Huntingtin gene; M = months of age; W = weeks of age; d = days; n.r. = not reported. BAC: bacterial artificial chromosome; YAC: yeast artificial chromosome. ↑= Increase in; ↓= Decrease in; f = female, ~ = approximately. Outlined rows reflect the mouse models used in this thesis. References reflect the first instance of an observed effect.

| | **PHENOTYPE PROFILE** | | | |
|---|---|---|---|---|
| **Model** | **Cognitive** | **Psychiatric/ Emotional** | **Motor deficits** | **Lifespan** |
| ***Transgenic models*** | | | | |
| R61 | ↓ exploratory behaviour (*Hodges et al, 2008)*, sensory discrimination deficits (*Mazarakis et al, 2005)* | ↓ anxiety [24w], depression-like symptoms (*Naver et al, 2003*) | Progressive [4m-]; seizures, ↓locomotion [23w], clasping [14w] (*Carter et al, 1999*) | 32-40 w |
| R62 | Deficits on: Morris water maze (*Murphy et al, 2000*); open-field (↑exploration [20d], ↓ [4-6w];*Bolivar et al, 2003*); T-maze (*Lione et al, 1999)* | Fear conditioning deficits [5 w] *(Bolivar et al, 2003)* | Progressive; hyperactive [3w], hypoactive [4.5w], rotarod deficits [40d], resting tremor, chorea, clasping behaviour, seizures, narcolepsy [9w], climbing and balance deficits [5w] (*Hickey et al, 2005*) | 10-13w |
| YAC 72Q / 128 | Discrimination reversal learning deficits [27w], extra-dimensional set-shifting deficit [69w] (*Brooks et al, 2012*) | Depressive-like [3-4m] (*Pouladi et al, 2009*) | Progressive co-ordination deficits [4m], hyperactive [3m], hypoactivity [12m]; rotarod deficits [11w-6m], balance beam deficits [3-4m] 72Q: clasping behaviour [3m] (*Brooks et al, 2012*) | n.r.(YAC128: 2 years [*anecdotal]*) |
| N171-82Q | Working and reference memory deficits [14w] (Ramaswamy et al. 2004). | n.r | Tremor, hypokinesia, rotarod and gait deficits, clasping behaviour [11w] (*McBride et al, 2006*) | 5-11m |
| BAC-HD | cognitive inflexibility and psychomotor slowing (Farrar et al, 2014) | Depressive-like [12m] *(Gray et al, 2008)* | Progressive: rotarod deficits [2m], startle response [12m] (*Gray et al, 2008*) | n.r. (*19 months [anecdotal]*) |
| ***Knock-in models*** | | | | |
| HdhQ92 | Deficits in: sensorimotor learning [4m]; delayed alternation [5m] (*Trueman et al, 2009*), watermaze [14m] (*Brooks et al,2012*), attention (*Trueman et al, 2012)* | n.r | Startle and grip strength deficit [4m] (*Brooks et al, 2012)* | Normal |
| HdhQ111 | spatial and recognition memory deficits in HdhQ7/Q111 mice (*Giralt et al, 2012)* | Anxio-depressive behaviour [13-15w]; gender differences | No clasping or rotarod deficits [15m]; gait abnormalities [24 m] (*Wheeler et al, 2002)* | Normal |
| HdhQ150 | Spatial learning memory deficit on Morris water maze [13m] | n.r. | **progressive from ~ 4m** | Normal |
| Hdh 94 | n.r. | n.r | biphasic: hyperactivity [2 m], hypoactivity [4 m] | |
| Hdh6/72<br>Hdh 4/80 | n.r. | Aggression [3m]; males > f | Rotarod deficits [4m] | 17 m + |
| Hdh(CAG)140 | Motor learning deficits [6m] | anxiety [1.5m]; ↑ freezing behaviour [4-6m] ~ fearfulness | biphasic: ↑ rearing [1m]; ↓ locomotion [4m]; gait deficits, ↓ climbing [1.5–6.5 m]; rotarod deficit [4m]; tremor [20-26m] (*Dorner et al, 2007)* | Normal |

Table 1.3 Neuropathology of HD mouse models. N.r: not reported, m: months, w: weeks. ↑= Increase in; ↓= Decrease in; ~ = approximately. Outlined rows reflect the mouse models used in this thesis.

| NEUROPATHOLOGY | | | |
|---|---|---|---|
| **Model** | **Neuronal Inclusions and aggregates** | **Grey matter** | **White matter pathology and inflammation** |
| ***Transgenic models*** | | | |
| R61 | Progressive throughout brain *(Davies et al, 1997)* | Overall brain atrophy; ↓ striatal volume (*Van Dellen et al, 2000)* | n.r |
| R62 | Inclusions [1m]; initially in cortex & hippocampus, progress to striatum. Widespread by 8w (*Morton et al, 2000)* | striatal neuronal atrophy [12w]<br>progressive loss in brain weight [4w]<br>loss of striatal neurons (Levine et al, 2004) | ↓ in microglia, structural microglial abnormalities [7w]<br>↓microglia size [14.5w]<br>Dystrophic microglia (*Simmons et al, 2007, Ma et al, 2003*) |
| **YAC 72 /128** | *Inconsistencies:* No inclusions but micro-aggregates [12m]; mutant *HTT* aggregates & inclusion bodies in striatum [12m] inclusions [18m)](*Li et al, 2001; Hodgson et al, 1999, Slow et al, 2003*) | Striatal atrophy [8m]; ↓ forebrain weight, normal cerebellar weight [12m]; cortical atrophy [12m] (*Lerch et al, 2008; Slow et al, 2003)* | n.r |
| N171-82Q | Cytoplasmic aggregates & diffuse nuclear staining [4w]; inclusions in striatum, hippocampus, and cortex [16w] | 25% neuronal loss in striatum, 20% cell shrinkage [16w] | **n.r** |
| BAC-HD *(Gray et al, 2008)* | Progressive inclusions in the striatum and cortex & aggregates [12 m]; No S830+ striatal aggregates [12m] | striatal and cortical volume loss, ↓ forebrain weight, normal cerebellar weight [12m] | n.r |
| ***Knock-in models*** | | | |
| HdhQ50 | Inclusions [>6m] | No abnormalities until 6m | n.r |
| HdhQ92 | Nuclear staining [5m]; nuclear microaggregates and inclusions [12m] | n.r | n.r |
| HdhQ111 (*Wheeler et al, 2002*) | Nuclear staining [~2m]; nuclear micro-aggregates [~5m]; intranuclear inclusion [12m]; neuropil aggregates [17m] | **n.r** | Gliosis [24m]<br>Axonal changes [17m] |
| **HdhQ150** | Nuclear staining [7-8m]; nuclear and neuropil aggregates and inclusions [14m] (*Lin et al, 2001*) | Striatal cell loss (*Bayram-Weston et al, 2012)* | Gliosis and axonal degeneration [14m] |
| Hdh 94 / 140 | Nuclear staining & microaggregates [6m] intranuclear inclusions [18m] (*Menalled, 2002*) | **n.r** | **n.r** |
| Hdh6/72 Hdh 4/80 | Inclusions from 12m (Li et al, 2001) | 15% ↓ brain size [4-6m] No neuronal loss [4-6m; 16-17m] (*Shelbourne et al, 1999*) | No gliosis (*Shelbourne et al, 1999*) |
| Hdh(CAG)140 | **Progressive Inclusions from 2-4m;** inclusions in the striatum, cortex, hippocampus, and cerebellum (*Menalled et al, 2003*) | 38% ↓ striatal volume, 40% ↓ striatal neurons [20–26 m] Brain weight ↓19%, medium spiny neurons ↓41% [12m)];<br>↓84% [20–26 m] *(Hickey et al, 2008)* | Cortical astrogliosis [12m], striatal gliosis [24m]; No difference in corpus callosum or globus pallidus (GFAP) (*Hickey et al, 2008*) |

### *Treatment options in Huntington's disease*

There are currently no treatments available to alter the course of HD, with treatment options limited to symptomatic therapies. As HD has a heterogeneous phenotype, with each patient experiencing a different profile of symptoms, symptomatic treatment options and their effectiveness differ between individuals and across the disease time course. As with other disorders aiming to treat multiple symptoms, side effects of one treatment are likely to exacerbate other symptoms. An ideal treatment for HD would prevent neuronal death that occurs as a consequence of the mutant *HTT* gene and precede the emergence of symptoms. There are currently two main targets to prevent neuronal loss in HD, the first being a cellular target which aims to replace lost neurons and/or provide nutritional and survival support to reduce cell loss in diseased tissue, whereas the second option is a genetic target to ablate the mutant huntingtin protein.

***Symptomatic treatments*** Pharmacotherapy treatment options for motor symptoms include the dopamine depleter tetrabenazine, benzodiazepines (e.g. diazepam) and neuroleptics (e.g. risperidone), whereas treatment options for non-motor symptoms include selective serotonin reuptake inhibitor antidepressants, antipsychotics (Correll, Leucht, & Kane, 2004), monoamine oxidase inhibitors, and mood-stabilizing agents to improve impulse control.

***Cell-based therapies*** There are a number of different cell-based therapies that have potential in HD treatment for the future. In vivo, the most evidence exists for foetal primary transplants. From work in mice, rats, and monkeys in which embryonic striatal tissue is transplanted into the site of excitotoxic striatal lesions, grafts were shown to survive, grow, express a wide range of cellular markers characteristic of the normal striatum and improve behavioural signs associated with the lesion (Dunnett, Nathwani, & Björklund, 2000; Döbrössy & Dunnett, 1998; Mayer, Brown, Dunnett, & Robbins, 1992). Importantly, host-to-graft afferent and efferent connections were shown to develop (Wictorin, 1992) and were functionally viable both neurochemically (K. Campbell et al., 1993; Sirinathsinghji et al., 1988; Sirinathsinghji, Heavens, Torres, & Dunnett, 1993) and electrophysiologically (Mazzocchi-Jones, Döbrössy, & Dunnett, 2009; Nakao, Ogura, Nakai, & Itakura, 1999; Xu, Wilson, & Emson, 1991). Foetal primary transplants have since been taken forward to clinical trials and in the past 14 years, there have been a number of clinical trials which have produced mixed results, with evidence of a short-term but not long-term clinical improvement (Bachoud-Lévi, 2009; Bachoud-Lévi et al., 2006; Bachoud-Lévi et al., 2000; Kopyov et al., 1998; Paganini et al., 2013; Philpott et al., 1997). A multi-centre study ("NEST-UK") is also underway in the UK, with reports on efficacy and safety recently published (Barker et al., 2013) . Despite this, a fundamental constraint is the limited supply of suitable donor tissues, which restricts the levels of standardization and quality control required for experimental medicine.

Alternative sources of tissue for neural transplantation have been explored, including human neural stem cells (Johann et al., 2007; Lee et al., 2006; J. L. McBride et al., 2004; Roberts, Price, Williams, & Modo, 2006; Ryu et al., 2004) Sources of neural stem cells which have been investigated in HD include: 1) *embryonic stem cells* (J. Song et al., 2007), which are derived from blastocysts, 2) *foetal stem cells*, with pluripotent progenitor cells taken from the embryo, foetus, or neonate, which are already partially committed down a neural lineage, 3) *adult neural stem cells*, with progenitor cells isolated from the adult subventricular zone (Vazey, Chen, Hughes, & Connor, 2006; Vazey & Connor, 2010), 4) *embryonic germ cells* that are isolated from the gonadal ridge of the embryo, 5) *non-neural stem cells*, such as adult bone marrow stem cells or umbilical cord cells, and 6) induced pluripotent stem cells (iPS cells) which can be generated from adult human fibroblasts (Consortium, 2012; Takahashi, Okita, Nakagawa, & Yamanaka, 2007).

. In addition, in response to work showing a reduction in neurotrophic support required for neurogenesis in HD (Ciammola et al., 2007; Conforti et al., 2008; Zuccato et al., 2008; Zuccato et al., 2011) the transplantation of genetically-engineered stem cells which over-express a range of neurotrophic factors (e.g. BDNF, glial-cell derived neurotrophic factor and nerve growth factor) has been shown to improve motor function and reduce striatal loss (Dey et al., 2010; Sadan, Melamed, & Offen, 2012) in rodent models of HD, although issues with poor survival of transplanted cells are reported (Sadan, et al., 2012).

The future of these cell-based therapies beyond pre-clinical trials will depend on practical issues such as achieving effective and reliable tissue survival and integration, feasibility, long term safety and ethical and regulatory restrictions (Dunnett & Rosser, 2014). Nevertheless, it is hopeful that with advancements in knowledge and refinements in cell transplant technology, cell-based therapeutics may still hold promise in HD.

***Gene-based therapies*** Gene-based therapies also offer a potential powerful treatment option for the future, aiming to prevent the expression of the mutant protein in order to circumvent the cytotoxic downstream effects. Gene silencing involves targeting RNA to prevent the mutant HTT protein from being formed and is close to reaching clinical trials. One example of gene silencing is antisense therapy (Lu & Yang, 2012), whereby a strand of nucleic acid is synthesised specifically to bind to the messenger RNA produced by the *HTT* gene in order to inactivate it, as mRNA needs to be single stranded for it to be translated. This technique has proven hopeful when applied to transgenic mouse models of HD, with antisense oligonucleotides found to reduce *HTT* expression by approximately 75% following injection into the lateral ventricle (Kordasiewicz et al., 2012). There are also a number of genome editing technologies that have been developed in recent years, such as zinc finger nucleases [ZFN's] (Gaj, Guo, Kato, Sirk, & Barbas, 2012; Y. G. Kim, Cha, & Chandrasegaran, 1996), transcription activator-like effector nucleases [TALENs] (Mussolino et al., 2011) and most recently, Clustered Regularly Interspaced Short Palindromic Repeats [CRISPR] (Gaj, Gersbach, & Barbas, 2013) which aim to cut DNA at a specific target sequence, such as near the expanded CAG tract in the HD gene.

As with cell-based therapies, one of the challenges for gene therapies is the method of delivery and the inability to stop in the event of adverse effects. Unlike pharmacotherapy, delivery may need to be directly into the brain and would thus require neurosurgery.

***Environmental enrichment*** A less invasive and more accessible therapeutic avenue that has received research attention in a range of neurodegenerative diseases is environmental modification. Environmental enrichment, defined as an increased level of novelty and complexity, inducing enhanced sensory, cognitive and motor stimulation (Nithianantharajah & Hannan, 2006) has been found to improve survival rates, reduce motor symptoms and disease-related neuropathology and decrease neuronal intranuclear inclusion load in mouse models of the disease (Benn et al., 2010; Hockly et al., 2002; T. L. Spires et al., 2004; Wood, Glynn, & Morton, 2011). Environmental enrichment may also be of benefit in an indirect way; research in mice who had received a unilateral quinolinic acid lesion of the striatum followed by an embryonic striatal graft found that environmental enrichment induced changes in long term potentiation and BDNF levels in both the intact and grafted striatum (Mazzocchi-Jones, Döbrössy, & Dunnett, 2011), suggesting environmental modification can improve the outcome of cell transplantation.

***Exercise*** Exercise based interventions conducted in both mouse models and HD patients have shown beneficial effects on behaviour (Busse et al., 2013; Khalil et al., 2013; van Dellen, Cordery, Spires, Blakemore, & Hannan, 2008) and a reduction in neuropathology (Harrison et al., 2013). Taken together, the results from environmental enrichment and exercise studies suggest that a more holistic approach, whereby any genetic or cellular intervention is combined with an optimised environment in terms of physical, social and cognitive activity, may bring us closer to a disease-modifying treatment in HD.

## 1.2 Magnetic resonance imaging to study HD neuropathology

### *Principles of magnetic resonance imaging*

Magnetic resonance imaging (MRI) has a dichotomous history; whereas the principles underlying MRI were first discovered in the early 20th century, it wasn't until much later, in 1973 that the first NMR image was produced, and not until the late 1970's and early 1980's that the clinical utility of MRI was recognised with the introduction of magnetic field gradients, which dramatically sped up the ability to acquire MR images. Today, more advanced sequences, gradient manipulations and enhanced software continue to be developed resulting in an evolving field with the associated clinical utility continuing to be realised.

Although other nuclei have been studied, the magnetic properties of the hydrogen nucleus are principally utilised, namely because of the high abundance of hydrogen in the body. The interaction between the magnetic properties of the hydrogen nucleus, a strong external magnetic field (B0) and applied radio waves forms the basis of the MRI image. The nucleus of the hydrogen atom consists of just one proton, which spins in a randomly oriented fashion around its own axis, producing a small magnetic field with a north and south-pole and an associated magnetic moment vector. When the proton is placed in an external magnetic field (B0), two changes occur. Firstly, the dipoles of the protons are no longer randomly oriented, but instead line up with the direction of the magnetic field, either in a parallel ("spin up") or anti-parallel ("spin down") position. Marginally more protons align parallel to the external field, resulting in a net magnetic moment parallel to the magnetic field. Secondly, this net magnetic moment *precesses* about the direction of the applied field. With a precessional frequency $\omega$, that is directly proportional to the strength of the external magnetic field Bo, i.e. $\omega=\gamma Bo$, where $\gamma$ is the gryomagnetic ratio. The varying molecular structures and amount of hydrogen atoms in different tissue types in the body affects the strength of this net magnetisation, and thus the precessional (Larmor) frequency.

In order to achieve a MR signal, a RF pulse, which is a magnetic field oscillating at radio frequency, is applied perpendicularly to B0 in order to cause a transition between these two energy states. The electromagnetic radiation is absorbed by the protons, causing protons in the parallel, low-energy state to excite and flip into the anti-parallel state whilst precessing in-phase, consequently flipping the net magnetisation towards the transverse plane. The angle through which the net magnetisation flips is dependent on the strength and duration of the RF pulse, whereas the frequency of the pulse is determined by the Larmor equation ($\omega=\gamma Bo$) introduced above. Once the RF pulse stops, the protons contributing to the net magnetisation start to lose their phase coherence, whilst some of the protons that had transitioned into the anti-parallel, high energy state give off their energy and flip back to the low energy, parallel state (“relaxation”), causing the net magnetisation to regrow in the B0 direction. During this relaxation period, a radio frequency signal is generated and measured by receiver coils. The rate of longitudinal relaxation varies between different tissue types and is known as T1. A second type of relaxation is transverse, or T2 relaxation which occurs in the *x-y* plane and refers to the decay of transverse magnetization as spinning dipoles lose phase coherence and dephase following a RF pulse.

In order to gain spatial information from these signals, additional magnetic fields are applied using three gradient coils (X, Y, Z) which are each oriented along a different orthogonal axis and are used to produce deliberate variations in the main magnetic field to encode spatial information. The intensity of the signal received and thus the MR image reconstructed depends on a number of parameters including: the T1 relaxation time, the T2 relaxation time and the proton density. The contrast of the image can be altered by changing the pulse sequence parameters, such as the strength, duration and timing of the RF pulse, resulting in different pulse programs for different purposes.

## *$T_1$- and $T_2$-weighted MRI to examine tissue macrostructure*

The spin echo sequence is the most commonly used MRI pulse sequence and generally refers to an echo formed after the application of two pulses: a 90° excitation pulse and a 180° refocusing pulse. The echo time (TE) is the time between the 90° RF pulse and MR signal sampling, which corresponds to the maximum of the echo; the 180° refocusing pulse is applied at ½ of the TE and flips the dephasing individual spins to the opposite side in the x-y plane so that after another ½ TE, they refocus. This series is repeated at each time interval TR (Repetition Time) and the longer the TR, the more complete the longitudinal relaxation. Thus, a short TR (<1000 ms) results in a $T_1$-weighted image as the differences between the longitudinal relaxation of the tissues' magnetization is emphasised. In contrast, $T_2$-weighted sequences use a long TR and TE (> 2000/80ms), producing distinctly different image contrast. $T_1$- and $T_2$-weighted MRI sequences can be used to quantitatively examine disease pathology, as well as the volume, thickness and shape of brain structures.

There are a number of different analysis approaches used in order to obtain such metrics, and the suitability of the different approaches is affected by the image quality and the type of neuropathology expected in the sample population. The software used for human image analysis is not directly translatable to pre-clinical image analysis, due to differences in brain shape, size and anatomy. The simplest but most labour-intensive method is slice-by-slice manual segmentation of the structures of interest. This is generally considered the 'gold standard' reference method, but depends on the expertise of the rater and is thus prone to issues with inter-rater reproducibility. Due to the time-consuming nature of manual segmentation, the majority of human morphometric studies instead use software which employs semi-automated and automated approaches with 3D image registration, electronic brain atlases and prior tissue probabilities (e.g. SPM, FSL, FreeSurfer, and BrainVoyager).

Voxel-based morphometry (VBM) (Ashburner & Friston, 2000) and deformation-based morphometry (DBM) (Ashburner et al., 1998) are both commonly applied whole-brain automated approaches which can be used to reveal structural differences between groups (i.e. between healthy controls and a patient group). Whereas with VBM statistical analysis is performed at each voxel separately to look for local differences in the density, with DBM, statistical analysis is multivariate and performed on the deformation fields used to non-linearly register the voxels.

### *$T_1$- and $T_2$- weighted MRI in HD*

In pre-symptomatic HD, both grey and white matter atrophy has been found, with enlarged gyri and abnormally thin sulci found globally in the cortex (Nopoulos, Magnotta, & Mikos, 2007). Intracranial adult brain volume has been found to be reduced in pre-symptomatic HD carriers (Nopoulos et al., 2010) and individuals with pre-symptomatic HD have been found to have significantly enlarged cortical grey matter volume and significantly smaller cerebral white matter volume compared to age-matched controls (J. Paulsen et al., 2006). White matter atrophy at the pre-symptomatic stage has also been found in two large-scale longitudinal studies (Aylward et al., 2011; Paulsen, et al., 2010; Tabrizi et al., 2012; Tabrizi et al., 2011)

In a regression analysis conducted to determine whether any brain volume measures contributed to a prediction of estimated diagnosis, only cerebral white matter volume was found to be a predictor of diagnosis proximity after total striatal volume was entered into the statistical model (Paulsen, 2010) whereas there was no relationship between grey matter atrophy and time to onset (Ciarmiello, et al., 2006). Even in pre-symptomatic patients classified as far from symptom onset, the rate of white matter atrophy was significantly greater compared to healthy controls over a 1-year period (Tabrizi, et al., 2011), and over 2 years, the rate of change in white matter volume was greater than that in grey matter volume in pre-symptomatic and early HD patients (Tabrizi et al., 2012). However, in other studies with pre-symptomatic groups who are far from predicted disease (motor symptom) onset, there was no evidence of white matter change in participants who were on average 18 years away from disease onset (Hobbs et al., 2010). Remarkably, when correcting for normal age-related changes over a 2-year period, disease-related atrophy was more pronounced in white matter than in the striatum in pre-symptomatic participants (E. Aylward, et al., 2011). Likewise, in a smaller study, whereas white matter volume was significantly reduced in pre-symptomatic participants, the reduction seen in grey matter did not meet the threshold for significance (Ciarmiello, et al., 2006). In a smaller scale study, the isthmus of the corpus callosum was significantly thinner in pre-symptomatic patients compared to controls (Paola et al., 2012).

In early HD, white matter atrophy continues to be evident (Ciarmiello, et al., 2006; Hobbs, et al., 2010); patients had significantly lower cerebral white matter volume, cerebellar white matter, and corpus callosum volume than matched healthy subjects (Beglinger, et al., 2005; Hobbs, et al., 2010). There are inconsistencies in the literature for cerebral grey matter volume, with some work showing no difference in volume between controls and early HD participants (Beglinger, et al., 2005) and other work showing regionally specific cortical atrophy in the parietal, frontal and temporal lobes and widespread losses in the occipital lobes (Hobbs, et al., 2010). The rate of both global white matter loss and corpus callosum thinning was found to be more rapid in HD gene carriers who develop symptoms earlier in life ( <40 years old; Rosas et al., 2011), whilst the entire corpus callosum was significantly thinner compared to healthy controls (Paola, et al., 2012). Similarly, longer CAG repeat lengths, inversely related to age of onset (Andresen et al, 2007) was significantly associated with higher atrophy in the internal capsule as well as frontal, occipital and parietal white matter regions (Hobbs, et al., 2010). The splenium was found to be more atrophied than the genu and body of the corpus callosum in the early HD stage (Hobbs, et al., 2010).

There are fewer studies with patients with more advanced stages of the disease, and white matter changes are often not reported (Aylward et al., 2000; R. Wolf, Vasic, Schönfeldt-Lecuona, Ecker, & Landwehrmeyer, 2009). In one study of gene-positive patients ranging from pre-symptomatic to advanced HD, a significant negative correlation was found between relative WM volume (corrected for intracranial volume) and disease duration (Ciarmiello, et al., 2006). However, a second follow up scan around 18 months later found no change in white matter volume specifically in the symptomatic patients, suggesting the rate of white matter atrophy may decline with disease progression.

Overall, results from structural $T_1$- and $T_2$-weighted studies suggest the rate of atrophy in white matter does not follow the same course as grey matter atrophy in HD, with white matter atrophy beginning earlier in life prior to symptom onset, with less prominent changes in global grey matter volume. White matter areas affected tend to be widespread and not restricted to subcortical white matter, with both anterior and posterior regions affected. In relationship to the earlier list of candidate white matter pathways, these results are consistent with atrophy of the corpus callosum in HD pathology, and atrophy in the internal capsule suggests corticospinal tracts may be affected. Furthermore, atrophy in frontal, parietal and temporal white matter areas may implicate long association fibers, such as the cingulum, which connects regions in the frontal lobe with posterior regions such as the posterior cingulate cortex, hippocampus, and parahippocampus (Schmahmann et al., 2007; Wakana, Jiang, Nagae-Poetscher, van Zijl, & Mori, 2004).

## ***Diffusion MRI to probe tissue microstructure***

Diffusion MRI is an imaging modality capable of characterising tissue microstructure on a scale not achievable with other in vivo imaging modalities. Diffusion MRI is concerned with the random bulk motion of water molecules in tissue. In the brain, white matter fibers are highly oriented resulting in a contrast between anisotropic diffusion of water due to highly orientated barriers, and isotropic diffusion in regions of the brain that are not directionally oriented, such as in grey matter and cerebrospinal fluid.

Echo-planar imaging (EPI) is the most widely used method for diffusion imaging (Crooks et al., 1988; Turner et al., 1990) and the development of EPI in combination with high gradient amplitude systems allowed the clinical utility of diffusion MRI to be realised, with high-quality images devoid of significant motion artefacts attainable in clinically relevant acquisition times. The trade-off for increased speed is a reduction in image resolution; EPI requires high bandwidths which causes SNR loss and is resolved by lower image resolution.

### ***Tensor-based models and metrics***

The most widely used diffusion MRI approach is diffusion tensor imaging (DTI), which utilises a tensor model for diffusion, and assumes a 3-dimensional symmetrical Gaussian distribution. The diffusion weighted signal is acquired using a non-zero b-value with diffusion gradients applied along at least six non-collinear, non-coplanar directions (Basser, Mattiello, & LeBihan, 1994). Anisotropic diffusion is modelled as a diffusion ellipsoid and is a function of three orthogonal eigenvectors. The diffusivities along the eigenvectors are described by three eigenvalues ($\lambda_1$, $\lambda_2$, $\lambda_3$) which determine the size and shape of the ellipsoid, and this information is represented mathematically by a tensor. The most commonly reported DTI indices are the mean diffusivity (also known as the apparent diffusion coefficient), or MD value, which refers to the average diffusivity across the three eigenvalues, and fractional anisotropy, or FA value, which refers to the directional dependence of diffusion and informs only on the rate of anisotropic diffusion in the voxel, which is often interpreted as an indication of the integrity of the tissue.

The specific relationship between tissue microstructure and anisotropy is multifactorial. In animals, the association between radial diffusivity (the average of $\lambda_2$ and $\lambda_3$ of the diffusion tensor) and myelin content and between axial diffusivity ($\lambda_1$ of the diffusion tensor) and axonal structure has been made (Song et al., 2003; Song et al., 2002; Song et al., 2005). However, it has since been shown that in areas containing complex fiber configurations and in voxels affected by partial volume, the eigenvalues of the tensor may reflect different underlying structural characteristics, hindering the ability to make interpretations about underlying tissue structure (Wheeler-Kingshott & Cercignani, 2009).

### *Non-tensor based approaches*

A major limitation of the diffusion tensor model is that it can only account for Gaussian diffusion processes that dominate signal attenuation at relatively low b-values. Due to the heterogenous nature of biological tissue, with different cell types, barriers and compartments, the diffusion displacement probability distributions can deviate considerably from a Gaussian form (Cohen & Assaf, 2002). In recent years, a number of new methods have been developed to more adequately model diffusion in white matter. High angular resolution diffusion imaging, or HARDI, methods increase sampling in q-space to produce an improved diffusion profile using a variety of different approaches (Alexander, 2005; Frank, 2002; Tuch et al., 2002). Multi-compartment approaches, such as Assaf et al's (2004) composite hindered and restricted model of diffusion model (CHARMED) models the restricted diffusion component (intra-axonal compartments which correspond to distinct fiber populations) separately from the hindered-diffusion component in the extra-cellular space through the use of multiple b-values per direction and a hybrid HARDI approach. The ability to model the intra-axonal diffusion may provide a more biologically specific and/or sensitive characterisation of white matter changes in disease. The work conducted in Chapter 4 of this thesis demonstrates the first application of the CHARMED model in HD.

Other non-diffusion techniques are available to examine changes in myelin content. Multicomponent analysis of T1 and T2 relaxation data, or multicomponent relaxometry, is a quantitative MR technique that is sensitive to changes in myelin content (Deoni, Rutt, Arun, Pierpaoli, & Jones, 2008; Spader et al., 2013). This technique is based on the observation that there are multiple water compartments in a cell: the 'free' water that exists in both the intra- and extra-axonal space and water contained within the layers of the myelin sheath which has a shorter T2. Each water compartment has been shown to have a unique MR signal signature, and these signal signatures can be fitted from multiple MR images in order to calculate the relative signal from the myelin, known as the myelin water fraction (MWF). This metric has been shown to be strongly correlated with histological measures of myelin content (Laule et al., 2006; Webb, Munro, Midha, & Stanisz, 2003), and along with being more specific than DTI, is not influenced by other biological changes, such as inflammation (Gareau, Rutt, Karlik, & Mitchell, 2000). The work conducted in Chapter 5 of this thesis demonstrates the first application of the multicomponent driven equilibrium single-pulse observation of T1 and T2 (mcDESPOT) model (Deoni, et al., 2008) in Huntington's disease.

### *Diffusion Tractography*

Fiber tractography is a mathematical technique to trace the fiber tract trajectories from the acquired diffusion MRI data and allows for the 3-dimensional reconstruction of white matter pathways in the brain (Basser, Pajevic, Pierpaoli, Duda, & Aldroubi, 2000). Tractography algorithms can be separated into two major classes: *deterministic* and *probabilistic* tractography. In deterministic tractography, a tractogram is generated based on a best estimate of the underlying fiber orientation, starting from an initial user-defined ‘seed’ location and propagating through 3-D space according to the specific tractography algorithm until some termination criteria is met (i.e. curvature angle or anisotropy threshold). For example, in DTI tractography, the directional information from the diffusion tensor is used, with streamlines following the principal eigenvector (Basser, 1998). In contrast, probabilistic tracking uses the diffusion MR data to infer fiber orientation along with an estimate of orientation uncertainty in each voxel, and uses the estimates and uncertainty to build a probabilistic map of connections (Parker, 2004). Streamlines are propagated from a seed point but at each propagation step, an orientation is chosen randomly from the underlying distribution, and a spatial distribution of streamlines is built.

The diffusion tensor model is limited in areas of complex fiber architecture as it can only have a single maximum in an imaging voxel, thus a voxel-averaged tensor is unable to adequately describe voxels with crossing, diverging, or converging white matter tracts (Basser, Mattiello, & LeBihan, 1994; Lazar & Alexander, 2003; Pierpaoli, Jezzard, Basser, Barnett, & Chiro, 1996). This is particularly problematic for tractography, where white matter tracts are likely to traverse voxels containing multiple fiber orientations at some point along the path. Alternative algorithms are capable of modelling multiple fiber orientations within a single voxel, for example, spherical deconvolution (SD) methods estimate the fiber orientation distribution function f(ODF) directly (Tournier, Calamante, Gadian, & Connelly, 2004; Tournier et al., 2008). With this method, the expressed signal is the convolution over spherical coordinates of the response function with the fiber orientation distribution, with the response function describing the DW signal intensity measured as a function of orientation for a single fiber bundle (Tournier et al., 2004).

A number of different approaches use spherical deconvolution but differ in terms of the way the diffusion profile is obtained and the use of additional prior information. For example, constrained spherical deconvolution (CSD) (Tournier, Calamante, & Connelly, 2007; Tournier, Calamante, Gadian, & Connelly, 2004) uses spherical harmonics to model the high angular resolution diffusion-weighted imaging (HARDI) signal (Tuch et al., 2002) to generate estimates of the fiber orientation distribution within each imaging voxel, and has been shown in phantom data and in vivo data to be robust to crossing fibers (Farquharson et al., 2013; Tournier, et al., 2008).

### *Diffusion MRI in HD*

The majority of studies in HD have applied diffusion MRI based on the tensor model, either applying whole-brain tract based spatial statistics (S. M. Smith et al., 2006), voxel based whole brain statistics, or region of interest based analysis. The research focus has been on the basal ganglia although results to date have been inconsistent; some studies have reported lower FA values in the putamen, caudate nucleus (Reading et al., 2005) and thalamus (Magnotta et al., 2009) in pre-symptomatic gene-positive individuals whereas other studies report higher FA values in the putamen and pallidum (Douaud et al., 2009; Klöppel et al., 2008; Rosas et al., 2006) and others report no difference in FA between controls and pre-symptomatic gene-positive individuals (Dumas et al., 2012). Lower FA values and higher MD values have been reported in the internal capsule and corpus callosum, in both pre-symptomatic and symptomatic HD patients, suggesting white matter changes contribute to the disease in some way (Dumas et al., 2012; Magnotta et al., 2009; Rosas et al., 2006). One reason for the inconsistencies is the heterogeneity of patient groups; the average and range of CAG repeats in the patient group will vary between studies, as will the variance in disease stage, all of which introduces variance into the studies. Although ROI analysis of DTI indices is useful in examining a priori regions of interest, the technique has a number of limitations including bias in ROI selection, inter-subject variability, issues with artefacts and decreased resolution when drawn onto diffusion-weighted images, versus issues with registration when drawn on higher resolution anatomical images. Fewer studies have applied diffusion tractography in HD; Bohanna et al (2011) applied probabilistic tractography in symptomatic HD participants to examine connectivity to the caudate and putamen. In HD participants relative to controls, a reduction in FA and an increase in MD were found in the connections between both the caudate and putamen and the prefrontal, primary motor, and primary somatosensory cortices. Crucially, motor symptoms were shown to correlate with mean diffusivity in sensorimotor striatal sub regions, supporting the idea that the motor cortico-striatal circuit is selectively vulnerable in symptomatic HD (Bohanna et al., 2011).

### *Pre-clinical experimental MRI as a translational tool to study HD*

MRI has the benefit of allowing disease to be studied in the living animal non-invasively, creating the opportunity to study disease progression and evaluate therapeutic efforts. Furthermore, MRI allows for the acquisition of whole brain 3-dimensional data as opposed to highly localised histological measurements from tissue sections in a single plane. A mouse brain is approximately 1000 times smaller than a human brain in terms of total volume, thus, high field strength is required in order to obtain adequate SNR and resolution. Pre-clinical imaging at high field strength presents a number of unique technical challenges which need to be considered before comparisons can be made to clinical MRI. Firstly, higher magnetic fields shorten tissue T2 and T2* and lengthen tissue T1. Anaesthesia is also a requirement when scanning small animals which limits the viable *in vivo* scan time.

Diffusion MRI is particularly challenging in the mouse brain; it is a low SNR technique due to the attenuation of the signal magnitude in diffusion weighted images by the diffusion sensitizing gradients. EPI sequences are required in order to obtain a diffusion MRI image with sufficient SNR in a time frame that can be tolerated. However, EPI at high field is difficult to achieve due to the combination between short T2 and the amplification of a number of artefacts at higher field strengths. Geometric distortions due to local magnetic field inhomogeneities increase linearly with field strength and T2* decreases at high field, thus the reduction in signal amplitude during the echo train is increased, reducing the spatial resolution in the phase encoding direction. The frequency difference between fat and water is also increased linearly with field strength, resulting in more pronounced fat/water spatial displacement in the phase encoding direction. Because EPI requires high bandwidths which reduce the spatial resolution, and high spatial resolution is necessary because of the small size of the mouse brain, segmented EPI (i.e. multi-shot) sequences are necessary which increases motion artefacts. Image analysis software are also not as advanced for rodent imaging, with standard software packages having in-built human-specific priors and templates, and basic pre-processing steps such as image registration are more challenging.

Despite these challenges, there have been a number of MRI studies in mouse models of Huntington's disease. Structural (Heikkinen et al., 2012; Rattray et al., 2013; Sawiak, Wood, Williams, Morton, & Carpenter, 2009), functional (Cepeda-Prado et al., 2012) and metabolic (Heikkinen, et al., 2012) imaging studies in HD mouse models have all revealed abnormalities of differing degrees depending on the mouse model used. Nevertheless, preclinical imaging in HD is still in its infancy; there is only a single published study applying diffusion MRI in a mouse model of HD, revealing white matter abnormalities in the corpus callosum (Xiang, et al., 2011). Likewise, despite the potential, only one published study has used MRI (T2-weighted structural) as an outcome measure for therapeutic intervention (Aggarwal et al., 2012) thus it remains to be seen whether different MRI sequences can produce sensitive outcome measures for pre-clinical therapeutic trials.

## Aims of this thesis

This thesis aims to characterise the structural brain changes that occur in Huntington’s disease across the disease course, using multi-modal translational neuroimaging. Novel imaging sequences will be used to characterise white matter microstructural changes in a number of different pathways implicated in HD, and results will be examined alongside macrostructural changes and behavioural results, in the context of discovering imaging biomarkers in HD.

# 2 Methods to characterise Huntington's disease

This methods chapter is split into two sections: 'pre-clinical' and 'clinical' methods. The first gives an overview of the methods used for examining structural changes in mouse models of HD and the second section describes the methodology for examining differences in a patient cohort of HD.

For the MRI methods for both the pre-clinical and clinical studies, there was an effort to ensure the pulse sequences were as similar as possible in order for comparisons to be drawn. However, because of: a) differences in the relative size of the brain compared to the scanner bore, b) differences in magnetic field strength between the pre-clinical and human MR system resulting in differences in the Larmor frequency and relaxation parameters, and c) differences in $T_1$ of brain tissue across species, there are differences in the scan parameters used between the two systems and experimnts. A comparison of scan parameters is shown in Table 2.1.

## 2.1 Pre-clinical Methods

### *In vivo methods*

***Ethical statement*** All experimental procedures in this thesis followed protocols in accordance with the United Kingdom Animals (Scientific Procedures) Act of 1986. All experimental procedures performed on mice were approved by Cardiff University Ethical Review Process Committee and carried out under Home Office License 30/3036.

***Breeding*** In experimental chapter 6, heterozygous HdhQ150 mice on the original 129/Ola x C57BL6/J background (Lin, et al., 2001) were bred in-house using a heterozygous mutant (-/+) x heterozygous mutant (-/+) breeding regime. Male homozygote $Hdh^{Q150/Q150}$ mice and male wild-type $Hdh^{+/+}$ mice were used in the experiment. In experimental chapter 7, YAC128 (Hodgson et al., 1999b) were congenic on a C57BL6/J background. This strain was initially sourced from the Hayden laboratory at the University of British Columbia, Vancouver, and the strain was maintained in-house by backcrossing on to BL/6 with every breeding cycle.

***Genotyping*** Genotype was confirmed by tail tipping at approximately 5 weeks old and carried out commercially (Laragen Inc., Los Angeles, CA, USA).

***Housing*** All mice were housed in age- and sex-matched groups of between 1 and 3 mice with mixed genotype cages where possible. Mice were subject to a 12-hour light: 12-hour dark cycle with controlled room temperature (21 ± 3 °C) and relative humidity (60 ± 3%). All home cages contained moderate enrichment conditions including play tunnels and nesting material. All animal were weighed on a monthly basis in order to monitor general health.

***Behaviour Assessment***. Both cognitive and motor tests are available to examine mouse behaviour, however cognitive testing is associated with long training periods which may confound MRI measures due to training-induced plasticity (Sagi et al., 2012). Thus, in Chapter 6 where the primary aim was to measure structural brain changes longitudinally, only motor testing was conducted to reduce learning-induced confounding effects.

Table 2.1 Comparison of mouse and patient MRI parameters. RARE: Rapid Acquisition with Refocused Echoes. FSPGR: Fast spoiled gradient echo EPI: echo-planar imaging. TRSE: Twice-refocused spin echo. HARDI: high-angular resolution diffusion imaging. TR: Repetition time. TE: Echo time.

| | Mouse models | | HD patients | |
|---|---|---|---|---|
| | Chapter 6 | Chapter 7 | Chapter 4-5 | |
| Hardware | 9.4 T Bruker Biospin | | 3T GE HDx | |
| **Anatomical Scan** | | | | |
| | $T_2$-weighted | $T_2$-weighted | $T_1$-weighted | |
| TR/ TE (ms) | 1750/17.5 | 4000 /35 | 7.9/3.0 | |
| Sequence | Turbo RARE | RARE | FSPGR | |
| Dimensions | 3D | 2D | 3D | |
| Matrix | 128 x 128 | 128 x 128 | 256 x 256 | |
| In-plane resolution (mm) | .12 x .12 | .12 x .12 | 1 x 1 | |
| Slice thickness (mm) | 0.12 | 0.4 | 1 | |
| **Diffusion MRI** | | | | |
| | | | *DTI-optimised* | *HARDI-optimised* |
| TR/ TE (ms) | 8500/18.7 | 14600/ 20 | cardiac gated TR / 84.6 | cardiac gated TR / 97.3 |
| Sequence | 4-shot DTI-EPI | 4-shot DTI-EPI | TRSE | TRSE |
| Matrix | 96 x 96 | 96 x 96 | 96 x 96 | 96 x 96 |
| Resolution (mm) | .213 x .213 | .213 x .213 | 1.8 x 1.8 | 1.8 x 1.8 |
| Slice thickness (mm) | 0.32 | 0.32 | 2.4 | 2.4 |
| B value (s /mm$^2$) | 1000 | 1000 | 1000 | 2000 |
| Gradient directions | 30 | 30 | 30 | 45 |

***Open-field locomotion.*** The open field test was conducted using Ethovision Pro version 2.3.19 software (Noldus Information Technology, Netherlands) to investigate anxiety-related and exploratory behaviour. The open field was an empty square test arena (81 x 81 cm) containing 9 equally-spaced quadrants, in which the

animal's activity was measured using a camcorder (Sanyo CCD camera) and the recording software over a 20 minute period. The software measured the centre-point, nose point and tail base of the mouse. This allows a variety of different behaviours to be measured, such as locomotion (total distance moved), rearing, turning and freezing, as well as the amount of time spent close to the wall (an anxiety-like response, termed *thigmotaxis*) compared to the amount of time spent in, and frequencies of visits to, the inner quadrants. After each animal was removed from the arena, it was thoroughly cleaned with alcohol wipes to remove any scent information that may affect behaviour.

***Automated home-cage analysis of activity***. Animals were transferred to cages similar to their home cage containing access to food and water in order to test motor activity under non-stressed conditions. This test measured locomotion over a 24-hour period in order to measure both the light and dark phases of the diurnal cycle. Clear Perspex activity chambers containing food and water were fitted with 8 infra-red sensors (40 cm x 24 cm x 18 cm), and the total number of beam breaks made in 5-minute intervals were recorded over a 24-hour time period on MED Associate hardware and MED-PC® software (Vermont, USA). Lights were set on a timer to come on and go off every 12 hours, in order to study behaviour during periods of peak activity without experimenter interference. Animals were placed in the cages for 27 hours, with the first three hours not included in the main analysis to allow for acclimatisation and avoid detecting novelty or anxiety-related behaviour.

***Rotarod.*** The rotarod test (B. Jones & Roberts, 1968) is a classic test in HD and was used to assess overall performance in motor coordination, balance and endurance (Alvarez-Fischer, et al., 2008; Schallert, et al., 2000). Mice were trained and tested on the accelerating rotarod apparatus (Ugo Basile Research Apparatus, Varese, Italy). Mice were trained on 2 separate trials each lasting for 5 minutes on 2 consecutive days on an alternating fixed / accelerating speed protocol; Figure 2.1 shows the training protocol. The protocol involved 15 seconds of fixed speed, followed by a period of accelerating speed, with each successive period increasing in duration. During training, when mice fell off the rod (3.1cm diameter) they were placed back on until the full time had elapsed. The testing day followed the training days. On the testing day, the mice were tested twice on the accelerating version of

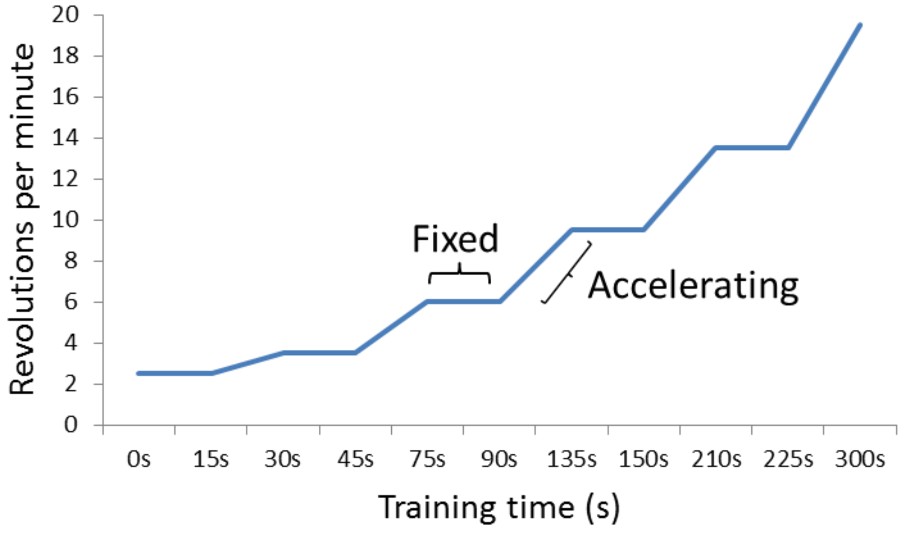

Figure 2.1 Training procedure for the Rotarod test. An alternating fixed/accelerating speed protocol was used during training for a maximum of 5 minutes. The line represents the speed of the rod in revolutions per minute (r.p.m).

the rotarod; the speed of revolutions increased from 4 to 44 r.p.m over a maximum period of 300 s. The two trials were 15 minutes apart. When the mouse fell from the rod the latency to fall from the rod was recorded for each trial.

***MRI Acquisition*** All preclinical MRI was conducted on a 9.4 Tesla small bore (20 cm) Bruker Biospin system, equipped with BGA12-S (12 cm inner bore size, integrated shims) gradients. A transmit 1H 500 Watt echo-planar imaging (EPI) volume coil was used for all in vivo scan acquisitions. For the scans described in Chapter 7 (YAC128), a mouse head receive-only surface coil was used, however, for the remaining experiments, a phased array 4-channel surface coil was acquired and used for all ex vivo MRI scans and for in vivo scans described in Chapter 6. Paravision software (Bruker Biospin) was used for data acquisition (version 5.0 for data in Chapter 7, version 5.1 for data in Chapter 6).

For in vivo scans, animals were anaesthetised with isofluorane (5% for induction, 1.8-2.2% for maintenance) mixed with carrier gas delivered at a flow rate of 1 litre/minute. The carrier gas changed during the course of the PhD based on advice from the Cardiff University vet. For the YAC128 mice described in Chapter 7, the carrier gas was 30% pure oxygen, 70% medical air, however this was less well tolerated by the HdhQ150 mice where longer scan times were used, and the carrier gas was changed to 100% pure oxygen.

The magnetic field homogeneity was optimized with a localized shimming procedure (Fastmap, Bruker Biospin) on a volume of interest (4 x 4 x 4 $mm^3$) placed in the centre of the mouse brain. A PRESS-waterline sequence (Bruker BioSpin) was used with outer volume suppression without water suppression to evaluate water line width (TR/TE = 2500/20 ms respectively) to evaluate the shim performance and the peak line width of the water signal was evaluated and iterations were repeated until all line widths < 40Hz.

Animals were positioned on a heated water bed, secured using tooth and ear bars and inserted into a nose cone (provided by Bruker) for the delivery of anaesthesia. The temperature and respiration rate (Small Animal Instruments Inc, New York, US) were monitored throughout the scan.

For the RARE $T_2$-weighted sequences, the TR and TE values were selected based on the T1 and T2 relaxation times of a normal mouse brain for grey and white matter (Kuo, Herlihy, So, Bhakoo, & Bell, 2005). For diffusion MRI sequences, the TR value was selected in line with previous work detailing $T_1$ relaxation times in the mouse brain at 9.4 T and the knowledge that the TR should be at least 5 times the $T_1$ in order to allow the magnetization to relax to 99% of its initial value and avoid $T_1$-weighting effects. In the mouse brain at 9.4 T, $T_1$ in white matter is ~ 1.7 s (Kuo, Herlihy, So, Bhakoo, & Bell, 2005; van de Ven et al., 2007), thus TR should be > 8.5s. Table 2.1 details the scan parameters for each experiment. Specific details can be found in individual experimental chapters.

***MRI Image Processing*** For volumetric measurements, analysis was conducted using Analyze software (v 10.0, Mayo Clinic, Rochester, MA, USA).

Diffusion weighted images were analysed using Explore DTI version 8.3 (Leemans, et al., 2009). Diffusion images were first corrected for motion artefacts and eddy current induced geometric distortions (Leemans & Jones, 2009). Images were corrected for distortions due to motion using a global affine registration of each image volume to the first non-diffusion weighted volume, normalised mutual information was the cost-function, and the encoding vectors were then re-orientated (Leemans & Jones, 2009) and the signal intensity modulated by the Jacobian determinant of the transformation (Jones & Cercignani, 2010). Skull stripping was performed using a brain extraction tool (Smith, 2002), modified for rodent brains and kindly provided by Dr David Lythgoe. The linear robust estimation of tensors by outlier rejection (RESTORE) algorithm was used to estimate the tensor and remove outliers (L.-C. Chang, Jones, & Pierpaoli, 2005); artefactual data points were identified by robust fitting and excluded on a voxel-by-voxel basis. The images were then corrected to account for contamination due to partial volume (Pasternak, et al., 2009).

### *Ex vivo methods*

All of the solutions used in the experiments can be found in Appendix 1.

***Perfusion*** Mice were terminally anaesthetised via intraperitoneal injection of 0.1 ml Euthatal, and then perfused through the heart with approximately 60 ml of phosphate buffered saline (PBS) followed by approximately 150 ml of 4% paraformaldehyde (PFA) in PBS (pH 7.3) at a flow rate of 30ml/min. After decapitation, the skulls underwent post-fixation in 4% PFA in PBS overnight and were transferred to a 25% sucrose solution.

***Ex vivo MRI tissue preparation*** One week before ex vivo imaging, the skulls were soaked in chemical-grade PBS and washed daily ( see Appendix 1 for solution) to regain some signal due to tissue rehydration (Petiet, Delatour, & Dhenain, 2011) and to remove all free fixative solution (Calamante et al., 2012). To prevent the skulls from drying out and to minimize magnetic susceptibility artefacts during scanning, skulls were immersed in a proton-free susceptibility-matching fluid (Fluorinert) in a 15ml Falcon tube on the day of the scan. Immediately after scanning, skulls were returned to PBS.

***Immunohistochemistry*** For the HdhQ150 mice, skulls were removed following MRI and the brains then transferred to a 25% sucrose solution (in PBS) until they sank. Brains were then bisected at the midline with the left hemisphere being used for immunohistochemistry. Future planned work involves using the right hemisphere for electron microscopy analysis. Coronal sections of 40 um were cut on a freezing sledge microtome and stored at −20°C in tissue cryoprotective solution until staining. All brains were stained at the same time to ensure consistency in the staining intensity. A 1 in 6 series was stained, with sections first placed in a pH = 7.4 Tris buffered saline (TBS) and washed twice. Following this, they were incubated in a solution of 80% water / 10% methanol / 10% $H_2O_2$ (at 30% concentration) for 5 minutes to inhibit peroxide activity and were then washed in TBS (pH 7.4). After washing, a 3% horse serum solution (Invitrogen, Paisley, UK) in TBS + 0.2% Triton X100 (TXTBS; pH 7.4) was applied to the sections for 1 hour to block non-specific binding sites. Immediately after this, sections were transferred into the primary antibody in a solution of 1% horse serum and TXTBS (specific details in Experimental Chapters) and left at room temperature overnight. The sections were then washed several times in TBS and incubated with biotinylated secondary antibody (depending on the primary antibody used) at a 1:200 concentration (Vector Laboratories, Burlingame, CA, USA) with 1% horse serum and TBS for 3 hours at room temperature. The sections were washed several times and a biotin–streptavidin (ABC) kit was then applied for 2 hours according to the manufacturer's instructions (Vector Laboratories). Finally, the sections were washed in TBS and then in 0.05M Tris non-saline (TNS). Following this, sections underwent staining with diaminobenzidine (DAB; Sigma, Poole, Dorset; 0.5 mg/ml in fresh TNS with 3% $H_2O_2$ [30% concentrated] at 1 in 5 dilution) was applied. Sections were then washed in TNS followed by TBS and mounted on gelatinised slides and dehydrated in ascending concentrations. Counterstaining was then completed where relevant (details in experimental Chapter) and sections were all finally dehydrated in a graded alcohol series, cleared in xylene, cover slipped and mounted on gelatine coated slides with DPX mounting medium (RA Lamb, Eastbourne, UK).

## 2.2 Human Methods

### *Ethics*

All work with patients was first approved by the Research Ethics Committee (REC number 12/WA/0184), the NHS Research and Development Forum (Cardiff and Vale University Health Board reference 12/IBD/5488; NISCHR PCU reference 98601) and Cardiff University School of Psychology Ethics committee. Training in Informed Consent was completed and an Honorary Research Passport was obtained in order to enter NHS clinics for recruitment purposes.

### *Recruitment*

Patients were recruited from the South Wales HD service. The clinic has around 150-200 HD patients registered, and >95% of patients are already recruited on a longitudinal observational study of all stages of HD (Registry: A study by the European Huntington's Disease Network; MREC number 10/WSE04/7). Thus there were baseline motor, cognitive, psychiatric, demographic and CAG repeat data available. Recruitment was based on whether patients matched the following criteria:

### Inclusion criteria

- Participants had genetically-confirmed HD. Patients with cognitive impairment (UHDRS cognitive score <200) were the main target group but pre-symptomatic patients were also considered.

### Exclusion criteria

- Participants under 18 and over 65.
- Individuals whose attention and/or cognition was felt to be too low to understand or complete the tasks or to give informed consent, as assessed by the lead physician (Prof A. Rosser) using clinical judgement.
- Individuals with any contraindications to MRI
- Patients with neurological disorders (other than Huntington's Disease) including light-induced seizures
- Pregnant women.
- Participants with a past history of moderate to severe head injury, prior or current alcohol and/or drug abuse,
- Previous stroke or cerebral haemorrhage, or significant vascular disease elsewhere (peripheral vascular disease, carotid or vertebral artery stenosis, or previous coronary intervention), structural heart disease or heart failure.

There were two recruitment pathways for HD patients. Patients who were already on the Registry database and thus had previously given their permission to be contacted by researchers through the HD clinic were contacted directly with an invitation letter and information sheets sent in the post. A second route was for the consultant neurologist (Prof A. Rosser) to identify potential participants attending the clinic who were not currently registered on the Registry database who met the inclusion and exclusion criteria of the study. These patients were informed of the study and given a 'Consent to Contact' form to indicate whether they would like to be contacted. Potential participants were then contacted by telephone to discuss the study and receive further information. If the patient was still interested in participating, information packs were sent in the post and followed up one week later by a telephone call to arrange dates for testing sessions and to answer any questions.

There were two recruitment pathways for control participants. Carers, spouses and /or family members of patients who had expressed interest in participating were contacted. For patients registered on the Registry database, when the initial information packs were sent, a leaflet advertising the study and Consent to Contact form for healthy controls was included. The second pathway was to recruit participants registered on Cardiff University School of Psychology Community Panel and through local advertising. As participants on the database are already consented to be contacted, an information pack containing an invitation letter was mailed to all participants who were either age or gender-matched to recruited patients, followed up by a phone call one week later.

### ***Participants***

19 HD gene-positive participants (11 pre-symptomatic, 8 early symptomatic) and 19 healthy age-matched controls were recruited in total. 6 healthy controls were recruited from route 1 (family members, spouses and/or carers), whereas the remaining 13 healthy control participants were recruited through advertising and participant panels. Throughout this thesis, 'HD participants' will refer to this combined pre-symptomatic and early HD group. Independent t-tests found no difference in age between the HD and control group, $t(34) = 0.106$, $p > 0.05$. The healthy control group was also matched for gender and educational background; demographic information is shown in Table 2.2.

Matching for educational attainment was conducted based on research showing that in comparison to people with low educational attainment, people with higher educational attainment have delayed symptom onset, or equivalent cognitive impairment despite a greater degree of neuropathology (Stern, 2009). Figure 2.3 shows the educational background of participants as scored using the

International Standard Classification of Education (ISCED) scale (Appendix 2). Educational information was not available for 1 patient and 1 control. The Disease Burden index, a measure of disease severity, was used according to the previously described formula (age × [CAG-35.5]), where CAG is the number of CAG repeats (Penney, Vonsattel, MacDonald, Gusella, & Myers, 1997) and is a presumed index of the cumulative toxicity of mutant Huntingtin. This indexed score was used in Chapters 4 and 5 to examine the relationship between a genetic marker of disease severity and neuropathology.

17 out of 19 HD participants had been assessed with the Unified Huntington’s Disease Rating Scale ’99 (UHDRS) in the one-year period prior to participating in this study by a research nurse at the Cardiff Huntington’s Disease Centre as part of the Registry study. The UHDRS was developed to assess the clinical features of HD and includes motor, cognitive, behavioural, and functional subscales ("Unified Huntington's Disease Rating Scale: reliability and consistency. Huntington Study Group," 1996) with each section consisting of multi-step subscales, and has been shown to have high inter-rater reliability and internal consistency. As shown in Figure 2.2, the motor assessment examines 15 motor behaviours with a maximum score of 60 indicating maximum motor disability. The functional assessment contains 25 questions relating to daily functioning with a maximum score of 20 indicating functional capacity. The independence scale is measured in percentage, with 100% representing no special care needed, and 10% representing tube fed / total bed care. The Total Functional Capacity scale (Shoulson & Fahn, 1979) is the main assessment tool of functional status in HD clinical care and research, designed to assess progression of HD in symptomatic patients with emphasis on self-care, mobility, and independence. A maximum score of 13 indicates full capacity in all domains assessed. However, this scale may be less sensitive to functional changes in patients far from symptom onset. The cognitive assessment score is a summation of performance on the verbal fluency test (letters and categories), symbol digit modality test, and Stroop interference test, with a score > 200 indicating cognition

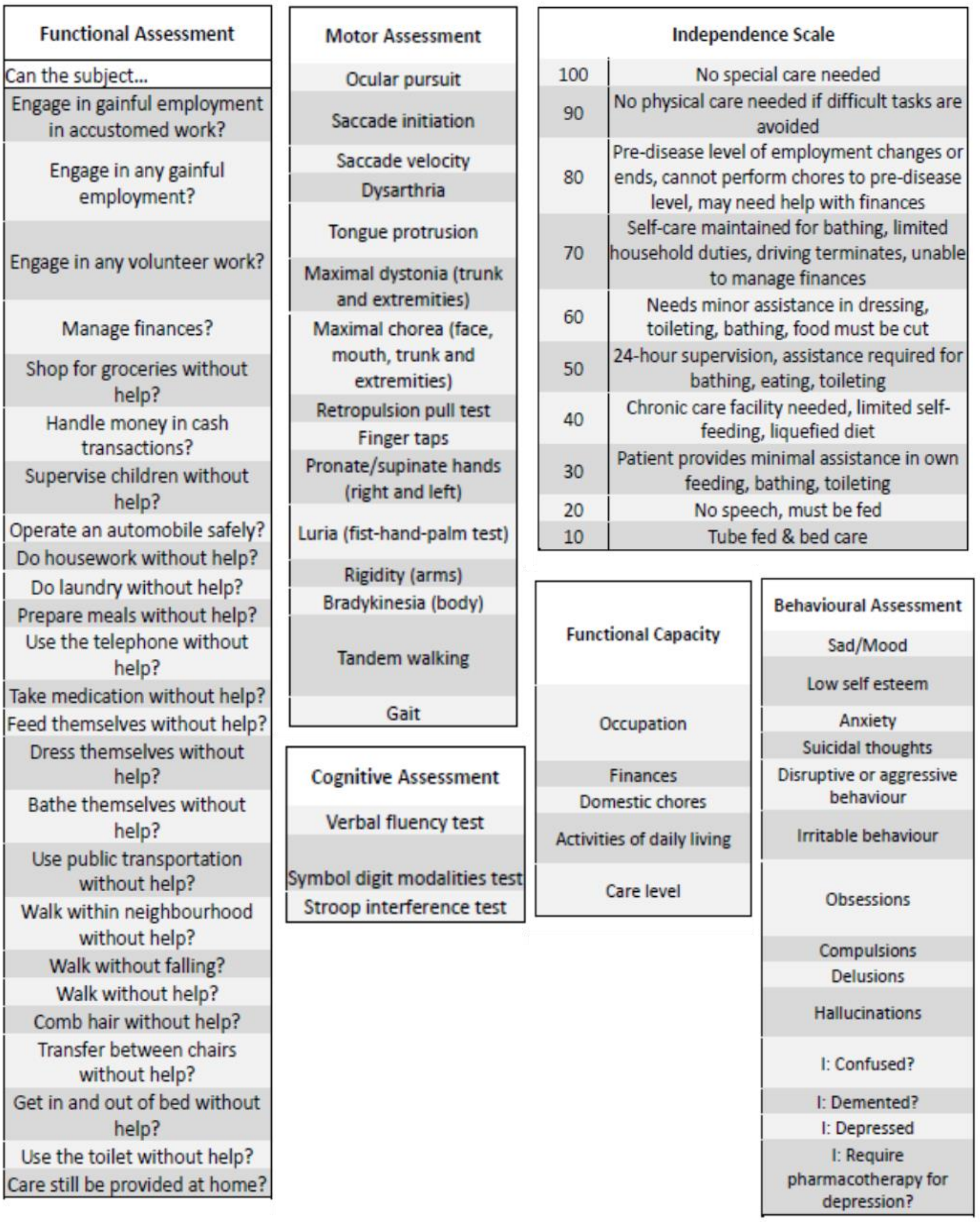

| Functional Assessment |
|---|
| Can the subject... |
| Engage in gainful employment in accustomed work? |
| Engage in any gainful employment? |
| Engage in any volunteer work? |
| Manage finances? |
| Shop for groceries without help? |
| Handle money in cash transactions? |
| Supervise children without help? |
| Operate an automobile safely? |
| Do housework without help? |
| Do laundry without help? |
| Prepare meals without help? |
| Use the telephone without help? |
| Take medication without help? |
| Feed themselves without help? |
| Dress themselves without help? |
| Bathe themselves without help? |
| Use public transportation without help? |
| Walk within neighbourhood without help? |
| Walk without falling? |
| Walk without help? |
| Comb hair without help? |
| Transfer between chairs without help? |
| Get in and out of bed without help? |
| Use the toilet without help? |
| Care still be provided at home? |

| Motor Assessment |
|---|
| Ocular pursuit |
| Saccade initiation |
| Saccade velocity |
| Dysarthria |
| Tongue protrusion |
| Maximal dystonia (trunk and extremities) |
| Maximal chorea (face, mouth, trunk and extremities) |
| Retropulsion pull test |
| Finger taps |
| Pronate/supinate hands (right and left) |
| Luria (fist-hand-palm test) |
| Rigidity (arms) |
| Bradykinesia (body) |
| Tandem walking |
| Gait |

| Cognitive Assessment |
|---|
| Verbal fluency test |
| Symbol digit modalities test |
| Stroop interference test |

| Independence Scale | |
|---|---|
| 100 | No special care needed |
| 90 | No physical care needed if difficult tasks are avoided |
| 80 | Pre-disease level of employment changes or ends, cannot perform chores to pre-disease level, may need help with finances |
| 70 | Self-care maintained for bathing, limited household duties, driving terminates, unable to manage finances |
| 60 | Needs minor assistance in dressing, toileting, bathing, food must be cut |
| 50 | 24-hour supervision, assistance required for bathing, eating, toileting |
| 40 | Chronic care facility needed, limited self-feeding, liquefied diet |
| 30 | Patient provides minimal assistance in own feeding, bathing, toileting |
| 20 | No speech, must be fed |
| 10 | Tube fed & bed care |

| Functional Capacity |
|---|
| Occupation |
| Finances |
| Domestic chores |
| Activities of daily living |
| Care level |

| Behavioural Assessment |
|---|
| Sad/Mood |
| Low self esteem |
| Anxiety |
| Suicidal thoughts |
| Disruptive or aggressive behaviour |
| Irritable behaviour |
| Obsessions |
| Compulsions |
| Delusions |
| Hallucinations |
| I: Confused? |
| I: Demented? |
| I: Depressed |
| I: Require pharmacotherapy for depression? |

Figure 2.2 **The Unified Huntington's Disease Rating Scale (UHDRS)** (" Huntington Study Group," 1996) . Motor assessment graded 0 = normal, 4, = unable to complete task. The cognitive assessment is based on raw test scores. On the behavioural assessment, each point is graded for severity (0 – Absent, 4 – Severe), with the prefix 'I' indicating that the rating is based on the investigator's observations of the individuals behaviour. Functional capacity is graded from 0 (requiring total care) to 3 (normal) for occupation, finances and daily activities, and 0-2 for domestic chores (2 = normal) and care level (0= full time skilled nursing, 2= home) and requires yes/no responses.

in the normal range. The Problem Behaviour Score examines psychiatric and emotional symptoms including the prevalence and severity of a depressed mood, suicidal ideation, anxiety, irritability, anger and aggression, apathy, perseverative thoughts and behaviour, obsessive-compulsive behaviour, delusions and hallucinations, and disorientation, with a maximum score of 132 indicating severe and daily experiences of all of these behaviours. The availability of these assessment results is useful in terms of characterising the HD group in terms of heterogeneity of symptoms and their severity, and for comparison with other study cohorts. Although the majority of neuroimaging studies in HD stratify participants according to the presence of motor symptoms (e.g. pre-symptomatic group vs early symptomatic group), in this study both pre-symptomatic and early symptomatic HD participants were recruited. This is because there is robust evidence demonstrating that cognitive decline and psychiatric symptoms, together with subtle motor signs, become detectable well before the formal diagnosis of HD (Papoutsi, Labuschagne, Tabrizi, & Stout, 2014), and thus the diagnosis of 'symptomatic HD' is constrained by the sensitivity of measurements scales. The increase in statistical power associated with recruiting both pre-symptomatic and early symptomatic HD participants and including them in the same analysis may allow for more subtle yet informative changes to be detected.

### *Consent*

After completing NHS Informed Consent training, the author took informed consent for all participants. Consent was taken upon arrival at the imaging centre, where the information sheets were discussed and an opportunity to ask any further questions was provided, before participants were asked to read and sign the consent forms. Only individuals who were considered by the consultant neurologist (Prof A. Rosser) to be cognitively able to understand the consent forms were included in this study. Participants were informed of their right to withdraw from the study at any point without giving a reason and were informed that they could request that their data be destroyed and not included in the study.

Table 2.2 Demographic information for participants. Standard deviation in parentheses. CAG: repeat length of CAG mutation, m : male, f: female

| | HD | Healthy controls |
|---|---|---|
| Age | 44.7 (10.6) | 45.9 (11.8) |
| Gender | 10 m / 9 f | 8 m / 11 f |
| CAG | 43.4(3.27) | |
| Disease Burden | 338.1 (110.3) | |
| UHDRS Motor | 23.3 (23.1) | |
| UHDRS Cognitive | 224.3 (96.5) | |
| Total Functional Capacity | 10.3 (3.3) | |
| UHDRS Functional | 21.8 (4.15) | |
| UHDRS Independence Scale | 87.9 (13) | |
| Problem Behaviour Score | 11.8 (11.8) | |

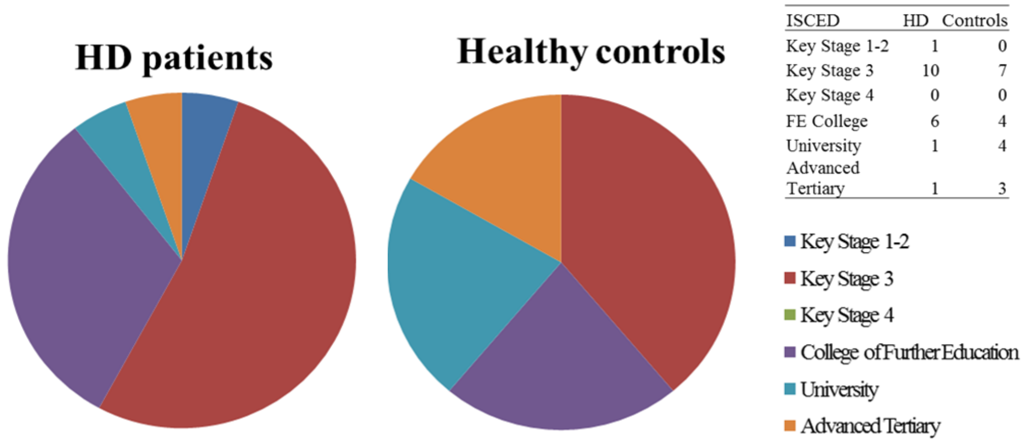

| ISCED | HD | Controls |
|---|---|---|
| Key Stage 1-2 | 1 | 0 |
| Key Stage 3 | 10 | 7 |
| Key Stage 4 | 0 | 0 |
| FE College | 6 | 4 |
| University | 1 | 4 |
| Advanced Tertiary | 1 | 3 |

Figure 2.3 Educational attainment for HD and healthy control participants. The International Standard Classification of Education (ISCED) ordinal scale was used to facilitate education matching. Key stage 1,2 : primary school, key stage 3: comprehensive/secondary school, key stage 4: sixth form college.

## *Cognitive Testing*

The cognitive testing session was conducted prior to MRI scanning and lasted approximately 45 minutes after which the participant was offered a break. The battery was adapted from a battery of publicly available cognitive assessment tools that were designed and validated at the Medical Research Council Cognition and Brain Sciences Unit (Owen et al., 2010) and made freely available at http://www.cambridgebrainsciences.com. Testing was conducted in a cognitive testing room at Cardiff University Brain Research Imaging Centre (CUBRIC). The tests were conducted on a laptop (Acer Aspire 5742Z) with a 15.6 inch HD LED LCD screen, with responses made using a mouse unless instructed otherwise. A finger tapping task was also included as motor speed may confound performance on the cognitive tasks. The researcher was sat beside the participant for the duration of the test battery and was thus available to answer questions regarding the task instructions

The 10 tests were chosen to cover a wide spectrum of cognitive functioning across a number of cognitive domains. Where tasks were timed, a timer was shown in the top right of the screen. Where tasks were performance based, a maximum of 3 errors were allowed before the task terminated, the number of ‘lives’ remaining was shown on the right of the screen. Task difficulty was dynamically varied in a ‘ratchet-style’ approach in which each completely successful trial was followed by a new trial involving increased difficulty, and each unsuccessful trial was followed by a new trial of reduced difficulty in order to maintain motivation.

***Stroop Task.*** The Stroop task (Stroop, 1935) is an attentional task based on the phenomenon of increased difficulty in naming the colour a word is printed in when the semantic text of that word is an incongruent colour. For example, people are slower to name the ink colour when the word that is written in red ink is the word 'green'. This difficulty in colour naming vanishes when the semantic meaning of the word is the same (congruent) as the text colour (e.g. the word ' red ' written in red ink) or is semantically unrelated (e.g. the word ' window ' written in red ink) (Scheibe, Shaver, & Carrier, 1967). This effect is thought to be the result of interference caused by automatic word recognition. The task used in this study was a 'double Stroop' task, with participants being required to both respond to the colour word but also distinguish between one of two possibilities, adding an extra cognitive step. A single word (either 'red' or 'blue') was printed on a black background and displayed at the top of the screen. The colour word was printed either in a congruous colour (i.e. the word red printed in red ink) or in an incongruous colour (i.e. the word red printed in blue ink). At the bottom of the screen, two colour words were displayed (red, blue) and participants were required to indicate which of two coloured words at the bottom of the screen describes the colour of the ink that the word at the top of the screen is presented in, ignoring the word itself.

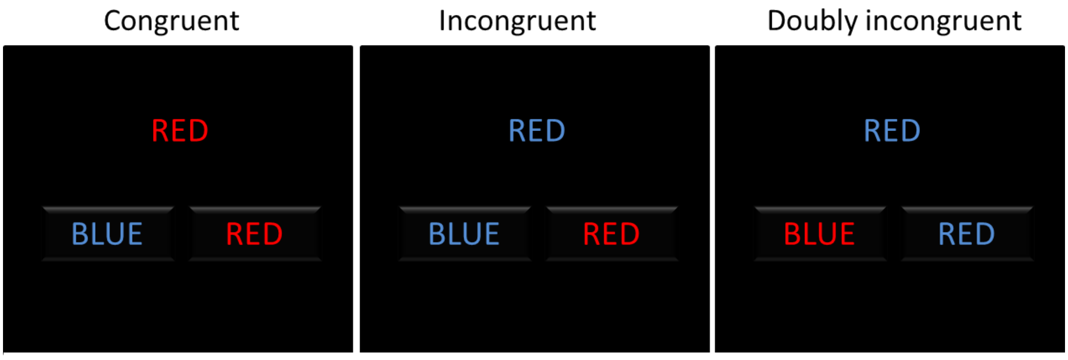

Figure 2.4 The three different trial types on the colour-word Stroop task. Participants are required to select the word at the bottom of the screen that describes the colour of the ink in the top word.

As shown in Figure 2.4, the colour word mappings may be congruent, incongruent, or doubly incongruent, depending on whether or not the colours that a given words describes matches the colour that it is drawn in. The colour-word mappings were congruent on approximately 25% of the trials, incongruent on approximately 50% of trials, and doubly incongruent on 25% of trials. The correct colour mapping was presented in the bottom-left and the bottom-right of the screen an equal number of times. The participant solved as many problems as possible within 90 seconds. The total score increased by 1 after a correct response and decreased by 1 after an incorrect response on a trial-by-trial basis. The total score was the outcome measure.

***Grammatical Reasoning.*** This task was based on Baddeley's grammatical reasoning test (Baddeley, 1968). As shown in Figure 2.5a, participants were presented with a pair of shapes displayed in the centre of the screen (e.g. a circle and a square) with a grammatical statement written above it, for example, "the circle is not smaller than the square". Participants had to indicate (True vs. False) whether the sentence accurately described the relationship between the shapes, and had 90 seconds to complete as many trials as possible. Participants were instructed to work as quickly and accurately as possible. The outcome measure was the total number of trials answered correctly in the 90-seconds, minus the number answered incorrectly. Task difficulty was dynamically varied (increase/decrease of complexity).

***Paired Associate Learning.*** This task required participants to remember the spatial location of a series of objects. Boxes are displayed at random locations on an invisible 5 x 5 grid and the boxes open one after another to reveal an enclosed object. The same objects are then displayed in random order in the centre of the grid and the participant must click on the boxes (in the correct location) that contained them. Task difficulty was varied dynamically ( ± 1 window). Participants were allowed to make three errors in total before the test was terminated. The main outcome measure was the average number of correct object-place associations ('paired associates') in the trials that were successfully completed. The test starts with two boxes (object-location pairs). The maximum level that could be achieved was 24. This task has been shown to be highly sensitive to various neuropathological conditions, and is commonly used to assess memory impairments in aging clinical populations (Gould et al., 2005).

a. Grammatical reasoning b. Paired Associates

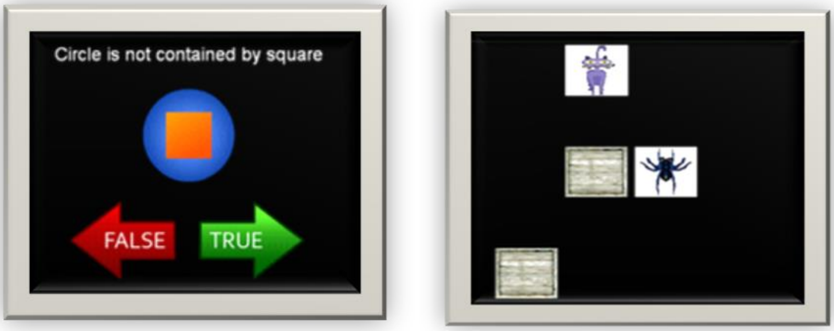

c. Feature Match d. Spatial Rotations

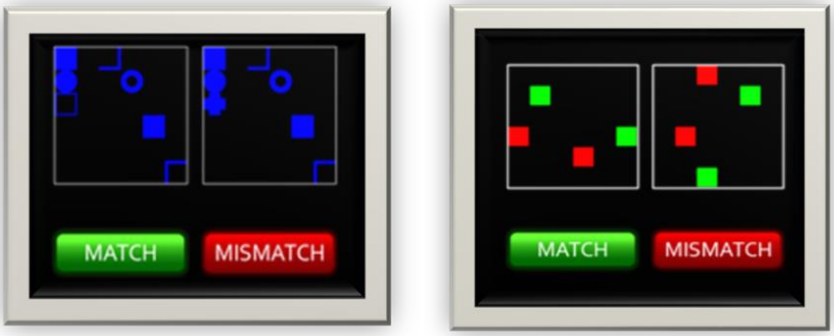

Figure 2.5 Example trials from four different cognitive tasks.

***Intradimensional/Extradimensional Shift (ID/ED) task*.** This test was developed from a similar task from the CANTAB test series and is designed to tap prefrontal executive function, namely set-shifting or cognitive flexibility. It is functionally similar to the category shifting required in the Wisconsin Card Sorting test, with the extra-dimensional stage equivalent to the change in category in the Wisconsin Card Sorting Task. However this task is conceptually simpler with only 2 distinct categories. Participants were presented with compound stimuli, which were composed of stimuli from 2 different object dimensions: block coloured shapes and coloured lines. This task required participants to learn, via trial and error, which stimulus, of the 2 presented on the screen, was designated as the target image. The 2 stimuli were presented in either the top, bottom, left or right of the screen and participants had to use the computer mouse to select the image. Participants were presented with feedback after every trial (response) in the form of an auditory tone. Participants were initially required to respond to the compound stimuli containing a target stimulus from the block shape dimension and ignore the line dimension. After a number of trials, the rule changes and participants need to respond to the second block shape (same dimension), and again ignore the line dimension, known as an ‘intra-dimensional (ID) reversal/switch’. A second type of ID rule change is an ‘intra-dimensional (ID) shift’ where the set of compound stimuli changes but the block shape remains the relevant dimension to respond to. Later, an extra-dimensional (ED) shift is introduced where the compound stimuli changes, but now participants need to respond to the line figures, with the previously trained block shapes now irrelevant. Whereas the ED shift specifically requires conceptual flexibility (i.e., shifting from one concept or cognitive set to another, such as from shape to line); the ID shift requires perceptual flexibility, or a shift from one exemplar to another within the same cognitive set (e.g., shape).

Participants had to make 6 consecutively correct responses to the target image. After reaching criterion, participants move onto the next stage of the test. If participants did not reach criterion within 30 trials, participants moved to the next stage of the test. If the new target stimulus was drawn from the same category as the previous one, this was termed ID. If it was drawn from the other category, it was termed ED. For each ID/ ED shift and reversal stage, trials to criterion was the outcome measure with 6 being the minimum and 30 being the maximum.

***Feature Match.*** This task is designed to examine attentional processing and is based on the classic feature search task (Treisman & Gelade, 1980). Two grids are displayed on one screen, each containing a set of abstract shapes. In half of the trials the grids differ by shape. Participants must assess whether or not the abstract shapes are identical (*see* Figure 2.5*c*). Task difficulty was dynamically varied (±1 shapes in the grid and total score changed by ± number of shapes in grid), with the first grids containing two abstract shapes each. The total score after 90 seconds was the outcome measure.

**Spatial Rotations** This task is based on the mental rotation tasks first introduced by Shepard and Metzler (1971) and was used to measure the participant's ability to mentally manipulate the spatial layout of objects. In this computerised version, two grids of coloured squares were displayed on either side of the screen with one of the grids rotated by a multiple of 90 degrees (*see* Figure 2.5*d*). When rotated, the grids were either identical or differed by the position of just one square. The task was to indicate: *"If you could rotate one of the panels would it be identical to the other or would it be different?"*

Participants were instructed that in order to gain maximum points, they must solve as many problems as possible within 90 seconds. After a correct response, the total score increased by the number of squares in the grid on that trial and the subsequent trial contained more squares. After incorrect responses, the total score decreased by the number of squares in the grid and the subsequent trial contained fewer squares, with the total score after 90 seconds being the outcome measure. For the first trial, the grids contained 4 coloured squares each. Mental rotational abilities are linked to perspective taking and navigation, and significantly correlated with route learning ability (Silverman et al., 2000).

**Digit Span** A computerised version of the verbal working memory component of the WAIS-R intelligence test (Wechsler, 1981) was used. Participants were presented with a sequence of digits that appear on the screen one after another. Subsequently, they were required to recall the sequence of numbers by entering them on the keyboard. Difficulty was varied dynamically (±1 digit) with the test terminating after 3 errors; the maximum achievable level was 25 and maximum level achieved was the outcome measure.

**Go/No-Go Task** In this task examining response inhibition, participants were presented with one of two cues : a frequent cue, which required a rapid button press response within 1s of the cue appearing on the screen, and an infrequent cue, which required participants to not respond, and inhibit the button press. Both cues were neutral stimuli and were presented in the centre of the screen against a black background. Following both types of cues, feedback was provided in terms of an auditory tone regarding the accuracy and/or speed of the response. There were 150 trials in total, 90% contained the frequent cue in order to create a prepotent tendency to respond and to increase the inhibitory effort required to successfully withhold responding on ‘stop’ trials where the infrequent cue was displayed. Reaction time was recorded for successful responses and failed inhibitions. The outcome measures were the total number of ‘failed stops’ to the infrequent cue and the number or ‘correct go’ button presses to the frequent cues, as well as the corresponding reaction times. The frequent cue was an image of a magnifying glass, and the infrequent cue was a cartoon image of a cat.

Table 2.3 Reward contingencies and win/loss frequency associated with each deck of cards in the Gambling Task.

| | Trial ratio | | Monetary value | | |
|---|---|---|---|---|---|
| Deck | Win (%) | Loss (%) | Average win ($) | Average loss ($) | Overall deck value ($) |
| A | 70 | 30 | 100 | 300 | -2000 |
| B | 50 | 50 | 100 | 100 | 0 |
| C | 80 | 20 | 100 | 50 | 7000 |
| D | 80 | 20 | 70 | 200 | 1600 |

***Gambling Task*** This was a version of the Iowa Gambling task (Bechara, Damasio, Damasio, & Anderson, 1994) and was designed to assess decision making and risk-taking behaviour in a more naturalistic manner and dissociated from learning ability. Because there was no ‘wait’ period between responses, this task may also be sensitive to impulsivity. Participants were presented with 4 decks of cards, and were instructed to selects cards one at a time from 1 of the desks. Participants were instructed that each card selected would result in either winning money or losing money. The goal of the task was to accumulate as much money as possible. After selecting a card, participants were informed how much money they had won or lost, with this information presented above the deck of cards. As shown in Table 2.3, different decks contained a higher probability of wins versus losses; two of the decks are advantageous, i.e., over the long run, the participant can expect to win money because these decks include cards that offer small rewards with cards that offer modest losses. There were 100 cards in total. The outcome measure was the total money won after 100 trials.

***Spatial Planning*** This task was a measure of higher-level planning ability, requiring participants to plan ahead in order to work out the correct sequence of responses to complete a series of puzzles (Owen et al., 1992). Participants were presented with numbered tiles on the screen, arranged in numerical order on a grid. The tiles were then shuffled so that some were no longer in the correct positions. The task was to rearrange the tiles into the correct order in as few moves as possible by sliding them in and out of the blank spaces. Participants were instructed to solve as many problems as possible in 3 minutes in order to gain maximum points. The outcome measure was the number of problems solved in the time limit.

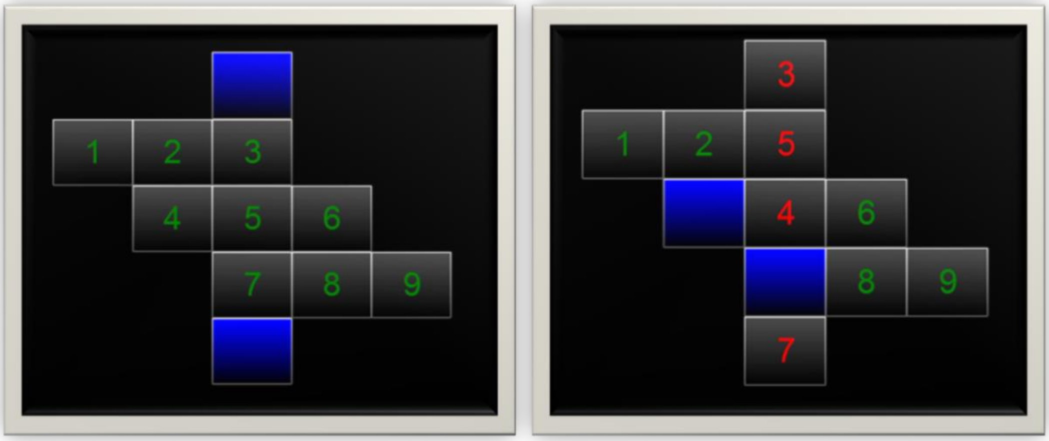

Figure 2.6 Spatial Planning Task. The left panel shows the pattern to be achieved, the right panel shows the re-arranged tiles which need to be ordered using the empty blue boxes.

***Finger Tapping Task*** The Speeded Tapping Test (Reitan, 1979) was used as a measure of motor speed. The test was performed on the computer and participants were required to press a button on the keyboard as quickly as possible. The outcome measure was the average tapping rate over 3 trials. For consistency, participants were instructed to form a fist shape with their dominant hand, with their finger nails touching down in front of the keyboard space bar. They were then instructed to extend their index finger in order to contact the 'space' bar on the keyboard, and to move only their index finger to tap the space bar as quickly as possible. After 20 taps, the average number of taps per minute was calculated.

## *MRI Acquisition*

Participants were screened for MR contraindications on the telephone prior to attending the Imaging Centre and again on the day of scanning. Prior to the scan session, all participants were shown a near-identical "mock" MRI scanner (General Electric), which is a model of a 3 T GE HDx MRI system but with no magnetic field. This can help to acclimatize volunteers to the MRI environment.

MR data were acquired using a 3 T GE HDx MRI system (General Electric). 7 different sequences were used to obtain measures of macrostructure and microstructure, with a total acquisition time of between 75-90 minutes depending on the heart rate of the participant. A localiser sequence was first acquired in order to know the position of the brain in order to prescribe the slice locations. Parallel imaging was used for the diffusion-weighted imaging, thus an array spatial sensitivity encoding (ASSET) scan was acquired to assess the sensitivity of the 8 coils, so that fewer phase encoding directions could be sampled during EPI readout. Although the cost of parallel imaging is a reduction in signal to noise ratio (SNR), the ability to use a shorter TE and sample earlier with fewer distortions is advantageous for EPI based sequences.

***$T_1$-weighted anatomical scan.*** A 3-dimensional $T_1$-weighted FSPGR scan was used to characterise tissue macrostructure, with an acquisition matrix of 256 x 256, and slice thickness of 1 mm giving a resolution of 1mm x 1mm x $1mm^3$, TR/TE of 7.904/2.996 ms.

***Diffusion MRI sequence***. Two separate diffusion-weighted MRI acquisitions were collected: a sequence optimised for diffusion tensor imaging (DTI) and a HARDI-based sequence more suited for recovering fibre orientations through spherical deconvolution approaches. Both sequences were peripherally gated to the cardiac cycle and parallel imaging [ASSET factor = 2] was used for both. For both diffusion-weighted sequences, a twice-refocused spin-echo echo-planar imaging (EPI) sequence was used which provided whole oblique axial brain coverage; gradient onset times and diffusion times (δ) are shown in Table 2.4. For both sequences, data were acquired from 60 axial slices with a resolution of 1.8 x 1.8 x 2.4 mm and an acquisition matrix of 96 x 96. For the sequence optimised for DTI, the b-value was 1000 s/$mm^2$, the TE was 84.6 ms and data was acquired with diffusion encoded along 30 isotropic gradient directions with 3 non diffusion-weighted images acquired. Cardiac-gating was used, resulting in a variable TR for individual participants.

Table 2.4 Diffusion parameters for the twice-refocused spin echo (TRSE) sequences used, with onset time for diffusion gradients of length δ (ms).

| | TRSE b = 1000 s /$mm^2$ | | TRSE b = 2000 s /$mm^2$ | |
|---|---|---|---|---|
| Diffusion gradients **G** | onset time (ms) | δ (ms) | onset time (ms) | δ (ms) |
| G1 | 16.47 | 8.13 | 16.06 | 11.41 |
| G2 | 29.8 | 18.55 | 32.67 | 21.83 |
| G3 | 48.35 | 18.95 | 21.83 | 22.2 |
| G4 | 73.2 | 8.13 | 82.63 | 11.4 |

Table 2.5 CHARMED Gradient Orientations Scheme

| b-value (s/mm$^2$) | Number of gradient orientations |
|---|---|
| 1093 | 6 |
| 2188 | 3 |
| 3281 | 4 |
| 4375 | 5 |
| 5469 | 6 |
| 6563 | 6 |
| 7656 | 7 |
| 8750 | 8 |

For the HARDI-based sequence, the b-value was 2000 s/mm$^2$, TE was 97.3 ms and data was acquired with diffusion encoded along 45 optimally-ordered and arranged isotropic gradient directions with 3 non diffusion-weighted images acquired. Again, cardiac gating was used, resulting in a variable TR for individual participants. A higher b value was employed because higher b values have been shown to give better angular resolution (A. L. Alexander, Hasan, Lazar, Tsuruda, & Parker, 2001). It was decided to use different parameters in order to maintain a reasonable scan time that would be tolerated by all participants, including HD patients. Because there was the risk that not all scans would be run to completion, with the potential for issues with HD-related excessive motion, prior to acquisition, the gradient directions used were optimally re-ordered so that if the scan was stopped before completion, the measurements already taken would be uniformly distributed in the sampling space, compared to if randomly ordered diffusion direction were used. This was conducted using the approach proposed by Cook et al. (2007)  and using the Camino software package (P. A. Cook et al., 2006).

***Multi-shell diffusion MRI***. For the CHARMED protocol, spin-echo diffusion weighted EPI sequences (TE/TR = 128.2 /17,000 ms) were performed with up to 38 axial slices (to cover the majority of the brain with the exception of the temporal lobes), and a resolution of 1.8 x 1.8 x 2.4 mm$^3$. Diffusion time ($\Delta$) and the diffusion gradient length time ( $\delta$ ) were 55.71 and 50.9 ms respectively. The gradient orientation scheme is shown in Table 2.5, and has been shown to be an optimal compromise between scanning duration and the quality of the estimated parameters for restricted volume fraction (De Santis, 2013). 40 gradient orientations are used, with 5 additional gradient orientations in the inner shell in order to calculate conventional DTI maps that are used as a reference in the registration to correct for eddy current distortions and motion (Ben-Amitay, Jones, & Assaf, 2011).

***Relaxometry*** The Multi-Component Driven Equilibrium Single Pulse Observation of T1/T2 (mcDESPOT) (S. Deoni, B. Rutt, T. Arun, C. Pierpaoli, & D. Jones, 2008a) protocol consisted of a combination of sagittally oriented spoiled gradient echo (SPGR), balanced steady state free precession (bSSFP) and inversion-recovery prepared SPGR (IR-SPGR) sequences (Deoni et al. 2008; Deoni et al. 2008). All three sequences were acquired with a field of view (FOV) of 220 mm; 1.7 x 1.7 x 1.7 mm$^3$, and frequency encoding in the superior-inferior direction for a total scan time of approximately 8 minutes. The SPGR parameters were TE/TR = 2.1/4.7 ms, bandwidth= ±25 kHz; and flip angle (α) = [3◦, 4◦, 5◦, 6◦, 7◦, 9◦, 13◦, 18◦]. The bSSFP parameters were TE/TR = 1.8/3.5 ms, bandwidth= ±62.5 kHz; α = [10.6◦, 14.1◦, 18.5◦, 23.8◦, 29.1◦, 35.3◦, 45◦, 60◦] for both phase-cycling acquisitions of 0◦ and 180◦. Finally, the IR-SPGR parameters were TE/TR = 2.1/4.7 ms; bandwidth = ±25 kHz; α = 5◦; inversion time = 450 ms. One patient was not scanned with the mcDESPOT sequence due to their weight exceeding the specific absorption rate (SAR) limit for this sequence. Another patient did not undergo this sequence due to permanent eye makeup and risk of heating.

## *MRI Image Processing*

***Diffusion MRI*** In Chapter 4, deterministic tractography was conducted to examine the corpus callosum, corticospinal tract and cingulum bundle. As with the mouse diffusion MRI processing, pre-processing involved estimating the tensor using the linear RESTORE algorithm (Chang, et al., 2005) and correcting images for motion and eddy currents (Leemans & Jones, 2009), EPI distortions and contamination due to partial volume (Pasternak, et al., 2009). During the EPI distortion correction, both the b=1000 s/mm$^2$ and the b= 2000 s/mm$^2$ images were registered to the $T_1$-weighted image. Given that the majority of white matter voxels contain multiple fiber orientations (B. Jeurissen, Leemans, Tournier, Jones, & Sijbers, 2012) spherical deconvolution based tracking algorithms were employed on the b= 2000 s/mm$^2$ images in order to achieve a more reliable reconstruction (Alexander, 2005; Tuch, et al., 2002). For each voxel, the fiber orientations were extracted using two different, readily available spherical deconvolution approaches: constrained spherical deconvolution (CSD) (Tournier, et al., 2007) and damped Richardson-Lucy (Dell'Acqua et al., 2007; Dell'acqua, et al., 2010) along with the traditional tensor algorithm for comparison (Basser, et al., 2000). To estimate fiber orientations using CSD (Tournier, et al., 2007), the acquired diffusion signal was modelled as a convolution of the fibre orientation density function with the ‘response function’ from a single fibre population, which corresponds to the diffusion MRI signal expected from an ideal fiber population aligned along the z-axis (FA > 0.7), fitted with maximum harmonic degree L = 8 (Tournier, et al., 2007; Tournier, et al., 2004). To estimate fiber orientations, DRL instead assumes a diffusion tensor model when obtaining the diffusion profile, and uses adaptive regularization, which includes an isotropic term to model partial volume. Specific tractography details are detailed in the Experimental Chapters. For the tract reconstructions, DTI indices were calculated from the b= 1000 s /mm$^2$ data.

***CHARMED*** Processing of the multi-shell data was conducted using Matlab code written by Silvia De Santis (Cardiff University) and modified by Cyril Charron (Cardiff University) using the following processing stages:

1. To correct for intra-scan motion and eddy currents, the non-diffusion weighted images ($b = 0\ s/mm^2$) from the CHARMED dataset were linearly registered using an affine (12 degrees of freedom) technique based on mutual information to the first image in the diffusion MRI sequence (Jenkinson and Smith 2001) and the transformation matrix applied to all volumes.

2. The gradient vectors were reoriented using the transformation matrix (A. Leemans & D. Jones, 2009).

3. Although the most widely used approach to correct for motion and distortion in diffusion weighted (DW) images is to apply an affine registration of the DW images to the non-DW images (Haselgrove & Moore, 1996) as in step 1, this approach only works at low b-values (up to $1000s/mm^2$) where most features found in the DW images are also found in the non-DW image, albeit with different contrasts. At much higher b-values, only those parts of white matter presenting restricted diffusion perpendicular to the applied diffusion weighting will be visible. The approach used here is to first estimate the diffusion tensor from the low b-value images ($<1000s/mm^2$, and affine-registered using normalized mutual information). The CHARMED model is then applied in a forward sense, assuming colinearity of the restricted and hindered components. This produces, for each unique diffusion-weighting, a unique 'template' image as the target for registration. As shown by Ben-Amitay et al. (2011) this results in more accurate correction for motion and distortion of high b-value images.

4. Using this template image, the high b-value ($>1000\ s/mm^2$) images were then co-registered to the DTI data.

5. The individual estimates of shift, shear and scale obtained for each pair-wise co-registration of a DW image to the non-DW images were then fed into a linear model, assuming linear dependence of eddy-current effects on gradient amplitude and slowly varying trends for motion. This results in a more robust estimate of the correction parameters.

6. The data was corrected for free water contamination approach, where two compartments (tissue / CSF) are fitted to the diffusion signal (Pasternak, et al., 2009).
7. Pre-processed data were fit to the parameters of the CHARMED model (Assaf & Basser, 2005) using a nonlinear least-square estimation procedure according to Assaf et al (2004).

The outputs of the fitting routine were the intra-axonal diffusivity, the fibre orientation and the restricted fraction.

***McDESPOT*** FSL software was used to analyse the relaxometry data alongside c-code written by Sean Deoni (Brown University). The following processing steps were conducted:

1. To correct for inter-scan and intra-scan motion, SPGR and bSSFP images for each participant were linearly registered using an affine (12 degrees of freedom) technique based on mutual information to the first image in the sequence (Jenkinson and Smith 2001).
2. All images were masked using the brain extraction tool provided in FSL.
3. To obtain B1 field and T1 maps, SPGR and IR-SPGR images were used for DESPOT1 with High-speed Incorporation (DESPOT1-HIFI) of RF Field Inhomogeneity processing as described in (Deoni et al. 2006; Deoni 2007), and using in-house c-code.
4. The B1 field and T1 maps were then used in the calculation of the B0 field and T2 maps using the bSSFP data and the DESPOT2 with full modeling (DESPOT2- FM) algorithm (Deoni et al. 2004).
5. The high-resolution DESPOT1-HIFI and DESPOT2-FM 3D sequences were combined in order to fit the multi-component DESPOT model (Deoni et al. 2008; Deoni et al. 2008).

This model provided whole brain estimates for myelin water fraction (MWF), myelin water residence time and intra- and extra-cellular (IE) water and myelin water $T_1$ and $T_2$.

## Statistical analysis

For all statistical analyses, outlier profiles and QQ plots were first examined and values over 3 standard deviations from the mean were deemed to be extreme outlier values and were excluded case-wise.

Where an ANOVA or ANCOVA analysis was used, the assumptions of the analysis were first tested (see Appendix 3 for results of the tests). To test whether the data were normally distributed, the Shapiro-Wilk test was used at $\alpha = 0.001$. Homogeneity of regression slopes was tested for all covariates. Levene's test was used to assess homogeneity of error variance. When this test was violated, and when the group standard deviations were proportional to the group means, a log transformation (log base 10) was used. If this was not possible, then non-parametric tests were used, as detailed in individual experimental chapters. When a repeated measures ANOVA was planned, Mauchly's sphericity test (Mauchly, 1940) was carried out as a validation to ensure the variances of the differences between the levels of the independent variable were equal and that the F-ratio was not inflated. Where the assumption of sphericity was violated, the Greenhouse-Geisser correction (Greenhouse & Geisser, 1959) was used which alters the degrees of freedom and produces an F-ratio where the Type I error rate is reduced.

# 3 Cognitive Characterisation of Huntington's disease

## Chapter Summary

The purpose of the work in this chapter was to develop a method of measuring cognition for use in the imaging studies in later chapters through two objectives. The first was to objectively measure cognitive function in a cohort of pre-symptomatic and early-stage HD participants across a range of domains using a novel battery of cognitive tests. The Cambridge Brain Sciences battery has not previously been reported in published work in Huntington's Disease (HD), yet offers a number of advantages in comparison to more commonly used cognitive test batteries in HD, with quick and consistent test delivery across participants, and the availability of population mean data from a study of over 44,000 individuals for comparison (Hampshire, Highfield, Parkin, & Owen, 2012). The second objective was to develop a composite cognitive score using principal components analysis that could adequately describe the variance in the data across a number of tests, and that could be used in future chapters to examine the relationship with brain structure.

## Introduction

Cognitive problems are a key feature in Huntington's disease and typically manifest earlier than motor symptoms. Impaired awareness is a feature of HD which yields self-report cognitive tests inappropriate, thus more objective neuropsychological test batteries are required to characterise the profile of changes.   It is important to be able to reliably and sensitively characterise cognitive function in HD: cognitive and behavioural changes are the most highly associated with functional decline, can be predictive of institutionalisation, and place the greatest burden on families (Hamilton, et al., 2003; Nehl, Paulsen, & Group, 2004; Williams et al., 2010).

Various neuropsychological measures have been applied to the study of pre-symptomatic and manifest HD in order to characterise the cognitive profile at different disease stages and identify potential cognitive markers of disease for use in clinical trials. Despite this, no single cognitive measure has emerged as more robust than others in detecting changes or tracking disease. There is also no universally accepted cognitive battery for assessment in HD, although the cognitive section of the Unified Huntington Disease Rating Scale (UHDRS) is widely used. The cognitive section of the UHDRS comprises the Symbol Digit Modality Test, the Stroop Colour Word tests, and a Verbal Fluency test, with the summed score used to indicate the degree of cognitive impairment. Alternative assessments include the Montreal Cognitive Assessment (MoCa) and Mini Mental State Examination (MMSE); the MoCa has been found to have greater utility compared to the MMSE in characterising dementia in HD (Mickes et al., 2010). The UHDRS is more commonly used in research either to track progression or to use as a correlate in brain imaging studies (e.g. (Kobal, Melik, Cankar, & Strucl, 2014; Politis et al., 2011; Wolf et al., 2008). Recent work has shown that the cognitive component of the UHDRS has low variance over time and is more reliable than either the MMSE or MoCA in monitoring cognitive changes in HD patients over 12 months (Toh et al., 2014). Despite this, many research studies in HD choose to supplement the UHDRS with additional cognitive tests in order to achieve a more comprehensive cognitive assessment (Hart et al., 2014; Holl, et al., 2013; Tabrizi, et al., 2013).

There has been a wealth of research examining cognitive changes in HD, and this literature has been comprehensively reviewed (Craufurd & Snowden, 2002; Craufurd & Snowden, 2002; Dumas, et al., 2013; Harrington et al., 2012; Paulsen, 2011; Stout, et al., 2011). Although there are discrepancies in the literature, and understanding regarding the progression of cognitive decline over the disease course continues to be improved, in general cognitive deficits have been shown to emerge prior to motor symptom onset, initially as subtle deficits in domain-specific functions. In pre-symptomatic gene carriers there are typically no or few deficiencies in memory, language or global cognitive functions, with subtle deficits in psychomotor speed, negative emotion recognition, and in some executive functioning sub-domains (Duff, et al., 2010; Harrington, et al., 2012; Paulsen, Smith, Long, & Group, 2013; Stout, et al., 2011; Stout et al., 2012; Tabrizi, et al., 2013). After the onset of motor symptoms, language and global functional domains are thought to be spared for the longest period, with progressive cognitive decline resulting in dementia during the end stage of the disease (Dumas, et al., 2013).

An important consideration when conducting cognitive testing in a clinical group for research and clinical purposes alike is the time required. There has been an increasing tendency for traditional pen-and-paper tests to be adapted to computerised forms. The CANTAB is arguably the most well-known computerised battery of memory, attention and executive function (Fray & Robbins, 1996), whereas the Cambridge Brain Sciences battery used in this work is similar but has the distinct advantage of being freely available. Computer based testing benefit from being time efficient both in terms of experimenter and participant time. A shorter test time means results are more likely to be specific to true cognitive function and less affected by factors such as fatigue and frustration. Whereas pen-and-paper batteries requires a high degree of training to achieve consistency from experimenters in terms of test delivery, with issues associated with inter- and intra-rater reliability for delivery and scoring, computer-based tests are easy to administer, allowing for test delivery in a variety of environments, and can be administered in a consistent and controlled way. Computer based tests also allow measurements to be recorded that are not possible with paper based assessments, such as trial-specific reaction time. Whereas a major problem with pen-and-paper tests is the effect of practice, alternate versions can be easily developed for computerised tests.

The Cambridge Brain Science is a freely-available validated test battery that has not previously been applied to characterise cognitive deficits in HD. A key benefit of the battery is that cognitive tests are short, with each test taking approximately 3 minutes. Secondly, data has previously been acquired on over 44,000 participants who completed the testing online. Thus, there is a sufficiently large population sample to compare against, and this data has been comprehensively analysed (Hampshire, et al., 2012) allowing for comparisons with normal population means as well as with the small well-defined matched healthy control group.

In the current study, 10 tests were selected from the large battery of tests available in order to capture functioning across a wide range of cognitive domains include working memory, visual episodic memory, attention, reward sensitivity, response inhibition, verbal reasoning, planning and set-shifting.  Multiple tests were selected to examine executive function as the research literature suggests there may be domain-specific executive dysfunction in HD (Dumas, et al., 2013; A. Lawrence, Watkins, Sahakian, Hodges, & Robbins, 2000). Ardila et al (2013) proposed that executive dysfunction can be separated into two distinct classes. The first class, referred to as  a "*metacognitive executive dysfunction syndrome*" includes problem solving, abstracting, planning, anticipating the consequences of behaviour, strategy development and implementation, and working memory, and is associated with dorsolateral frontal damage (Ardila, 2013). A second distinct "*motivational and emotional executive dysfunction syndrome*" was proposed that is associated with orbitofrontal and medial frontal pathology and symptoms related to behavioural control (Ardila, 2013). Cognitive deficits in the "*metacognitive*" executive function domain have previously been shown in manifest HD in visuo-spatial planning (Bäckman, Robins-Wahlin, Lundin, Ginovart, & Farde, 1997; Watkins et al., 2000) cognitive flexibility (Bäckman, et al., 1997; Jason et al., 1988;

A. Lawrence et al., 1996), and verbal fluency (Franciosi, Shim, Lau, Hayden, & Leavitt, 2013). In pre-symptomatic HD participants, results are more varied, which different studies producing contradictory findings (see Dumas et al. (2013) for a review). In the motivation / emotional executive function domain, deficits in manifest HD have been observed in response inhibition (Beste, Saft, Andrich, Gold, & Falkenstein, 2008), and in risky decision making (Stout, Rodawalt, & Siemers, 2001), with evidence showing that the effect of experiencing loss on decision-making is reduced in HD patients (Campbell, Stout, & Finn, 2004). In contrast, in early HD, no deficits were found on the Iowa Gambling Task which measures risky decision making (Holl, et al., 2013). Thus, in this study, cognitive tests were selected that measure executive function in both the "meta-cognitive" domain (e.g. the Intra-dimensional/ Extra-dimensional set shifting task and Grammatical Reasoning) and in the motivational/emotional domain (e.g. a version of the Iowa Gambling task and the Go/No-Go task).

It is often necessary to form composite scores from multiple cognitive tests in order to provide a single summary score. One motive is to reduce the number of multiple comparisons, for example, when examining the relationship between cognition and neuropathology. Both the UHDRS cognitive score and the MMSE are composite cognitive scores; however a major limitation with both is the way in which the cognitive elements are combined. Both the MMSE and the UHDRS combine the individual cognitive tests in an additive manner, despite the tests using different measurement scales. In contrast, the ideal approach would be to statistically model the individual cognitive tests so that an optimised weighting of the most sensitive measures are used. Moreover, the ability to combine tests in a manner that can capture the latent properties being measured would produce a composite score more reflective of the cognitive domains affected in HD. In this chapter, the purpose of creating a composite cognitive score was not to be able to distinguish HD participants from controls, but rather to produce a single score that encompassed many cognitive domains to be used to analyse the relationship with brain structure measured using MRI.

### *Declaration of Collaborations*

The Unified Huntington's Disease Rating Scale '99 (UHDRS) assessment was conducted by Kathy Price (research nurse) in a separate research session as part of the Registry study (MREC number 10/WSE04/7).

## Methods

### *Participants*

15 HD gene-positive (asymptomatic and early HD) participants and 13 age, gender and education-matched healthy control participants completed the cognitive testing session. Demographic information is provided in Chapter 2 along with details of the experimental conditions.

### *Cognitive Test Battery*

The 10 cognitive tests are described fully in detail in Chapter 2 and are available for evaluation at www.CambridgeBrainSciences.com. They were designed based on well-established paradigms from the cognitive neuroscience literature, to measure planning, reasoning, attention and working memory abilities. The tests took approximately 45 minutes to complete and were presented in a fixed order. Brief descriptions of the tests are as follows:

***Motor speed*** The Speeded Tapping Test (Reitan, 1979) is a computerised test of finger tapping speed that requires a participant to press a button on the keyboard as quickly as possible. Participants were instructed to use the index finger on their dominant hand and instructions were provided to ensure consistency in the position of the hand. The outcome measure was the average tapping rate over 3 trials.

***Digit Span*** This test of verbal working memory required participants to recall a sequence of digits in the same order in which they were presented. Difficulty was varied dynamically (±1 digit); the outcome measure was the maximum number of digits recalled.

***Paired Associate Learning (PAL)*** This task measuring visual episodic memory required participants to remember the spatial location of a series of objects. Task difficulty was varied dynamically (± 1 window). The main outcome measure was the maximum number of correct object-place associations (‘paired associates’) in the trials that were successfully completed.

***Gambling*** This test of risky decision making required participants to select cards one at a time from 1 of 4 decks, with each card selected resulting in either a gain or a loss of money (Bechara, et al., 1994). Different decks contained a higher probability of wins versus losses and the aim was to accumulate as much money as possible. The outcome measure was the total money won after 100 trials/cards selected.

***Go / No-Go*** This task measures response inhibition by the ability to inhibit prepotent responses (Verbruggen & Logan, 2008). Participants were presented with one of two cues: a frequent cue (90% of trials), which required a button press response and an infrequent cue (10% of trials), which required participants to not respond, and inhibit the button press. The outcome measures were the number of ‘failed stops’ to the infrequent cue and the number or ‘correct go’ button responses to the frequent cue, as well as the corresponding reaction times.

**ID/ED shift Task** This task required participants to learn, via trial and error, which stimulus, of the 2 presented on the screen, was designated as the target image. The 2 stimuli were compound images composed of 2 different object dimensions: block shapes and line drawings. There were 8 stages of this test as shown in Figure 3.1. For each stage, the criterion was 6 consecutively correct responses, before moving to the next stage. If participants did not reach criterion within 30 trials, participants moved to the next stage of the test. For each ID/ ED shift and reversal stage, the number of trials to criterion was the outcome measure (range 6-30). In order to have a single empirical measure for set formation and flexibility, the sum of the number of trials for criterion for ID conditions (ID shift + ID reversal) was subtracted from the ED conditions (ED shift + ED reversal), according to Fallon et al (2013), based on the lower error rate typically observed for ID shifts compared with ED shifts.

**Spatial Planning** This task required participants to reposition a number of squares on a grid so that they are configured in ascending numerical order. Puzzles become progressively harder with the total number of moves required and the planning complexity increasing in steps. The outcome measure was the total number of puzzles solved within 3 minutes.

**Colour-word stroop** A single word (either ‘red’ or ‘blue’) was displayed at the top of the screen, either in a congruous colour (i.e. the word red printed in red ink) or in an incongruous colour (i.e. the word red printed in blue ink). At the bottom of the screen, two colour words were displayed (red, blue) and participants were required to indicate which of two coloured words at the bottom of the screen describes the colour of the ink that the word at the top of the screen is presented in, ignoring the word itself. The participant solved as many problems as possible within 90 seconds. The total score increased by 1 after a correct and decreased by 1 after an incorrect response on a trial-by-trial basis. The total score was the outcome measure.

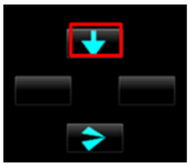

**1. One-dimension Rule**: Participants first had to learn a rule that existed between 2 stimuli that were from the same category (Rule = target object is block object A).

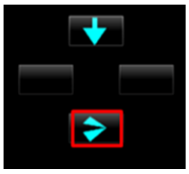

**2. One-dimension Reversal**: the target object is reversed (Rule = target object is block object B).

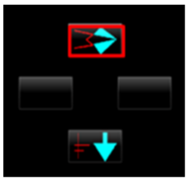

3. **Two-dimensions :** A second category (line drawings) is introduced to each image but this category must be ignored ( Rule = target object is the image containing block object B)

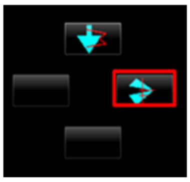

4. **Two-dimensions overlap**: The two categories are now overlapped in space, the second category must still be ignored ( Rule = target object is the image containing block object B)

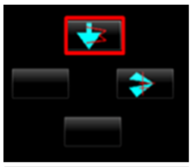

5. **Intra-dimensional reversal:** the target object is reversed (i.e. target object is image containing block object A).

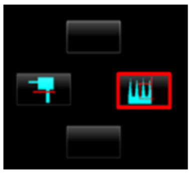

6. **Intra-dimensional shift:** a new set of stimuli from the same 2 categories are shown. The target object is from the same category as the previous trial (Rule = target object is image containing block object C)

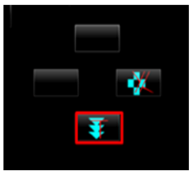

7. **Extra-dimensional shift :** The target image changes dimensions, from a solid object to a line drawing (Rule = target image is image containing line drawing C)

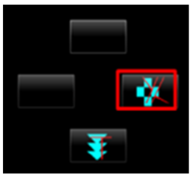

**8. Extra-dimensional reversal** The target image line drawing is reversed, but within the same category (Rule = target image is image containing line drawing D)

Figure 3.1 The 8 stages of the Intra-dimensional /Extra-dimensional (ID/ED) Task. The red box indicates the correct response for the trial. Stages 1-4 were training stages. From stage 3 onwards, images were always compounds of the two object dimensions (line drawings + block object).

***Grammatical Reasoning*** Participants were presented with a pair of shapes and a grammatical statement described the relationship between the two shapes (Baddeley, 1968). Participants had to indicate (True vs. False) whether the sentence accurately described the relationship between the shapes, and had 90 seconds to complete as many trials as possible. The outcome measure was the total number of correct trials minus the number answered incorrectly. Task difficulty was dynamically varied.

***Feature Match*** Participants were presented with two grids, each containing a set of abstract shape and were required to assess whether or not the abstract shapes were identical. Task difficulty was dynamically varied. The total score was the sum of the number of shapes in the grid for each correct trial. The task was terminated after 90 seconds.

***Spatial Rotations*** Two grids of coloured squares were displayed on either side of the screen with one of the grids rotated by a multiple of 90 degrees. When rotated, the grids were either identical or differed by the position of just one square. The task was to indicate whether the grids were identical if one of the grids was rotated. The total score increased or decreased by the number of squares in the grid on that trial for correct and incorrect responses respectively. The total score after 90 seconds was the outcome measure.

### *Statistical analysis*

One-way analysis of covariance (ANCOVA) was used to examine differences in cognitive functioning between HD and control participants, controlling for the effect of age. The assumptions of the ANCOVA were first tested. All of the measures were found to be normally distributed when tested using the Shapiro-Wilk test at $\alpha = 0.001$. Homogeneity of regression slopes was tested for all covariates added to the analysis. The Kruskal-Wallis non-parametic test was used to examine group based differences for the ID/ED test as the assumption of normality was violated. The principal components analysis does not make any assumptions about the underlying assumption, thus the ID shift component of the ID/ED test was included in this analysis.

As well as looking at differences between controls and HD participants, one-sample T-tests were conducted to examine differences against the population mean for these tests from a dataset of 44,600 participants aged 12-70 year old, as reported in Hampshire et al (2012).

Where mean responses are reported, the corresponding ± standard error of the mean is also reported.

## Results

The population mean from a study of 44,000 participants (Hampshire, et al., 2012) was available for 6 of the tests used in this study. Descriptive statistics and the results of statistical testing against the sample mean are shown in Figure 3.2.

### *Finger tap speed*

HD participants were significantly slower (19.9%) on the test of finger tapping speed compared to healthy controls, $t\ (26) = 2.76$, $p < 0.05$. Finger tapping speed did not correlate with age, $p > 0.05$. In HD participants, finger tapping speed did not significantly correlate with disease burden, $r = -.467$, $p > 0.05$, but did correlated with the UHDRS motor score, $r = -.703$, $p < 0.01$.

### *Age as a confound*

Age was found to be related to cognitive performance on a number of the tests (see Appendix 3), thus age was added as a covariate in the analyses.

### *Motor speed as a confound*

On 6 of the tests, a timed response was required. Thus, a correlational analysis was performed to examine whether motor speed confounded cognitive performance on these timed tests. Because of the difference between HD and control participants in finger tap speed, the correlations were examined separately for each group and the results of the analysis are shown in Table 3.1. Finger tap speed was correlated with performance on the Feature Match test, $r = .54$, $p < 0.05$ in the HD participants. The same relationship was not found in healthy control participants, however a comparison of regression slopes found no interaction between gene status, age and finger tapping speed for performance on this test, $F (2,23) = 1.60$, $p > 0.05$. Finger tap speed was also correlated with performance on the Go-No-Go task in healthy controls, specifically in the trials requiring response inhibition, $r=-.74$, $p < 0.05$ FDR-corrected. The same relationship was not found in HD participants, however a comparison of regression slopes for both groups of participants found there was no interaction between gene status and finger tapping speed for response inhibition during the Go-No-Go task, $F (2, 23) = .30$, $p > 0.05$, justifying the addition of motor speed as a covariate for both of these tests.

Table 3.1 Cognitive tasks with a timed element and the corresponding correlation coefficient with finger tap speed. s: seconds

| | | **Finger-tap speed** | | | |
|---|---|---|---|---|---|
| | | controls | | HD | |
| Timed Tasks | Allocated time | *r* | *p* | *r* | *p* |
| Stroop | 90s | 0.26 | .41 | 0.53 | .09 |
| Grammatical Reasoning | 90s | -0.05 | .888 | 0.46 | .151 |
| Spatial Planning | 180 s | 0.37 | .241 | -0.04 | .898 |
| Feature Match | 90s | 0.32 | .305 | 0.54 | **.037** |
| Spatial Rotations | 90s | 0.41 | .181 | -0.53 | .090 |
| Go-No-Go | | | | | |
| *Failed Stop* | Timed trials | -0.74 | **.005** | 0.21 | .534 |
| *Missed Go* | | 0.01 | .971 | -0.33 | .319 |
| *Mean RT* | | 0.58 | .049 | -0.29 | .390 |

### *Memory domain*

**Digit Span** HD participants had a digit span that was on average 1.63 digits shorter than healthy controls, controlling for age, F (1, 25) = 7.71, $p < 0.05$. Although the test did not require timed-responses, given the requirement to enter digits on the laptop keyboard, it was plausible that impaired motor speed may also be a confound on this test. A correlational analysis found that this was the case, with finger tapping speed being strongly associated with digit span only in HD participants, r = .765, $p < 0.01$, with no relationship found in controls, r = 0.025, $p > 0.05$. Repeating the ANOVA with finger tapping speed as a covariate resulted in the previous main effect of gene status now not being significant, F (1, 24) = .1.37, $p > 0.05$. There was no relationship between disease burden and digit span, with or without finger tapping speed partialled out, $r < 0.3$, $p > 0.05$.

**Paired Associate Learning** HD participants performed significantly worse on the paired associate learning task compared to matched control participants, in which an association between an object and location was required, F (1,25) = 4.58, $p < 0.05$. Descriptive statistics are shown in Figure 3.2. Paired associate learning was not related to disease burden in HD participants, r = .01, $p > 0.05$.

### *Top-down processes / executive functions*

**Gambling Task** Overall, performance on this task was highly variable in both groups of participants ($57.69 ± 117.38 for healthy controls, $250.00 ± 141.79 for HD participants). There was no difference in overall performance on the gambling task, with HD and control participants responding equally to rewards and punishments associated with specific card decks after controlling for age, F (1,25) = 1.00, $p > 0.05$. The score on this test was not related to disease burden, r = -.236, $p > 0.05$.

***Go / No-Go*** On the inhibition or 'no-go' trials, where participants were required to cancel the frequent response when presented with an infrequent cue, participants had a high failure rate (63.5 ± 6.69 % for controls, and 56.44 ± 6.53 % for HD participants) and a rapid reaction time ( control mean = .293 ± .015 s, HD mean = .342 ± .027 s). Whereas there was no difference in the failure rate between HD and control participants (F (1, 24) = .915, p > 0.05 with motor speed as a covariate, F (1, 25) =.577, p > 0.05 without accounting for motor speed), HD participants had a longer reaction time, F (1, 23) = 5.03, p < 0.05 uncorrected, p > 0.05 FDR-corrected. This difference in reaction time was not found when motor speed was not included in the analyses as a covariate, F (1, 24) = 2.31, p > 0.05. On the response, or 'go' trials, participants had to respond with a button press to a frequent stimulus within 1s. Control participants had a higher success rate on these trials (mean = 85.74 %) compared to HD participants (mean = 74 %), although this difference was not statistically significant, F (1, 23) = 1.53, p > 0.05, and there was no difference in reaction time for successful trials (control mean = .32 ± .01 s, HD mean = .36 ± 0.03 s). In HD participants, disease burden was correlated with response accuracy to no-go trials, r = -.716, p < 0.05 uncorrected, p > 0.05 FDR-corrected.

### *Intra-dimensional / Extra-dimensional set shifting*

There was a significant difference between HD and control participants on a measure of set-formation and set-flexibility (trials to criterion on ED blocks minus ID blocks), *F (*1, 25) = 5.66, < 0.05. Set-formation and flexibility was moderately correlated with disease burden in HD participants although the relationship was not statistically significant, r = .535, p = 0.059. There was no interaction between gene status and shift; both groups of participants found the ED shift significantly more difficult than the ID shift, F (1, 26) = 42.54, p < 0.001, however, after accounting for age, this difference was not significant, F (1, 25) = 1.263, p > 0.05. To understand what was driving the difference between HD and control participants, trials requiring an attentional shift were examined separately from trials requiring a rule reversal. There was no difference between HD and control participants in the median number of trials to learn the intra-dimensional shift rule, $\chi^2 = 2.53$, $p > 0.05$. The HD participants required significantly more trials to learn the extra-dimensional shift rule compared to control participants, $\chi^2 = 4.26$, $p < 0.05$; however this did not survive FDR-correction, $p > 0.05$. In HD participants, ID shift was significantly correlated with disease burden, $r = -.638$, $p < 0.05$ FDR-corrected. The same relationship was not found for ED shift, $r = .456$, $p > 0.05$.

***Spatial Planning*** There was no difference in the spatial planning performance of HD participants compared to healthy controls, $F(1, 25) = 2.038$, $p > 0.05$. Spatial planning ability was not related to disease burden in HD participants, $r = -.295$, $p > 0.05$.

***Colour-word Stroop*** There was no difference between HD participants and healthy controls in performance on the stroop task overall, controlling for age, $F(1, 28) = 1.58$, $p > 0.05$. Examining the congruent, incongruent, and doubly incongruent trials separately also did not reveal any significant differences between groups in terms of accuracy or reaction time (controlling for finger tapping speed), all $p > 0.05$. Both HD and control participants performed significantly worse on this test compared to the large population sample (Hampshire, et al., 2012), $t(14) = -5.94$ and $t(12) = -3.33$ respectively, $p < 0.01$. Overall stroop performance was not associated with disease burden, $r = .194$, $p > 0.05$.

***Grammatical Reasoning*** HD participants scored significantly lower on the grammatical reasoning task, $F(1, 25) = 6.40$, $p < 0.05$. HD participants attempted a similar number of trials compared to controls, $F(1, 25) = 3.52$, $p > 0.05$, thus the difference in score was caused by a higher error rate in HD participants. Overall grammatical score was not associated with disease burden, $r = -.468$, $p > 0.05$, whereas the number of trials attempted was associated with disease burden, with increased disease burden associated with a reduction in the number of trials attempted, $r = -.626$, $p < 0.05$ FDR-corrected.

a. Memory tests

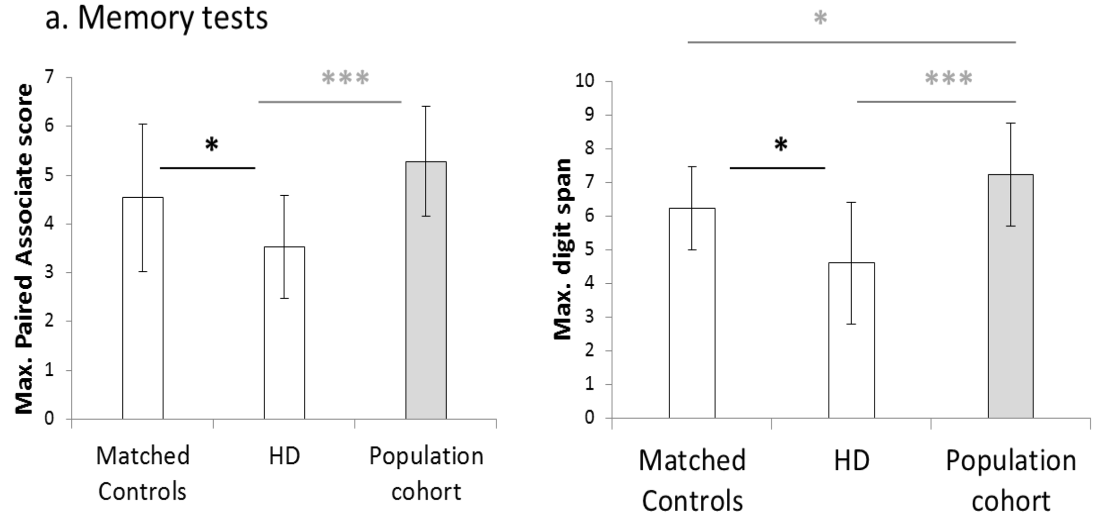

b. Executive function tests

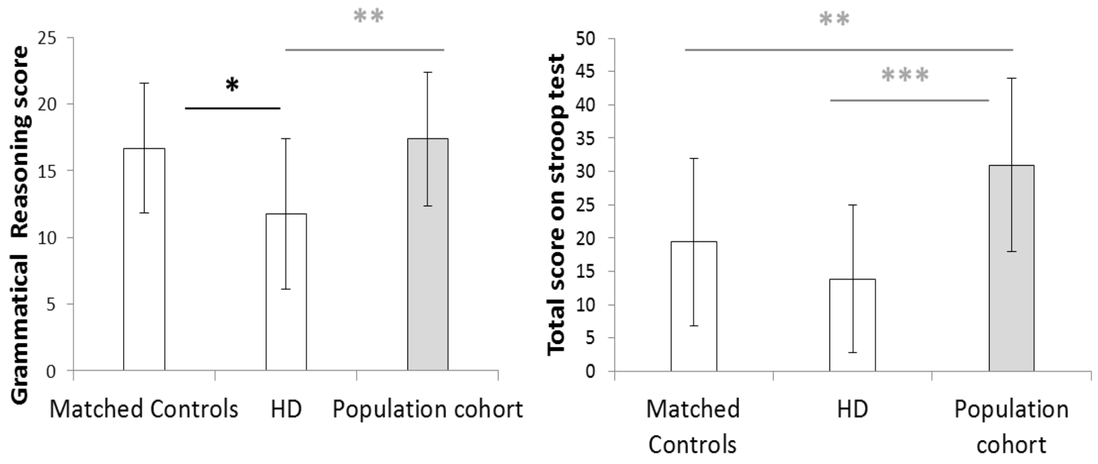

c. Spatial attention tests

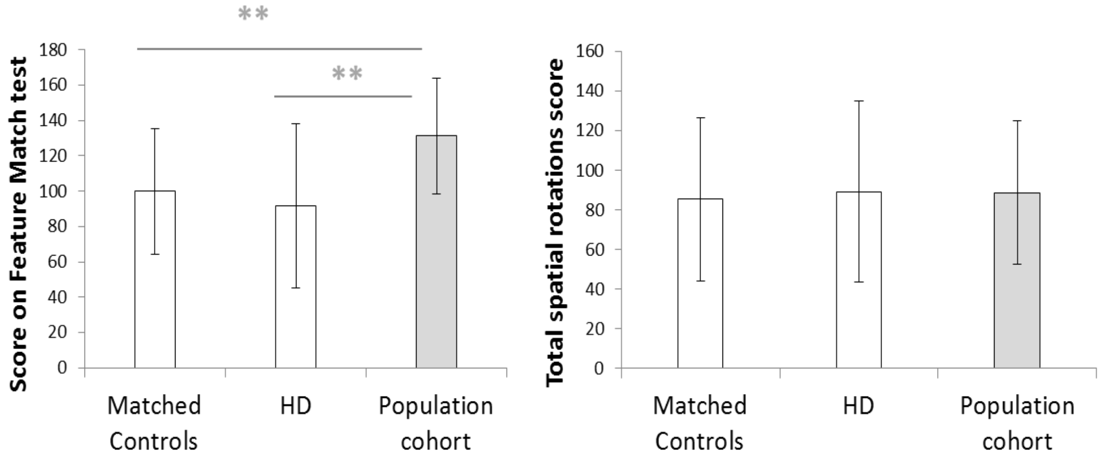

Figure 3.2 Descriptive statistics for cognitive test performance. Population cohort refers to the 44, 600 data sets reported in Hampshire et al (2013). Error bars represent ± 1 standard deviation. * $p < 0.05$, ** $p < 0.01$, *** $p < 0.001$. ANOVA's conducted between matched controls and HD participants were controlled for the effects of age.

### *Attention domain*

**Feature Match** There was no difference in performance between HD and control participants with motor speed as a covariate, F (1, 24) = .417, $p > 0.05$, and without motor speed in the analysis, F (1, 25) = 1.54, $p > 0.05$. Both HD and control participants performed significantly worse on this test compared to the large population sample (Hampshire, et al., 2012), t (14) = -3.29, and t (12) = -3.18 respectively, $p < 0.01$. After controlling for finger tapping speed, there was no relationship between disease burden and performance on this test, r = -.063, $p > 0.05$.

**Spatial Rotations** HD participants were able to mentally rotate a similar number of objects correctly (8.6 ± .54 rotated grids) within the time limit compared to control participants (8.9 ± .65 grids). HD participants made a similar number of errors (3.6 ± .66) compared to healthy control participants (3.8 ± .42), there was no statistical difference in overall performance on this task between groups, F (1, 26) =.084, $p > 0.05$. There was also no difference in average performance by HD and control participants and the large population sample (Hampshire, et al., 2012), t (14) = .041, and t (12) = -.292 respectively, $p > 0.05$. There was no relationship between disease burden and performance on this test, r = .106, $p > 0.05$.

### *Composite cognitive score*

In order to examine the relationship between cognition and MRI measures, it was necessary to reduce the number of dimensions for analyses. Thus all 10 cognitive tests were added to a principal component analysis using SPSS software (IBM, version 20). The number of Correct-Go and Failed-Stop responses from the Go/No-Go tasks were added to the analysis separately, as there was a low correlation (r=-0.068) between the two measures, suggesting they tap different cognitive processes, response execution and response inhibition. Similarly, the score on intra-dimensional (ID) shift trials was added separately to the score on the extra-dimensional (ED) shift trials from the ID/ED task, due to the low correlation between the two measures (r=0.13). In order to improve the interpretation of the resulting composite score; ED and ID shift were transformed: *[minimum number of trials to criterion (6) – achieved trials to criterion].* This resulted in a high value being indicative of a good performance, rather than a poor performance (number of trials to criterion).

Bartlett's test of sphericity was significant, $\chi^2$ (66) = 144.19, $p < .05$, suggesting that the model is appropriate. However, the Kaiser-Meyer-Olkin measure of sampling adequacy was 0.579, just below the recommended value of 0.6, and the diagonals of the anti-image correlation matrix were below 0.5 for 4 of the measures (Failed Stop, ID shift, gambling, and spatial rotations), indicating that these measures lack sufficient correlation with the other measures and supporting the exclusion of these items and the inclusion of the remaining measures in the analysis. The PCA was then recalculated with the 4 measures excluded. The Kaiser-Meyer-Olkin measure was now 0.686, and Bartlett's test of sphericity remained significant, $\chi^2$ (28) = 100.79, $p < .05$. Oblique rotation was used based on correlations (>0 .3) in the component correlational matrix, suggesting overlap in variance. As shown in Table 3.2, the first principal component was extracted and these regression values used as the composite cognitive score for each participant. This first principal component accounted for 56.3 % of the total variance and included measures from 8 out of the 10 test domains.

HD participants had a lower composite score (-.32 ± .22) compared to control participants (.34 ± .30), although this difference did not meet statistical significance when controlling for age, F (1, 24) = 3.40, p = 0.078. Although underpowered [*df =6*], there was a moderate correlation between the composite cognitive score and performance on the UHDRS cognitive scale, r = .562, p > 0.05. There was no relationship between disease burden and composite cognitive score, r = -.15, p > 0.05.

Table 3.2 Principal Component Analysis (PCA) of cognitive performance in all participants with oblique rotation.

| | Component matrix | | |
|---|---|---|---|
| | Component | | |
| | 1 | 2 | 3 |
| Stroop | .939 | .241 | .293 |
| Paired Associates | .773 | .690 | .260 |
| Feature Match | .651 | .588 | .334 |
| Grammatical Reasoning | .640 | .594 | .402 |
| ED shift | .549 | .266 | .347 |
| Spatial Planning | .316 | .971 | .268 |
| Response production (Go/No-Go) | .341 | .267 | .996 |
| Digit Span | .561 | .476 | .646 |

Rotation Method: Promax with Kaiser Normalization.

## Discussion

It is known from previous studies that cognitive deficits commonly occur prior to the onset of motor symptoms in HD, although no single cognitive measure has emerged as superior in terms of robustly detecting changes or tracking disease. The use of the Cambridge Brain Sciences computerised battery in HD participants has not previously been reported in the published literature. Using this battery, HD participants were found to have deficits in verbal working memory, visual episodic memory and verbal reasoning, along with evidence of both psychomotor slowing and motor slowing. HD participants were selectively impaired in their ability to shift their response set to a previously irrelevant dimension (extra-dimensional set-shifting, [EDS]), but were not impaired when shifting attention to new exemplars of a previously relevant dimension (intra-dimensional shift [IDS]). By contrast, HD participants were not found to have impairments in three separate tests sensitive to frontal lobe dysfunction, namely a version of the Tower of London test of spatial planning ability, a visual discrimination learning paradigm and the colour-word

Stroop interference task. This discrepancy may be due to the many integrated cognitive functions that are required to perform different executive function tasks, resulting in many factors confounding performance on each test (Lezak, Howieson, & Loring, 2004). By breaking down the individual elements of the Go / No-Go task, it was found that HD participants did not have deficits in response inhibition compared to healthy controls, although they did take longer to respond to cues signally a ‘No-Go’ response, suggestive of psychomotor slowing. There were no deficits seen on a version of the Iowa Gambling task, suggesting that at this early stage in the disease, there are no differences in sensitivity to reward contingencies.

The selective deficit seen in EDS shifting is in agreement with Lawrence et al (1996) who also found impaired EDS shifting with intact IDS shifting specifically in early HD participants. The same selective deficit has previously been shown in a cohort of neurosurgical patients with localised excisions of the frontal lobes (Owen, Roberts, Polkey, Sahakian, & Robbins, 1991) and in patients with early-stage Parkinson’s disease (Downes et al., 1989). In Parkinson’s disease, this selective deficit was explained in terms of a dysfunction of fronto-striatal circuity. Previous explanations of the selective EDS shifting deficit seen in HD suggested the inability to switch between response sets is caused by a breakdown of inhibitory associative and attentional control mechanisms controlled in part by the head of the caudate nucleus (A. Lawrence, et al., 1996; Robbins & Brown, 1990; Sutherland & Mackintosh, 1971). The lack of a deficit in spatial planning is in agreement with the literature, given the time limits used in the version of the task. For example, performance on the Tower of London spatial planning task was previously shown to be impaired in early HD participants but only on the most difficult 5-move problems, whereas deficits were not seen on less challenging tasks (A. Lawrence, et al., 1996). Because of the time limit imposed, it is likely in this study that the task did not become sufficiently difficult for differences to emerge, and is an element of the task that could be altered for future use.

Memory deficits were observed in verbal working memory and visual episodic memory. Previous work has also shown a deficit in performance on the forward digit span, but only in manifest HD participants (Lemiere, Decruyenaere, Evers-Kiebooms, Vandenbussche, & Dom, 2004). Because it was not possible in this study to stratify according to pre-symptomatic or early manifest status due to sample size limitations, it is not possible to ascertain if the significant deficit seen in this study were driven by changes specifically in the manifest participants or whether changes were also evident in the pre-symptomatic participants. Previous work has shown that performance on the forward digit span test of verbal working memory is not susceptible to significant decline in early HD (Lemiere, et al., 2004; Mason et al., 2010). The lack of a relationship found between disease burden and digit span supports this. The deficit seen on the paired associate learning task is suggestive of a deficit in visual episodic memory in the very early stages of HD. In the literature, there have been equivocal findings regarding the episodic memory impairments in HD, although a recent meta-analysis found that recall, cued recall, and recognition memory were are all profoundly impaired in symptomatic HD participants, but only slightly impaired in pre-symptomatic participants (Montoya et al., 2006). The results in this study of a cohort of pre-symptomatic and early-stage HD participants fit with this finding.

The mean performance on a number of tests in both HD participants and healthy matched control participants was found to differ significantly from the mean performance reported from a sample of 44,600 participants (Hampshire, et al., 2012). There are a number of factors that may explain this difference. Firstly, testing in this study was conducted under controlled laboratory conditions, whereas the population mean from the large cohort was obtained from participants who completed the testing on the internet. Thus, it may be that participants did not complete the tests alone, or completed the test multiple times and thus the higher mean scores can be explained by practice effects. Secondly, the participants whom chose to complete the tests which were accessed via the internet can be assumed to have a certain level of computer literacy, in order to be able to view the online advertisement and navigate to the test website. In the cohort used in this study, computer literacy was not uniform, for example, some participants needed instructions on operating the computer mouse, which may have affected performance.  Secondly, the healthy control group in this study were recruited specifically to match the HD group in terms of age, gender and education. As HD is typically an adult-onset neurodegenerative disease, it is likely that the average age was significantly greater and the range of participant ages smaller than the larger population sample used. Furthermore, participants were drawn from a smaller geographical pool, thus socioeconomic status is likely to be less varied, and the education level was skewed towards fewer years in education, compared to the sample used in Hampshire et al (2012).

The influence of motor function on cognitive testing is an important factor that needs to be considered. Bradykinesia, or motor slowing, is a feature of the motor phenotype in HD (Tabrizi, et al., 2013) and was tested in this study using the Speed Finger Tapping test (Reitan, 1979) , with a reduced tapping speed found in HD participants. In contrast, psychomotor speed refers to the speed of thinking and acting, and is a feature of the cognitive phenotype in both pre-symptomatic and manifest HD (Tabrizi, et al., 2013). On the Go/No-Go task, HD participants were found to be significantly slower in responding to infrequent cues requiring a response inhibition (‘No-Go’ trials) which may be suggestive of subtle psychomotor slowing. It is not clear in what way motor slowing and psychomotor slowing interact and affect performance on tasks. In the test battery used in this chapter, this is important as a number of the tests have a timed element, so interpreting poor performance may not be specific to the cognitive domain being measured in the task, but may also be influenced by psychomotor and/or motor speed. Previous longitudinal work in HD by Hart (2013) showed that significant cognitive results were reduced by 20% when motor speed was taken into account, affecting the overall statistical outcome and interpretation of the results.  Thus, there is the risk that cognitive deficits are overestimated when motor slowing is not controlled for. Despite this, performance on the Speeded Finger Tapping test is not commonly included as a covariate in the analyses of cognitive performance (Paulsen, 2011; Tabrizi, et al., 2013). In this study, where a significant relationship was found between speeded tapping and cognitive performance, motor speed was added as a covariate and the result with and without this covariate is reported. This proved to be important when examining response inhibition on the Go / No-Go task, with a difference in reaction time between HD and control participants specifically to trials requiring response inhibition only detectable when motor speed was included as a covariate. This suggests that the effects of motor speed deficits may dilute the effects of psychomotor speed deficits if not controlled for, thus masking potential relevant deficits in HD.

A strength of this chapter was the formation of a composite cognitive score using a statistically sound approach in order to produce a score that was weighted and encompassed different aspects of cognition. This single score is more appropriate given the small sample size and can be used in future work to examine the relationship with brain structure. Furthermore, it is likely to be more sensitive that the UHDRS cognitive score which is formed in an ad hoc, non-optimal manner. In this study, only the first principal component was extracted, however with a greater sample size that would be more robust to multiple comparisons, it would also be worthwhile to examine the second and third components to avoid losing potentially meaningful data.

A limitation with the work in this chapter is related to some of the tasks included in the battery of cognitive tests. Two of the tests lacked sensitivity to the construct being measured, potentially leading to misleading findings. As previously mentioned, the time limit imposed in the spatial planning task meant that the outcome measure, the total number of trials completed within this limit, lacked sensitivity. In practice, this meant that a number of participants made progress in solving a problem and were close to completing the problem when the time ran out, and their effort on that trial was not recognised in the overall score. Whereas previous work has found reduced accuracy in spatial planning in early HD (Watkins, et al., 2000), it is difficult to ascertain whether the lack of a difference found in this study is because the cohort study included pre-symptomatic participants, or because the test was not a sensitive measure of performance. Similarly, the gambling task produced highly variable performance in both control and HD participants, with this variance not related to the construct under examination. Because there was no wait period between trials, some participants appeared to rapidly work through the trials disregarding the feedback information required to complete the task, which may explain the variance and the lack of a correlation with other test dimensions, leading to the test being excluded from the composite score. Furthermore, the overall measure of total money earned in the test is not informative of the strategy used by participants, which may be more sensitive to differences between groups. Future improvements include modifying these two tests to include a wait period for the gambling task, as well as a more prominent display of the monetary gain/loss for each trial, and for the spatial planning task to not be time-limited, but rather examine the number of moves taken to complete a set number of puzzles.

Although computerised testing offers many advantages in terms of speed, ease and accuracy of delivery, there are a number of drawbacks that also need to be considered when using computer-based approaches. Irrespective of the clinical group, there is likely to be variance in terms of computer literacy and experience amongst participants, which may introduce bias in terms of response times and the perception that tasks are too fast spaced. For example, in the Hampshire et al. (2012) study, the frequency with which individuals played computer games was positively related to the mean cognitive score, suggesting that computing experience affects performance on these tests. In addition, both motor and cognitive deficits may interfere with the ability to adapt to a keyboard and/or mouse. The effect of computing experience be minimised by including practice trials and an assessment of basic computer skills to use as a potential confounding variable in the analysis.

A final consideration is the importance of premorbid intelligence in HD, which may be related to cognitive reserve and thus the rate and severity of cognitive decline in HD (Papoutsi, et al., 2014). In this study, attempts were made to account for premorbid intelligence by ensuring that the healthy control group were matched for educational attainment, although it is acknowledged that years in education may not be a sensitive marker of premorbid intelligence, especially given the research showing cognitive decline up 15 years before the onset of motor symptoms, which conceivably could affect higher education progression.

Overall, this chapter has shown that in general, the short yet extensive battery of computerised cognitive tests used are sensitive to cognitive changes that occur in pre-symptomatic and early-stage Huntington's disease. Moving forward to examining changes in cognition over the disease course, a computerised battery such as the one used has distinct advantages over pen-and-paper tests, such as those used in the UHDRS cognitive battery. Computerised batteries can produce multiple versions of tests, minimising any effects of learning and practice that may confound longitudinal analyses. The computerised battery is quick to deliver and minimises frustration and boredom in a patient population and healthy control population alike, meaning that any other tests obtained following the cognitive test session are less confounded by fatigue or motivational issues. The ability to create a composite score that encompassed multiple cognitive domains allows for the relationship with brain structure to be explored whilst minimising the number of multiple comparisons required.

# 4 Higher-order deterministic tractography of white matter pathways in Huntington's disease

## Chapter summary

The primary aim of this chapter was to examine quantitatively the differences in metrics obtained from deterministic tractography reconstructions of white matter pathways in patients with Huntington's disease (HD) compared to healthy matched controls. The second aim was to assess the correlation between quantitative fiber tractography metrics, cognitive and motor performance and disease burden in HD.

Analysis was focused on data obtained from multicomponent relaxometry and from 3 separate diffusion MRI sequences: a diffusion sequence optimised for tensor based metrics, a HARDI-based sequence more suited for recovering fibre orientations through spherical deconvolution approaches, and a multi-shell diffusion MRI sequence (CHARMED). Whole-brain HARDI deterministic fiber tractography was conducted and the corpus callosum, cingulum bundle, and corticospinal tract were reconstructed in both hemispheres. Tensor based metrics, axon density (restricted volume fraction) and myelin water fraction were obtained along the tracts. Differences between HD and healthy control participants were examined, along with the relationship between metrics obtained along the reconstructed white matter tract, motor speed, cognitive function, UHDRS scores and disease burden in HD.

## Introduction

Despite a growing body of evidence showing that white matter plays a role in HD pathology, the impact of the HD mutant gene on specific white matter pathways is not known, and likewise, the specific contribution any white matter abnormality makes to the clinical features of the disease is not understood. In HD, the majority of investigations into white matter changes have been focused on either whole brain white matter (Bohanna et al., 2011; Mascalchi et al., 2004; Rosas et al., 2006) or a region-of-interest analysis (Matsui et al., 2013). To date, only a handful of studies have focused on reconstructing individual white matter pathways. Given the heterogeneous nature of psychiatric, cognitive and motor symptoms, it is plausible that multiple pathways are involved either as a direct effect of pathology, or are recruited as part of a compensatory network as a result of damage elsewhere in the brain.

As described in Chapter 1, deterministic tractography is an approach to analysing diffusion MRI data in which white matter fiber pathways can be reconstructed in 3-dimensions in vivo (Jones, 2008), therefore allowing the comparison between anatomically known white matter pathways across groups. The reconstruction of fiber bundles has traditionally been carried out by the propagation of streamlines along the single path of least hindered diffusion, namely the principal eigenvector of the diffusion tensor (Basser, et al., 2000). The limitations of the diffusion tensor model which were described in Chapter 1 have resulted in the development of advanced algorithms capable of modelling multiple fiber orientations within a single voxel. High angular resolution diffusion imaging, or HARDI, methods use a large number of unique gradient orientations to acquire the data, with this increased sampling in q-space improving the diffusion profile (D. Alexander, 2005; Frank, 2002; Tuch, et al., 2002).

In this chapter, two different spherical deconvolution (SD) methods were implemented and compared. SD methods are capable of recovering the fiber orientation distribution (FOD) in each imaging voxel directly by weighting the measurement from each orientationally-distinct fiber population with the fraction of fibers with that orientation. As described in chapter 2, this is achieved by modelling the acquired diffusion signal as a convolution of the fiber orientation distribution function (fODF) with the response function from a single fiber population (Tournier, et al., 2004). A number of different SD approaches exist, and differ in terms of the way the diffusion profile is obtained and the use of a priori information as regularization terms. Constrained spherical deconvolution (CSD) is one SD method which measures the diffusion profile directly from the data, and contains a non-negativity constraint on the fiber orientation distribution, improving the accuracy of the estimation of the fODF (Tournier, et al., 2004). Without the non-negativity constraint, noise in the data can introduce large spurious negative lobes in the reconstructed fiber orientation distribution which are not physically possible (Tournier, et al., 2008). Damped Richardson-Lucy is an alternative SD approach (Dell'acqua, et al., 2010) that instead assumes a diffusion tensor model when obtaining the diffusion profile, and uses adaptive regularization, which includes an isotropic term to model partial volume. Both methods will be used in this chapter as it is plausible that they may differ in terms of the specificity and sensitivity to reconstruct certain fiber pathways.

In terms of the quantitative indices used to evaluate white matter pathways, there is still a reliance on tensor-based scalar measures in the literature, despite the adoption of more advanced tracking algorithms. Diffusion tensor indices have the advantage of being highly sensitive to local changes in diffusivity properties yet are inherently non-specific, containing both an interesting source of variation (e.g. axon density and diameter, myelin water) and an uninteresting source of variation (the orientational dispersion), thus it is not possible to accurately infer the biophysical basis of any change in tensor metric. In recent years, a number of different approaches have been developed showing specificity to changes in myelination and axonal structure. Multi-shell diffusion MR sequences, such as Assaf et al.'s (2004) composite hindered and restricted model of diffusion model (CHARMED), models intra-axonal, or restricted diffusion, separately from extra-axonal, or hindered diffusion through the use of a multi-shell approach. The extra-axonal compartment is characterised by a single diffusion tensor, whereas the restricted intra-axonal compartment is characterised by impermeable cylinders with radii that follow a fixed Gamma distribution (Assaf & Basser, 2005; Assaf, et al., 2004). The parameters obtained from this approach, such as the restricted volume fraction, may provide more biologically sensitive and specific measures compared to tensor-based metrics.

Multicomponent analysis of T1 and T2 relaxation, or multicomponent relaxometry, is a quantitative MR technique that is sensitive to changes in myelin content (Spader et al., 2013), and is described fully in Chapter 2. The multicomponent driven equilibrium single-pulse observation of T1 and T2 (mcDESPOT) proposed by Deoni and colleagues (2008b) allows for quantitative analysis of myelin with scan times suitable to clinical imaging research. Neither CHARMED or mcDESPOT acquisitions have previously been published in the HD literature, and may be useful in disentangling the contribution of specific white matter cell populations to HD pathology.

In this study, the focus was on three large white matter tracts all with a well-known structure and function and a clear hypothesis when looking for abnormalities in HD.

### *Corpus Callosum*

The corpus callosum is the most studied white matter pathway in HD research. It is the largest white matter fiber tract in the brain containing more than 200 million commissural fibers that transfer information between the two hemispheres and is one of the few fiber systems that can be readily identified and isolated without the need for tractography, perhaps explaining the concentration of research attention here. The transfer of information between the two hemispheres is crucial for a variety of cognitive processes, such as perception, memory, attention, and learning (Aboitiz & Montiel, 2003; Engel, König, Kreiter, & Singer, 1991; T. Matsuzaka et al., 1999; T. Matsuzaka et al., 1993). The majority of callosal fibers arise from neocortical pyramidal cells (Le Bé, Silberberg, Wang, & Markram, 2007), which is a cell population known to be affected early on in the disease course of HD (Sach et al., 2004).

The corpus callosum has been reported to be affected in HD using a variety of approaches, including TBSS (Di Paola et al., 2012; Kincses et al., 2013; Weaver, et al., 2009), region-of-interest based analysis (Di Paola, et al., 2012; Dumas, et al., 2012), and tractography (Dumas, et al., 2012; Klöppel et al., 2008; Phillips et al., 2013). Callosal thinning and reduced FA has been found in HD even in the pre-symptomatic stage, with thinning initially only evident in the isthmus, and progressing in an anterior direction in the symptomatic stage of the disease, with the callosal body showing thinning compared to pre-symptomatic HD patients (Di Paola, et al., 2012). In symptomatic HD, the anterior corpus callosum was found to be affected using probabilistic tractography (S. Klöppel, et al., 2008). MRI metrics obtained from the corpus callosum have been found to correlate with behavioural measures in HD, with both motor and cognitive scores correlating with diffusivity values in the corpus callosum (Bohanna, Georgiou-Karistianis, Sritharan, et al., 2011; Dumas, et al., 2012).

The corpus callosum is not a homogenous tract, with fibers varying in terms of size and age of myelination; larger and early myelinated fibers are found in posterior callosal regions whereas smaller and late myelinating fibers are found in anterior regions (Aboitiz & Montiel, 2003; Aboitiz, Scheibel, Fisher, & Zaidel, 1992). Thus, analysing the corpus callosum in terms of sub-divisions rather than as a uniform tract may be more fruitful in understanding pathology and regional differences in HD in terms of changes in myelination and/or axonal structure.

### *Corticospinal Tract*

The corticospinal tract is the main white matter pathway that carries motor signals from the spinal cord to the motor cortex. Approximately half of the population of white matter fibers in the corticospinal tract originate from the primary motor cortex (Kandel, Schwartz, & TM, 2000; Schultz, 2001), and motor dysfunction in HD has been found to be correlated with cell loss in the primary motor cortex (E. H. Kim et al., 2014; Thu et al., 2010) whilst altered functional (BOLD) activation in this area has been reported (Georgiou-Karistianis, Poudel, et al., 2013). The pathway is connected to the basal ganglia, which is the hallmark area of neuropathology in HD, and as with the corpus callosum, the majority of fibers originate from pyramidal cells in the cerebral cortex, which are known to be affected in HD. In terms of function, the corticospinal tract is involved in voluntary movement (Kandel, et al., 2000; Schultz, 2001), which is altered in HD, with reduced precision on a self-paced timing motor task (Rowe et al., 2010) and evidence of disordered eye movements (Patel, Jankovic, Hood, Jeter, & Sereno, 2012).

Only a handful of studies have examined changes in the corticospinal tract in HD, with macrostructural changes reported in the internal capsule from VBM studies (Della Nave, et al., 2010; Fennema-Notestine, et al., 2004) and microstructural changes in the internal capsule from diffusion tensor ROI studies (Magnotta et al., 2009; H. Rosas, et al., 2006), whilst CAG repeat length and motor score were related to the degree of atrophy in the internal capsule (Hobbs, et al., 2010). Phillips and colleagues (2014) were the first to examine the corticospinal tract as a distinct fiber pathway. The authors used diffusion tensor based tractography to reconstruct the tract in both pre-symptomatic and early-HD patients, and found a reduction in fractional anisotropy (FA), an increase in diffusivity values (radial diffusivity [RD] and axial diffusivity [AD]), and cortical thinning in the primary motor cortex bilaterally in HD patients compared to both controls and pre-HD patients. Pre-HD patients had higher RD values compared to controls. A limitation of this study is the reliance on the tensor model to reconstruct the pathway, which can lead to erroneous fiber tractography results in areas where fiber bundles cross each other. This is an issue in the corticospinal tract, where the lateral projections to the upper extremity and face region of the motor cortex intersect the superior longitudinal fasciculus. Previous work has demonstrated that with single tensor tractography, only part of the corticospinal tract is reconstructed, whereas a two-tensor deterministic streamline tractography algorithm was able to accurately identify fiber bundles consistent with anatomy (Qazi et al., 2009). Thus, this limitation will be addressed in this chapter through the use of high-angular resolution diffusion imaging (HARDI) and tractography analysis based on spherical deconvolution.

### *Cingulum Bundle*

The cingulum bundle is the most prominent white matter fiber tract in the limbic system and contains afferent and efferent fibers of different lengths (Mufson & Pandya, 1984) with the longest fibers running from the anterior temporal gyrus to the orbitofrontal cortex (Catani, Howard, Pajevic, & Jones, 2002). Anatomically, the tract is longitudinally oriented above the corpus callosum from the genu to the splenium and underlies the cingulate cortex. It is a complex tract, with work in the primate brain showing that the cingulum contains afferent and efferent short U fibers associated with the rostral, mid, and caudal cingulate cortices and connections to the medial and dorsal prefrontal, parietal, occipital, and temporal lobes (Catani, et al., 2002).

The cingulum is known to be involved in attention, memory and emotions (Catani & Thiebaut de Schotten, 2008) and although the cingulate cortex has been implicated in HD, with major loss of interneurons found in the anterior cingulate cortex in HD (Kim, et al., 2014) and loss of pyramidal projection neurons in the cingulate gyrus (Cudkowicz & Kowall, 1990) the cingulum bundle has not yet been examined in HD.

Reconstructions of the cingulum bundle using diffusion tractography have tended to portray the cingulum as a continuous white matter pathway (Catani & Thiebaut de Schotten, 2008) whereas the cingulum is not uniform in terms of the underlying function of the white matter connections, and instead consists of three major fiber components, originating from the thalamus, cingulate gyrus, and cortical association areas (Armstrong, 1990; Bürgel et al., 2006) with only a small fraction of the total white matter in the cingulum traversing the length of the tract. It was recently shown that the diffusion tensor metrics varied significantly between different subdivisions of the cingulum bundle corresponding to known anatomical connectivity (Jones, Christiansen, Chapman, & Aggleton, 2013), with the ‘parahippocampal’, ‘retrosplenial’, and ‘subgenual’ portions of the cingulum forming a topographic arrangement of cingulum fibers. Whereas the subgenual subdivision is implicated more in top-down attentional control, goal-directed behaviour, motivation, reward and cognitive modulation of affect (Amft et al., 2014; Vann, Aggleton, & Maguire, 2009), all of which are clinical features of HD, the retrosplenial subdivision, which contains connections to the retrosplenial cortex, has been implicated more in memory processes, such as scene learning and episodic memory (Vann, et al., 2009). The retrosplenial cortex has been shown to have correlated activity with the thalamus (Aggleton & Nelson, 2014; Vogt, Vogt, & Laureys, 2006), a key relay system in the basal ganglia, which is known to be affected in HD. Thus, based on the symptom profile in HD and the known neuropathology, it is possible that both the subgenual and retrosplenial cingulum fibers are affected in HD but not necessarily in the same way.

Thus, the overall aim of this chapter was to characterise the tissue microstructure along three white matter pathways that are implicated either theoretically or empirically in HD using multi-modal MRI acquisitions, in order to achieve both a sensitive and specific characterisation of white matter abnormalities in pre-symptomatic and early-stage HD.

## Methods

### *Participants*

A sub-set of participants comprising 14 HD gene-positive ( 10 pre-symptomatic, 4 early HD) and 13 healthy controls underwent a more extensive MRI scan session to examine changes in white matter. For one HD participant, it was not possible to acquire all of the sequences due to severe HD-related motion in the scanner. For the mcDESPOT acquisition, data were not acquired for 2 HD participants due to specific absorption rate (SAR) concerns related to MRI contraindications and weight limits. The mcDESPOT data were not acquired for a further HD participant due to a technical fault at the end of the scan session.

### *Psychometric data*

Outcome measures from the computer-based cognitive battery described fully in Chapter 2, were analysed using a principal components analysis (full details in chapter 3), and the composite cognitive values were used to examine relationships with white matter microstructure. In addition, the majority of HD participants recruited were also enrolled on the longitudinal REGISTRY study, which involves yearly assessments by a trained research nurse. Thus, there was data available from the most recent REGISTRY study (within the past 12 months), including the UHDRS assessment ("Unified Huntington's Disease Rating Scale: reliability and consistency. Huntington Study Group," 1996). The UHDRS motor score, total functional capacity, independence and UHDRS functional score were therefore also used as variables to examine relationships with white matter microstructure. The UHDRS cognitive score was not used as not all HD participants had completed this component, thus the sample size was too small to examine meaningful relationships. Finger tapping speed was also used as a measure of motor speed, which was recorded on the day of the MRI session. For details on the UHDRS, see Chapter 2.

## *MRI Data Acquisition*

As detailed in chapter 2, two different diffusion MRI sequences were acquired in order to perform the tractography analysis. Whole brain tractography was performed on a HARDI-based sequence more suited for recovering fibre orientations through spherical deconvolution approaches (b-value = 2000 s/mm$^2$, 45 gradient directions) and the tensor based metrics along the reconstructed tracts were then obtained from a co-registered diffusion sequence optimised for tensor based metrics (b-value = 1000 s/mm$^2$, 30 isotropic gradient directions). A multi-shell CHARMED sequence was acquired in order to obtain a measure of restricted volume fraction. The sequence used 8 shells (1093, 2188, 3281, 4375, 5469, 6563, 7656, and 8750 s/mm$^2$) and 40 gradient orientations. A Multi-Component Driven Equilibrium Single Pulse Observation of T1/T2 (mcDESPOT) (S. Deoni, et al., 2008a) protocol was acquired to measure myelin water fraction. The protocol combined spoiled gradient echo (SPGR), balanced steady state free precession (bSSFP) and inversion-recovery prepared SPGR (IR-SPGR) sequences according to Deoni et al. (2008). The acquired $T_1$-weighted FSPGR scan was used for image registration.

### *MRI Post-processing*

For the acquired diffusion images, ExploreDTI software (Leemans, et al., 2009) was used for image pre-processing. As shown in Figure 4.1, images were corrected for distortions due to motion and the tensor was estimated using the RESTORE algorithm (Chang, et al., 2005) as detailed in Chapter 2. Images were corrected for EPI distortions using a non-rigid registration of the FA map to the $T_1$-weighted map which had the same image contrast as the participants FSPGR image.

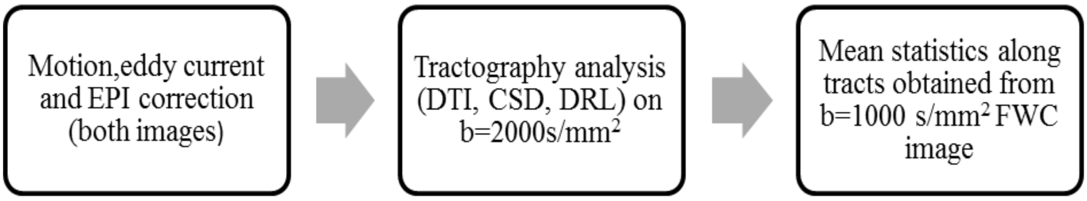
Motion,eddy current and EPI correction (both images)
Tractography analysis (DTI, CSD, DRL) on b=2000s/mm²
Mean statistics along tracts obtained from b=1000 s/mm² FWC image

Figure 4.1 Analysis pipeline for both the low and high b-value diffusion MRI images. ExploreDTI software (Leemans, et al., 2009) was used for all steps. FWC: free water correction (Pasternak, et al., 2009).

There were 4 resolution steps, 20000 data samples, and the deformations were constrained to the phase-encoding direction of the diffusion acquisition. The images were then corrected to account for contamination due to free water using the Pasternak approach (Pasternak, et al., 2009). Free water volume fraction maps were examined to look for differences due to gene status.

In order to obtain a measure of myelin water fraction, the image maps was linearly registered to the $T_1$-weighted image using 6 degrees of freedom using FMRIB's Linear Image Registration Tool (FLIRT) (Jenkinson & Smith, 2001). For the restricted volume fraction obtained from the CHARMED analysis, linear registration did not produce satisfactory results, thus registration was conducted using the *ELASTIX* software (Klein, Staring, Murphy, Viergever, & Pluim, 2010; Shamonin et al., 2013) where the combination of a rigid and a B-spline transform is applied. All registrations were visually inspected for accuracy.

### ***Deterministic Tractography***

Deterministic whole-brain tractography (Basser, et al., 2000) was performed using the tensor model, and 2 different high-angular resolution diffusion imaging (HARDI) spherical deconvolution methods, constrained spherical deconvolution (CSD) (Tournier, et al., 2004; Tournier, et al., 2008) and the iterative damped Richardson Lucy (DRL) approach (Dell'acqua, et al., 2010). The SD approaches were chosen due to the well-established limitations of tensor-based tracking in resolving voxels containing multiple fiber orientations. Many of the candidate pathways were in regions of crossing/kissing fiber combinations, thus tensor-based tracking was insufficient for this purpose.

The selected tracking algorithm was able to reconstruct fibers by estimating the fODF peak at each seed-point and then propagating from here in 0.5 mm steps along the axis subtending the smallest angle to the current trajectory, thus allowing for multiple fiber orientations within a voxel. A fiber pathway was traced through the data for fibers greater than 5 mm in length and less than 500 mm in length until the fODF fell below an arbitrary threshold (0.1) or the direction of the pathway changed through an angle greater than 45°. The SH order was 8 and for both CSD and DRL, for one fiber profile, the expected ADC ($mm^2/s$) was 0.0007 and FA was 0.8. DRL algorithm parameters were $\alpha$ =1, algorithm iteration = 400, $\eta$ =0.06 and $\nu$ =8 as regularisation terms.

### P*arcellation of the corpus callosum*

The corpus callosum was reconstructed using the Hofer and Frahm (2006) approach (Figure 4.2) which uses 5 vertical subdivisions to parcellate the corpus callosum in accordance with defined cortical connections. Briefly, a geometric baseline was established in the midsaggital slice by connecting the most anterior and posterior points of the corpus callosum. Seed points were drawn on this mid-sagittal slice, and NOT gates used to remove spurious fibers not travelling to the cortical region.

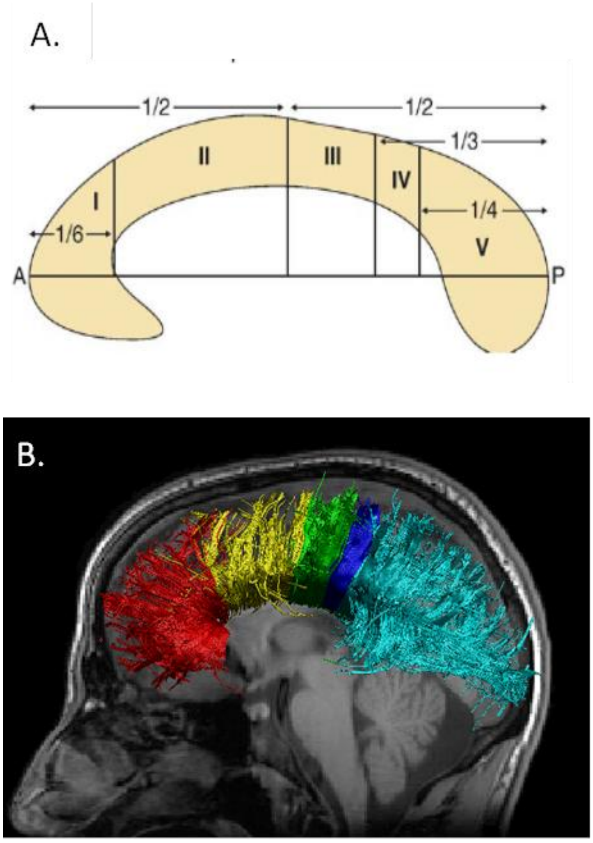

Figure 4.2 A. Schematic of corpus callosum parcellation. Reproduced from Hofer & Frahm (2006). B. Transcallosal fiber tracts from a single male healthy control subject overlaid onto native T1 reference image. Sagittal view of reconstructed fibers projecting into the prefrontal lobe (red), premotor and supplementary motor areas (yellow), primary motor cortex (green), primary sensory cortex (dark blue), parietal, occipital and temporal lobe (light blue).

***Parcellation of the cortico-spinal pathway***

The corticospinal tract (CST) was defined as pathways between the primary motor cortex and the midbrain. The first ROI was drawn in the axial plane to include the entire cerebellar peduncle at the level of the decussation of the superior cerebellar peduncle, which is a clear anatomical landmark that can be seen in Figure 4.3, marked by an arrow. The ROI was drawn on the most dorsal slice where the decussation was visible. The registered T1-weighted image was used to aid in the identification of the central sulcus. A second ROI was then drawn in the primary motor cortex on the axial slice. A 'NOT' operation was placed in the mid-sagittal slice to remove any streamlines entering the contralateral hemisphere.

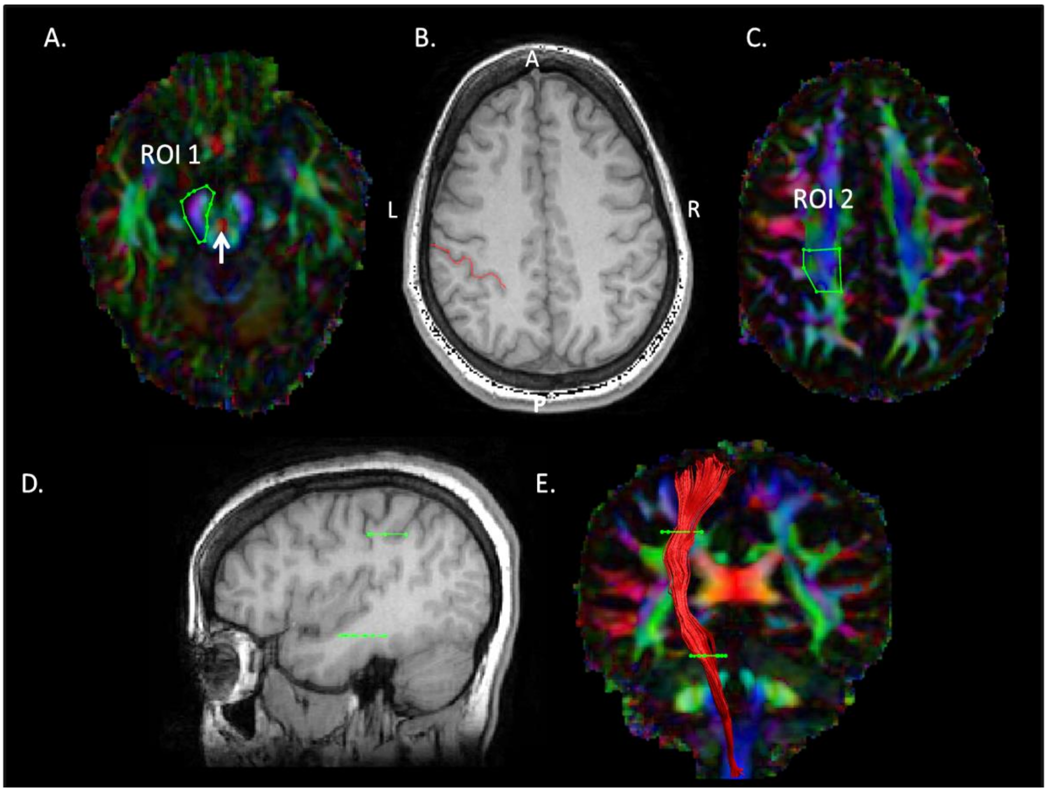

Figure 4.3 Parcellation of the Corticospinal Tract. A. Placement of ROI on most dorsal axial slice where the decussation of the cerebellar peduncle (arrow) is seen. B. Identification of the central sulcus (red line) in the left hemisphere on the $T_1$ image. C. Placement of ROI on axial slice in the primary motor cortex, D. Position of both ROI's from a sagittal view, imposed on the $T_1$ image. E. Reconstructed tracts in the coronal plane shown on the colour-coded principal component image.

### *Parcellation of the cingulum*

The cingulum and the subgenual and retrosplenium subdivisions were parcellated according to the protocol detailed by Jones et al. (2013) for all participants, as shown in Figure 4.4. Briefly, for each hemisphere, the parasagittal level that provided the most extensive visualisation of the cingulum bundle was identified and the position of the corpus callosum in that same plane was used to derive a set of fixed landmarks for subsequent ROIs. For all segmentation, "NOT" ROIs were occasionally placed after visual inspection to exclude any outlier tracts that were inconsistent with the known anatomy of the cingulum bundle.

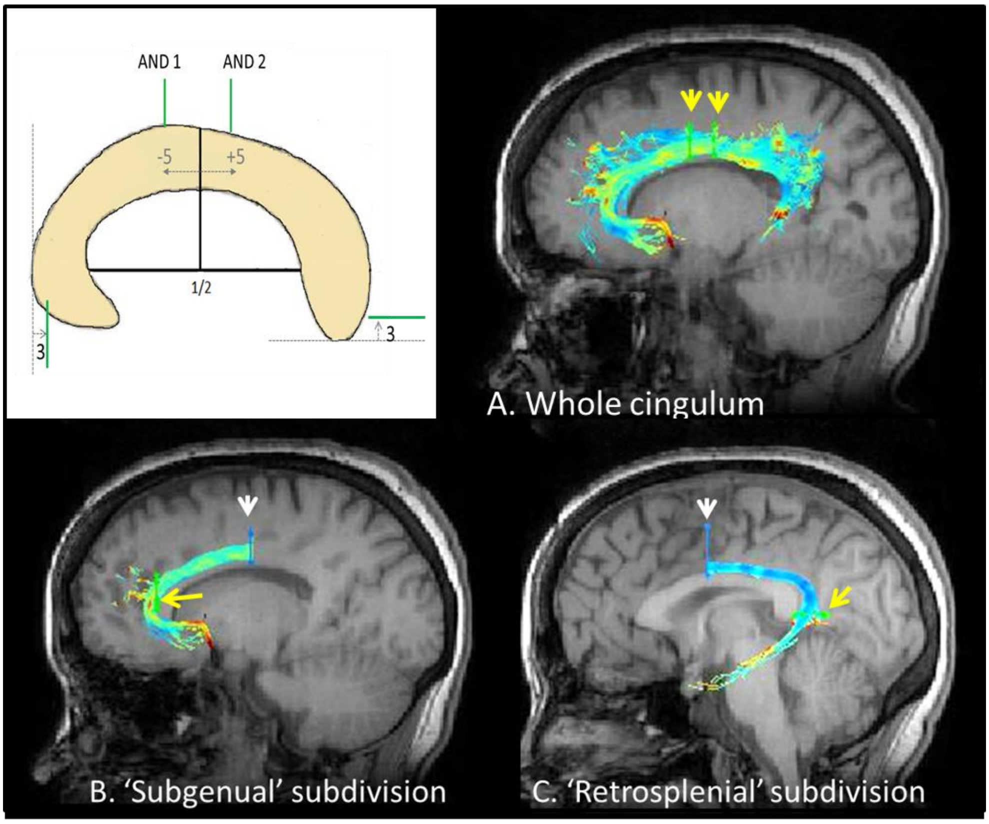

Figure 4.4 Segmentation of the cingulum bundle. Schematic shows placement of ROI's (green lines) with reference to anatomical landmarks (dashed lines). A-C show reconstructed tracts from one control participant shown colour-coded for mean diffusivity (MD) and overlaid on a $T_1$-weighted image. ROI's shown: seed point 'OR' gates in blue (white arrows), 'AND' gates are in green (yellow arrows).

***Whole Cingulum*** The rostral–caudal midpoint of the body of the corpus callosum was first determined, defined as the mid-way point between the back of the curve of the genu (i.e., its most posterior part at the flexure) and the front of the splenium (i.e., its most anterior part at the flexure). The two AND gates were drawn in the coronal plane on the coronal sections five slices anterior and five slices posterior to the rostral–caudal midpoint. All streamlines that passed through both regions of interest were retained as 'cingulum' pathways.

***'Subgenual' subdivision*** Two ROIs was employed. One ROI was in the same location as the caudal ROI used for the whole cingulum reconstruction (AND 2 in Figure 4.4), and the second ROI was placed in the subgenual part of the cingulum on the third coronal slice caudal to the most anterior part of the genu.

***'Retrosplenial' subdivision*** Two ROIs were used for dissecting the 'retrosplenial' subdivision. One ROI was placed in the same location as the rostral ROI used for the whole cingulum (AND 1 in Figure 4.4). The location of the second ROI was determined by finding the most ventral plane of the splenium and was drawn in the axial plane three axial slices above the base of the splenium.

### *Statistical analysis*

A mixed-model ANOVA was used to examine the effect of HD on white matter pathways, with disease status (control, HD) as the between-subject variable, and/or segment (for corpus callosum and cingulum) and hemisphere (for cingulum and corticospinal tract) as within-subject factors. Where age was found to correlate with the dependent variable (defined as $r > 0.30$); age was added as a covariate to the analysis (see Appendix 3 for statistical tests). The assumptions of a mixed-model ANOVA were tested (see Appendix 3) and appropriate corrections made where assumptions were violated. For diffusion tensor metrics, FA and MD values were principally examined. Where significant main effects of interactions surviving post-hoc analysis were found, the component AD and RD values were then examined.

A mixed-model ANOVA was also used to examine the effect of the choice of tractography algorithm, with 2 within-subject factors (callosal segment and algorithm) and 1 between-subject factor (gene status).

A correlational analysis was conducted to assess the relationship between composite cognitive scores (see chapter 2 for details on PCA), motor speed on the Speeded Finger Tapping test, UHDRS scores and MR measures. Normality testing on the composite cognitive scores found data was normallydistributed at $\alpha = 0.001$. Where age was found to be significantly correlated with any of the measures, a partial correlational analysis was performed with age partialled out.

## Results

### *Corpus Callosum Reconstructions with different tractography algorithms*

There was a significant interaction between corpus callosum segment and tractography algorithm for FA values, F (2, 26) =10.27, $p \leq 0.001$. Post-hoc analyses found that there was a significant effect of algorithm choice on FA values in every segment ( segment I : F (2,46 ) = 5.89, $p \leq 0.05$ FDR-adjusted; segment II: F (2,38) = 15.15 $p \leq 0.001$ FDR-adjusted; segment III: F (2,40) = 12.31, $p \leq 0.001$ FDR-adjusted, segment IV : F (2,36) = 16.97, $p \leq 0.001$ FDR-adjusted; segment V: F (2,30) = 19.69, $p \leq 0.001$ FDR-adjusted). Paired t-tests found that DTI tracking produced significantly higher FA values in comparison to both CSD and DRL tracking results in callosal segments II – V ( all $p \leq 0.05$ FDR-adjusted), whereas FA values were not significantly different across algorithms in the most anterior callosal segment, $p > 0.05$. FA values sampled by CSD compared to DRL tracking did not differ in segments I – IV, whereas in the most posterior segment, DRL tracking produced higher FA values compared to CSD, $p = 0.045$ FDR-adjusted. There was no main or

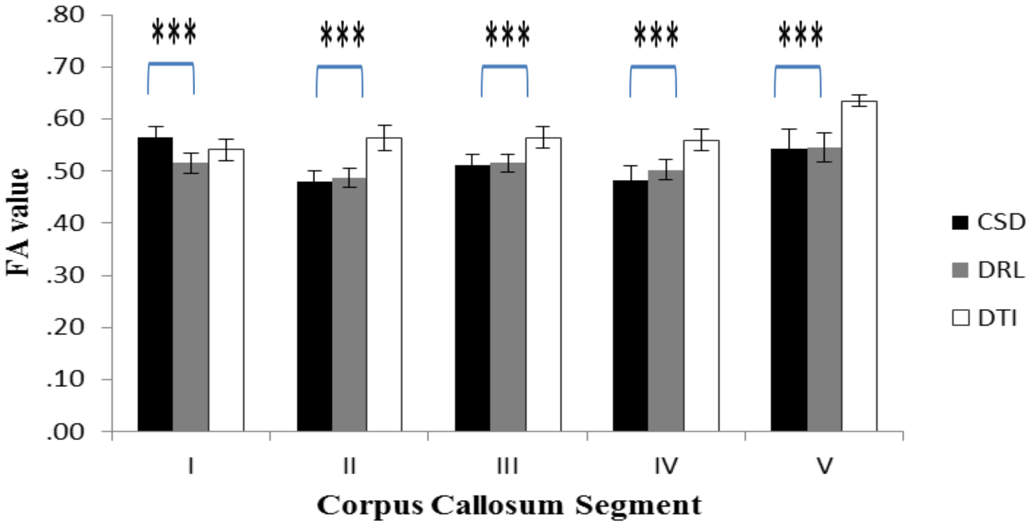

Figure 4.5 The effect of tracking algorithm on fractional anisotropy (FA) estimates in different segments of the corpus callosum. Error bars represent ± standard error of the mean. *** represents statistical significant of $p < 0.001$ for the main effect of tractography algorithm (no post-hoc tests shown).

interactive effect of tractography algorithm on MD values in the corpus callosum when age was added as a covariate, all $p > 0.05$

In terms of the effect of gene status on MR measures, there was a discrepancy between a main effect versus an interactive effect for FA values estimated with CSD compared to DRL, and a difference in the degree of significance for MD values. Using CSD as the tractography algorithm, there was a significant interaction between callosal segment and gene status for FA values, F (4, 56) = 2.59, $p \leq 0.05$. Post-hoc t-tests revealed a significant reduction in FA in segment II, which contains motor connections, and in segment V, which contains parietal, temporal and occipital connections in HD participants compared to controls, t (19) = 2.13, and t (17) = 2.24 respectively, $p \leq 0.05$ uncorrected. This did not survive correction for multiple comparisons using the FDR, all $p > 0.05$. HD participants had significantly higher MD values in the corpus callosum, F (1, 18) = 4.63, $p \leq 0.05$, although this did not survive correction for multiple comparisons. Post-hoc analysis of the component eigenvalues AD and RD found no difference between HD and control participants, $p > 0.05$.

In contrast, when using DRL as the algorithm, FA was significantly lower in HD participants compared to controls, F (1, 19) = 4.51, $p \leq 0.05$ uncorrected, $p > 0.05$ FDR-corrected, and there was no interaction with callosal segment, $p > 0.05$. MD was significantly higher in HD participants compared to healthy controls, F (1, 22) = 8.14, $p \leq 0.05$ FDR-corrected. Post-hoc analysis of the component eigenvalues AD and RD found no difference between HD and control participants for both algorithms, $p > 0.05$. All results were corrected for partial volume effects, however there was no effect of gene status on free water fraction, F (1, 19) = 2.99, $p > 0.05$ for CSD, and F (1, 21) = 0.467, $p > 0.05$ for DRL. There was a trend for myelin water fraction to be reduced in the corpus callosum in HD participants, with the magnitude of difference being greater than 10% in more anterior callosal segments, as shown in Table 4.1. However, this difference was not statistically significant when derived from tractography using CSD, F (1, 15) = 1.44, $p > 0.05$, or from tractography using DRL, F (1, 18) = 2.51, $p > 0.05$.

Results from CSD and DRL converged to show no difference in restricted volume fraction (a proxy estimate of ‘axon density’) from the CHARMED analysis between HD and control participants, F (1, 19) = 2.83, and F (1, 23) = 1.152 respectively, both $p > 0.05$. For both algorithms, and as with the other measures, there was a main effect of callosal segment, Greenhouse-Geisser adjusted F (2.63, 49.94) = 6.77, and F (2.51, 57.74) = 17.74, $\varepsilon = .657$ and .628 respectively, both $p < 0.05$, but no interaction between gene status and segment, $p > 0.05$.

When using DTI as the tractography algorithm, there was no main effect of gene status for FA values across the corpus callosum, F (1,17) = 0.467, $p > 0.05$, although there was a significant difference in FA values depending on callosal segment, F (4,68) = 12.44, $p \leq 0.001$. HD participants had significantly higher MD values in the corpus callosum, F (1, 22) = 9.96 $p \leq 0.01$, with no interaction across different callosal segments. There was no effect of gene status on myelin water fraction or restricted volume fraction in the corpus callosum derived from tractography using DTI, F (1,18) = 2.25, $p > 0.05$ and F (1,21) = 1.03, $p > 0.05$ respectively. All results were corrected for partial volume effects, however for the free water fraction, there was an interaction between gene status and callosal segment, Greenhouse-Geisser adjusted F (2.63, 49.96) = 3.63, $p \leq .05$, $\varepsilon = 0.66$. Post-hoc tests found a difference between controls and HD participants specifically in segment II and V, F (1, 18) = 4.58 and 6.75 respectively, $p \leq 0.05$; however these results did not survive correction for multiple comparisons using the FDR, all $p > 0.05$.

### *Relationship between corpus callosum and disease burden in HD*

In measures obtained using the CSD algorithm, disease burden was positively correlated with free water fraction in the first 3 segments of the corpus callosum, r = .584 , .683,  .670 respectively, $p < 0.05$ uncorrected, whereas no relationship was found in the 4th and 5th segments, $p > 0.05$. Restricted volume fraction was negatively correlated with disease burden in the second callosal region which contains inter-hemisphere connections to the premotor and supplementary motor areas, r = -.65, *n = 10*, $p < 0.05$ uncorrected, however did this not survive correction for multiple comparisons. Similarly, a negative relationship was found between disease burden and myelin water fraction in the same callosal region (segment II), with a higher disease burden associated with a reduction in myelin water fraction in these tracts, r = -.89, *n = 7*, $p < 0.01$ uncorrected. This result did survive FDR-correction across myelin water fraction measures in the 5 segments, $p < 0.05$, however did not survive correction across both the 5 segments and the 4 remaining outcome measures (FA, MD, FWF, restricted volume fraction) , with 25 comparisons in total.

In measures obtained using the DRL algorithm, disease burden was positively correlated with free water fraction in the 2nd and 3rd segment, r = .58 and .69, $p < 0.05$ uncorrected, similar to the findings with CSD tracking. MD values were positively correlated with disease burden in the 3rd and 4th segments, which contain inter-hemispheric connections to the primary motor and primary sensory cortex respectively, r = .655 and .723, $p < 0.05$ uncorrected. The result in the 4th segment survived FDR-correction across MD measures in the 5 segments, $p < 0.05$, however did not survive correction for all 4 outcomes measures and 5 segments combined.

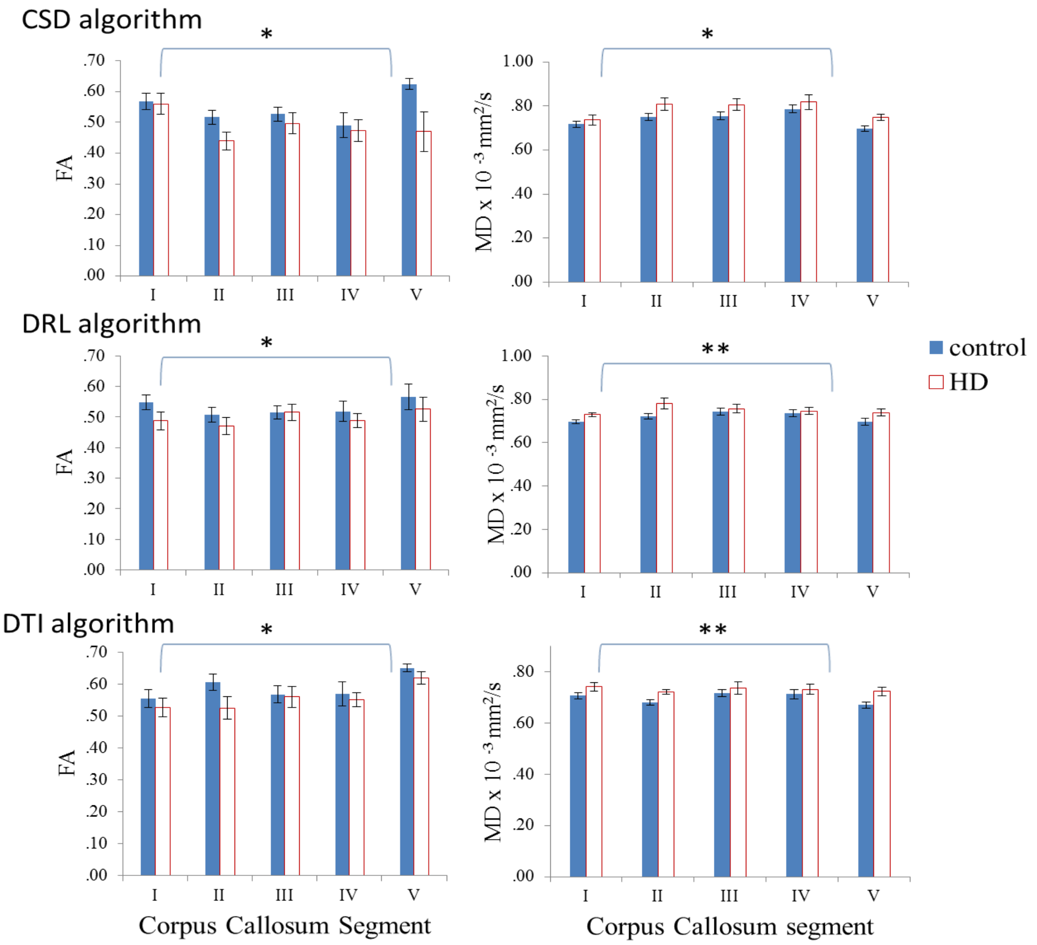

Figure 4.6 Average tensor metrics in each segment of the corpus callosum obtained using different tractography algorithms. * $p \leq 0.05$, ** $p \leq 0.01$ significant level. Error bars represent ± standard error of the mean

### Relationship between corpus callosum and motor dysfunction

In HD participants [ n =13], a negative correlation was found between average free water fraction across the segments of the corpus callosum reconstructing using DRL tracking, and finger tapping speed, r = -.609, $p < 0.05$ uncorrected. Similarly, a strong negative correlation was found between free water fraction across the segments of the corpus callosum reconstructing using both DRL and CSD tracking algorithms, and UHDRS Total Functional Capacity [ *n =9*], r = -.899 and -.901 respectively, $p < 0.05$ FDR-corrected. Additionally, for tracts sampled by CSD, a significant relationship was found with UHDRS motor score and FA, MD and restricted volume fraction in the corpus callosum, r = -.859, -.765, and -.794 respectively, all $p < 0.05$ FDR-corrected.

### Relationship between corpus callosum and cognitive scores

Partial correlations were conducted between the composite cognitive score produced in chapter 3, and the metrics obtained along the corpus callosum segments, with age partialled out. In the HD participants, and using values obtained from the DRL algorithm, a negative relationship was found between cognitive score and MD in the corpus callosum segment containing inter-hemispheric pre-motor and supplementary motor area connections, r = -.668, df = 8, $p < 0.05$ uncorrected, $p > 0.05$ FDR-corrected. The same relationship was less strong when the corpus callosum was reconstructed using CSD, r = -.583, $p > 0.05$. There were no significant relationships between cognitive score and average MR measures in the control group.

Table 4.1 Corpus Callosum Reconstruction. Descriptive statistics for the non-tensor based metrics using different tractography algorithms. Standard error of the mean shown in blue.

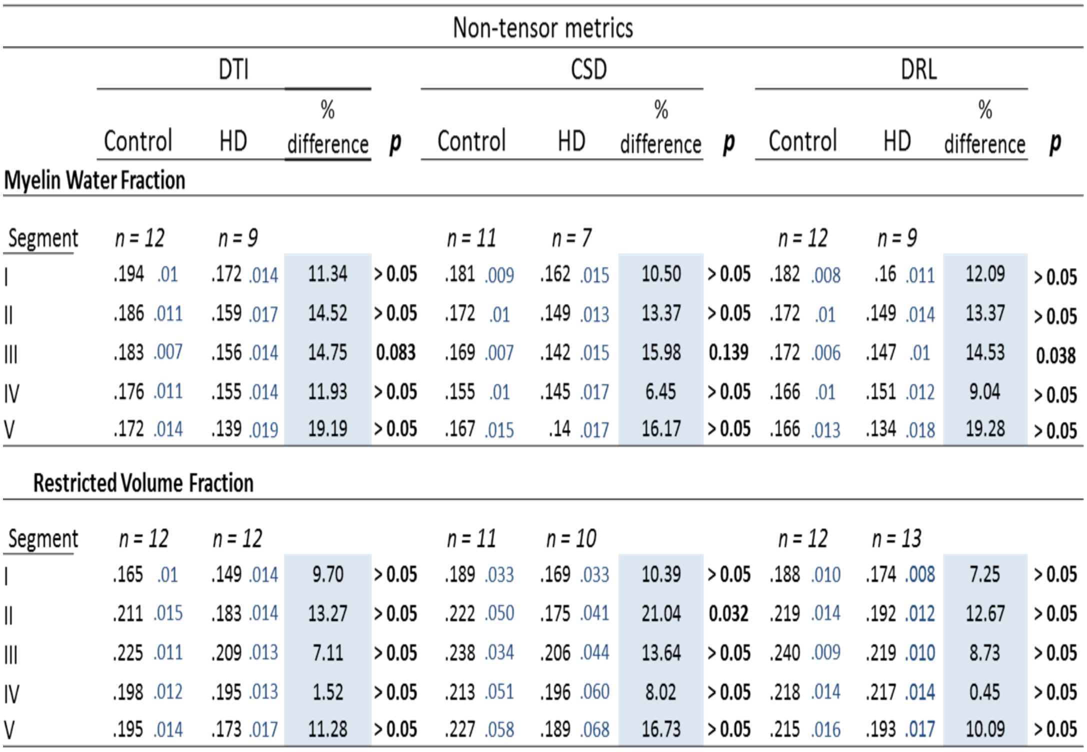

| Non-tensor metrics | | | | | | | | | | | | |
|---|---|---|---|---|---|---|---|---|---|---|---|---|
| | DTI | | | | CSD | | | | DRL | | | |
| | Control | HD | % difference | **p** | Control | HD | % difference | **p** | Control | HD | % difference | **p** |
| **Myelin Water Fraction** | | | | | | | | | | | | |
| Segment | n = 12 | n = 9 | | | n = 11 | n = 7 | | | n = 12 | n = 9 | | |
| I | .194 .01 | .172 .014 | 11.34 | > 0.05 | .181 .009 | .162 .015 | 10.50 | > 0.05 | .182 .008 | .16 .011 | 12.09 | > 0.05 |
| II | .186 .011 | .159 .017 | 14.52 | > 0.05 | .172 .01 | .149 .013 | 13.37 | > 0.05 | .172 .01 | .149 .014 | 13.37 | > 0.05 |
| III | .183 .007 | .156 .014 | 14.75 | 0.083 | .169 .007 | .142 .015 | 15.98 | 0.139 | .172 .006 | .147 .01 | 14.53 | 0.038 |
| IV | .176 .011 | .155 .014 | 11.93 | > 0.05 | .155 .01 | .145 .017 | 6.45 | > 0.05 | .166 .01 | .151 .012 | 9.04 | > 0.05 |
| V | .172 .014 | .139 .019 | 19.19 | > 0.05 | .167 .015 | .14 .017 | 16.17 | > 0.05 | .166 .013 | .134 .018 | 19.28 | > 0.05 |
| **Restricted Volume Fraction** | | | | | | | | | | | | |
| Segment | n = 12 | n = 12 | | | n = 11 | n = 10 | | | n = 12 | n = 13 | | |
| I | .165 .01 | .149 .014 | 9.70 | > 0.05 | .189 .033 | .169 .033 | 10.39 | > 0.05 | .188 .010 | .174 .008 | 7.25 | > 0.05 |
| II | .211 .015 | .183 .014 | 13.27 | > 0.05 | .222 .050 | .175 .041 | 21.04 | 0.032 | .219 .014 | .192 .012 | 12.67 | > 0.05 |
| III | .225 .011 | .209 .013 | 7.11 | > 0.05 | .238 .034 | .206 .044 | 13.64 | > 0.05 | .240 .009 | .219 .010 | 8.73 | > 0.05 |
| IV | .198 .012 | .195 .013 | 1.52 | > 0.05 | .213 .051 | .196 .060 | 8.02 | > 0.05 | .218 .014 | .217 .014 | 0.45 | > 0.05 |
| V | .195 .014 | .173 .017 | 11.28 | > 0.05 | .227 .058 | .189 .068 | 16.73 | > 0.05 | .215 .016 | .193 .017 | 10.09 | > 0.05 |

### *Cortico-spinal tract*

Descriptive statistics for all outcome measures are shown in Figure 4.7. Mixed-model ANOVA found no difference between CSD and DRL sampling for any measure. Both CSD and DRL algorithms found no difference between HD and control participants in FA and MD values in the corticospinal tract (*CSD: F (1, 20) = 1.01, and F (1, 19) = 1.74 respectively; DRL: F (1, 21) = 0.128, and F (1, 22) = 2.90 respectively; all p > 0.05).*

For the non-tensor based metrics, there was also no difference in myelin water fraction and restricted volume fraction between HD and control participants using either the CSD or DRL algorithm (*CSD: F (1, 16) = 2.43, and F (1, 20) = 1.74 respectively; DRL F (1, 17) = 1.42, and F (1, 22) = 0.236 respectively; all p > 0.05).* There was also no difference between HD and control participants for free water fraction (*CSD: F (1, 20) = 3.24; DRL: F (1,22) = 0.260; both p > 0.05),* although there was a difference between hemispheres using CSD, with a higher fraction in the right corticospinal tract compared to in the left hemisphere, F (1, 20) = 6.04, $p < 0.05$.

### *Relationship between microstructure and disease burden in HD*

There was no relationship between disease burden and tensor based metrics estimated obtained using the CSD algorithm [*n =12*], all $p > 0.05$. In contrast, when using the DRL algorithm [*n =13*], a positive relationship was found between disease burden and MD values in the left corticospinal tract, r = .615, $p < 0.05$ uncorrected, and between disease burden and free water fraction in the left and right hemisphere alike, r = .775 and .821 respectively, $p < 0.05$ FDR-corrected.

### *Relationship between microstructure and motor/functional dysfunction in HD*

The relationship between baseline UHDRS motor scores and metrics obtained in the corticospinal tract was not significant, $p > 0.05$. A significant negative relationship was found between the UHDRS functional assessment (high score = high functional ability), which is focused on assessing whether an individual can engage in everyday tasks (e.g. management of finances, grocery shops), and MD in the left corticospinal tract, r = - .777, $p < 0.05$ FDR-adjusted. There was no relationship between MR measures obtained from either DRL and CSD in the corticospinal tract and finger tapping speed.

For MR measures obtained using CSD whole-brain tracking, a significant positive correlation was also found between UHDRS motor score (high score = more impaired) and MD in the left and right corticospinal tract, r = .742 and .747, respectively, $p < 0.05$ FDR-corrected. There was no relationship between MR measures and any of the other UHDRS measures.

### Relationship between microstructure and cognitive scores

In the healthy control participants and in tracts obtained using the CSD algorithm, a strong positive relationship was found between FA in the left corticospinal tract (CST) and cognitive function, $r = 0.70$, $p < 0.05$ uncorrected, between myelin water fraction in the left CST and cognitive function $r = 0.669$, $p < 0.05$ uncorrected, and between restricted volume fraction in the left CST and cognitive functioning, r =0 .668, $p < 0.05$ uncorrected. The same relationships were not found in HD participants, $p > 0.05$.

When using tracts obtained using the DRL algorithm, the relationship between FA and cognitive functioning, myelin water fraction and cognitive functioning, and restricted volume fraction and cognitive functioning were all weak in healthy control participants, r = .148, .085 and .08 respectively, $p > 0.05$ and HD participants alike, r = -.079, - .311, .085 respectively, $p > 0.05$.

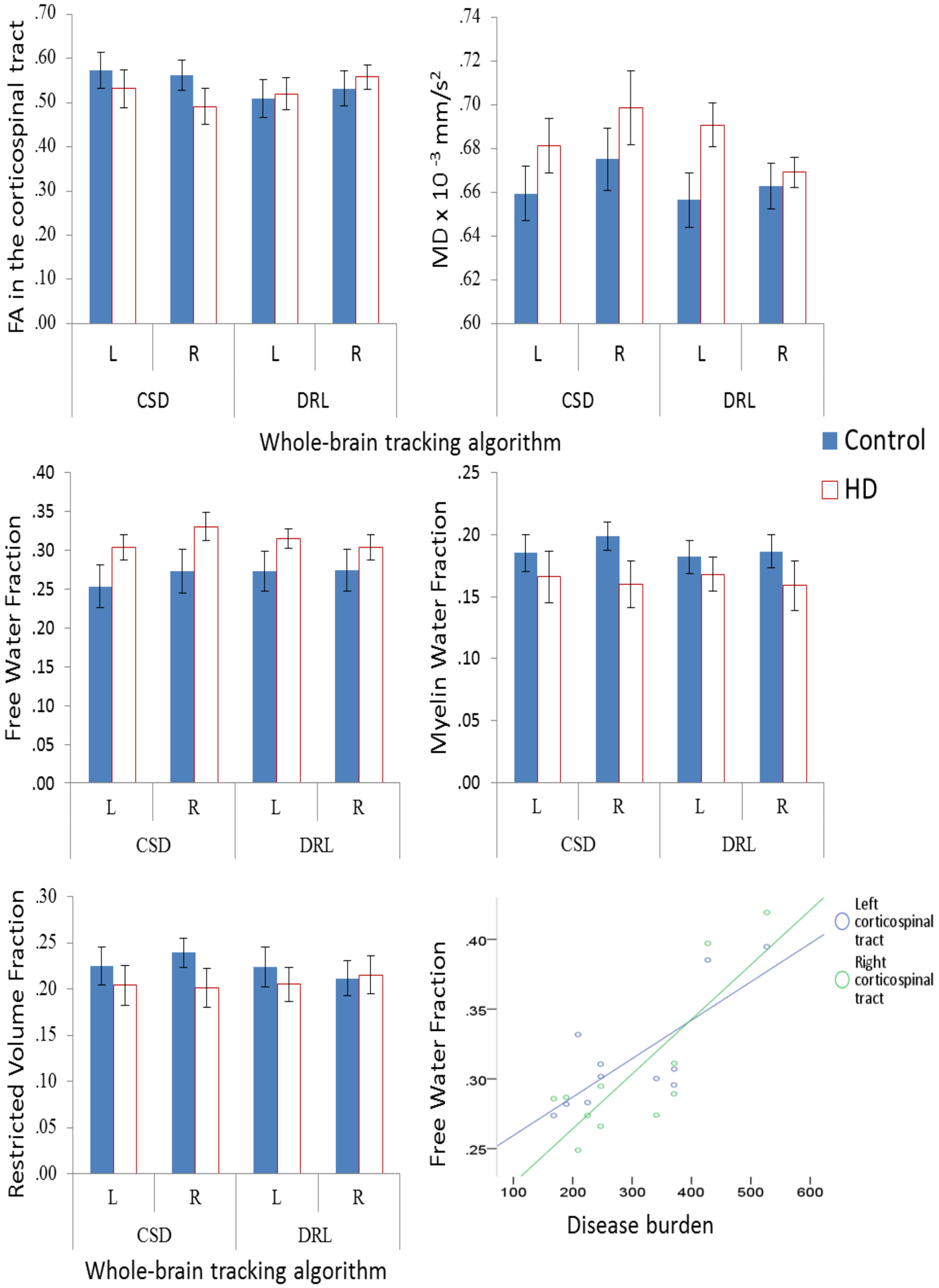

Figure 4.7 Results from the Corticospinal Tract reconstruction. Values are shown from tractography using two different spherical deconvolution approaches: constrained spherical deconvolution [CSD] (Tournier et al., 2008) and damped Richardson-Lucy [DRL] (Dell'acqua et al., 2010). Myelin water fraction obtained from multicomponent relaxometry, restricted volume fraction obtained from CHARMED, a multi-shell diffusion MR sequence. L: left hemisphere, R : right hemisphere. For the scatterplot, $r^2$ = .60 and .67 for left and right hemisphere respectively. Error bars represent standard errors of the mean.

### *Cingulum Bundle*

Reconstructing the cingulum bundle was not as effective with CSD-based whole brain tracking compared to DRL; 8/25 of the cases produced either very poor tract reconstructions not representative of known anatomy, or failed to reconstruct any tracts. The effect of this loss of data on an already small sample size meant that any statistical analysis would not be robust, thus only results from DRL reconstructions were statistically analysed.

### *Differences between HD participants and controls*

Mean tensor and non-tensor values are shown in Figure 4.8 along with standard errors of the mean.

***Whole cingulum*** For FA in the whole cingulum, there was a significant interaction between hemisphere and genotype, F (1, 17) = 4.76, $p < 0.05$. Post-hoc t-tests found a laterality effect in control participants, t (9) = -3.018, $p < 0.5$, but not in HD participants, t (8) = .480, $p > 0.05$. In the left hemisphere, FA was 10.7% higher in HD participants compared to controls, however this did not meet statistical significance, t (17) = -1.31, $p > 0.05$. In comparison, in the right hemisphere, the difference in FA between HD participants and controls was 0.79%, t (17) = .106, $p > 0.05$. There was no effect of gene status on MD values in the whole cingulum, F (1, 17) = .426, $p > 0.05$, and no interaction between gene status and hemisphere, F (1, 17) = .602, $p > 0.05$. Because of the interaction seen for FA, the component eigenvalues were examined. For both AD and RD values, there was no difference between HD and control participants, F (1, 17) = .281 and .049 respectively, $p > .05$, and no interaction between gene status and hemisphere, $p > 0.05$.

There was no effect of gene status on free water fraction values in the whole cingulum, F (1, 18) = .217, $p > 0.05$. Similarly, there was no difference in myelin water fraction, F (1, 14) = .138, $p > 0.05$, or restricted fraction, F (1, 18) = .018, $p > 0.05$.

***Subgenual Cingulum.*** There was no difference in FA values between HD and control participants in the subgenual section of the cingulum bundle, F (1, 21) = 1.36, $p > 0.05$. MD values were higher in HD participants compared to healthy controls, F (1, 21) = 6.86, $p < 0.05$ uncorrected. A main effect of hemisphere was also found, F (1, 21) =10.12, $p < 0.01$ uncorrected. Post-hoc analyses of the component eigenvalues found that whereas there was no difference between groups in axial diffusivity (AD, $\lambda_1$) values (F (1, 21) = 2.02, $p > 0.05$), radial diffusivity (RD; $[\lambda_2+\lambda_3]/2$) was significantly higher in HD participants (0 .54 ± .015 x$10^{-3}$ $mm^2/s$) compared to healthy control participants (0.50±0.016 x$10^{-3}$ $mm^2/s$), F (1,21) = 5.43, $p < 0.05$ uncorrected, $p > 0.05$ FDR-adjusted.

There was a trend towards higher free water fraction in HD participants [*n = 13, M = .344 ± .026*] compared to healthy controls [*n = 10, M=.268±.031*] in the subgenual cingulum, F (1, 21) = 3.97, p = 0.059.

Restricted volume fraction, a proxy for axon density, was found to be significantly reduced (-17.9% and -15.8% in the left and right hemisphere respectively) in HD participants compared to healthy controls, F (1, 21) = 8.50, $p < 0.05$ FDR-corrected. Myelin water fraction was reduced in HD participants [n=9] compared to control participants [n=10] in both the left (-16.70%) and right (-11.1%) hemisphere, however this difference did not survive statistical significance, F (1, 17) = 2.09, $p > 0.05$.

***Retrosplenial cingulum*** There was no difference in FA, MD or free water fraction between HD and control participants in the retrosplenial subdivision of the cingulum, $p > 0.05$. Similarly, there was no difference in myelin water fraction or restricted volume fraction between groups, $p > 0.05$.

### *Relationship between microstructure and disease burden*

***Whole cingulum*** As seen in Figure 4.8C, in the HD participants, free water fraction in the cingulum was positively correlated with disease burden, r = 0.746

and 0.669 in the left and right hemisphere respectively, $p < 0.05$ uncorrected, FDR-corrected $p > 0.05$.

***Subgenual subdivision*** Free water fraction in the left subgenual division of the cingulum was positively correlated with disease burden in the HD participants, r = .577, $p < 0.05$ uncorrected, FDR-corrected $p > 0.05$, see Figure 4.8D.

***Retrosplenium subdivision*** There was no correlation between disease burden and any of the white matter microstructure measures in the retrosplenial subdivision, all $p > 0.05$, see Figure 4.8E.

### *Relationship between cingulum and motor dysfunction*

***Whole cingulum*** In HD participants, both finger tapping speed and UHDRS motor score (high score = more motor impairment) were correlated with free water fraction in the right cingulum, r= -.707 and .735 respectively, $p < 0.05$ uncorrected, whereas the same relationship with finger tapping speed was not present in control participants, $p > 0.05$. Both UHDRS total functional capacity and independence sub-scales were strongly negatively associated with free water fraction in the right cingulum, r = -.829 and -.856 respectively, $p < 0.05$, although only the relationship with total functional capacity was significant after multiple comparison correction, $p < 0.05$ FDR-adjusted. There was no relationship between either finger tapping speed or UHDRS and other MR measures.

***Subgenual subdivision*** There was no relationship between finger tapping speed and MR measures in the subgenual cingulum for HD participants, all $p > 0.05$ at an FDR-adjusted level. In control participants, finger tap speed was negatively correlated with FA values and myelin water fraction, r = -.650 and -.722 $p < 0.05$ uncorrected, $p>0.05$ FDR-corrected.

For the UHDRS motor score, a moderate relationship was found with free water fraction in the right subgenual subdivision, r = .583, $p < 0.05$ uncorrected, however $p>0.05$ at an FDR-adjusted level. UHDRS independence score and total functional capacity were not related to any microstructural measures, all $p > 0.05$.

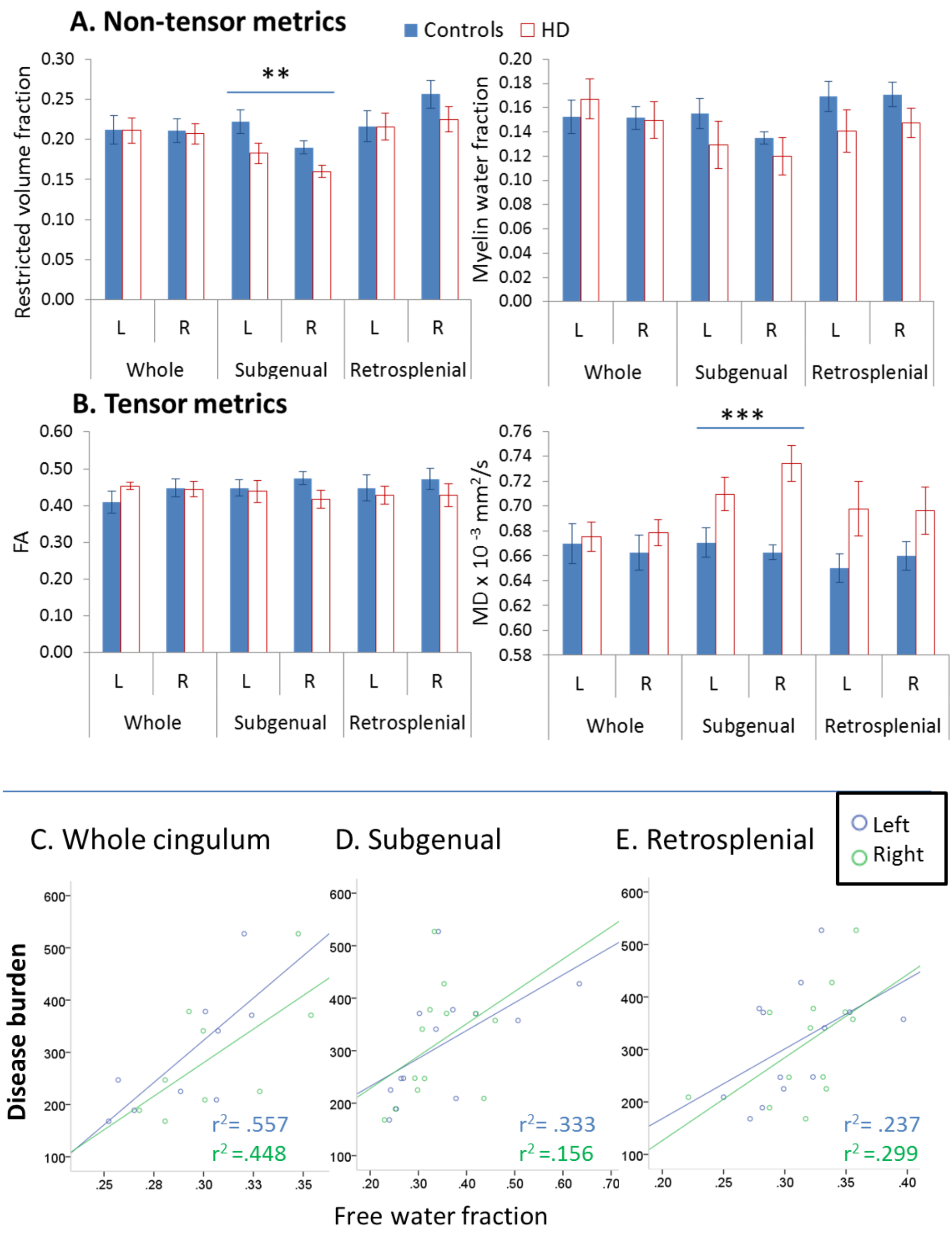

Figure 4.8 **A-B.** Group differences in the cingulum bundle and its subdivisions, with selective effects seen in the subgenual subdivision. L: left hemisphere, R: right hemisphere. Error bars represent standard errors of the mean. ** p < 0.01 uncorrected, ** < 0.001 uncorrected.

**C-E.** Relationship between free water fraction (FWF) and disease burden, a presumed index of the cumulative toxicity of mutant huntingtin, in the whole cingulum and cingulum subdivisions. The relationship is significant in the whole cingulum and left subgenual cingulum (p<0.05 uncorrected). Line of best fit overlaid on scatterplots with Pearson's $r^2$ shown in blue and green ink for the left and right hemisphere respectively.

***Retrosplenial subdivision*** There was no relationship between finger tapping speed and MR measures in the retrosplenial cingulum for control and HD participants alike, all $p > 0.05$. There was a moderate positive relationship between UHDRS motor scores and MD values in the left and right hemisphere, $r = .591$ and $.61$ respectively, $p < 0.05$ uncorrected, as well as with restricted volume fraction in the right hemisphere, $r = -.663$, $p < 0.05$ uncorrected. UHDRS independence score was also correlated with free water fraction in the left cingulum, $r = -.753$, $p < 0.05$ uncorrected, FDR-adjusted $p > 0.05$.

### Relationship between microstructure and composite cognitive scores

***Whole cingulum*** There was no correlation between composite cognitive scores and any of the measures in control or HD participants, all $p > 0.05$.

***Subgenual subdivision*** Restricted volume fraction, which was shown to be reduced in HD participants in the above section, was found to be correlated with cognitive functioning in HD participants specifically, $r = .585$, $p < 0.05$ uncorrected, with higher cognitive functioning associated with greater axon density in this sub-division of the cingulum. The same relationship was not significant in control participants, $r = -.463$, $p > 0.05$.

***Retrosplenial subdivision*** There was no correlation between composite cognitive scores and any of the measures in control or HD participants, all $p > 0.05$.

## Discussion

Although the neuropathological hallmark of HD is loss of medium spiny neurons in the striatum, there is increasing evidence that pathology also affects white matter; however there is no clear consensus on whether white matter damage is secondary to or independent of atrophy in the grey matter. The ability to characterise white matter degeneration would improve our understanding of the evolving process of neurodegeneration in HD, and could potentially inform future trials in terms of cell populations to target. In order to probe the white matter, multi-modal MRI measures were used to gain both a sensitive and specific characterisation of tissue microstructure in key white matter pathways in the brain. This is the first study to apply the CHARMED model in HD in order to examine the intra-axonal compartment separately from the extra-axonal compartment, and is also the first study to apply multi-component relaxometry to examine myelin water fraction.

### *Corpus callosum abnormalities*

In line with previous work using DTI-based tractography (Phillips, et al., 2013), a reduction in FA was found in HD participants in the corpus callosum using a more advanced tractography algorithm capable of resolving crossing fibers within the voxel. Two different SD approaches were used and a reduction in FA in HD participants was found with both approaches. Constrained spherical deconvolution (CSD)-based tracking was sensitive to specific differences in callosal regions as seen in a previous study (O. Phillips, et al., 2013), whereas a general reduction in FA was found using damped Richardson-Lucy (DRL), an alternative SD approach. HD participants were also found to have increased mean diffusivity (MD) in the corpus callosum, whereas the component eigenvalues were not significantly affected. MD values were not reported in the previous work (O. Phillips, et al., 2013), although component eigenvalues AD and RD were reported, and both were found to be higher in HD compared to control participants.

In terms of the clinical relevance of these findings, a higher disease burden, calculated from the individuals age and CAG repeat length, was associated with an increase in mean diffusivity (MD), specifically in the the 3rd and 4th segments, which contain inter-hemispheric connections to the primary motor and primary sensory cortex respectively. MD values were significantly higher in HD participants compared to controls, thus establishing a relationship between disease burden and microstructural abnormalities in the corpus callosum in HD. This supports the findings of Phillips et al. (2013), in which a correlation between callosal FA and RD and disease burden was reported. Finally, higher MD values were associated with a reduction in cognitive functioning in HD participants only, demonstrating the functional relevance of the microstructural changes observed.

### *Corticospinal tract*

The second pathway examined in this chapter was the corticospinal tract (CST), which is the main motor pathway in the brain. The only previous published work using deterministic tractography to reconstruct the CST in HD showed a reduction in FA and increase in axial and radial diffusivity in symptomatic HD patients compared to controls, with no difference in tensor based metrics between controls and pre-symptomatic HD (Phillips, et al., 2014). In this study, although MD was increased and both myelin water fraction and restricted volume fraction were reduced in HD participants compared to controls, this observation was only a trend and did not survive statistical significance. The sample size in this study was considerably smaller than that used by Phillips and colleagues (2014) and did not stratify HD participants as pre-symptomatic and early HD, which may explain the differences in results. However, in agreement with the previous study, a strong relationship was found between disease burden (CAG repeat length in conjunction with age) and both MD values and free water fraction in the CST, adding support to the idea that white matter abnormalities in the CST are a pathological feature of HD.

### *Cingulum bundle*

Finally, the cingulum bundle was reconstructed using deterministic tractography for the first time in HD participants. The whole cingulum was reconstructed as well as the subgenual and retrosplenial subdivisions of the cingulum separately, based on work showing distinct fiber populations within the cingulum (Jones, et al., 2013), which may be differentially affected in HD. Whereas there were no differences found between HD and control participants in the whole cingulum, mean diffusivity was found to be increased, radial diffusivity was found to be reduced, and restricted volume fraction, a non-tensor derived proxy of axon density, was found to be reduced (>15%) in HD participants compared to controls in the subgenual subdivision of the cingulum. There was also a trend for an increase free water fraction and a reduction in myelin water fraction (11-16% observed change) in this anterior portion of the cingulum. In contrast, there were no differences found between HD and control participants in the retrosplenial subdivision.

These results support the work showing distinct fiber populations in the cingulum bundle (Jones, et al., 2013), and suggest the subgenual cingulum is selectively vulnerable to neuropathology in HD. This fits with evidence showing a direct disease process in the anterior cingulate cortices in HD. The anterior cingulate cortex has previously been shown to be selectively vulnerable to neurodegeneration in HD (Davies et al., 1999; E. H. Kim, et al., 2014), with dystrophic neurites (huntingtin protein aggregates formed in axons and dendrites) found in the cingulate of post-mortem HD brains (Cammarata, Caponnetto, & Tabaton, 1993). Furthermore, it is known that the medium spiny neurons which selectively die in HD receive dense innervation from the anterior cingulate cortex (van Dellen, Deacon, York, Blakemore, & Hannan, 2001). Thus, this work suggests that the white matter tracts running between the striatum and anterior cingulate cortex are also affected, and represents the first observation of distinct abnormalities in this pathway in humans. Furthermore, this is the first observation of a reduction in restricted volume fraction in HD, and suggests that changes to axonal structure contribute to white matter pathology in HD.

The functional relevance of a reduction in restricted volume fraction was examined using a correlational analysis to probe the relationship with motor speed, motor functioning, cognitive functioning and total functioning capacity. Whereas there was no relationship with any motor measurements in the subgenual cingulum, a selective association was found with cognitive functioning, with an increase in restricted volume fraction associated with an increase in cognitive functioning specifically in HD participants; thus axon density in this fiber population may be important for cognition in HD. Although free water fraction was not increased in the cingulum in HD participants, it was found to be associated with disease burden, finger tapping speed and UHDRS motor and independence scores in the whole cingulum, suggesting that free water fraction is sensitive to measures of clinical severity.

### *Free water fraction as a biomarker of disease severity*

A novel finding to emerge from this work was the relationship between disease burden and free water fraction in HD participants in many of the fiber pathways studied. The relationship survived correction for multiple comparisons and was strongest in the corticospinal tract, with increased disease burden associated with an increase in isotropic partial volume. An increase in isotropic partial volume along a white matter pathway is suggestive of a reduction in packing density in the tissue, which may be due to a number of factors such as neuronal loss in neighbouring grey matter, and/ or white matter atrophy, such as a loss of axons or demyelination. This interesting and novel finding warrants further attention, but demonstrates the benefit of mapping the free water volume in diseases where atrophy is a pathological feature. Furthermore, considering that the DRL algorithm for whole-brain tractography recognises the contribution of isotropic partial volume effects to the signal, these results suggest that DRL is more appropriate for whole-brain tractography in the HD brain compared to CSD, based on the functional relevance of free water.

A surprising finding in this study was the relationship between UHDRS scores which were recorded months before the scan session, and microstructural measures in relevant white matter pathways. In both the corpus callosum and the cingulum, both of which are pathways known to contain distinct fiber populations, there was a strong relationship between free water fraction and total functional capacity. The Total Functional Capacity scale (Shoulson & Fahn, 1979) is the main assessment tool of functional status in HD clinical care and research, designed to assess progression of HD in symptomatic patients with emphasis on self-care, mobility, and independence. The direction of the relationship indicated that impaired functional capacity was associated with an increase in free water in the corpus callosum, whereas independence in terms of self-care was associated with free water fraction in the cingulum. This may reflect the multiple cognitive domains that contribute to everyday functioning and independence, and the effect of mutant huntingtin on the multiple fiber populations that are contained within these two white matter pathways, although this warrants further investigation. White matter microstructure was also found to be functionally significant in the motor domain in HD participants, with strong relationships found between UHDRS motor scores and MR measures obtained along the corpus callosum and cingulum bundle. In the corpus callosum, there was a discrepancy between the two different tracking algorithms in terms of which measures were correlated, however strong relationships emerged for both algorithms.

### *Non-tensor based microstructure metrics*

The differences seen in myelin water fraction, obtained using multi-component relaxometry, and in restricted volume fraction, obtained using a multi-shell diffusion MR sequence, require further study and attention. The significant reduction in restricted volume fraction of more than 15% found selectively in the subgenual cingulum in HD participants, and the trend for a reduction in restricted volume in HD participants in the corpus callosum suggests that axonal structure is affected in HD pathology at this early stage of the disease.  Thus, this work affirms the importance of going beyond the diffusion tensor and using more advance non-tensor based acquisitions in clinical research. The relationship found between restricted volume fraction and both UHDRS motor scores and disease burden in the corpus callosum, and between restricted volume fraction and cognitive functioning in the subgenual cingulum in HD participants, demonstrates that this metric is not only sensitive to differences between groups, but also sensitive to markers of clinical functioning and severity in HD. The differences seen in myelin water fraction between HD and control participants were also large (more than 10% difference), although not significant when correcting for multiple comparisons. Recently published work using R2* relaxometry found lower R2*(a marker of iron concentration) in the isthmus of the corpus callosum in early HD (Di Paola et al., 2014), suggesting myelin may be affected in the corpus callosum in HD. In healthy control participants, myelin water fraction was found to be related to finger tapping speed in the subgenual division of the cingulum, and to cognitive functioning in the corpus callosum.

Taken together, these findings are promising in terms of increasing the biological specificity to understand how HD affects white matter microstructure, and require further attention in a larger sample size.

### *Choice of tracking algorithm*

Previous studies have been reliant on the diffusion tensor model to conduct whole brain tractography, despite the well-established limitations with this approach. A comparison of measures obtained from tracts sampled using the tensor model and the two difference SD approaches found that FA values in the corpus callosum obtained from DTI tracking were significantly higher than corresponding FA values obtained using both of the SD approaches, with no significant differences found between the two SD approaches. Recent work estimates that 90% of white matter voxels contain crossing fibers (Jeurissen, Leemans, & Tournier, 2010), suggesting that the diffusion tensor model is inadequate in the vast majority of white matter regions. Considering this, the current work showing that tractography performed using the tensor model leads to statistically different results compared to tractography algorithms capable of resolving crossing fibers has serious implications for the interpretation of previous work showing changes in anisotropy and diffusivity measures in HD.

### *Methodological considerations*

A strength of this work is that unlike previous studies, all of the tensor-based metrics presented in this chapter have undergone correction for partial volume effects due to intra-voxel contamination by cerebrospinal fluid (CSF). The replication of previous findings in the corpus callosum (Phillips, et al., 2013) after correcting for partial volume demonstrates that white matter microstructural abnormalities in HD are a robust finding. The CHARMED model also includes a partial volume correction stage, whereas the code used to create myelin water fraction maps did not contain a compartment to model free water, which is likely to lead to an underestimation of myelin water fraction. Recent optimisation work has included a free water component in the mcDESPOT pipeline (Deoni, Matthews, & Kolind, 2013), and was shown to perform advantageously within partial volume regions. Thus, future work will involve repeating the analysis with the optimised code in order to achieve a more accurate estimate of myelin water fraction.

A discrepancy in findings for metrics sampled using either DRL or CSD tracking algorithm was observed and is likely driven by a difference in statistical power. The sample size was marginally higher for tracts obtained using DRL compared to tracts reconstructed using CSD. This was because whole-brain tracking with CSD occasionally failed to reconstruct any tracts for a given pathway, whereas DRL was capable of recovering tracts more often. One reason for this difference is the different way in which partial volume effects are treated by the two algorithms. Whereas CSD uses a non-negativity constraint to reduce spurious fiber orientations, the damped Richardson-Lucy algorithm recognises the contribution of isotropic partial volume effects to the signal, and addresses this using adaptive regularization (Dell'acqua, et al., 2010), resulting in a reduction in the number of false positives and spurious fiber orientations in areas of partial volume without a cost to angular resolution. In comparison, in areas of partial volume, CSD will not be able to adequately recover fiber orientations, producing erroneous results. This may explain why the cingulum reconstructions were particularly poor with CSD, with sub-cortical atrophy increasing the partial volume effects which would have affected the ability to reconstruct the subgenual subdivision of the cingulum. Thus, the differences seen between metrics sampled using CSD and DRL are likely due to differences in statistical power due to reduced numbers with CSD sampling, and differences in terms of accuracy in reconstructing the pathway of interest.

Statistical power was affected by the methodological decision to conduct the tractography on a higher b-value image more suited for recovering fiber orientations through spherical deconvolution approaches, and then to extract the tensor based statistics from a lower b-value image optimized for DTI. Although striving for greater accuracy by using the sequences in the most optimal way, in practice, this meant that two complete data sets acquired with different sequences were required from each participant in order to gain a measure for each tract. In practice, with some images suffering motion artefacts, it was not always possible to use both images, which became problematic for achieving statistical power with a small sample size.

### *Concluding comment*

This chapter has shown that the structural connectivity of both the corpus callosum and the cingulum bundle is altered in Huntington’s disease. This work adds a key finding to the literature with regards to the relationship between free water along white matter pathways and disease burden in HD, and suggests researchers should be both aware of, and take steps to address the issue of free water contamination in their analysis of diffusion MR data in Huntington’s disease. This work is the first to reconstruct the cingulum bundle as a distinct white matter fiber in HD, and using a multi-shell diffusion MRI sequence, found specific changes in a proxy measure of axon density. Finally, the relationship between metrics in both the corpus callosum and cingulum and UHDRS clinical scores suggests an important functional role for these white pathways in HD.

# 5 Moving beyond volume: Macrostructural changes in Huntington's disease

## Chapter Summary

The purpose of this chapter was to quantitatively examine the differences in grey matter morphometrics obtained from $T_1$-weighted MRI in patients with Huntington's disease (HD) compared to healthy matched controls. The second aim was to assess the correlation between different measures of grey matter macrostructure and cognitive performance, motor function and disease burden in HD.

Data analysis was conducted using a variety of approaches, including whole-brain exploratory VBM, a region-of-interest (ROI) analysis, a surface-based analysis of cortical thickness, surface area and curvature, and shape based analysis of subcortical regions implicated in HD.

## Introduction

In Chapter 1 the background literature on macro-structural changes previously found in HD was reviewed. The focus of research using $T_1$- and $T_2$-weighted MRI in HD has predominantly been looking at regions of atrophy in relation to disease stage, in order to gain an understanding of the pattern of atrophy with disease progression. Overall, this literature suggests that whereas HD affects both the grey and white matter in terms of volumetric change, the rate of atrophy in white matter does not follow the same course as grey matter atrophy in

HD, with white matter atrophy beginning earlier in life prior to symptom onset, with less prominent changes in global grey matter volume at this stage.

To examine changes in local volume, either a whole-brain hypothesis-free or a region-of-interest hypothesis-driven approach can be taken. Given the specific cell loss that is known to occur in the striatum and cerebral cortex, a region-of-interest (ROI) based analysis would arguably be most appropriate in HD (Aylward, et al., 2000). For example, ROI analyses of $T_1$-weighted images from pre-symptomatic HD participants from multiple research sites worldwide ($n > 500$) found that the volume of basal ganglia structures contributed more highly to the prediction of most motor and cognitive variables than volumes of other brain regions (Aylward et al., 2013).

However, work showing more widespread changes in HD (Kassubek et al., 2004; Wolf, et al., 2009) and the concept of compensatory networks in response to neurodegeneration (Klöppel et al., 2009) has also justified more exploratory whole-brain approaches. Voxel based morphometry (VBM) is an automated whole-brain approach that allows for the anatomical localisation of differences in volume between two groups (Ashburner & Friston, 2000) and has been applied in a number of studies of HD (Hobbs, et al., 2010; Kassubek, et al., 2004; Scahill et al., 2013; Wolf, et al., 2009; Wolf et al., 2013). One of the limitations of VBM is that the accuracy of the spatial normalisation affects the results. Furthermore, there are inconsistencies in the way in which VBM is applied across studies. The implications of these inconsistencies was demonstrated in a HD dataset where it was shown that changing user-specified options (e.g. smoothing kernel size, software version) can alter the results in a way that is similar to the biologic differences being examined (Henley et al., 2010; Jones, Symms, Cercignani, & Howard, 2005; Jones, Symms, Cercignani, & Howard, 2005). Thus, the robustness of results obtained using VBM is questionable and would be strengthened by the convergence of results using different analysis techniques and software packages.

Examining the shape of specific brain structures may be an additional informative metric to understand how HD progresses and the relevance of structural changes to disease-related symptoms. Shape-based deformation analysis examines the localised change in the outer surface of structures and can inform on both the location and pattern of changes. For each participant, the displacement of the surface of structures can be measure against a deformable surface mesh model that is based on the average segmentation for all participants. Displacement of the surface can be inwards, representing atrophy, or outwards, representing hypertrophy. Considering the specific efferent and afferent connections to different areas within a structure, such as the sub-nuclei of the thalamus, understanding localised changes within a structure may be informative in terms of interpreting white matter changes and understanding the neural basis of specific symptoms. To the best of this author's knowledge, shape analysis has only been applied in two studies in HD (van den Bogaard et al., 2011; Younes et al., 2014). In pre-symptomatic HD small areas of inward displacement (representing atrophy) were found in the putamen, pallidum, accumbens and caudate nucleus, with the most pronounced inward displacement evident in the caudate and putamen in HD participants closest to expected diseased onset (van den Bogaard, et al., 2011).

Cortical atrophy is well-documented as a site of HD pathology and there are a number of measurement tools available to examine changes specifically in the cerebral cortex. Although cortical neuronal loss is less severe than striatal neuronal loss, post mortem studies have reported approximately a 30% reduction in neurons in neocortical regions, including the associative frontal, temporal and parietal regions, and primary somatosensory cortices (Heinsen et al., 1994). Research in post-mortem brains has shown that degeneration of cortical neurons follows a specific pattern, with large projection neurons specifically vulnerable, especially in layers V and VI and to a lesser extent in layer III (Hedreen, Peyser, Folstein, & Ross, 1991; Macdonald & Halliday, 2002), as well as in the primary motor cortex and the premotor area (Macdonald & Halliday, 2002; Thu, et al., 2010). However, postmortem cytoarchitectural measurements have a number of limitations, with artefacts associated with the tissue fixation process, limited ante-mortem characterization, and a bias towards the late disease stage.

Thus, the availability of imaging software to generate surface-based cortical representations overcomes both the limitations of post-mortem studies and the limitations of volume-based representations. Cortical volume is influenced by both cortical thickness and surface area (Qiu et al., 2014), with cortical volume driven mostly by cortical surface area rather than cortical thickness (Im et al., 2008; Pakkenberg & Gundersen, 1997; Winkler et al., 2010). There is a large variability in the pattern of gyral folding across individuals and twin studies have provided evidence for a genetic influence on sulcal patterning (Im et al., 2011). Changes in cortical thickness may reflect a change in the size, density and arrangement of neurons, dendritic arborisation, change in myelination, and neuroglia, and therefore measuring cortical thickness can provide unique and important information about the effects of HD on cortical neuroanatomy not captured by cortical volume alone. The Freesurfer surface-based segmentation package was applied in this study, which uses the major sulcal and gyral patterns for inter-subject registration and overcomes some of the limitations of VBM in terms of spatial normalisation. Previous analysis of cortical thickness using the PREDICT-HD multi-site database with more than 500 $T_1$-weighted images from pre-symptomatic HD participants found that changes in cortical volume began to appear in participants who were classified as ‘midway to symptom onset’ with atrophy found mostly in the posterior and superior cerebral regions. With increased disease progression, changes were more evident in cortical thickness compared to surface area, with fewer changes in ventral and medial regions of the frontal and temporal cortex (Nopoulos, et al., 2010).

Thus, there is a range of techniques available to examine grey matter macrostructure beyond changes in regional volume. However, each analysis approach and corresponding software package comes with its own set of limitations. Combining different analysis methodologies to look for the convergence of results will improve the robustness of findings; the convergence and consistency of findings is important in a heterogeneous condition such as Huntington's disease. The first aim of this chapter was to test whether macrostructural results obtained in this specific HD cohort converge to replicate findings in the literature using a range of analysis techniques. HD is a heterogeneous condition and in order to be able to interpret findings obtained from more novel MRI acquisition sequences and analysis techniques, it is important to ascertain how comparable the recruited HD cohort is in comparison to other studies. A second aim was to examine the relationship between tissue macrostructure and cognitive function, using a validated cognitive test battery that has not been applied in HD previously. It is known from previous studies that cognitive measures correlate with structural changes in HD, therefore this chapter aims to examine whether the specific battery used in this thesis can reflect changes in tissue macrostructure.

## Methods

### *Participants and Data Acquisition*

17 HD gene-positive participants and 18 healthy controls participants had a $T_1$-weighted structural MRI scan on a 3T GE system; methodological details can be found in Chapter 2. Scans of the two groups (HD gene positive vs. controls) were acquired in an interleaved fashion. For the HD gene-positive participants, a disease burden score was calculated as a measure of disease severity, according to the previously described formula (age × [CAG-35.5]), where CAG is the number of CAG repeats (Penney, et al., 1997).

### *Cognitive Scores*

The composite cognitive scores were used to examine the relationship with tissue macrostructure. Details of the principal components analysis to produce the composite scores can be found in Chapter 3.

### *Region-of-Interest (ROI) Analysis*

Macrostructural changes are strongly hypothesised in the basal ganglia, thus a region of interest approach was used to examine changes in these areas. However, because HD is known to also affect more widespread areas to a lesser extent, exploratory whole-brain analyses were also conducted.

***Image Segmentation*** Image processing and analysis was performed using *Freesurfer* version 4.4.0 (Dale, Fischl, & Sereno, 1999; Fischl et al., 2002; Fischl, Sereno, & Dale, 1999). To cross-validate the segmentation results, the FMRIB Integrated Registration and Segmentation Tool (FIRST), a model-based segmentation/registration tool, was also used to generate subcortical region-of-interest (ROI) masks from each participant's $T_1$ anatomical image using FMRIB Software Library (FSL) version 5.0.1 (S. M. Smith et al., 2004). The *Freesurfer* image analysis package (http://surfer.nmr.mgh.harvard.edu/) was used for cortical reconstruction and parcellation of the cortex using the Desikan–Killiany atlas for each participant. These cortical and subcortical structure parcellations were then used for the volumetric analysis and vertex-based analysis. The rationale to use FSL FIRST and Freesurfer as registration and segmentation tools was that both tools have an automated set-up and therefore offer an unbiased approach.

***ROI Volume Analysis*** ROI and intracranial volumes were calculated from the $T_1$-weighted segmentations using Freesurfer (Dale, et al., 1999). Grey matter volume was examined in 10 ROI's: the cerebral cortex, cerebellar cortex, thalamus, caudate, putamen, globus pallidum, nucleus accumbens, amygdala, hippocampus and the brainstem. The hippocampus and amygdala were control regions, where atrophy relative to intracranial volume was not expected.

White matter ROI's were cerebral white matter, cerebellar white matter, and the corpus callosum (anterior, mid-anterior, central, mid-posterior, posterior sub-sections).

Sub-cortical ROI's obtained from the FSL segmentation were the thalamus, caudate, putamen, globus pallidum, nucleus accumbens, amygdala and the hippocampus. Brain tissue volume and total grey and white matter volumes, normalised for subject head size, were estimated with SIENAX (S. M. Smith et al., 2002), part of FSL (S. M. Smith, et al., 2004). All registrations and segmentations were visually inspected for accuracy.

***Vertex-Based Shape Analysis*** To investigate localised shape differences in the basal ganglia and thalamus, a vertex-based analysis was performed which examined group differences using permutation testing (randomise, FSL) making use of the segmentations acquired from FIRST (FSL). FIRST creates a surface mesh for each subcortical structure using a deformable mesh model. The mesh is composed of a set of triangles and the apex of adjoining triangles is called a vertex. The number of vertices for each structure is fixed. In order to investigate group differences, the surfaces were aligned (rotation and translation, minimising sum-of-squares difference) to MNI152 space.

Group comparisons of vertices were carried out using randomise (FSL) (Winkler, Ridgway, Webster, Smith, & Nichols, 2014), with the statistics rendered onto the shape surface (see Figure 5.1) to represent the signed, perpendicular distance from the average surface, providing a map of the localised regions where the structure changed significantly between groups. The results were corrected for multiple comparisons using the family-wise error (FWE). Again, the hippocampus was a control region where no group differences were expected.

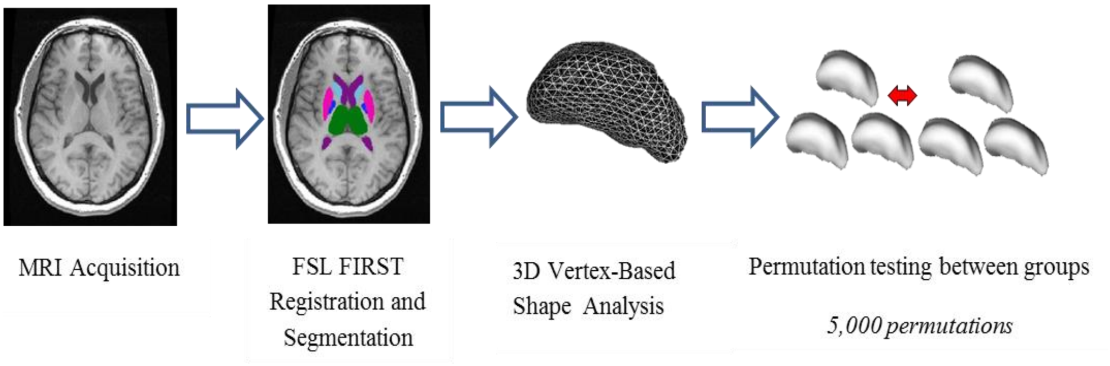
MRI Acquisition
FSL FIRST Registration and Segmentation
3D Vertex-Based Shape Analysis
Permutation testing between groups
5,000 permutations

Figure 5.1 Schematic of analysis pipeline for shape analysis performed using FMRIB Software Library (FSL) version 5.0

***Surface-based Cortical Morphometry.*** The automated *Freesurfer* pipeline was used to extract measures of cortical thickness, surface area and curvature. Processing steps included registering to a template image, intensity normalisation, removal of non-brain tissue, automated Talairach transformation, segmentation of white matter, and then the identification of the grey matter (GM) and white matter (WM) boundary and the pial surface (Dale, et al., 1999; Fischl, et al., 1999) using a tessellation technique. Neighbourhood intensity information was used to identify likely white matter voxels. White matter and pial surfaces were constructed after refining the initial surfaces generated for each hemisphere using surface deformation to optimally place the borders between grey and white matter, and between grey matter and CSF at the location where the greatest shift in intensity defines the transition to the other tissue class (Fischl & Dale, 2000). Cortical thickness is defined by Freesurfer as the average of the distance between the pial surface and the GM-WM boundary and the distance between the GM-WM boundary and the pial surface (Fischl & Dale, 2000) and was examined across every vertex. The surface area was computed from the surface at the boundary between WM and GM. The curvature was measured as 1/r, where r is the radius of an inscribed circle.

***Voxel-Based Morphometry (VBM)*** To examine the relationship between gene status and volume across the whole brain without specific a priori regions of interest, VBM was used. VBM was performed using VBM8, a toolbox in SPM (version 8), and analysis followed a number of stages:

- Images were visually inspected to ensure an appropriate level of alignment (within 5 cm and 20°) to a template image released with SPM.
- $T_1$ images were non-linearly normalised using high-dimensional DARTEL (Ashburner, 2007) to the Montreal Neurological Institute (MNI) ICBM European brain template space with 6 iterative steps. The DARTEL template used for the normalisation was derived from 550 healthy controls subjects from the IXI---database (http://www.brain-development.org).
- Images were then segmented into GM, WM and CSF. Segmentation parameters include a very light bias regularisation (0.0001), a 60mm bias FWHM cut-off, warping regularisation of 4 and a sampling distance of 3 mm. The segmentation approach was based on an adaptive Maximum A Posterior (MAP) technique, whereby local parameter variations are modelled as slowly varying spatial functions (Rajapakse et al.1997). *A priori* information about tissue probabilities is not required and tissue probability maps are used only for the spatial normalisation step and not for segmentation as was the case in earlier VBM toolboxes.
- In order to correct for changes in brain volume caused by the non-linear spatial normalisation, a non-linear modulation processing step was used so that comparisons could be made between absolute volumes of GM or WM structures. Thus, using the Jacobian determinants of the deformation field, images were scaled by the amount of contraction that occurred during normalisation so that the total amount of grey matter remains the same as in the original images.
- A quality check of the segmented and normalised images was conducted.
- Normalised segmented images were then smoothed through convolution with a Gaussian kernel with a Full-Width at Half-Maximum (FWHM) of 10

mm, in order to be comparable with the cortical thickness analysis, which also used a 10 mm smoothing kernel. Previous research studies in HD have also used a 10 mm kernel (Gavazzi et al., 2007; Jech, et al., 2007; Ruocco, Bonilha, Li, Lopes-Cendes, & Cendes, 2008; Thieben et al., 2002) although there is no consensus or consistency in the kernel size used in HD research (Henley, et al., 2010).

After carrying out the statistical analysis, coordinates of significant voxels were given in MNI space. In order to obtain an estimate of Talairach coordinates, a non-linear transform was implemented using a Matlab code provided at www.imaging.mrc-cbu.cam.ac.uk (Calder, Lawrence, & Young, 2001; Duncan et al., 2000). Talairach software was then used to obtain neuroanatomical labels (Talairach Client) and these labels were checked for accuracy in the original statistical maps.

### *Statistical Analysis*

The different types of analysis methods require different statistical approaches, with the number of multiple comparisons differing dramatically depending on whether the analysis is based on a priori ROI's or is an exploratory whole-brain approach. Although it is preferable to use the same approach to conduct multiple comparison corrections throughout, this has not been possible due to software restrictions which only allow for a specific type of correction. Thus, a mixture of the family-wise error (FWE), which reduces the probability of any false discoveries, and the less-stringent false-discovery rate (FDR), which is concerned with the expected proportion of false discoveries, and has greater power but an associated increased rates of Type I errors, were used. For both multiple comparison correction approaches, statistics were corrected by controlling the FWE rate or FDR at 5%.

Differences in ROI volume were investigated using analysis of variance (ANOVA) in SPSS (IBM Statistics 20), with the within factors 'laterality' (left, right hemisphere) and the between group factor ‘gene status’ (HD gene positive, control gene-negative). For the corpus callosum ROI analysis, corpus callosum segment (anterior, mid-anterior, central, mid-posterior, posterior sub-sections) was a within-subject factor. To normalise for age-related structural changes, age was added as a covariate. To normalise for inter-individual variations in head size, regional volumes obtained from Freesurfer were analysed with ICV as a covariate, whereas regional volumes obtained using FSL were analysed with total brain volume as a covariate. This was to ensure that the two software packages were being compared in their entirety, rather than use a statistic obtained from one package as a covariate in an analysis of regional volumes produced by a different package, introducing bias and reducing the ability to compare across packages. However, the consequence of this is that the interpretation of any group differences is not directly comparable; Freesurfer does not produce a whole brain volume estimate, and ICV includes all tissue and CSF below the skull, thus is more representative of pre-morbid brain volume rather than FSL’s whole brain volume, which will be more sensitive to whole brain atrophy caused by disease. Statistics were FDR-corrected for multiple comparisons.

Local displacement (inwards or outwards) in shape of sub-cortical structures between groups was investigated using permutation testing (randomise, FSL), with a single F-contrast testing for group differences. Statistics were corrected for multiple comparisons by controlling the FWE rate. An arbitrary threshold of 6 was used to form supra-threshold clusters of voxels using the null distribution of the maximum cluster size across the image.

To examine surface-based differences in cortical thickness, analysis was carried out using a general linear model (Qdec v1.2, Freesurfer) co-varying for age, with a FWHM smoothing of 10mm. Multiple comparisons were taken into account by controlling the FDR. The relationship between cortical thickness and disease burden in the patient group was examined using a correlational analysis.

Correlations between MRI findings and cognitive measures were examined in order to understand the functional relevance of any structural abnormalities. The composite cognitive score from the PCA was partially correlated with the grey matter and white matter volume measures, controlling for age and intracranial volume using SPSS.

Statistical testing for the VBM analysis was conducted using SPM8. A between-subject two-tailed T-test was conducted with age and ICV as covariates, due to the range of ages in both groups. Both the uncorrected ($p < 0.001$) and FWE-corrected p values are reported at the voxel-level and cluster level.

## Results

### *Atrophy in HD patients*

Both the VBM and the ROI analyses were used to examine changes in volume between HD and healthy control participants. Results from the VBM analysis are shown in Figure 5.2. In order to cross-validate results in the ROI analysis, sub-cortical segmentation was conducted using two different software packages (FSL FIRST vs. Freesurfer). Table 5.1 shows the comparative p-values of the two software packages; a mixed-model ANOVA found a significant difference in the caudate and pallidum measures produced by the segmentation pipeline implemented in Freesurfer compared to FSL, with Freesurfer producing smaller estimates. As shown in Figure 5.3, there was no difference in intracranial volume (Freesurfer) between HD patients and controls, $F(1, 32) = 1.43$, $p > 0.05$, whereas HD patients had reduced whole brain volume (FSL) of -5.8% compared to controls and grey matter atrophy was evident (-4.9%), $F(1, 32) = 6.26$ and $10.25$, $p < 0.05$.

***Sub-cortical atrophy*** Descriptive statistics from the ROI analysis are presented in Table 5.2. HD patients had significant atrophy in the caudate, putamen, thalamus, pallidum, nucleus accumbens and brainstem, $F(1, 32) = 9.90$,

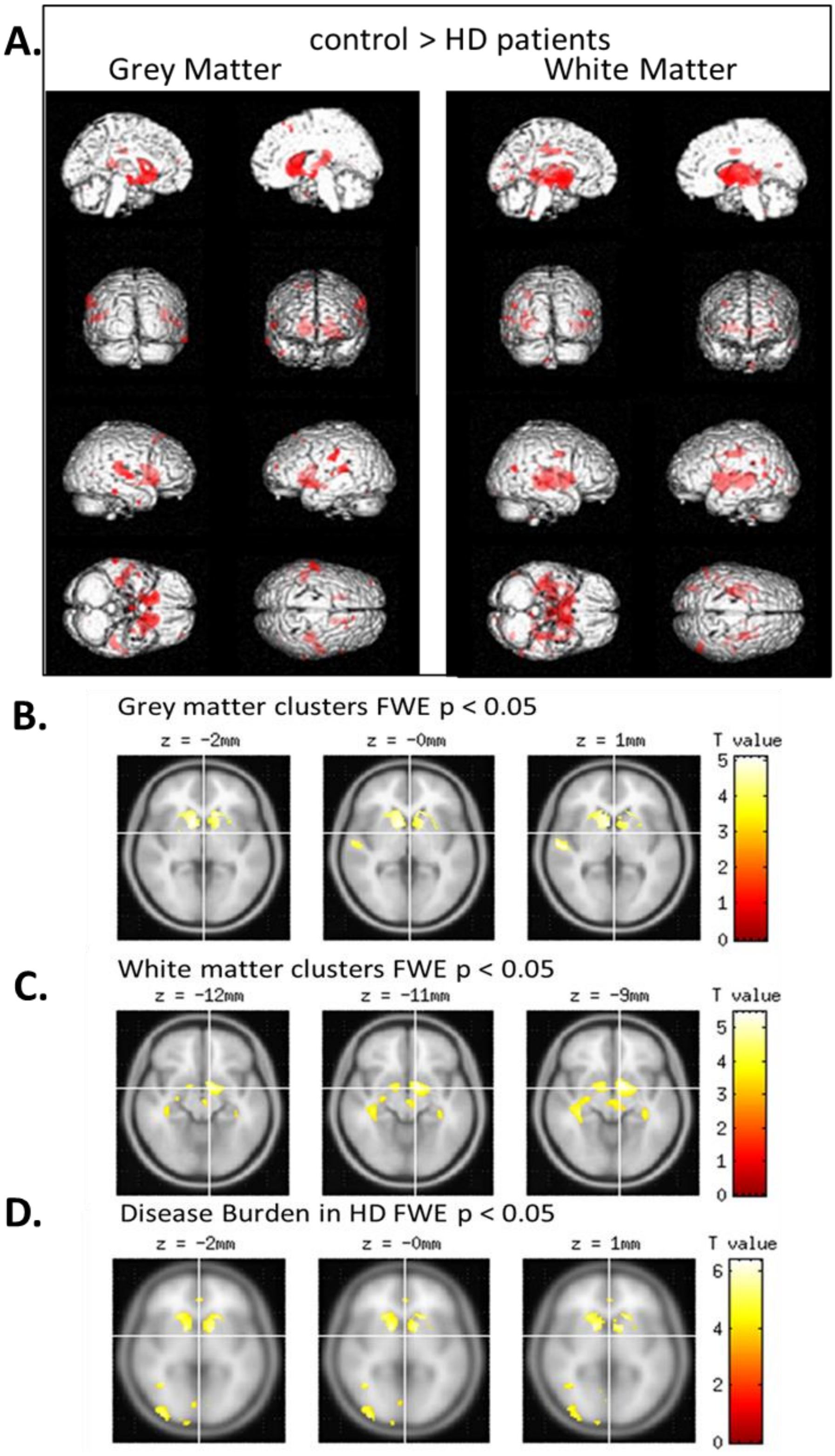
A.
control > HD patients
Grey Matter
White Matter
B.
Grey matter clusters FWE p < 0.05
z = -2mm
z = -0mm
z = 1mm
T value
5
4
3
2
1
0
C.
White matter clusters FWE p < 0.05
z = -12mm
z = -11mm
z = -9mm
T value
5
4
3
2
1
0
D.
Disease Burden in HD FWE p < 0.05
z = -2mm
z = -0mm
z = 1mm
T value
6
4
2
0

Figure 5.2 **Results of VBM Analysis.** A) Grey and matter volume differences in HD patients, T (31) = >3.37, $p < 0.001$ uncorrected B) Location of significant grey matter clusters, C) significant white matter clusters, and D) clusters of significant correlation with disease burden. Clusters significant at FWE-adjusted $p < 0.05$. All statistics shown overlaid on an average T1-template image provided by SPM99

Table 5.1 Mixed model ANOVA results of group differences in sub-cortical volume based on segmentation software package. FDR-adjusted p-values * p < 0.05, ** p < 0.01, *** p < 0.001

| ROI | Freesurfer segmentation | FSL segmentation | Freesurfer vs. FSL |
|---|---|---|---|
| Caudate | ** | ** | *** |
| Putamen | *** | *** | *p > 0.05* |
| Thalamus | * | ** | *p > 0.05* |
| Pallidum | *** | *** | * |
| Nucleus Accumbens | * | * | *p > 0.05* |
| Amygdala | *p > 0.05* | *p > 0.05* | *p > 0.05* |
| Hippocampus | *p > 0.05* | *p > 0.05* | *p > 0.05* |

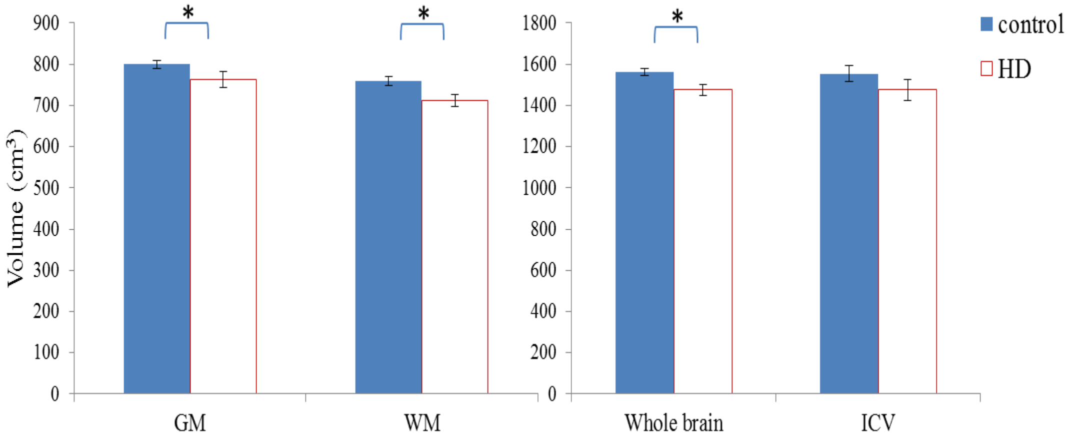

Figure 5.3 Total grey matter (GM), white matter (WM), whole brain volume and intracranial volume (ICV) in HD patients and healthy controls. Values shown are the observed unadjusted mean values. GM, WM and whole brain volumes from FSL analysis; ICV from Freesurfer ($cm^3$). Error bars represent ± standard error of the mean. Significance is after correction for age and multiple comparisons, * $p < 0.05$.

21.86, 8.76, 36.02, 6.81, and 12.74, respectively, $p < 0.05$ FDR-corrected. There was no difference in volume in the amygdala and hippocampus, all $p > 0.05$. Despite the differences in volumetric measures between Freesurfer and FSL, cross-validation with FSL also revealed sub-cortical atrophy in the HD patients in the caudate, putamen, thalamus, pallidum and nucleus accumbens, F(1, 32) = 11.24, 23.49, 14.49, 17.20 and 6.81, respectively, $p < 0.05$ FDR-corrected, with no differences in the amygdala, and hippocampus, all $p > 0.05$.The ROI comprising the brain stem combined with the fourth ventricle did not differ in volume between the HD patients and controls, $p > 0.05$. The magnitude of differences between HD patients and controls is shown in Figure 5.4 for both software segmentations.

A reduction in subcortical grey matter (GM) was also found in HD participants in the VBM analysis at an uncorrected p value < 0.001 (FWE-corrected p>0.05). At the cluster level, significant clusters of volume change which survived FWE-correction were found bilaterally in the basal ganglia, with the left hemisphere cluster (size = 17980) in the caudate head (MNI coordinates [x,y,z]= -12 22 -2), lateral globus pallidus (16 2 -9 mm) and putamen ( -15 8 -2 mm) , and the right hemisphere cluster (size = 18890) in the right putamen and caudate head (MNI coordinates 12 8 -4; 6 10 4 ; 10 20 1 mm).

***Cortical atrophy*** There was no difference in volume in the cerebellum or cerebral cortex as calculated using ROI's from Freesurfer software, $p > 0.05$. In the VBM analysis, a significant difference in volume was found in a cluster (size=13310) in the right superior temporal gyrus / Brodmann area 13/22 (MNI 57 -16 3 mm, Talairach 56 -15 4), $p < 0.05$ FWE-corrected.

***White Matter atrophy*** HD patients had significant atrophy in the cerebral white matter and corpus callosum compared to controls, F(1, 31) = 10.16 and 6.78 respectively, $p < 0.05$ FDR-corrected. There was no main effect of callosum segment, and no interaction between corpus callosum segment and gene status, both $p > 0.05$. There was no difference in white matter volume in the cerebellum, F (1, 31) = 1.82, $p > 0.05$. In the VBM analysis, a significant cluster which spanned both hemispheres and survived FWE-correction at $p < 0.05$ was found in the sub-cortical WM of the basal ganglia and temporal lobe. Segmenting the brain using FSL software also revealed white matter atrophy (-6.7%) in the HD patients (normalised for head volume) compared to controls, F (1, 28) = 7.23, $p < 0.05$.

There was no correlation between grey matter and white matter volume in the control group ($r$ (18) = 0.45, $p > 0.05$) or in the HD group, $r$ (17) = 0.18, $p > 0.05$.

Table 5.2 Descriptive statistics for raw volume measures (mm$^3$) from segmented images (Freesurfer). † Measured across hemispheres. S.E.M : standard error of the mean. WM: white matter.

| | **Controls** | | | | **HD** | | | |
|---|---|---|---|---|---|---|---|---|
| | Left | | Right | | Left | | Right | |
| | **Mean** | ***S.E.M*** | **Mean** | ***S.E.M*** | **Mean** | ***S.E.M*** | **Mean** | ***S.E.M*** |
| Intracranial Volume † | 1570612.00 | *36343.02* | | | 1467860.22 | *53057.23* | | |
| **Grey Matter ROI's** | | | | | | | | |
| Cerebral Cortex | 272073.94 | *8300.51* | 271997.13 | *8375.45* | 254834.63 | *8261.83* | 257143.00 | *8670.9* |
| Cerebellum Cortex | 55964.50 | *999.38* | 57542.56 | *1089.29* | 54028.94 | *1842.16* | 55456.25 | *2053.6* |
| Thalamus | 7309.44 | *189.85* | 7082.50 | *190.78* | 6540.56 | *193.93* | 6345.69 | *170.6* |
| Caudate | 3325.38 | *103.82* | 3197.56 | *124.27* | 2470.88 | *222.43* | 2367.25 | *211.1* |
| Putamen | 5442.94 | *180.25* | 5149.50 | *186.12* | 4138.44 | *306.74* | 3690.00 | *252.4* |
| Pallidum | 1639.00 | *40.83* | 1456.13 | *39.74* | 1185.75 | *71.87* | 1052.81 | *69.51* |
| Nucleus Accumbens | 629.44 | *31.15* | 546.94 | *25.57* | 537.88 | *38.48* | 434.75 | *25.52* |
| Hippocampus | 4520.19 | *108.53* | 4638.75 | *105.83* | 4465.06 | *113.69* | 4387.06 | *117.9* |
| Amygdala | 1487.88 | *32.70* | 1577.38 | *47.51* | 1381.56 | *43.22* | 1412.56 | *60.20* |
| Brain Stem† | 21636.75 | *474.37* | | | 18938.44 | *609.47* | | |
| **White Matter ROI's** | | | | | | | | |
| Cerebral WM | 238396.44 | *6203.46* | 243528.50 | *6203.46* | 205280.69 | *8255.84* | 206864.63 | *8828.4* |
| Cerebellum WM | 16088.13 | *358.30* | 16374.06 | *358.30* | 16754.88 | *889.37* | 16696.31 | *812.3* |
| Corpus Callosum† | | | | | | | | |
| *Anterior* | *873.19* | *44.70* | | | *665.06* | *58.36* | | |
| *Mid-Anterior* | *546.06* | *41.11* | | | *395.81* | *36.44* | | |
| *Mid* | *551.63* | *40.03* | | | *411.69* | *50.18* | | |
| *Mid-Posterior* | *503.56* | *22.13* | | | *406.13* | *35.77* | | |
| *Posterior* | *1015.94* | *45.27* | | | *902.06* | *39.69* | | |

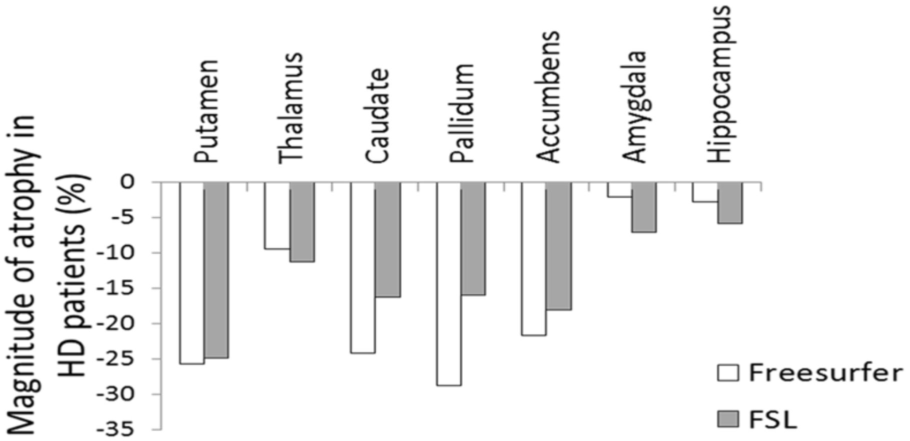

Figure 5.4 Percentage magnitude of sub-cortical atrophy in HD patients compared to controls depending on the software package used for segmentation

***Relationship between volume and motor functioning*** The average result from the Speeded Tapping Test (Reitan, 1979) was used as a measure of motor speed. The UHDRS motor score was used as a measure of overall motor functioning, whereas the UHDRS Total Functional Capacity (TFC) score was used as a more general measure of functioning not restricted to the motor domain. Partial correlations were conducted with age and either intracranial volume (for Freesurfer volumes) or total brain volume (for FSL volume) partialled out.

When volumes were calculated using the Freesurfer segmentation pipeline, average finger tapping speed for HD participants was correlated with volume in the left and right putamen ($r = 0.743$ and $0.734$ respectively, $p < 0.1$ uncorrected), although neither result survived correction for multiple comparisons using the FDR, $p = 0.084$ for both hemispheres. In healthy control participants, finger tapping speed was negatively correlated with volume in the left cerebral cortex ($r = -.807$, $p < 0.01$ uncorrected), and the right caudate ($r = .861$, $p < 0.01$ uncorrected), although neither result survived correction for multiple comparisons using the FDR, $p = 0.081$ and $0.054$ respectively. When volumes were calculated using the FSL segmentation pipeline, finger tapping speed in HD participants was significantly positively correlated with volume in the left and right putamen ($r = .73$ and $.79$ respectively), left and right caudate ($r = .70$ and $.71$ respectively), left and right thalamus ($r = .67$ and $.72$ respectively) and in the left and right globus pallidum ($r = .66$ and $.70$ respectively), all $p < 0.05$ FDR-corrected. There were no significant correlations between finger tapping speed and regional volume in the control participants, all $p > 0.05$.

For the UHDRS motor score, a strong negative relationship between motor score (high score = more motor impairments) and volume was found in the left and right putamen ($r = -.812$ and $-.795$, $p < 0.05$ FDR-corrected) the left and right globus pallidum ($r = -.791$ and $-.793$ respectively, $p < 0.05$ FDR-corrected) and in the right caudate ($r = -.728$, $p < 0.05$ FDR-corrected), as calculated using Freesurfer. When using volumes segmented using the FSL pipeline, the same regions were significantly correlated, whereas additional significant correlations were found with left caudate volume ($r = -.75$), left and right thalami volume ($r = -.68$ and $-.67$ respectively), and volume in the left nucleus accumbens ($r =-.72$), all $p < 0.05$ FDR-corrected.

Similarly, for the Total Functioning Capacity (high score = higher functional capacity), a strong positive relationship was found with putamen volume in the left and right hemisphere ($r = .802$ and $.74$, $p < 0.05$ FDR-corrected), and with globus pallidum volume in the left and right hemisphere ($r = .739$ and $.727$, $p < 0.05$ FDR-corrected) when calculated using Freesurfer. When using volumes segmented using the FSL pipeline, a strong positive relationship was also found with putamen volume in the left and right hemisphere ($r = .75$ and $.77$), whereas the left nucleus accumbens was also positively correlated with TFC score ($r = .82$), all $p < 0.05$ FDR-corrected.

Using VBM, at the voxel level, finger tapping speed was positively correlated with volume in a cluster in the left inferior occipital gyrus in HD participants, $t(12) = 5.71$ at peak voxel, $k = 790$, $p < 0.05$ FWE- and FDR-corrected. In control participants, there was no correlation between finger tapping speed and volume at the voxel-wise level after correcting for multiple comparisons, $p>0.05$. In HD participants, UHDRS motor score was negatively correlated with volume in clusters encompassing the left caudate head, medial globus pallidum and putamen ($t(13) = 6.10$ at peak voxel, $k = 2409$), right caudate tail ($t(13) = 7.07$ at peak voxel, $k = 860$) , and right putamen and ventral posterior medial nucleus of the right thalamus ($t(13) = 4.06$ at peak voxel, $k = 14640$), all $p < 0.05$ FWE- and FDR-corrected. A positive correlation was found between UHDRS motor score and volume in a cluster in the right posterior lobe of the cerebellum, $t(13) = 4.26$ at peak voxel, $k = 1539$, $p < 0.005$ FWE- and FDR-corrected. For Total Functioning Capacity (TFC), a strong positive correlation was found with volume in clusters encompassing the left inferior occipital gyrus ( $t(13) = 8.19$ at peak voxel, $k =5943$), right inferior frontal gyrus and caudate body ($t(13)=7.44$, $k=2528$), left caudate head and amygdala ($t(13)=7.26$, $k=6214$), right paracentral lobule (Brodmann area 5 and 31), (t(13)=7.10, k=1145) and right posterior insula and primary somatosensory cortex /postcentral gyrus (t(13)=6.02, k=1268), all $p < 0.01$ FWE- and FDR-corrected.

### *Relationship between volume and cognitive performance*

When examining the relationship with cognitive functioning, partial correlations were conducted using the composite cognitive scores from chapter 3, with age and either intracranial volume (for Freesurfer volumes) or total brain volume (for FSL volume) partialled out. For the HD participants, there was a strong and significant correlation between composite cognitive functioning and left hippocampal volume obtained using Freesurfer, $r = 0.832$, $p < 0.05$ FDR-corrected. The same relationship was not found in control participants, $r = -0.043$, $p > 0.05$. There was no correlation between composite cognitive scores and corpus callosum volume, cerebral white matter volume or cerebellum white matter volume, all $p > 0.05$. For volumes obtained using FSL segmentation, and adjusted for age and whole brain volume, non-significant yet moderate correlations were found with cognitive functioning in the right caudate and putamen and left hippocampus $r = 0.571$, 0.599 and 0.531 respectively, $p > 0.05$. Total white matter volume and total grey matter volume were both correlated with composite cognitive scores in HD participants, $r = -.645$ and 0.645 respectively, and in control participants, $r =-.621$ and 0.621, $p < 0.05$ uncorrected, all $p > 0.05$ FDR-corrected.

Using VBM, at the voxel level a number of widely distributed voxels showed a significant correlation in both the HD participants and healthy controls at $p < 0.0001$ uncorrected. In the HD participants at the voxel level, a correlation that was approaching the FWE-significance threshold ($p = 0.097$) was found in the right inferior temporal gyrus corresponding the Brodmann area 19, $t(11) = 5.45$, $z = 5.08$, $p < 0.0001$ uncorrected. This same correlation was significant at the cluster level, $t(11) = 4.02$, $k = 38$, $p < 0.001$ FDR- and FWE-adjusted. Volume in a second cluster was also found to be positively correlated with cognitive function in HD participants, in the right medial frontal gyrus, corresponding to the Brodmann area 8, t (11) = 4.02, k = 26, $p < 0.05$ FDR- and FWE-corrected.

In the control participants, analysis at the cluster-wise level found a positive correlation between cognitive scores and a single cluster in the grey matter in the right occipital lobe corresponding to Brodmann area 8 / visual association area, t (11) = 4.02, k = 39, $p < 0.05$ FDR- and FWE-adjusted, and a negative correlation in a single cluster in the posterior lobe of the right cerebellum, at the pyramis lobule, t (11) = 4.02, k = 67, $p < 0.01$ FDR- and FWE-corrected. There were no negative correlations found between cognitive function and volume at either the voxel of cluster level in HD participants, all $p > 0.05$ corrected.

***Relationship between volume and disease burden*** From the ROI analysis, sub-cortical volume was strongly negatively correlated with disease burden in the caudate (r = -.743 and -.840 left and right respectively), putamen (r= -.763 and -.808 left and right respectively), pallidum (-.753 and -.756, left and right respectively), and the left nucleus accumbens, r = -.658, all $p < 0.05$ FDR-corrected. There was no relationship between disease burden and white matter macrostructure, all $p > 0.05$.

The results from a regression analysis from the voxel-wise analysis also found the same relationship. A correlation between disease burden and GM volume was found in 3 clusters: in the left basal ganglia including the pallidum and putamen, in the right putamen, and an additional correlation was found in the right inferior occipital gyrus (Brodmann area 18), all FWE-adjusted $p < 0.05$. As with the ROI analysis, there was no correlation between disease burden and WM volume in any voxel, FWE-adjusted $p > 0.05$.

Table 5.3 Correlation coefficients between volume and disease burden in HD participants *(df = 14)*. P-values shown are uncorrected values; bold p-values indicate those that survive FDR correction at q< 0.05.

| | Huntington's Disease | | | |
|---|---|---|---|---|
| | Volume | | | |
| | Freesurfer | | FSL | |
| Measure | *r* | *p* | *r* | *p* |
| **Disease Burden** | | | | |
| Left caudate | -0.74 | **.001** | -0.57 | .021 |
| Right caudate | -0.84 | **.000** | -0.66 | .006 |
| Left putamen | -0.76 | **.001** | -0.55 | .026 |
| Right putamen | -0.81 | **.000** | -0.59 | .016 |
| Left pallidum | -0.75 | **.001** | -0.54 | .031 |
| Right pallidum | -0.76 | **.001** | -0.33 | .216 |
| Left thalamus | -0.38 | .147 | -0.27 | .318 |
| Right thalamus | -0.19 | .485 | -0.23 | .388 |
| Left accumbens | -0.66 | **.006** | -0.61 | .012 |
| Right accumbens | -0.39 | .140 | -0.39 | .141 |
| Left amygdala | 0.09 | .754 | -0.32 | .224 |
| Right amygdala | 0.05 | .846 | 0.15 | .569 |
| Left hippocampus | -0.07 | .810 | -0.19 | .478 |
| Right hippocampus | -0.10 | .719 | -0.23 | .383 |
| | | | | |
| Corpus callosum | 0.52 | .045 | n/a | |
| Left cerebral white matter | -0.32 | .235 | n/a | |
| Right cerebral white matter | -0.30 | .258 | n/a | |
| Left cerebellum white matter | 0.48 | .061 | n/a | |
| Right cerebellum white matter | 0.37 | .156 | n/a | |
| | | | | |
| Total grey matter | n/a | | -0.35 | .179 |
| Total white matter | n/a | | 0.35 | .179 |

### *Cortical thinning is related to disease burden*

There was no difference in cortical thickness, surface area or curvature in HD patients relative to controls when adjusting for multiple comparisons (FDR) and controlling for age. Figure 5.5 shows the correlation between cortical thickness and disease burden in HD patients. Disease burden was found to correlate negatively with cortical thickness in both hemispheres in the caudal and rostral middle frontal cortex, precentral gyrus, isthmus cingulate gyrus, precuneus, lingual gyrus, lateral occipital cortex, and middle and superior temporal cortex, all $p < 0.05$ FDR-adjusted. In the left hemisphere specifically, negative correlations were also observed in the superior frontal and lateral orbitofrontal cortex, transverse and inferior temporal cortex, inferior parietal cortex, paracentral sulcus and supramarginal gyrus, all $p < 0.05$ FDR-adjusted. Surface area in the left precentral sulcus and right superior temporal cortex was found to positively correlate with disease burden, $t(15) = 4.39$ and $4.37$ respectively, $p < 0.0001$ uncorrected, whereas surface area calculated from the pial surface rather than the GM/WM boundary surface, produced negative correlations with disease burden in the left middle temporal gyrus, left superior temporal sulcus, left lateral occipital gyrus, and right post-central gyrus, $t(15) = -4.3$, $-4.04$, $-4.19$ and $-4.42$ respectively, $p < 0.0001$ uncorrected. None of these correlations survived FDR-correction for multiple comparisons. Cortical curvature was not related to disease burden, $p > 0.05$ FDR-adjusted.

***Relationship between cortical thickness and motor functioning*** For control participants, there was no relationship between cortical thickness and finger tapping speed when accounting for ICV, all $p > 0.001$ uncorrected. Surface area in the right posterior cingulate was positively correlated with finger tapping speed, $t\ (10) = 3.90$, $p < 0.001$ uncorrected. For HD participants, cortical thickness in the left paracentral, right supramarginal gyrus, inferior parietal sulcus and superior frontal gyrus were positively correlated with finger tapping speed, after accounting for ICV, $t\ (11) = 3.16$, $3.49$,$3.74$ and $3.07$ respectively, $p < 0.001$ uncorrected. Cortical thickness was not correlated with UHDRS motor scores at an uncorrected p value of 0.001, whereas surface area in the right pars orbitalis gyrus and pericalcarine gyrus were positively correlated with UHDRS motor score, $t\ (11) = 3.64$ and $3.04$ respectively, $p < 0.001$ uncorrected. None of the relationships survived correction for multiple comparisons using the FDR.

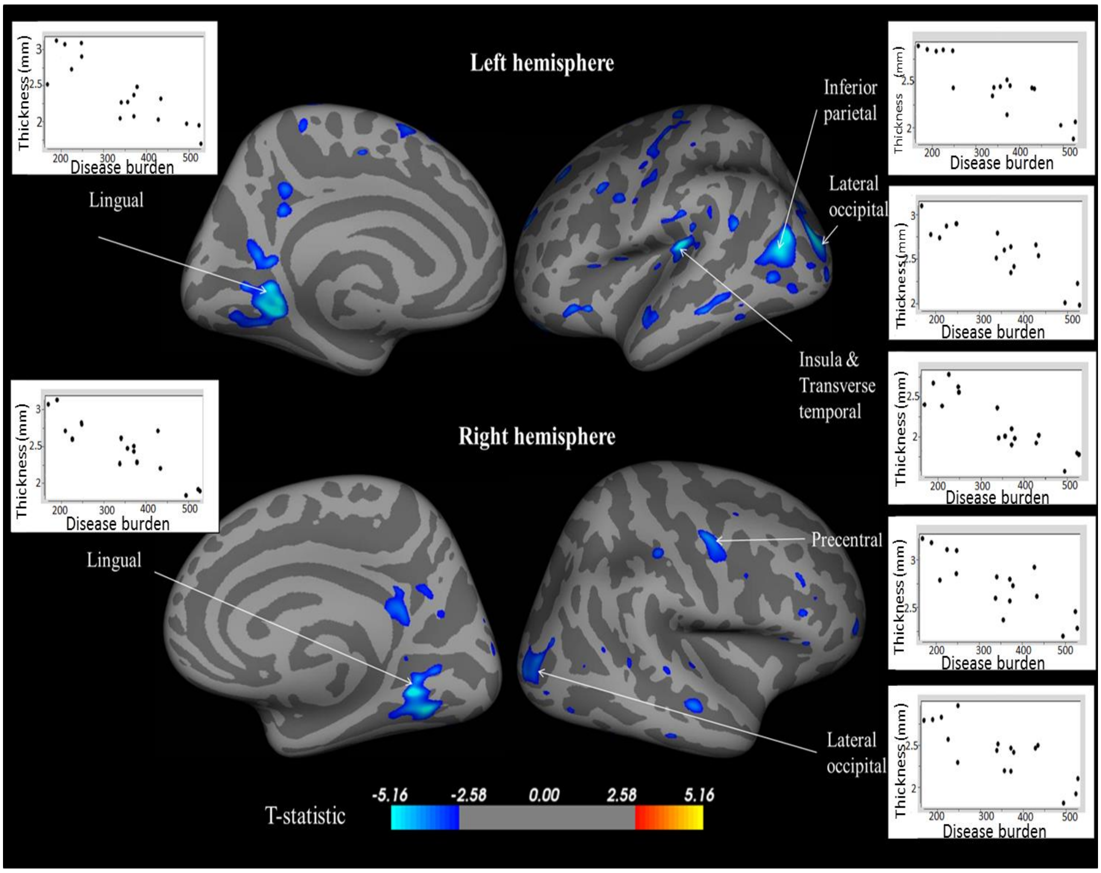
Left hemisphere
Right hemisphere
Lingual
Inferior parietal
Lateral occipital
Insula & Transverse temporal
Lingual
Precentral
Lateral occipital
T-statistic
-5.16
-2.58
0.00
2.58
5.16
Thickness (mm)
Disease burden
200
300
400
500
2
2.5
3

Figure 5.5 Correlation between cortical thickness (mm) and disease burden in HD patients. In the right hemisphere, negative correlations were also observed in the postcentral gyrus, fusiform, precuneus, and parstriangularis cortical areas, all $p < 0.05$ FDR-adjusted. Colour represents t-statistic, thresholded to only include statistics which survive FDR-correction. Scatterplots shown are for regions where $p < 0.0001$ uncorrected, disease burden is on the x axis and cortical thickness (mm) on y axis.

***Relationship between cortical thickness and cognitive function*** In the HD participants, there were no significant correlations between cortical thickness or cortical curvature and composite cognitive score, $p > 0.05$. Surface area in the left posterior cingulate gyrus was positively correlated with cognitive scores accounting for age, t (10) = 5.69, $p < 0.0001$ uncorrected, and the right superior parietal sulcus was negatively correlated with cognitive scores accounting for age, t (10) = -5.87, $p < 0.0001$ uncorrected. Notably, these t statistics were close to the threshold for FDR-significance (t = 5.73 and 5.91 for the left and right hemisphere respectively). When disease burden was accounted for, the relationship between surface area and cognitive function became weaker in the posterior cingulate gyrus (t (10) = 3.44), and in the right superior parietal sulcus (t (10) = -4.66).

In the control participants the correlation between cortical thickness in the right peri-calcarine sulcus and composite cognitive scores (t (10) = 4.86) was significant at $p < 0.0001$ uncorrected, FDR-corrected $p > 0.05$. Surface area was also positively correlated with cognitive function in the left precuneus sulcus (t (10) = 4.04) and right superior frontal gyrus (t (10) = 4.80), and negatively correlated with cognitive function in right inferior parietal gyrus, t (10) = -4.25, all $p < 0.0001$ uncorrected.

### *Sub-cortical shape analysis*

Results of the shape analysis are shown in Figure 5.6.

***Caudate nucleus*** Shape changes were more evident in the caudate head and body compared to the caudate tail. Some localised areas of change were seen in the left caudate tail. Localised inward displacement of the caudate surface (taken to represent local atrophy) was most pronounced in the medial caudate body in both hemispheres, with less change in the lateral edge.

***Putamen*** Significant shape deformation was evident almost throughout the whole structure, with the exception of the most posterior lateral region and medial middle region. Putamen changes were consistent in both hemispheres.

***Thalamus*** Localised changes were evident throughout the middle thalamus, whereas the medial and lateral surfaces were unchanged. The areas of no effect in the medial thalamus correspond to the medial dorsal subnuclei, whereas the areas of change in the middle thalamus cover a number of different subnuclei.

***Globus Pallidum*** In the pallidum, shape changes were evident throughout the dorsal middle region, and were more widely distributed in the

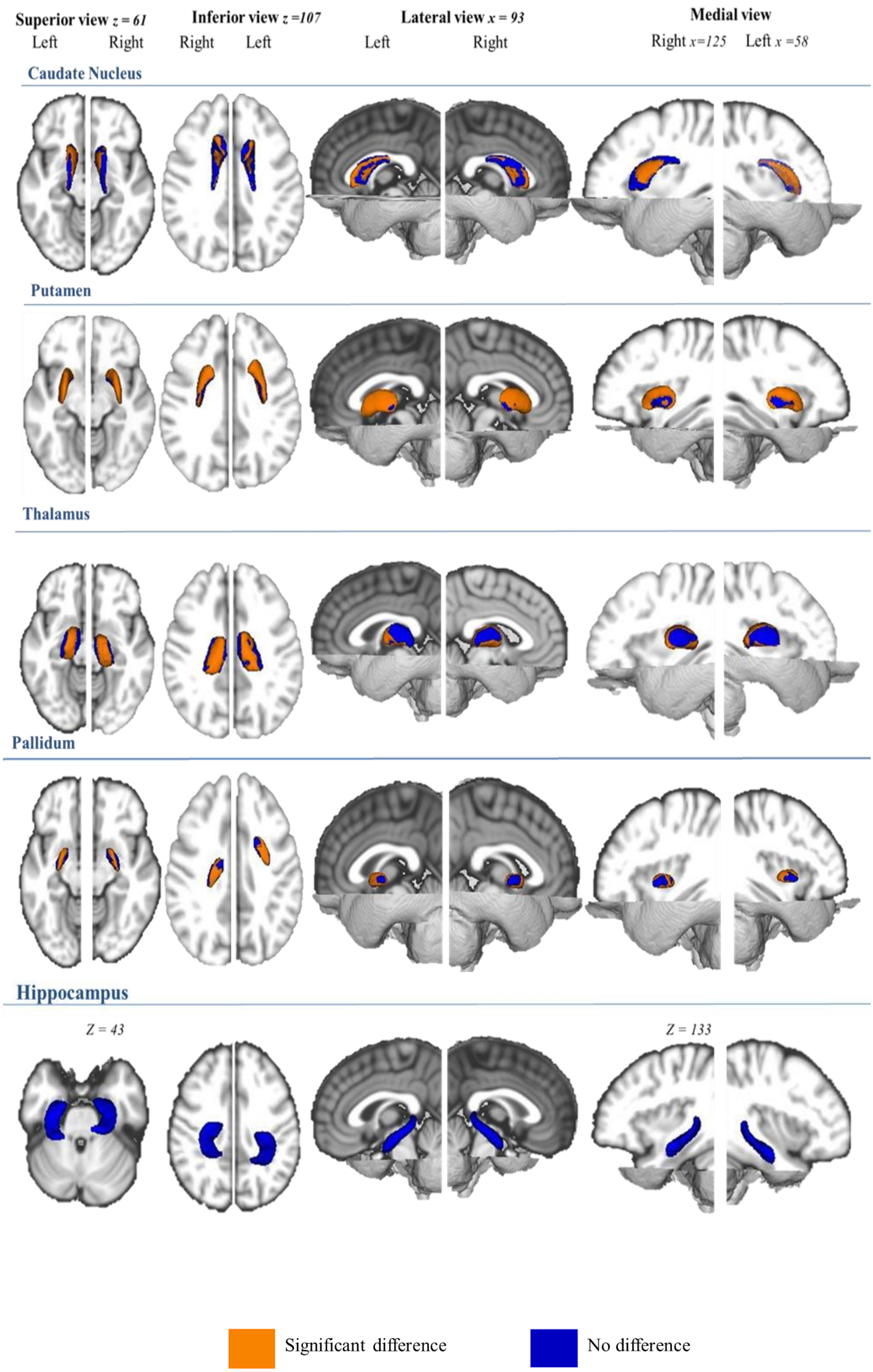
Superior view z = 61
Left
Right
Inferior view z =107
Right
Left
Lateral view x = 93
Left
Right
Medial view
Right x=125
Left x =58
Caudate Nucleus
Putamen
Thalamus
Pallidum
Hippocampus
Z = 43
Z = 133
🟧 Significant difference
🟦 No difference

*Figure continues onto next page…*

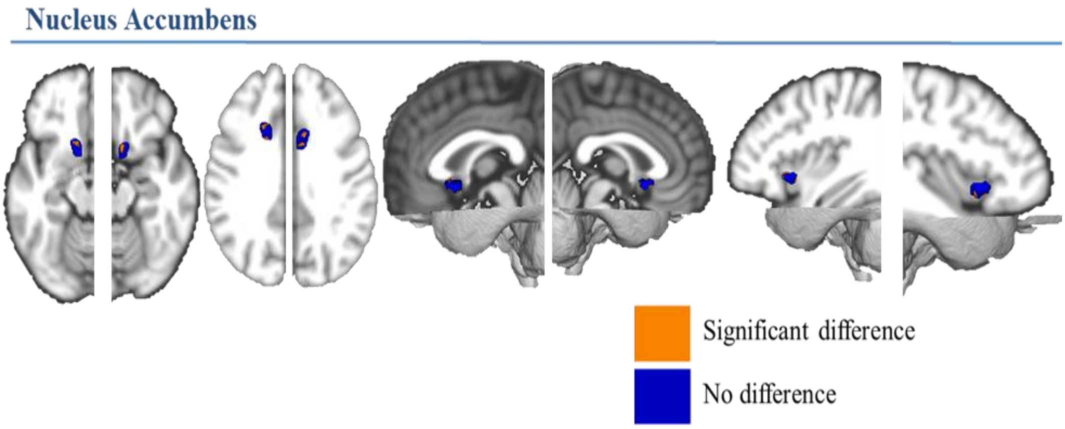

Figure 5.6 Shape analysis for sub-cortical regions, shown from different viewpoints. Orange regions indicate significant difference between HD and control participants after cluster-based multiple-comparison correction. All regions shown overlaid on an MNI-152 space $T_1$-weighted 1mm image.

ventral mid- and posterior pallidum. The medial surface was less affected, whereas the lateral anterior surface was altered in the left but not the right hemisphere. It is not clear how these shape changes relate to the globus pallidus interna and externa separately; whereas the interna segment is positioned medial to the externa segment, change is most evident in the middle of the structure, with image resolution not allowing for a segmentation of the internal structure boundaries.

***Nucleus accumbens*** Shape changes were seen in the middle surface region, both on the superior and inferior surface, although the middle-posterior accumbens was only altered on the anterior surface. There were no significant changes on the medial and lateral surface of the accumbens.

***Hippocampus*** The hippocampus was the control structure and no changes were evident throughout the surface of the structure.

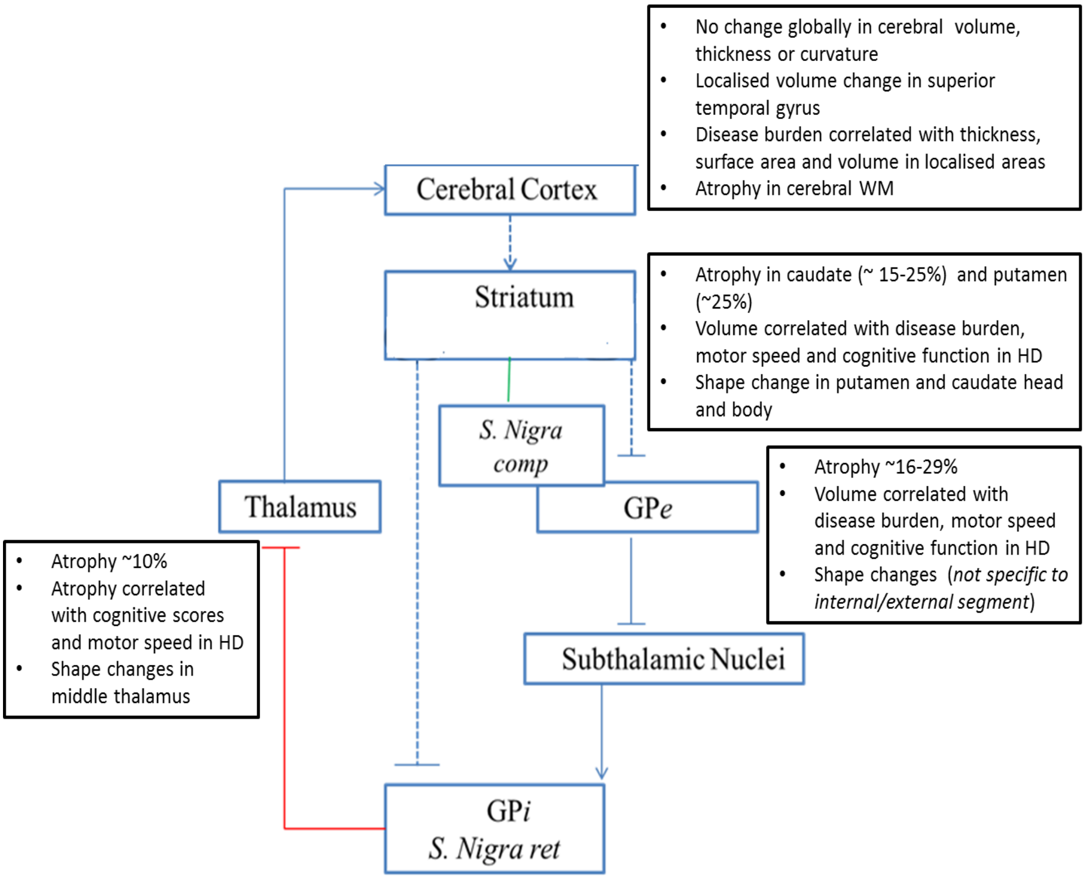
No change globally in cerebral volume, thickness or curvature
Localised volume change in superior temporal gyrus
Disease burden correlated with thickness, surface area and volume in localised areas
Atrophy in cerebral WM
Cerebral Cortex
Striatum
Atrophy in caudate (~ 15-25%) and putamen (~25%)
Volume correlated with disease burden, motor speed and cognitive function in HD
Shape change in putamen and caudate head and body
S. Nigra comp
Atrophy ~16-29%
Volume correlated with disease burden, motor speed and cognitive function in HD
Shape changes (not specific to internal/external segment)
Thalamus
GPe
Atrophy ~10%
Atrophy correlated with cognitive scores and motor speed in HD
Shape changes in middle thalamus
Subthalamic Nuclei
GPi
S. Nigra ret

Figure 5.7 Summary of results in relation to basal-ganglia-cortical circuity in HD participants relative to healthy controls. GM: grey matter. WM: white matter. GP: globus pallidum, i: interna, e: externa. S.Nigra comp: substantia nigra compacta.

## Discussion

Although it is known that macrostructural changes occur in Huntington’s disease prior to the onset of symptoms, this knowledge has arguably been achieved in a disjointed manner, with volume changes reported separately from cortical thickness changes, with either a region-of-interest based approach or a whole brain voxel or vertex-based approach. In this chapter, multiple analysis techniques were used to examine convergence across approaches in the same HD cohort, in order to build a picture of how difference findings relate to each other.

It was found that regionally specific sub-cortical atrophy was disproportionate to whole brain atrophy in the HD participants compared to controls, with the magnitude of atrophy greater than 15% in the caudate, putamen, pallidum and nucleus accumbens. Loss of grey matter volume was predominantly in sub-cortical structures. Both the ROI analysis and the surface-based analysis of the cortex found no abnormalities in cortical volume or cortical thickness, surface area or curvature. However, the whole brain voxel-based analysis found a significant volume change in the grey matter in the superior temporal gyrus, suggesting that cortical changes in HD begin in small localised areas, and supporting work showing a posterior-anterior gradient of cortical disease progression in HD (Rosas et al., 2002). In complement to the microstructural changes reported in Chapter 4, atrophy was evident in the corpus callosum of HD participants, vindicating the decision to correct for partial volume effects. Cerebral white matter and white matter in the basal ganglia was also atrophied in HD participants, supporting the body of evidence for white matter involvement in HD pathology, and suggesting that basal ganglia circuitry may be impaired even at this early stage of the disease. This pattern of results supports previous work which suggested that cortical changes tend to occur later in the disease process compared to changes in the striatum and white matter (Nopoulos, et al., 2010).

In line with previous work (Paulsen, et al., 2010; Tabrizi, et al., 2009), pre-symptomatic and early HD participants were found to have smaller whole brain volumes and grey matter atrophy compared to age, gender and educated-matched healthy controls. An apparent contradiction in the results was no difference in intracranial volume (ICV), which is likely due to the inexact way in which ICV is calculated using Freesurfer software, which can lead to systematic errors compared to manual segmentation (Malone et al., 2014; Nordenskjöld et al., 2013; Pengas, Pereira, Williams, & Nestor, 2009). ICV is estimated based on a linear talairach transform rather than being a direct count of the voxels inside the skull, because the skull is not distinguishable from CSF on $T_1$-weighted images.

### *Relationship between structure and functioning*

Sub-cortical atrophy was found to be functionally relevant, with a strong correlation found between atrophy and finger tapping speed in HD participants. In chapter 3, finger tapping speed was found to be significantly reduced in HD participants, suggestive of motor slowing. Thus, this finding suggests that motor slowing is related to the degree of sub-cortical atrophy. When using volumes segmented using the Freesurfer pipeline, a relationship was found selectively in the putamen, whereas when using FSL, atrophy in the caudate, putamen, thalamus and globus pallidum were also related to finger tapping speed.  The same relationship was not found in control participants.  In addition, the UHDRS motor score was also strongly associated with sub-cortical atrophy, with higher motor impairment associated with a greater degree of atrophy in numerous sub-cortical structures.

In contrast, there was no significant relationship between cognitive functioning and sub-cortical atrophy. Both total grey matter and total white matter atrophy were related to the composite measure of cognitive functioning (see chapter 3), which suggests that global macrostructural changes may be more prognostic in terms of cognitive functioning at this early stage in the disease.  An interesting association was found between larger hippocampal volume and greater cognitive functioning selectively in HD participants. In addition, increased surface area in the posterior cingulate gyrus was associated with greater cognitive functioning, again selectively in HD participants. Anatomically, the posterior cingulate is considered to be part of the limbic system and contains strong reciprocal connections with cortical regions implicated in learning and memory functions, including the hippocampus (Maddock, 1999), thus these two independent findings may be functionally related. One potential explanation for these findings is the concept of compensatory mechanism, whereby the brain undergoes reorganization in response to neurodegeneration to preserve cognitive performance (Papoutsi, et al., 2014). As was observed in both this and the previous two chapters, the severity of structural brain changes is not matched by widespread cognitive changes, and previous work has shown that structural brain changes appear years prior to cognitive decline (Tabrizi, et al., 2009; Tabrizi, et al., 2012; Tabrizi, et al., 2011). The recruitment of new regions to a compromised neural network is one mechanism which may explain this preserved cognitive performance. When faced with marked atrophy in sub-cortical structures centrally involved in cognitive functioning, recruitment of other brains regions involved in cognitive functioning, such as the hippocampus and connected paralimbic regions is plausible and requires further exploration.

A selective association between disease burden, a genetic marker of disease severity and cortical atrophy, sub-cortical atrophy, and topographical cortical thinning was found. These associations were found through a convergence of ROI analysis, VBM and surface-based cortical reconstructions and suggest that the pattern of disease progression is not global across the cortex or sub-cortical regions, but instead follows a selective pattern. Although cortical volume changes were only evident in posterior brain regions with no differences in cortical thickness, it was also found that cortical thinning in both anterior regions (e.g. superior frontal and lateral orbitofrontal cortex and middle frontal gyrus) and posterior regions (e.g. lateral occipital cortex and middle and superior temporal cortex) were related to increased disease severity. This challenges previous work suggesting that cortical thinning follows a posterior to anterior pattern with increased disease progression (H. D. Rosas, et al., 2002). The discrepancy could potentially be due to the limited range in terms of disease progression in this cohort, with pre-dominantly pre-symptomatic HD participants at different stages in terms of distance from disease onset, whereas a symptomatic cohort was used to draw conclusions about the directional trajectory of progression (Rosas, et al., 2002). The lack of a relationship between disease burden and white matter macrostructure suggests that white matter atrophy occurs early in the disease course but remains more stable across the disease stages of HD, whereas neurodegeneration of sub-cortical regions continues with increased disease progression.

Cortical surface area was found to be differentially related to disease burden compared to cortical thickness in HD participants. A novel and intriguing finding was a discrepancy between a positive relationship between cortical surface area and disease burden when calculated based on surface area at the GM/WM boundary, and a negative relationship between surface area and disease burden when calculated using the pial surface area. This discrepancy could be driven by the uneven distribution of neuronal loss across the cortical layers (Hedreen, et al., 1991; Sotrel et al., 1991), with selective degeneration of cells in layer VI of the cortex, and both cortical thinning and atrophy being especially marked in layer VI (Hedreen, et al., 1991; Wagster, Hedreen, Peyser, Folstein, & Ross, 1994), which is the cortical layer at the GM/WM boundary. Thus, surface area may be a more sensitive measure than cortical thickness in tracking layer-specific cortical neuropathology in HD.

### *Changes to the shape of sub-cortical structures*

In light of the sub-cortical atrophy evident at this early disease stage, the final analysis in this chapter considered whether changes in these sub-cortical structures occur in a widely distributed and uniform way, or if structural changes occurs in localised regions with the structure. The shape of a structure is of interest given the functionally distinct white matter circuitry, for example, different subnuclei of the thalamus have been hypothesised to be involved in functionally distinct basal ganglia-thalamo-cortical loops (G. E. Alexander, et al., 1990), and D3 dopamine receptors, affected in HD (Ariano et al., 2002), are distributed mainly in the ventral striatum, which contains limbic connections. There have been two previous studies examining the shape of sub-cortical structures in HD (van den Bogaard, et al., 2011; Younes, et al., 2014), both of which differ in terms of the statistical models used, however both use permutation testing for validation, which is consistent in this study. Van den Bogaard et al (2011) found small areas of deviation from the norm structure in prodromal HD subjects, with fewer areas of shrinkage in the gene positive participants who were far from disease onset. In this study, with a combination of both pre-symptomatic and early HD participants, localised displacement of the structure surface was found in the caudate head more prominently than in the caudate tail, and was more prominent in the medial surface compared to the lateral edges. This specific localised shape change in the medial caudate body was also reported in the Track-HD cohort (van den Bogaard, et al., 2011) suggesting this result is not specific to this patient cohort but may reflect early localised structural change. The medial caudate is known to contain afferent connections from the frontal cortex and limbic system, which may explain the emergence of cognitive and psychiatric changes earlier on in the disease course. In the putamen, changes to the surface shape were found throughout the whole structure. It has been shown that the degree of atrophy is greatest in the putamen (Harris et al., 1992), thus the whole surface may be altered due to the sheer degree of cell loss, or it may be that the putamen contains connections that are uniformly affected in HD, explaining the lack of localised displacement. In the thalamus, localised changes were evident throughout the middle surface, with no changes in the medial and lateral surfaces, suggesting sub-nuclei specific changes occur in the thalamus early in the disease course of HD. Evidence of localised shape deformation was found in both the nucleus accumbens and globus pallidum in HD participants, with the medial surface less affected in both structures. Importantly, in the hippocampus, which was not shown to be atrophied in the ROI analysis and was thus considered to be the control region, no localised shape changes were found.

A limitation of shape analysis is that changes in the exterior shape of a structure are not biologically specific, and may be reflective of a number of factors, such as neuronal loss and/ or white matter atrophy caused by factors such as as a loss of axons or demyelination. Despite this, examining the shape of structures may provide new insights in localized intra-structural atrophy patterns in HD; identifying the specific areas of earliest change may be useful for targeting therapies to slow disease progression.

### *Future work and concluding comment*

Although it was not possible in this dataset due to the limited sample size and large number of predictors, with 10 cases recommended as the minimum per independent variable (Hosmer & Lemeshow, 2000), a future area of analysis in a larger dataset would be to conduct a logistic regression to examine whether both macrostructural and microstructural measures contribute to predicting gene status. Furthermore, a linear regression including individual cognitive tests would be conducted to unpick the relationship between grey and white matter volume and composite cognitive scores, to determine which areas of cognition are most affected by grey and white matter atrophy.

In conclusion, the different analyses techniques in this chapter converge to show alterations in sub-cortical structures in terms of volume and localised shape deformation, with atrophy in these structures being related to a genetic marker of disease burden. There was less convergence across analyses for the cerebral cortex, with only a voxel-based approached finding evidence for cortical atrophy in a localised region in the temporal lobe. Despite this, cortical volume in a localised region in the occipital cortex, and cortical thinning in widely distributed regions were found to be related to disease burden, suggesting that the cerebral cortex contributes to disease pathology at this early stage. Finally, evidence was provided to support a pathological role of white matter in HD that is functionally relevant to cognitive function but less sensitive to changes in disease burden, in comparison to grey matter structures.

# 6 Longitudinal structural imaging of the HdhQ150 mouse model of Huntington's disease

## Chapter Summary

In this chapter, a knock-in mouse model was used to examine whether in vivo MRI can detect neuropathology both before the onset of motor signs, and at a second time point when motor signs are evident. Anatomical $T_2$-weighted MRI and diffusion MRI sequences were acquired using a 9.4T small animal system in order to examine tissue macrostructure and tissue microstructure across time. The relationship between brain structure and motor deficits was examined at the symptomatic time point, and in vivo techniques are presented along with ex vivo high-resolution MRI and immunohistochemistry analysis.

## Introduction

The mutant gene underlying HD was identified in 1993 (Group, 1993) and since then, non-human models of the disease have been developed. Genetic animal models have a similar genetic defect to that seen in the human disease, allowing for the study of early pathological, cellular and molecular alterations caused by the mutation, and can provide a direct measure of neuropathology, which is not possible in patients in vivo. A major benefit of animal models compared to patient studies is that they do not suffer the variance in terms of disease stage, number of CAG repeats and genetic background allowing for greater experimental control.

The longitudinal characterisation of Huntington's disease (HD) mouse lines is crucial in order to understand the developmental time course, nature and severity of phenotype progression over time (Brooks, Jones, & Dunnett, 2012) and ultimately be able to translate this knowledge to the human disease. A major benefit of being able to study disease progression with animals models is that whereas in patients with more advanced stages of HD it is difficult to study structural changes in the brain in vivo due to the incompatibility of chorea with MRI, with animal models the whole disease course can be studied, thus improving understanding of the later stages of the disease.

In recent years, MRI has been applied to animal models of disease in order to study changes in neuroanatomy caused by genetic mutations and/or pathology. The majority of MRI studies using mouse models of HD have been cross-sectional (Carroll, Lerch, Franciosi, & Spreeuw, 2011; Cepeda-Prado, et al., 2012; Lerch, Carroll, Dorr, et al., 2008; Sawiak, Wood, Williams, Morton, & Carpenter, 2009) however the primary value of pre-clinical MRI lies in the capability for within-subject longitudinal designs with increased power and experimental control to study the time course of disease and evaluate therapeutic outcomes and the interaction with disease stage. It is important to examine neuropathology longitudinally with MRI as this can inform the design of future animal studies, allowing for the most appropriate mouse line to be selected depending on the purpose of the study, and providing a readout of the regional and temporal specificity of neuropathology. One area that has not received attention in previous HD mouse studies is the impact on white matter, despite white matter abnormalities being evident at all disease stages in the human disease (Beglinger, et al., 2005; Ciarmiello, et al., 2006; de la Monte, et al., 1988; Dumas, et al., 2012; Klöppel, et al., 2008; Paulsen, et al., 2010; Reading, et al., 2005; Rosas, et al., 2010).

In order to study white matter microstructure, diffusion MRI combined with tractography analysis can provide in vivo 3-dimensional reconstructions of white matter pathways in the brain non-invasively. However, despite diffusion MRI now being a routine scan sequence in human imaging, diffusion MRI of the mouse brain presents significant challenges. A mouse brain is approximately 1000 times smaller than a human brain in term of the total volume (Zhang et al, 2009). Thus, whereas the resolution of human brain diffusion MRI is about 1 - 2 mm per pixel, in order to achieve the same anatomical resolution, the resolution for mouse brain diffusion MRI needs to be 0.1 - 0.2 mm per pixel (Zhang et al, 2009). This is technically challenging in terms of achieving adequate signal to noise ratio (SNR), as SNR is proportional to the volume of the voxel. Although a high field system improves the SNR achieved, it presents its own set of problems in terms of more severe field inhomogeneity and a shortened tissue T2, both of which affect echo planar imaging (EPI) sequences which are commonly used for diffusion MRI acquisition (Le Bihan, Poupon, Amadon, & Lethimonnier, 2006) on account of their ability to effectively freeze physiological motion during the read-out. Physiological motion during the acquisition is a challenge, and carefully controlled anaesthesia, animal constraints and respiratory triggering can minimize but not remove motion effects, whilst the effects of anaesthesia on tissue microstructure remains relatively unexplored.

As detailed in chapters 2 and 4, when analysing MR images acquired using a diffusion sequence, the diffusion tensor model is inadequate for reconstructing white matter pathways in the human brain due to the inability to describe voxels with crossing fiber configurations (Seunarine & Alexander, 2009). In response to this, more sophisticated approaches have been developed, including spherical deconvolution (SD) techniques which allow recovery of the fibre orientation density function (fODF) in tissue irrespective of complexity. In the mouse brain, crossing fibers are also an issue (see Figure 6.1), yet despite this, there are currently no published studies where non-tensor based tractography has been applied.

In this chapter, a spherical deconvolution based approach was applied to perform whole brain tractography analysis and gain information on tissue microstructure, along with $T_2$-weighted anatomical imaging to measure tissue macrostructure. The knock-in HdhQ150 mouse model was examined over the course of the animals' natural lifetime. Knock-in models in HD are generated by homologous recombination techniques using mouse embryonic stem cells. Thus, the HdhQ150 mice (Lin, et al., 2001) were created by directly replacing the normal mouse endogenous CAG repeat length with an expanded 150 CAG sequence in the mouse Htt gene without affecting the rest of the endogenous sequence of the gene. Behaviourally, the phenotype of $Hdh^{Q150/Q150}$ mice has been well characterised longitudinally. Just as in the human disease, $Hdh^{Q150/Q150}$ mice display cognitive deficits prior to the onset of motor abnormalities, defined as the benchmark for formal diagnosis in humans, with extra-dimensional set-shifting deficits (Brooks et al., 2006) and reduced reactivity to an acoustic startle evident at 6 months of age. Weight loss is not evident in male $Hdh^{Q150/Q150}$ mice until 13 months of age when other cognitive deficits emerge, such as impairments in finding the submerged platform on the Morris water maze (Heng, et al., 2007).

Neuropathological characterisation from ex vivo histological analysis has shown that $Hdh^{Q150/Q150}$ mice display many of the characteristics of the human disease including Htt aggregation that is most marked in the striatum but also evident to a lesser degree in the cortex, thalamus and hippocampus, as well as neuronal intra-nuclear inclusions (Bayram-Weston, Torres, Jones, Dunnett, & Brooks, 2012; Lin, et al., 2001). These neuropathological changes are evident from around 5 months of age followed by striatal cell loss at 8 months of age (Bayram-Weston, et al., 2012). Thus, this mouse model was chosen because both the appearance of cognitive and motor symptoms follows the temporal pattern seen in the human disease, neuropathological specificity has been demonstrated (Brooks et al., 2012) and because neuropathological changes are detectable prior to the onset of motor signs, in line with the human literature from the pre-symptomatic disease stage.

Based on the above research into the temporal appearance of symptoms, 7-months was selected as the first time-point to represent the pre-symptomatic stage of the human condition, as cognitive deficits and neuropathology is evident in the absence of motor signs. 19 months of age was selected to represent the symptomatic time point where both cognitive and motor deficits were evident.

## *Declaration of Collaborations*

In this chapter, the volumes of structures obtained from an automated atlas-based segmentation protocol are presented. The development of the protocol and the processing of the data through the pipeline were conducted by Ma Da at UCL as part of a collaborative project. In addition, perfusions were conducted with assistance from Jane Heath, a technician in the Brain Repair Group.

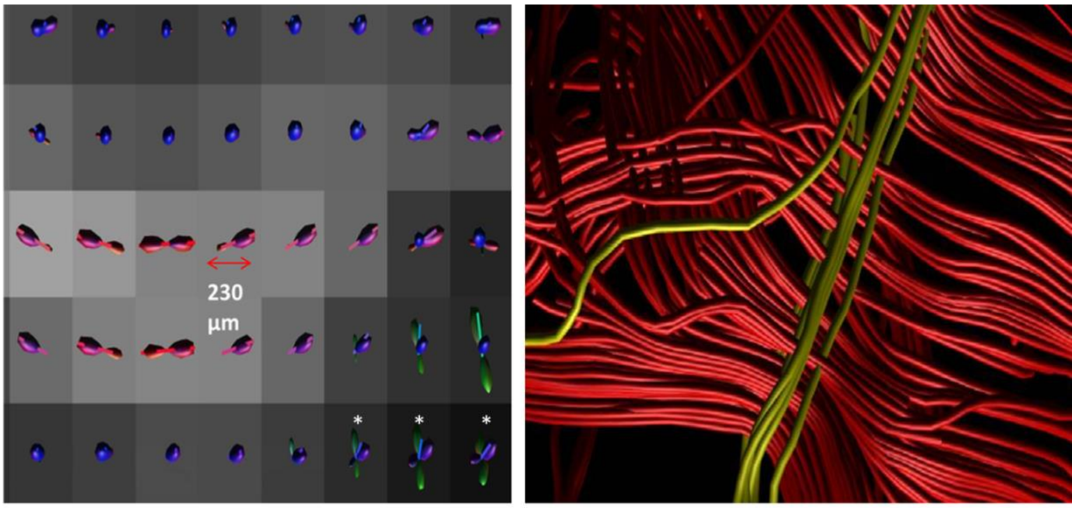

Figure 6.1 Demonstration of crossing fibers in the mouse brain using spherical harmonic tractography analysis (Tournier et al., 2008). On the left, in each voxel, the principaldiffusion direction (sticks) and the fiber orientation distribution (ellipsoids) are shown, the white stars showing examples of voxels containing more than one fiber orientation. Right: Corpus callosum tracts shown in red, cingulum fibers shown in yellow.

## Methods

### Subjects

Twenty-five homozygous knock-in ($Hdh^{Q150/Q150}$) male mice (mean CAG repeat length on allele 1: 147 ±7 SD, allele 2: 158 ± 5) and 25 age-matched wild type male mice ($Hdh^{+/+}$) were used in the study. Homozygote mice were used in order to be comparable to published behavioural work in this mouse model (Brooks, Higgs, Jones, et al., 2012). Details on breeding, animal housing and genotyping are described in Chapter 2. Due to long separation times during MRI scanning at 7 months, there was a problem with fighting between cage mates, thus all mice were individually housed from 7 months of age.

### Body weight

As a general indicator of mouse health, mice were weighed monthly throughout their lifetime. In HD mouse lines, progressive weight loss is a sign of the advancement of the disease state and is considered as a core feature of these

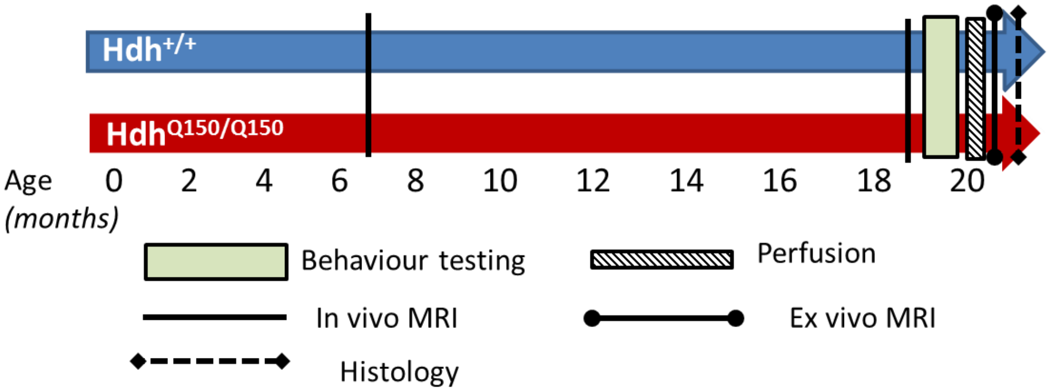
Hdh+/+
HdhQ150/Q150
Age
(months)
0
2
4
6
8
10
12
14
16
18
20
Behaviour testing
Perfusion
In vivo MRI
Ex vivo MRI
Histology

Figure 6.2 Experimental design from birth to 20 months. Wild-type mice: $Hdh^{+/+}$, homozygous mice: $Hdh^{Q150/Q150}$

models (Brooks, Higgs, Jones, et al., 2012).

### *MRI Acquisition*

The experimental design, showing the 3 MRI sessions, is detailed in Figure 6.2. MRI acquisition and animal preparation details are described fully in Chapter 2. A phased array mouse head surface coil was used in this study. Due to the long scan times and to improve animal health and recovery, 500 μl of glucose saline was administered via sub-cutaneous injection immediately prior to the MRI session and immediately after the MRI session. The anaesthesia protocol was amended on the advice of the vet following the first scan session, where 10% of the animals did not recover from anaesthesia. The carrier gas was changed from medical air to 100% $O_2$ and the scans were conducted in two separate sessions one week apart, with the $T_2$-weighted structural scan first.

***Macrostructural MRI*** For both in vivo and ex vivo acquisition, a 3D Turbo Rapid Acquisition with Refocused Echoes (RARE) $T_2$-weighted scan was used. For the in vivo sequence, parameters were: field of view (FOV) of 1.54 x 1.54 cm, in-plane resolution of 120 x 120 μm, matrix of 128 x 128 x 64, TR/ TE = 1750/17.5 ms, bandwidth 50000 Hz, RARE factor of 4, 1 average, with an acquisition time of approximately 1 hour 8 minutes. For the ex vivo scans, the resolution was 60um$^3$ with the following parameters: FOV 1.54 x 1.54cm x 1.02cm, matrix = 256 x 256 x 168, TR/TE = 1750/17.5 ms (effective echo time = 35 ms), bandwidth 50000 Hz, RARE factor of 4, 3 averages, with an acquisition time of 11 hours.

***Diffusion MRI*** 27 adjacent axial slices of 320 µm in thickness were acquired. Navigator echoes were used to minimise distortion artefacts due to multiple segments. 2 averages were used to increase the signal to noise ratio (SNR). The in-plane resolution was 213 x 213 µm at a FOV of 2.24cm x 2.24cm and an acquisition matrix of 96 x 96. Partial Fourier with an acceleration factor of

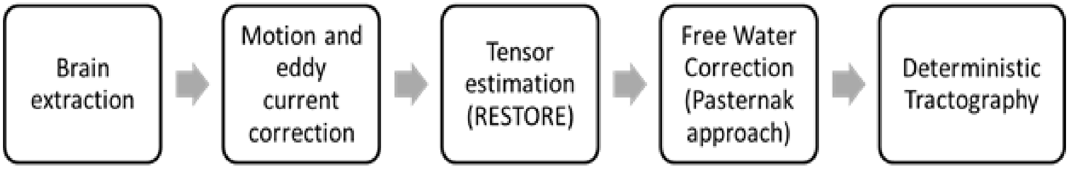
Brain extraction
Motion and eddy current correction
Tensor estimation (RESTORE)
Free Water Correction (Pasternak approach)
Deterministic Tractography

Figure 6.3 Preprocessing steps of diffusion MR data using ExploreDTI software (Leemans, Jeurissen, & Sijbers, 2009).

1.35 and 23 overscan lines were used in order to reduce the acquisition time. 4 dummy scans were used at the beginning of the acquisition in order to achieve magnetisation equilibrium. Respiratory-gating was used to minimise respiratory motion artefacts. At both time points, data were acquired with a b-value of 1000 s/mm$^2$ applied over 30 diffusion-weighted directions (Jones 30) in three dimensional space with 3 b0 images without diffusion weighting, TR/TE = 8500 /18.70 ms, δ /Δ = 4 /9 ms. The acquisition time was on average 1 hour but varied depending on the rate and stability of respiration for each mouse. Post-processing stages are represented in Figure 6.3 and described fully in Chapter 2.

## *MRI image analysis*

***Atlas-based segmentation of T2-weighted images*** In order to obtain a less labour-intensive measure that was not dependent on the expertise of the rater, raw $T_2$-weighted images were analysed using an automated multi-atlas based structural parcellation pipeline (D. Ma et al., 2014) as part of a collaboration with the Centre for Advanced Biomedical Imaging (CABI) in University College London. The following pipeline was developed by researchers at CABI and the pre-processing steps applied by Ma Da (CABI, UCL) according to the protocol outlined in (D. Ma, et al., 2014).

Briefly, the brain was first extracted to remove non-brain tissue. This was achieved by creating a mask for the native subject image from multiple atlas images (Leung et al., 2011). The MRM atlas (Y. Ma et al., 2005; Y. Ma et al., 2008) was selected for use after comparing parcellation results achieved with different atlases. The native subject image was globally registered to all atlas images (Ourselin, Roche, Prima, & Ayache, 2000) and the resulting transformation matrices were then inverted and used to propagate all the atlas brain masks to the native image. The mask was dilated to enhance the contrast between brain tissue and CSF. Due to the high field strength, it was necessary to correct for intensity non-uniformity which can cause misalignment during image registration, thus the non-parametric non-uniform intensity normalization technique (N3) (Sled, Zijdenbos, & Evans, 1998) was used to correct the bias field (

Figure 6.4). The affinely aligned atlas images from the brain extraction step were non-linearly registered to each Hdh$^{+/+}$/Hdh$^{Q150/Q150}$ mouse image (Modat et al., 2010) and the resulting deformation fields were then used to register the labels from the MRM atlas space to native space with nearest-neighbour interpolation to preserve the integer nature of the labels. These labels were then fused using the Multi-STEPS algorithm (Jorge Cardoso et al., 2013; D. Ma, et al., 2014), which utilised a locally normalised cross correlation similarity metric for atlas selection (Figure 6.4). From the labelled images, a number of regions of interest (ROI)'s were delineated and the total volume of these regions calculated. The total brain volume for the in vivo images was defined as the summed volume across all labelled brain regions (40 regions for the MRM atlas). ROI's were the caudate putamen, thalamus, globus pallidus, hippocampus, neocortex, cerebellum and ventricles. All masks and labels were visual inspected for quality.

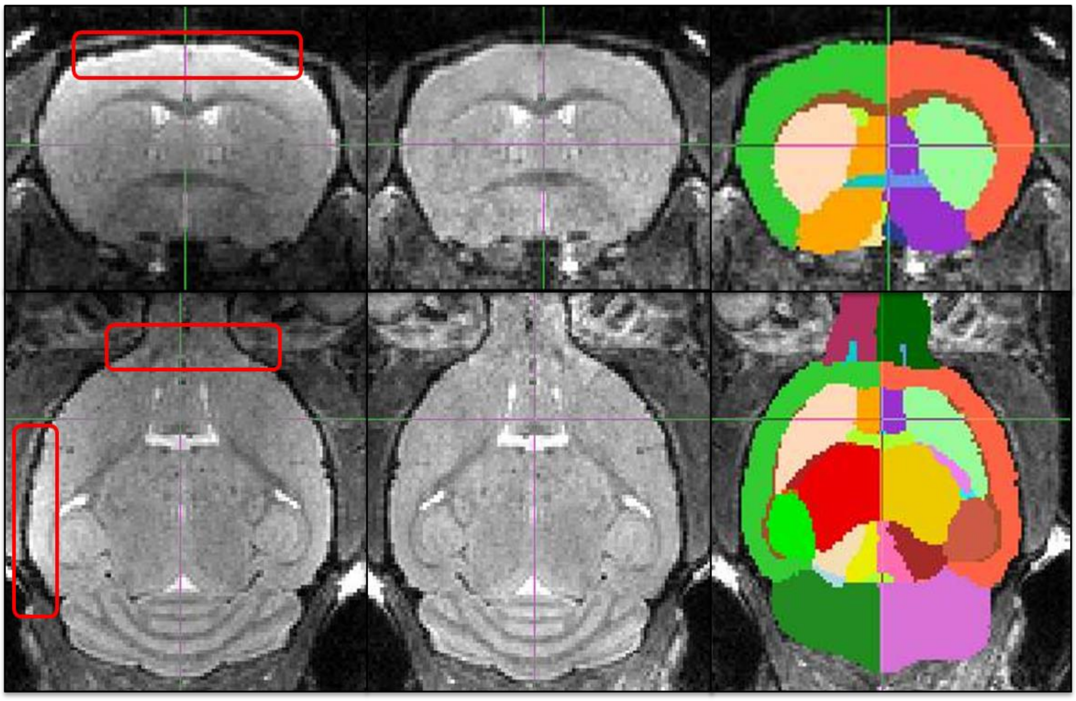

Figure 6.4 Atlas Based Segmentation of the HdhQ150 mouse brain. The left hand panel shows the raw in vivo $T_2$-weighted image of a representative $Hdh^{+/+}$ mouse brain at 19 months old in the coronal (top) and axial (bottom) plane. The red box shows areas of prominent non-uniformity. The middle plane shows the same brain slice after intensity non-uniformity correction. The right-hand plane shows the labelled regions based on the MRM atlas

***Voxel Based Analysis (VBA).*** VBA was performed in SPM8 (Wellcome Department of Clinical Neurology, London; http://www.fil.ion.ucl.ac.uk) using the SPMMouse toolbox (Sawiak et al., 2009). The grey/white matter tissue priors were not used as the grey matter segmentation results were not satisfactory. Instead, grey matter segmentation was achieved using the grey matter labels from the atlas-based approach detailed above. The intensity non-uniformity corrected images were registered to a C57/Bl6 atlas image (SPMmouse, Sawiak et al., 2009) using a 6-dof rigid body and similarity registration (three translations and three rotations, FSL). These images were then smoothed with a 500 µm isotropic Gaussian kernel to reduce the effect of imperfect image registration and non-normality in the data. A two-tailed Student's t-test was performed voxel-wise on the data to examine differences in localised density; multiple comparisons were corrected for using the false-discovery rate (FDR) technique (Benjamini & Hochberg, 1995) with a threshold of $p = 0.05$ for statistical significance. However, in order to control for the effect of individual brain sizes, the total intracranial volume was added as a covariate, as is standard practice for VBA.

***Deterministic Tractography*** For the tractography analysis of fiber pathways, whole-brain deterministic tracking was conducted using ExploreDTI (Leemans, et al., 2009). Deterministic tractography (Jeurissen, Leemans, Jones, Tournier, & Sijbers, 2011) was performed using the damped Richardson-Lucy algorithm (DRL; Dell-Acqua et al., 2010) as described in Chapter 2. The tracking algorithm estimated the fiber orientation distribution function (fODF) at each seed point and propagated in 0.05 mm steps along this direction, with an angle threshold of 40°; the SH order was 6. Three-dimensional reconstructions of the corpus callosum were then extracted from these whole-brain tractograms using multiple waypoint ROI’s which were drawn manually in native space on color-coded fiber orientation maps (Pajevic & Pierpaoli, 2000) by a single operator blinded to the genotype of the mouse. Representative ROIs are shown in Figure 6.5; ‘AND’ gate ROI’s are shown in green and select fibers that traverse both ROI’s. The corpus callosum was segmented with an initial ROI drawn on the colour-coded diffusion image in the sagittal plane on the midline slice in order to capture all the tracts passing through this ROI, which included many association fibers and fibers of the external capsule. The analysis was then restricted to the corpus callosum using two additional ‘AND’ gate ROI’s which were drawn in the sagittal plane in line with the medial cingulum in both hemispheres as visualised in the coronal plane. These two lateral boundaries were used to remove any external capsule pathways. Partial volume correction was performed to account for free water contamination as described in chapter 2 (Pasternak, et al., 2009) and the mean tensor based metrics (FA, MD) were obtained along the corpus callosum along with the free water fraction.

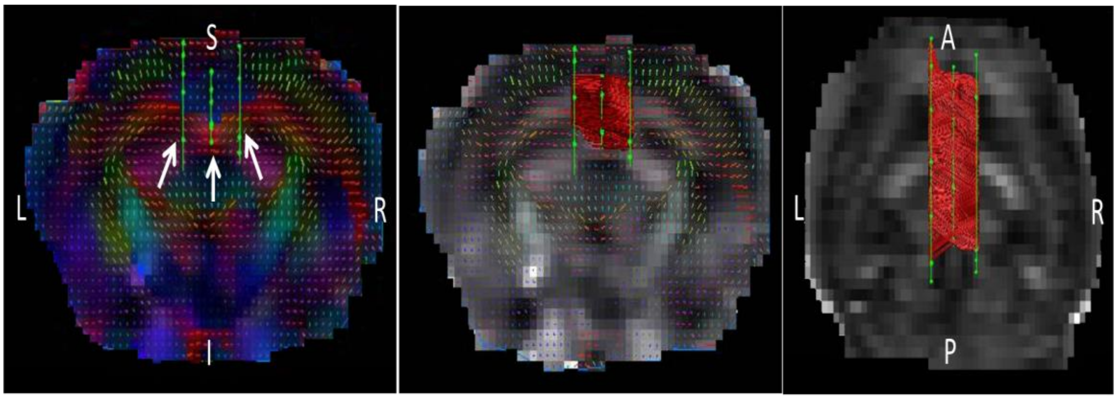

Figure 6.5 Deterministic tractography of the corpus callosum. Left: arrows indicate the placement of the 3 'AND' gates, shown in the coronal plane overlaid on a colour-coded FEFA map with principal diffusion vectors shown in each voxel. Middle pane shows reconstructed tracts in the coronal plane, right pane shows the same tracts in the axial plane, both overlaid on a single subject FA map.

### *Perfusion*

Mice were perfused using the methodology described in Chapter 2.

### *Immunohistochemistry*

The generic immunohistochemistry methodology is described in Chapter 2. Mouse anti-NeuN (1:1000, Millipore) was used to detect markers for neuronal nuclei. The sections were then washed several times in TBS and incubated with goat anti-mouse secondary antibody at a 1:200 concentration (Vector Laboratories, Burlingame, CA, USA) for 2 h at room temperature. Sections were then delipidised by dehydration in ascending alcohols and I hour in xylene before being counter-stained for myelin.

***Staining for myelin*** Solochrome (erichrome) cyanine was used to identify myelin. The sectioned tissue was hydrated by serial washes in 100%, 95% and 70% ethanol and distilled water for 5 minutes each and then immersed for 35 minutes in solochrome cyanine solution (Appendix 1). Sections were then thoroughly washed in distilled water and differentiation was carried out in 10% Iron Alum (Appendix 1) for 2-3 minutes and halted by thorough washing in distilled water. Sections were dehydrated by serial washes in 70% , 95% and 100% ethanol for 2 minutes each, cleared in xylene, and cover-slipped with DPX mounting medium (RA Lamb, Eastbourne, UK).

### ***Assessment of Cortical Thickness***

For comparison purposes, cortical thickness was measured on approximately the same coronal sections for both the MRI images and the prepared brain sections (see Figure 6.6). Analysis was conducted using Analyze software (version 10.0) for the MRI images and using a Leica microscope for the mounted brain sections.

For the mounted brain sections, measurements were made at a 5x objective with background correction for uneven illumination. In order to assess regional cortical atrophy, thickness measurements of primary motor cortex (M1) were taken. A vertical line was drawn covering all cortical layers from the most dorsal horn of the corpus callosum to the pial surface. The mean length taken was at approximately Bregma 1.10mm (at the section where the corpus callosum bridges across the two hemispheres), Bregma 0.14 mm (where the anterior commissure crosses the midline), Bregma -0.22mm (where the internal capsule, dorsal 3rd ventricle and 3rd ventricle can be seen), and Bregma -1.06 mm (where the lateral ventricles are lateral to the hippocampus). These sections provide consistent landmarks between animals and provide good coverage of the motor cortex.

### ***Behavioural measures***

At 20 months of age, mice were assessed for motor deficits. It was not possible to assess cognitive deficits due to the period of time required for training

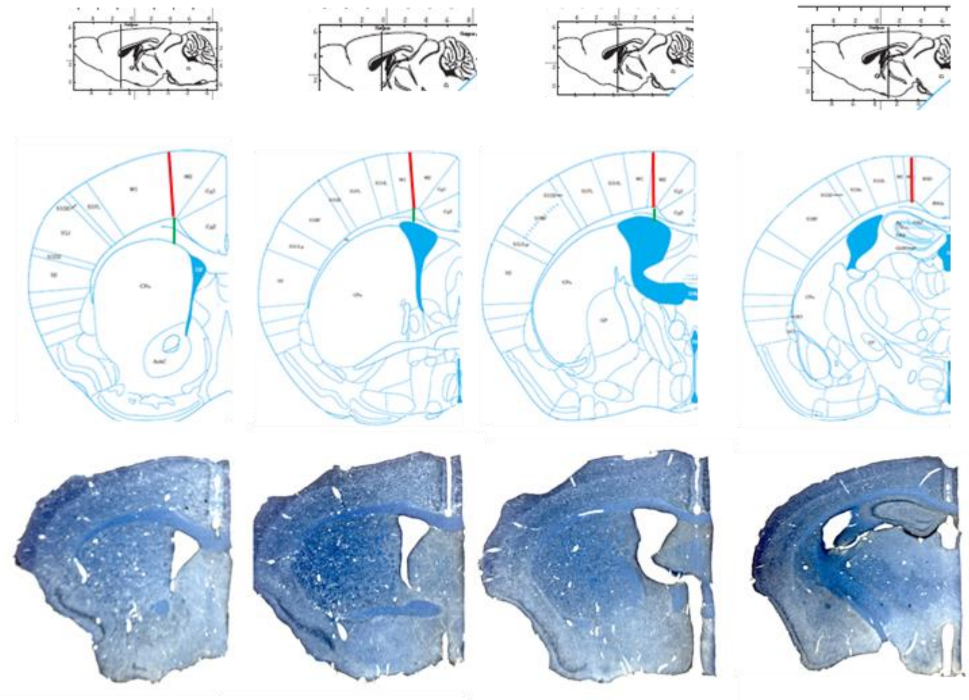

Figure 6.6 Approximate Bregma positions where measures of cortical thickness were made. Red line indicates approximate position of cortical measurement. Bottom image shows representative stained sections for cortical thickness measures (blue = myelin, brown = neuronal cells).

and the age of the mice. The Open Field test, locomotor activity over 24-hours, and Rotarod test were conducted as described in Chapter 2. For the Open Field test, statistical analysis was performed on the following dependent measures: total locomotion (cm), average time spent moving (seconds), velocity (cm/s) and rearing frequency.

### *Statistical Analysis*

It was not possible to assess the natural attrition rates across the life span of the mice because some mice did not recover from exposure to anaesthesia. Thus, a chi-square non-parametric test was used to examine survival during the first 7 months separately from survival during the two scan sessions. Finally, survival between the first and second time-point (7-19 months) was analysed separately.

For body weight, missing values were handled using SPSS IBM 20 Missing Values Analysis add-in; missing values were imputed based on expectation-maximization estimation. A mixed model ANOVA was then used to assess differences in weight due to genotype over multiple time-points. Post-hoc t-tests were then used to assess differences in weight between $\mathrm{Hdh}^{+/+}$ and $\mathrm{Hdh}^{Q150/Q150}$ mice separately for each month, and were corrected for multiple comparisons using the FDR.

For behavioural results, the correlation between weight and motor performance was first tested to decide if weight should be included as a covariate. Pearson’s correlation coefficients greater than 0.3 were treated as indicative of a moderate relationship and justified inclusion as a covariate. Before conducting the Analysis of Covariance (ANCOVA), the assumptions of homogeneity of regression slopes (between weight and behaviour) was tested across groups ($\mathrm{Hdh}^{Q150/Q150}$ vs. $\mathrm{Hdh}^{+/+}$ mice) to examine whether weight interacts with genotype. Where a significant interaction was found and the direction of the relationship was the same for both $\mathrm{Hdh}^{Q150/Q150}$ and $\mathrm{Hdh}^{+/+}$ mice, weight was added as a covariate and both the main effects of genotype and the corrected model, encompassing the contribution of weight, were reported, in the knowledge that the genotype effects are not fully separated from the effect of genotype on body weight.

For the tractography analysis of diffusion MRI images, a repeated-measures analysis-of-variance (ANOVA) design was used, with the corpus callosum segment (genu, body, splenium) as the within-subject variable, genotype as the independent variable and the tensor based metrics (FA, MD, AD, RD) as the outcome measure.

For both cortical thickness measures and volumetric analysis of $T_2$-weighted images, the correlations between total brain volume (TBV) and the MRI measures (thickness or volume) were first tested. The homogeneity of regression slopes (between TBV and either cortical thickness or volume) was tested across groups ($\mathrm{Hdh}^{Q150/Q150}$ vs. $\mathrm{Hdh}^{+/+}$ mice) to examine whether TBV interacts with genotype. Where an interaction was found, but results were in the same direction (i.e. a positive correlation found for both $\mathrm{Hdh}^{+/+}$ and $\mathrm{Hdh}^{Q150/Q150}$ mice), TBV was added as a covariate. An analysis of covariance (ANCOVA) approach was chosen over a proportional approach, whereby the ROI volume is divided by the total brain volume. The ANCOVA approach allowed the interactive effects resulting from a different relationship between the ROI and total brain volume depending on genotype to be incorporated into the analysis through an interaction term in the model. A mixed model ANCOVA was used, with hemisphere, and cortical region (4 Bregma positions) as within-subject variables and genotype as the between-subject factor. For the VBA analysis, a two-tailed t-test was conducted using SPM8 software (Wellcome Department of Clinical Neurology, London) with total intracranial volume added as a covariate.

## Results

### *Survival*

There was no difference in survival rate between Hdh$^{+/+}$ and Hdh$^{Q150/Q150}$ in the first 7 months of life and prior to the first MRI session ($\chi$ (1, n =50) = 1.02, $p > 0.05$). Similarly, for recovery from anaesthesia during the first MRI session at 7 months old, the relationship between genotype and recovery was not significant ($\chi$ (1, n =49) = 0.27, $p > 0.05$). From 7-19 months of age, there was also no significant difference between survival of Hdh$^{+/+}$ compared to Hdhq50 mice ($\chi$ (1, n =44) = 1.0, $p > 0.05$). During the 19-month scan, there was a relationship between genotype and recovery from the anaesthesia; Hdh$^{Q150/Q150}$ mice were less likely to survive the scan session compared to age-matched Hdh$^{+/+}$ mice ($\chi$ (1, n =38) = 4.02, $p < 0.05$). As a consequence, late stage behavioural tests and the histological analyses are based on correspondingly reduced and unequal group sizes.

### *Weight*

Figure 6.7 shows the weights of the two groups of animals throughout the lifespan. There was a significant interaction between genotype and time for body weight measured monthly from 2 to 19 months old (*Greenhouse-Geisser corrected* F (12.04, 145.89) = 27.30, $p < 0.001$, $\varepsilon = .179$). Post-hoc tests found that Hdh$^{Q150/Q150}$ had significantly smaller body weight compared to age-matched Hdh$^{+/+}$ mice at every time point from 3 months of age onwards, all $p < 0.05$ FDR-adjusted. Body weight was not significantly correlated with any of the behavioural measures for Hdh$^{Q150/Q150}$ mice and Hdh$^{+/+}$ mice alike, all $p > 0.05$. Modest, non-significant correlations with body weight were found with a number of measures (see Appendix 3), and body weight was included as a covariate where $r > 0.3$.

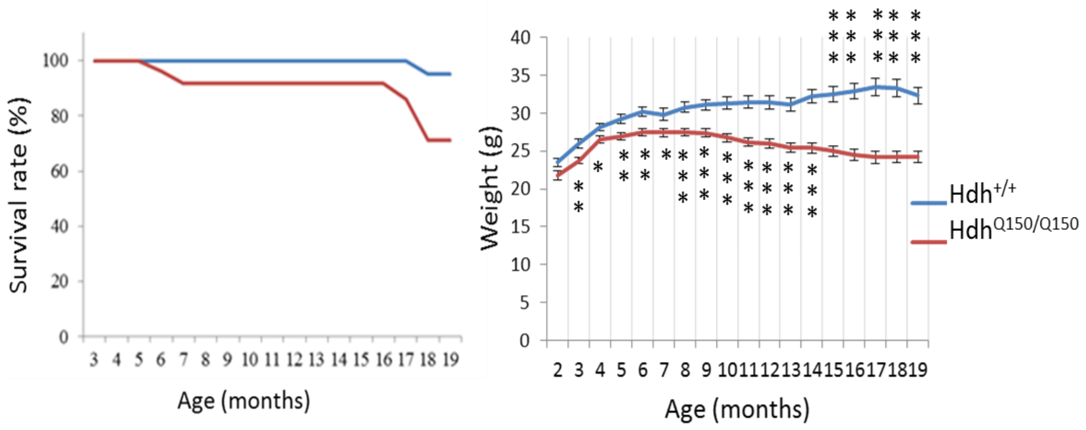

Figure 6.7 Left: Survival rates excluding cases where there was no recovery from anaesthesia (at 7 and 19 month scans). Right: Weights of animals weighed in the middle of each month. Error bars represent standard error of the mean (S.E.M). * $p < 0.05$ FDR-adjusted, ** $p < 0.01$ FDR-adjusted, *** $p < 0.001$ FDR-adjusted.

### *Behavioural changes at 19 months old*

Descriptive statistics for all behavioural tests are shown in Figure 6.8.

**Circadian-related activity** Transfer/habituation activity was measured over the first 2 hours of the testing period. There was no difference in activity levels between Hdh$^{Q150/Q150}$ mice and Hdh$^{+/+}$ mice (F (1, 26) = 0.003, $p > 0.05$). With weight as a covariate, Hdh$^{Q150/Q150}$ mice were more active than Hdh$^{+/+}$ mice during the light phase (F (1, 26) = 5.26, $p < 0.05$ FDR-corrected), and during the dark phase (F (1, 26) = 4.49, $p < 0.05$ FDR-corrected).

**Rotarod** Hdh$^{Q150/Q150}$ mice had a significantly shorter latency to fall from the rotating rod averaged over 2 trials compared to Hdh$^{+/+}$ age-matched mice, F (1,27) = 9.8, $p<0.05$.

**Open Field Test** Individual t-tests found that total distance moved, total time spent moving, velocity, and rearing frequency were significantly reduced in Hdh$^{Q150/Q150}$ mice compared to Hdh$^{+/+}$ mice (t (20) = 2.39, 2.42, 2.31 and 2.75 respectively, all $p < 0.05$ FDR-corrected). However, when body weight was a covariate, the difference between groups was no longer significant, all $p > 0.05$. Analysis of the univariate main effects revealed that the difference in performance between Hdh$^{Q150/Q150}$ and Hdh$^{+/+}$ mice was driven by Hdh$^{Q150/Q150}$ mice engaging in rearing behaviour significantly less frequently compared to Hdh$^{+/+}$ mice, (F (1,22) = 10.075, $p < 0.05$). There was also a main multivariate effect of weight (Wilks' $\lambda$ = .333, F (4, 19) = 5.58 $p > 0.05$), however this did not affect any one behavioural measure specifically, with no univariate main effect of weight for any measure, all $p > 0.05$.

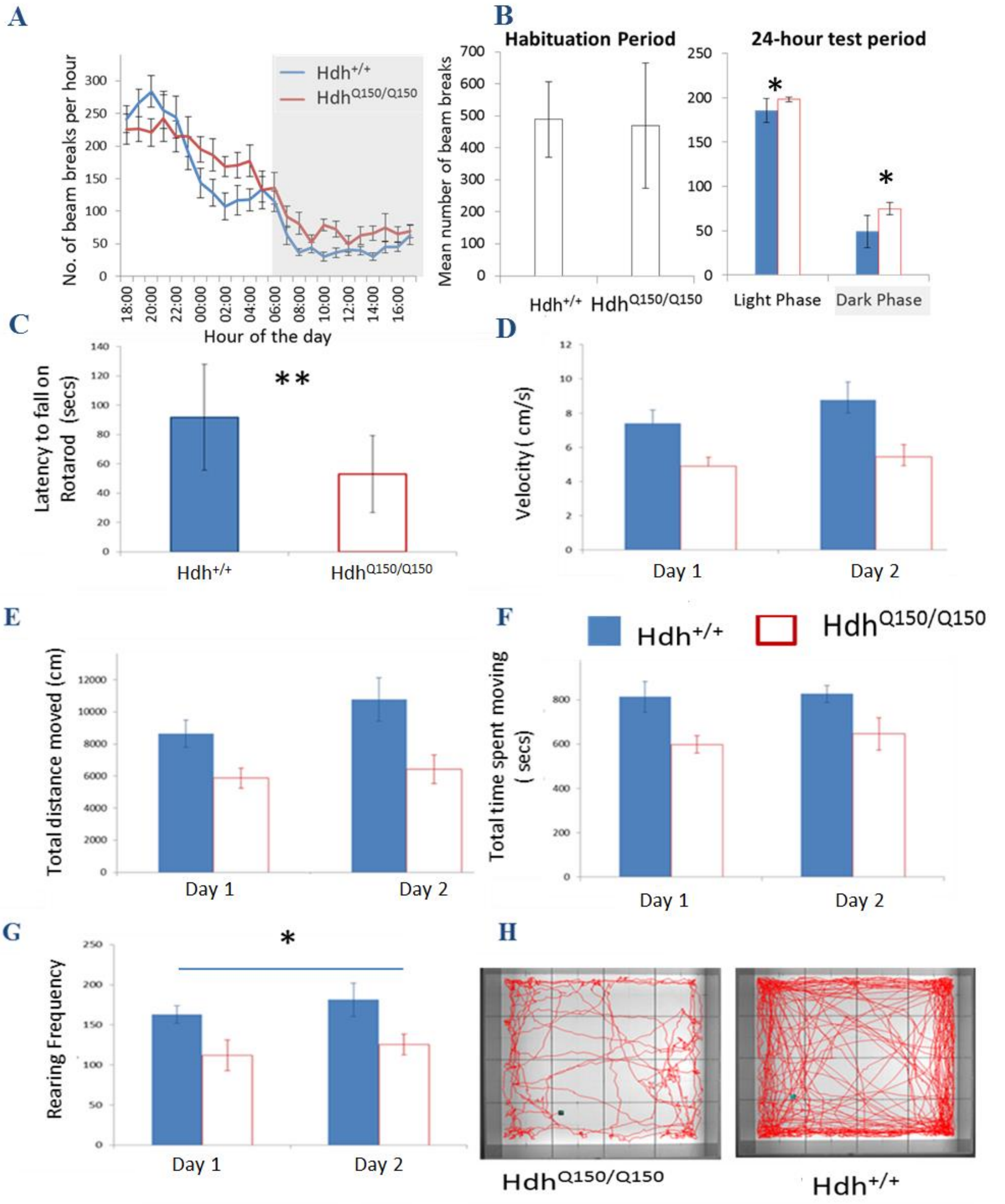

Figure 6.8 Behavioural Assessment at 19 months old. A: Total number of beam breaks per hour over a 24-hour period B: Average number of beam breaks in the first 2 hours in the boxes, during the light phase (18:00-05:59) and the dark phase (06:00-17:59) C. Latency to fall on Rotarod test, averaged over 2 trials. D-H Open Field Test measured on 2 consecutive days. D: Velocity (cm/s) E: Total Distance Moved (cm), F: total time spent moving, G: Frequency of rearing behaviour. F. Map of movements made in 20-minute period by a single $Hdh^{Q150/Q150}$ mouse and single $Hdh^{+/+}$ mouse. Error bars A-E represent ± standard error of the mean. * $p < 0.05$, ** $p < 0.01$, all FDR-adjusted for multiple comparisons.

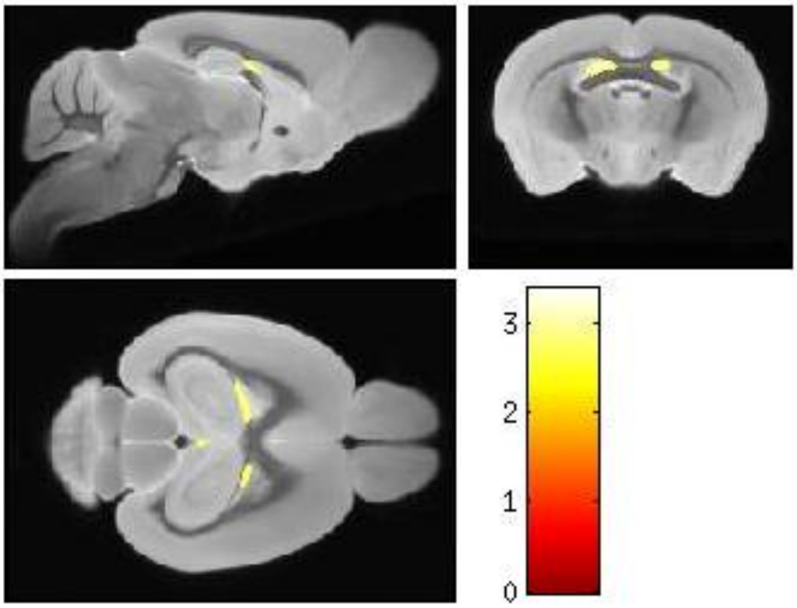

Figure 6.9 Results of the VBA analysis at 7 months of age. Colour bar represents t-statistics. T = 3.301 represents $p < 0.001$ uncorrected. T = 2.42 represents $p < 0.01$ uncorrected. Statistics are showed overlaid on an average C57 / Bl6 T2-weighted image.

### *Structural changes detectable with MRI*

***Voxel Based Analysis*** At 7 months old, with TBV as a covariate, results from the voxel-wise analysis revealed an increase in localised relative density in the lateral ventricles in $Hdh^{Q150/Q150}$ mice compared to $Hdh^{+/+}$ mice at the voxel level at $p \leq 0.001$ uncorrected, df = 41, z = 3.07, and at the cluster-level (k = 936), $p < 0.05$ uncorrected. The results are shown in Figure 6.9. At 20 months, with the reduced sample size, there were no differences between $Hdh^{+/+}$ and $Hdh^{Q150/Q150}$ mice at $p < 0.001$ uncorrected. For the $Hdh^{Q150/Q150}$ mice and $Hdh^{+/+}$ mice alike, there was no difference found in density from 7 months to 20 months, $p > 0.001$ uncorrected.

***Atlas based morphometry*** After visual inspection, segmented volumes for the globus pallidum and lateral ventricles were removed from the analysis for 2 $Hdh^{+/+}$ mice and 2 $Hdh^{Q150/Q150}$ mice at 7 months due to imperfect segmentation. For ex vivo images, the cortex was not included in the analyses for 5 $Hdh^{+/+}$ mice, due to imperfect segmentation and/or damage to the cortex in sample preparation. The relationship between TBV and volume in the specific regions of interest are shown in Table 6.1. When testing the homogeneity of regression slopes between $Hdh^{+/+}$ and $Hdh^{Q150/Q150}$ mice, a significant interaction effect was seen for all of the regions with the exception of the globus pallidum and right thalamus, indicating that the relationship between TBV and both cortical and sub-cortical volume differs between $Hdh^{+/+}$ and $Hdh^{Q150/Q150}$ mice, such that any differences seen between the two groups of mice will also be dependent on a difference in TBV. Thus, TBV was added as a covariate and statistical analyses on both the absolute volumes and the volumes with TBV as a covariate are reported.

TBV was significantly reduced at 7 months of age in $Hdh^{Q150/Q150}$ mice (-5.66%) compared to age-matched $Hdh^{+/+}$ mice (F (1, 43) = 11.03, $p < 0.01$). Similarly, at 19 months of age, TBV was also significantly reduced (-11.68%) in $Hdh^{Q150/Q150}$ mice compared to $Hdh^{+/+}$ mice (F (1, 26) = 20.35, $p < 0.001$). There was no main effect of time-point on TBV (F (1, 25) = .431, $p > 0.05$) with no significant change in volume observed from 7 to 19 months old in either $Hdh^{+/+}$ of $Hdh^{Q150/Q150}$ mice. For ex vivo images acquired at 20 months old, the cerebellum and brain stem were not included in the measure of TBV due to artefacts related to ex vivo preparation in this region in a number of images, thus TBV is not directly comparable to the in vivo measurements. There were no genotype differences in TBV in these ex vivo images (4.08%, F (1, 34) = 1.70, $p > 0.05$).

In the basal ganglia, absolute caudate-putamen volume was significantly reduced in $Hdh^{Q150/Q150}$ mice at 7 months (-7.5%, F (1, 42) = 16.65, $p < 0.01$ FDR-corrected), and at 19 months (-14.3%, F (1, 26) =13.35, $p < 0.01$ FDR-corrected). In the ex vivo images acquired at 20 months, the reduction in absolute caudate-putamen volume in $Hdh^{Q150/Q150}$ was smaller than the in vivo measurements (-5.63%), and this difference was not significant (F (1, 34) = 1.82, $p > 0.05$).

Table 6.1 Relationship between total whole brain volume (TBV) and volume in regions of interests (ROI's) at 7 and 19 months in vivo, and at 20 months ex vivo. Genotype*TBV: interaction between TBV and genotype. **$p < 0.001$, * $p < 0.05$.

| | Caudate-Putamen (L) | Caudate-Putamen (R) | Thalamus (L) | Thalamus (R) | GP(L) | GP (R) | Hippocampus (L) | Hippocampus (R) | Neocortex (L) | Neocortex (R ) | Cerebellum (L) | Cerebellum (R) | Ventricles (L) | Ventricles ( R) |
|---|---|---|---|---|---|---|---|---|---|---|---|---|---|---|
| ***7 - months*** | | | | | | | | | | | | | | |
| ***Correlation with TBV*** | | | | | | | | | | | | | | |
| **Pearson's Correlation Coefficient** | | | | | | | | | | | | | | |
| $Hdh^{+/+}$ | .708** | .826** | .827** | .863** | 0.305 | .745** | .895** | .953** | .589** | .642** | .823** | .870** | .606** | .783** |
| $Hdh^{Q150/Q150}$ | .641$^{**}$ | .687$^{**}$ | .765$^{*}$ | .789$^{**}$ | 0.329 | .648$^{**}$ | .784** | .760$^{**}$ | .585** | .847$^{**}$ | .674** | 0.746** | .493* | .526* |
| ***Test of homogeneity of regression slopes*** | | | | | | | | | | | | | | |
| **p-values (uncorrected)** | | | | | | | | | | | | | | |
| **Genotype * TBV** | 0.00 | 0.00 | 0.00 | 0.053 | 0.115 | 0.053 | 0.00 | 0.00 | 0.00 | 0.00 | 0.00 | 0.00 | 0.00 | 0.00 |
| ***19 - months*** | | | | | | | | | | | | | | |
| **Pearson's Correlation Coefficient** | | | | | | | | | | | | | | |
| $Hdh^{+/+}$ | .847$^{**}$ | .754$^{**}$ | .866$^{**}$ | .908$^{**}$ | .690$^{**}$ | 0.438 | .688$^{**}$ | .675$^{**}$ | .603** | .636** | 0.465 | .491* | 0.296 | 0.174 |
| $Hdh^{Q150/Q150}$ | .967$^{**}$ | 898** | .923** | .947** | .896$^{**}$ | .713$^{*}$ | .774$^{**}$ | .863$^{**}$ | .892** | .909** | .915** | .911** | .847** | .873** |
| ***Test of homogeneity of regression slopes*** | | | | | | | | | | | | | | |
| **p-values (uncorrected)** | | | | | | | | | | | | | | |
| **Genotype * TBV** | 0.00 | 0.00 | 0.00 | 0.00 | 0.00 | 0.01 | 0.00 | 0.00 | 0.00 | 0.00 | 0.00 | 0.00 | 0.00 | 0.04 |
| ***20-months ex vivo*** | | | | | | | | | | | | | | |
| **Pearson's Correlation Coefficient** | | | | | | | | | | | | | | |
| $Hdh^{+/+}$ | .800$^{**}$ | .794$^{**}$ | .682$^{**}$ | .723$^{**}$ | 0.275 | .470$^{*}$ | .596$^{**}$ | .648$^{**}$ | .954$^{**}$ | .576* | n/a | n/a | -0.157 | |
| $Hdh^{Q150/Q150}$ | .647$^{**}$ | .675$^{**}$ | .703$^{**}$ | .688$^{**}$ | 0.329 | 0.287 | .698$^{**}$ | .522$^{*}$ | .857$^{**}$ | .782** | n/a | n/a | 0.233 | |
| ***Test of homogeneity of regression slopes*** | | | | | | | | | | | | | | |
| **p-values (uncorrected)** | | | | | | | | | | | | | | |
| **Genotype * TBV** | 0.00 | 0.00 | 0.00 | 0.00 | 0.47 | 0.539 | 0.00 | 0.002 | 0.00 | 0.00 | n/a | n/a | 0.068 | |

After adding TBV as a covariate in the analysis, caudate-putamen atrophy in the Hdh$^{Q150/Q150}$ mice was still evident at 7 months (F (1, 41) = 4.46, $p < 0.05$ uncorrected), whereas at 19 months and 20 months ( ex-vivo) there was no localised atrophy in the caudate-putamen (F (1, 25) = 0.069, $p > 0.05$, and F (1,33) = .279, p>0.05 respectively). Absolute globus pallidum volume was also reduced in Hdh$^{Q150/Q150}$ mice at 7 months (- 7.8 %, F (1, 38) = 9.55, $p < 0.01$ FDR-corrected), and at 19 months (-16.16%, F (1, 26) = 5.92, $p < 0.05$ FDR-adjusted), whereas at 20 months, there was no difference in volume on ex vivo images (1.69%, F (1, 34) = .156, p >0.05). After adding TBV as a covariate in the analysis, there was no difference in globus pallidum between Hdh$^{Q150/Q150}$ and Hdh$^{+/+}$ mice at 7 months (F (1, 37) = 1.25, $p > 0.05$), 19 months of age (F (1, 25) = 0.01, $p > 0.05$), and at 20 months ex vivo (F (1, 33) = .766, $p > 0.05$).

The volume of the absolute thalamus shows a similar reduction to the basal ganglia structures in Hdh$^{Q150/Q150}$ mice (- 7.19%) compared to Hdh$^{+/+}$ mice at 7 months old (F (1, 42) = 12.14, $p < 0.01$ FDR-corrected). At 19 months, absolute thalami volume was also reduced (-12.20%) in Hdh$^{Q150/Q150}$ mice (F (1, 25) = 17.77, $p < 0.01$ FDR-corrected). Similarly, in ex vivo images acquired at 20 months, absolute thalami volume was also reduced (-7.11%) in Hdh$^{Q150/Q150}$ mice (F (1, 34) = 4.73, $p < 0.05$ uncorrected). The right thalamus was found to be larger than the left thalamus at each time point, $p < 0.05$ uncorrected. After adding TBV as a covariate in the analysis, there was no difference in volume between the two groups of mice at 7 months (F (1, 41) = 1.73, $p > 0.05$), 19 months (F (1, 24) = 0.099, $p > 0.05$), and 20 months ex vivo (F (1, 33) = 2.87, $p > 0.05$).

Absolute hippocampus volume was significantly reduced in Hdh$^{Q150/Q150}$ mice at 7 months (- 6.61%, F (1, 42) = 12.98, $p < 0.01$ FDR-corrected), and at 19 months old (-12.44%) compared to Hdh$^{+/+}$ mice (F (1, 26) = 20.45, $p < 0.01$ FDR-corrected). In the ex vivo images acquired at 20 months, absolute hippocampal

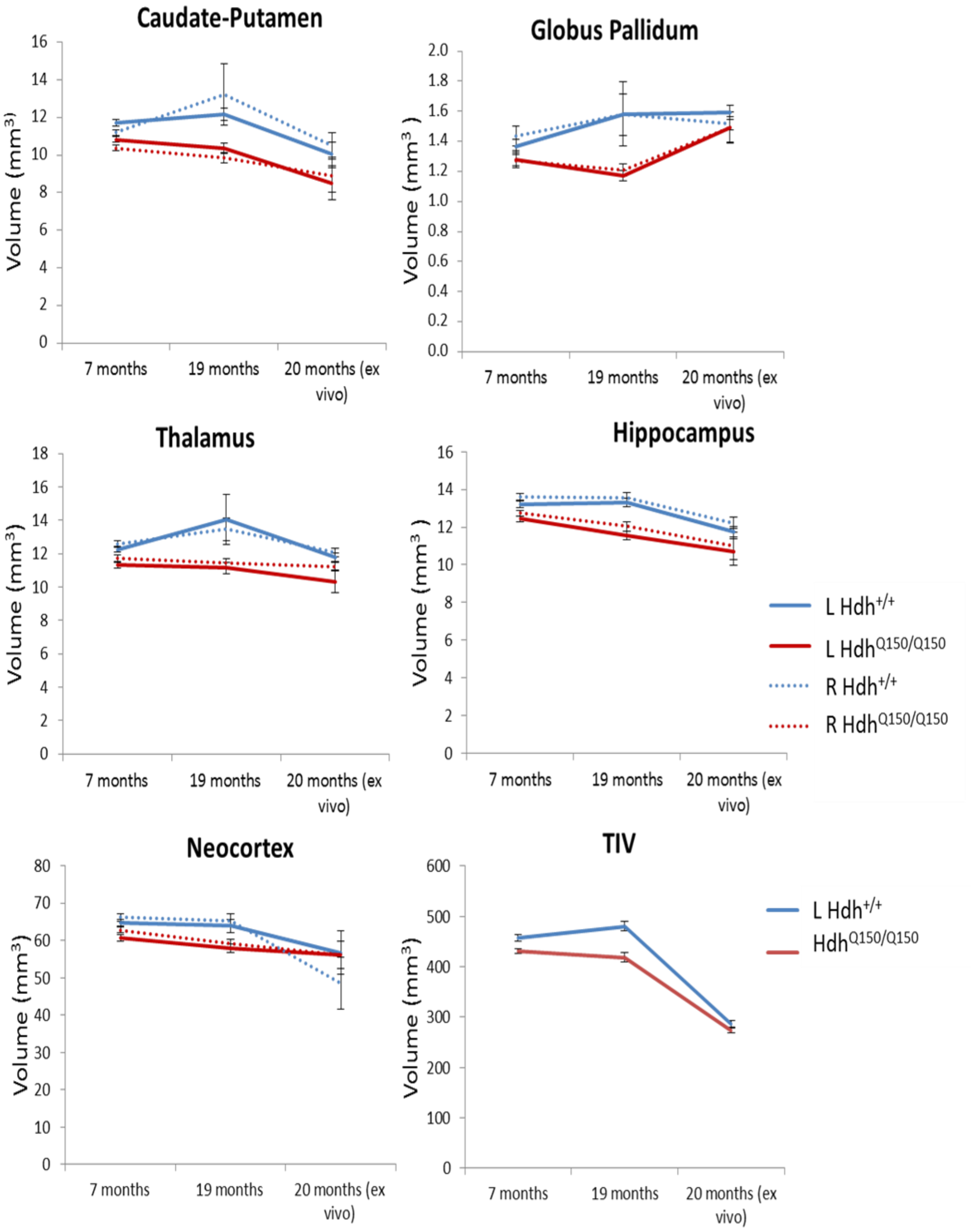

Figure 6.10 Absolute results of Atlas-Based Segmentation of T2-weighted images. Error bars represent standard errors of the mean. TBV: Total brain volume; L: left hemisphere, R: right hemisphere. Note that for TBV calculations from ex vivo images at 20-months, the cerebellum and brain stem were excluded due to artefacts.

volume showed a similar decrease as total brain volume (-4.11%) in Hdh$^{Q150/Q150}$ mice (F (1, 34) = 1.39, $p > 0.05$). After adding TBV as a covariate in the analysis, hippocampi volume was unaltered at 7, 19, and 20 months of age (F (1, 41) = 1.53, $p > 0.05$, F (1, 25) = 1.74, $p > 0.05$, and F (1, 33) = .198, $p > 0.05$ respectively).

Compared to total brain volume, the absolute neocortex volume showed a similar degree of atrophy (-5.70%) in Hdh$^{Q150/Q150}$ mice at 7 months (F (1, 42) = 9.34, $p < 0.05$ FDR-corrected), and at 19 months old (-10.53%, F (1, 26) = 8.07, $p< 0.05$ FDR-corrected). At 20 months ex vivo, the absolute neocortex volume reduced by 9.00% in Hdh$^{Q150/Q150}$ mice (F (1, 29) = 5.43, $p < 0.05$ uncorrected). After adding TBV as a covariate in the analysis, there was no difference in volume between the two groups of mice at 7, 19, and 20 months old (F (1, 41) = .965, $p > 0.05$, F (1, 25) = 0.02, $p > 0.05$ and F (1, 28) = .180, $p > 0.05$ respectively).

Similarly, the absolute cerebellum appeared to be relatively spared in Hdh$^{Q150/Q150}$ mice; absolute cerebellum volume was not significantly reduced at 7 months old (-2.29%; Hdh$^{Q150/Q150}$ = 27.04 ± .32 mm$^3$, Hdh$^{+/+}$ = 27.67 ± .52 mm$^3$, F (1, 42) = 1.06, $p > 0.05$), or at 19 months (-4.24%; Hdh$^{Q150/Q150}$ = 26.96 ±.83 mm$^3$, Hdh$^{+/+}$ = 28.21 ± .48 mm$^3$, F (1, 26) = 1.96, $p > 0.05$). However, after adding TBV as a covariate, the difference in cerebellum volume between Hdh$^{Q150/Q150}$ and Hdh$^{+/+}$ mice was significant at 7 months of age (F (1, 41) = 6.71, $p < 0.05$ uncorrected), but not at 19 months old (F (1, 25) = 2.25, $p > 0.05$). In order to examine whether cerebellum volume was relatively larger or smaller at 7 months after accounting for total brain volume (TBV), the normalised ([ROI/TBV]*100) statistics were calculated and revealed that normalised cerebellum volume is larger in Hdh$^{Q150/Q150}$ mice (12.54 ± .11 % of TBV) compared to Hdh$^{+/+}$ mice ( 12.09 ± .12 %). Thus, the cerebellum appears to be spared at both timepoints in Hdh$^{Q150/Q150}$ mice.

For the ventricles, the difference in absolute volume between Hdh$^{Q150/Q150}$ (mean = 3.08 ± .0.058 mm$^3$) and Hdh$^{+/+}$ mice (mean = 3.31 ± .065 mm$^3$) was significant at 7 months old (6.82%, F (1, 40) = 7.35, $p < 0.05$), whereas at 19 months, the 4.54% difference in ventricular volume was not significant ( mean Hdh$^{Q150/Q150}$ = 3.59 ±.31 mm$^3$, mean Hdh$^{+/+}$ = 3.76 ± .18 mm$^3$, F (1, 27) =.288, $p > 0.05$). Ex vivo measurements at 20 months showed that absolute ventricular volume was reduced by 15.10% in Hdh$^{Q150/Q150}$ mice (2.29 ± .11mm$^3$ vs. 2.69 ± .11 mm$^3$ for Hdh$^{+/+}$ mice, F (1, 33) = 6.67, $p < 0.05$ uncorrected). After TBV was added as a covariate, the difference in ventricular volume was not significant at 7 months (F (1, 39) = .437, $p > 0.05$), and at 19 months (F (1, 25) = 3.04, $p > 0.05$), whereas ex vivo measurements of ventricular volume were significantly reduced in Hdh$^{Q150/Q150}$ mice (F (1, 32) = 6.23, $p < 0.05$ uncorrected).

In the Hdh$^{Q150/Q150}$ mice, after accounting for TBV, there was a strong negative correlation between latency to fall on the rotarod test, and volume in the right thalamus, r = -.832, $p < 0.05$ FDR-corrected. A moderate relationship was found with the left thalamus, r = -.668, $p < 0.05$ uncorrected. In Hdh$^{+/+}$ mice, the relationship with the thalamus was weak, r = -.299 and -.098 for left and right hemisphere respectively, $p > 0.05$. Performance on the Open Field test was not significantly correlated with regional volume for Hdh$^{Q150/Q150}$ mice and Hdh$^{+/+}$ mice alike, all $p > 0.05$ FDR-corrected. Average non-perseverative behaviour over a 24-hour period was found to be correlated with neocortical volume in Hdh$^{+/+}$ mice, r = .642, $p < 0.05$ FDR-corrected, whereas the same relationship was weaker in Hdh $^{Q150/Q150}$ mice, r= .304, $p > 0.05$. There was no relationship with perseverative behaviour.

***Cortical thickness*** Hdh$^{Q150/Q150}$ mice had significantly thinner cortices compared to Hdh$^{+/+}$ mice on in vivo MRI images (F (1, 24) = 13.30, $p < 0.001$). Post-hoc tests, with TBV as a covariate, at the two time-points separately found that at 7 months old, prior to the onset of motor signs, the difference in cortical thickness between Hdh$^{Q150/Q150}$ and Hdh$^{+/+}$ (-2.8%) was not statistically significant (F (1, 37) = 2.53, $p > 0.05$). At 19 months old, the motor cortices in the Hdh$^{Q150/Q150}$ mice were approximately 8.7 % thinner compared to age-matched Hdh$^{+/+}$ mice (F (1,23) = 9.226, p < 0.01). In accordance with the in vivo results, for measurements made on higher-resolution images acquired ex vivo at 20 months, the motor cortices were approximately 9.3% thinner in Hdh$^{Q150/Q150}$ mice compared to age-matched Hdh$^{+/+}$ mice (F (1,30) = 9.33, p < 0.01 with TBV as a covariate).

For measurements from histologically stained sections, the motor cortices in the Hdh$^{Q150/Q150}$ mice were approximately 5.4 % thinner compared to age-matched Hdh$^{+/+}$ mice, but this difference did not meet statistical significance (t (15) = 1.05, p > 0.05). A multivariate analysis found that cortices were significantly thinner when measured using chemically stained tissue sections, compared to ex vivo MRI (Wilks' λ =.117, F (1,12) = 90.37, p < 0.001).

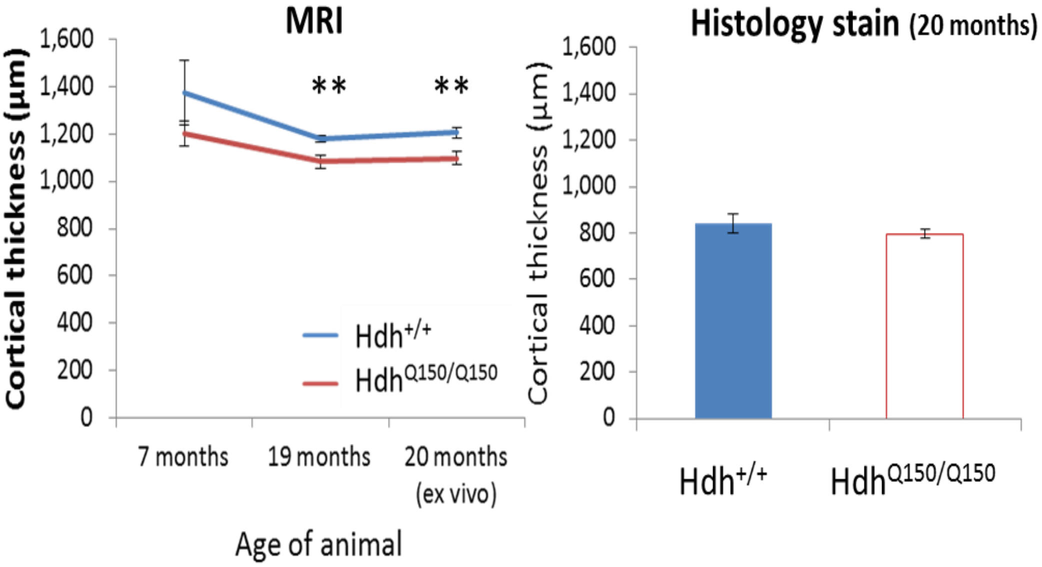

Figure 6.11 Cortical thickness measures from MRI images at different ages (left) and myelin-stained 40 µm brain sections at 20months old (right). Error bars represent standard errors of the mean. ** represents p< 0.01. Both the 7 and 19 month scans were acquired in vivo. All data are averaged across Bregma positions, and MRI measures are averaged across hemispheres.

Figure 6.11 shows the cortical thickness MRI measurements at each time-point and the measurements obtained from the stained sections. There was a main effect of Bregma position for the in vivo measurements at 7-months (F (3,126) = 275.5 and 191.8 for left and right hemisphere), and at 19 months (F (3,78) = 73.73 and 85.2 for left and right hemisphere respectively), and ex vivo MRI measures ( F (2.27, 74.80) = 148.84, ε = .756) and measurements made on stained sections (F (1.54, 20.02) = 13.11, ε = .513), all $p < 0.001$. For all main effects, the cortex was significantly thicker in more anterior brain slices compared to more posterior slices in measurements. However there was no interaction between Bregma position measured and genotype, all $p > 0.05$. In terms of laterality effects, there was no difference between measurements taken in the left and right hemisphere from in vivo measurements at 7 months (F (1, 37) =4.08, $p > 0.05$) and 19 months (F (1, 23) 2.47, $p > 0.05$), however there was a difference between hemispheres on the ex vivo MRI images at 20 months (F (1, 30) = 13.95 $p < 0.01$). For both $Hdh^{+/+}$ and $Hdh^{Q150/Q150}$ mice, there was no relationship between cortical thickness at any age/preparation, and motor function, after correcting for multiple comparisons using the false discovery rate (FDR), all $p > 0.05$.

### *White matter microstructural changes*

At 7-months of age, prior to the onset of motor signs, there was no difference in tensor based values or free water fraction in the corpus callosum between $Hdh^{Q150/Q150}$ mice [*n =20*] and age-matched $Hdh^{+/+}$ mice [*n = 23*], all $p > 0.05$. At 19-months of age, prior to correcting for free water contamination, all diffusivity values were lower in the $Hdh^{Q150/Q150}$ mice compared to $Hdh^{+/+}$ mice (t(30) = 2.3, 2.13, and 2.3 for MD, AD and RD respectively, $p < 0.05$ uncorrected, $p = 0.056$ FDR-corrected). After free water correction, the differences in diffusivity values were not significant (t (29) = 1.77, 1.72, and 1.60, $p > 0.05$ uncorrected), and there was no difference in FA values between groups (t (29) = .567, $p > 0.05$). The free water fraction did not differ between $Hdh^{Q150/Q150}$ (.282 ± .011) and $Hdh^{+/+}$ mice (.281

±.010), at 7 months (t, 41) = -.077, $p > 0.05$), or at 19 months, (Hdh$^{Q150/Q150}$=.239± .014, Hdh$^{+/+}$ = .253±.011; t (29) = .790, $p > 0.05$). There was a significant difference between uncorrected and free water corrected tensor values for FA at 7-months (F (1, 40) = 953.65, $p < 0.001$), and 19-months, (F (1, 29) = 264.56, $p < 0.001$), and MD at 7-months (F (1, 40) = 884.28, $p < 0.001$), and at 19-months (F (1, 29) = 583.56, $p < 0.001$). Examining change over time, free water corrected FA values were found to be significantly reduced at 19-months of age compared to 7-months in both Hdh$^{Q150/Q150}$ mice (t (13) = 2.93, $p < 0.05$ FDR-corrected) and Hdh$^{+/+}$ mice (t (15) = 2.92, $p < 0.05$ FDR-corrected). There was no change in MD values over time for either group of mice, both $p > 0.05$. Free water fraction in the corpus callosum was found to decrease from 7-months to 19- Months (t (29) = 2.16, $p< 0.05$) although this did not survive correction for multiple comparisons. Free water correction FA was positively correlated with locomotor velocity on the Open Field task in Hdh$^{Q150/Q150}$ mice, r = .691, $p < 0.05$ uncorrected, whereas the same relationship was not found in Hdh$^{+/+}$ mice, r = -.240.

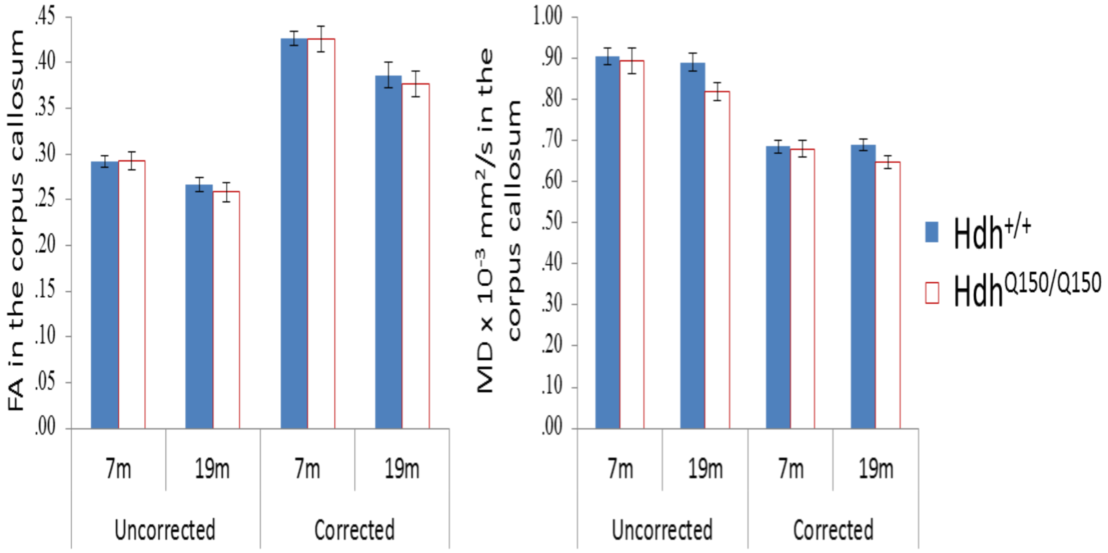

Figure 6.12 Mean tensor-based values for tract reconstructions along the corpus callosum at 7 months and 19 months of age, for uncorrected values and values corrected for free water contamination (Pasternak, Sochen, Gur, Intrator, & Assaf, 2009). Error bars represent standard error of the mean.

Free water fraction was negatively correlated with rearing frequency (normalised for body weight) on the Open Field task in Hdh$^{+/+}$ mice, r = -.574, $p < 0.05$ FDR-corrected, whereas the same relationship was not significant in Hdh$^{Q150/Q150}$ mice, $p > 0.05$.

## Discussion

The HdhQ150 mouse model of HD has previously been well characterised in terms of behavioural phenotype and neuropathology (Brooks, Jones, et al., 2012). However, characterisation of neuropathology has been restricted to ex vivo techniques that are limited to cross-sectional designs and beset by methodological issues with tissue fixative altering the tissue structure under examination. In this first application of in vivo MRI to the HdhQ150 model, total brain volume (TBV) was reduced at 7-months, prior to the onset of motor signs, and at 19-months of age, when motor signs were present. TBV was found to interact with genotype in accounting for differences in regional volume loss; at 7-months old, the relationship between TBV and regional volume was stronger in Hdh$^{+/+}$ mice compared to Hdh$^{Q150/Q150}$ mice, whereas at 19-months old, the relationship between TBV and regional volume was stronger in Hdh$^{Q150/Q150}$ mice. Localised atrophy not wholly accounted for by global volume loss was evident in the caudate putamen at 7-months of age along with an increase in localised density in the lateral ventricles. The cerebellum was relatively spared at both time points in Hdh$^{Q150/Q150}$ mice. At 19-months old, localised atrophy in numerous sub-cortical and cortical regions was not significant after controlling for global volume loss, although cortical thinning was evident. White matter microstructural abnormalities were not detected in the corpus callosum at any age. The results of this study partly fit with previous work in the same mouse model suggesting neuropathology follows a ventral to dorsal pattern (Brooks, Jones, et al., 2012), and the selective sparing of the cerebellum fits with the anterior to posterior pattern of pathology previously observed. The results also fit with the findings observed in patients; a smaller intracranial adult brain volume was also found in pre-symptomatic HD carriers (Nopoulos, et al., 2010).

## *Relationship between brain structure and motor function*

Hdh$^{Q150/Q150}$ mice were found to have prominent motor deficits at 19-months, with a shorter latency to fall from the accelerating rotarod, a reduction in rearing frequency on the open field test, and altered non-perseverative locomotion averaged over a 24-hour period. A novel finding was a relationship between motor function and brain structure in Hdh$^{Q150/Q150}$ mice detected with in vivo MRI. Fractional anisotropy in the corpus callosum, measured using tractography analysis of diffusion MRI data, was positively correlated with motor speed in Hdh$^{Q150/Q150}$ mice, suggesting that observed changes are not purely driven by changes in grey matter and that altered white matter microstructure may be related to some of the behavioural symptoms seen in HD. A counter-intuitive relationship was found between thalami volume and the latency to fall on the rotarod test specifically in Hdh$^{Q150/Q150}$ mice; larger thalami were associated with a shorter latency to fall on the rotarod test. This direction of effects highlights the difficulty in interpreting regional volume measures as a reduction in volume does not necessarily indicate cell loss, but could be sensitive to other pathological processes such as cellular swelling or an inflammatory response. The same relationship was not evident in Hdh$^{+/+}$ mouse, suggesting that this relationship is specific to HD. Future work would involve testing other symptom modalities to ascertain whether this structure-function relationship is specific to motor signs or whether cognition is also associated with atrophy.

## *White matter microstructure in the HdhQ150 model of HD*

The lack of any white matter microstructural changes in the Hdh$^{Q150/Q150}$ mice can be interpreted in a number of ways. In patients, diffusion MRI has revealed abnormalities in the corpus callosum in pre-symptomatic and manifest HD participants alike (Di Paola, et al., 2012; Di Paola, et al., 2014; Phillips, et al., 2013), also see Chapter 4. However, white matter anatomy differs between species (Treuting & Dintzis, 2012), and it is not known if there are functional subdivisions in the mouse corpus callosum as there are in human neuroanatomy that may dilute any effects when analysed as a single homogenous structure. Furthermore, the diffusion MRI sequence acquired is likely to be less optimal compared to the sequences acquired in patient work, with more issues with image artefacts caused by the higher magnetic field and motion artefacts due to differences in positioning in the scanner and respiration speed compared to human imaging. Many of the post-processing stages in this chapter were not originally designed for mouse brain, and were modified for use in this study. Thus some of the processing may be sub-optimal, for example, it was not possible to conduct EPI-correction on the images. Thus, it is not clear whether tissue microstructure is not a feature of pathology in the $Hdh^{Q150/Q150}$ mouse model, or whether methodological limitations means that sensitivity is not sufficient to detect an effect. Future planned electron microscopy analyses would be able to resolve this.

### *Sub-cortical atrophy in the HdhQ150 model of HD*

In this study, localised caudate-putamen atrophy was only evident at 7-months old, with no continued decline in localised volume found at 19-months old after accounting for whole brain volume. In contrast, in patient studies caudate and putamen volume were found to be significantly reduced over a 12-month, 24-month, and 36-month period in pre-symptomatic and manifest participants alike (Tabrizi, et al., 2012; Tabrizi, et al., 2011; Tabrizi, et al., 2013). Reasons for the discrepancy in results include the inability to delineate the caudate from the putamen in the mouse brain as they are not separated by the internal capsule as in the human brain, which may dilute any specific effects. Further, a change in volume over 12-months in the mouse lifespan does not readily translate to a period of time in patient work, although clearly 12-months for a mouse line with a lifespan of approximately 22 months represents a much longer lag period, which may explain the lack of selective, localised changes.

Although atrophy was evident in many structures in Hdh$^{Q150/Q150}$ mice, the degree of atrophy was not found to be significant in any region except from the caudate-putamen after accounting for total brain volume. The pattern of atrophy observed in this study is different to what is seen in the pre-symptomatic stage of the human disease, where localised sub-cortical atrophy is evident in many structures (as shown in Chapter 4). Interpreting a reduction in whole brain volume in terms of biophysical changes and in relation to previous immunohistochemistry findings is not straightforward due to the difference in the scale of the results. A progressive pathology has been shown in Hdh$^{Q150/Q150}$ mice in the striatum in the number of cells which stain for S830, an antibody for mutant huntingtin (Sathasivam et al., 2001), and the number of intra-nuclear inclusions, with an increase from 8- to 18-months of age observed (Bayram-Weston, et al., 2012). The volume of the striatum was found to be reduced compared to Hdh$^{+/+}$ mice from 6 months of age onwards (Bayram-Weston, et al., 2012), which was detected in the current study in vivo as localised striatal atrophy at 7 months of age. Similarly, the total number of neurons was also found to be reduced compared to Hdh$^{+/+}$ mice from 6 months of age onwards, however both the volume and neuronal count did not continue to decline with increased age (Bayram-Weston, et al., 2012), and nuclear inclusions were observed in widespread areas of the brain from 6 months of age. This specific lack of a progressive phenotype combined with evidence showing diffuse mutant huntingtin staining from an early age supports the pattern of results observed in this study.

### *Evidence for developmental effects*

An unexpected finding was the lack of decline in whole brain volume from 7- to 19-months of age, suggesting either that widespread atrophy occurs early in the disease course in this mouse model and is not progressive, or that the mutant gene has an effect on development. A smaller intracranial volume has previously been found in pre-symptomatic HD participants (P. Nopoulos et al., 2010), and in chapter 4, pre-symptomatic and early HD participants were found to have reduced whole brain volume, however whole brain volume loss has been found to increase over time in both pre-symptomatic and manifest HD participants (Domínguez et al., 2013; Majid et al., 2011; Tabrizi, et al., 2011), suggesting that there is further loss with subsequent neurodegeneration.

$Hdh^{Q150/Q150}$ mice had a significantly reduced body weight compared to age-matched $Hdh^{+/+}$ mice from 3 months of age onwards, suggesting that developmentally, these mice do not reach the normal mature adult weight seen in $Hdh^{+/+}$ mice. Combined with evidence showing reduction total brain volume at 7 months, these results could be indicative of abnormal developmental processes in this model of HD. Although this cannot be determined from the data, the concept that mutant huntingtin may have effects on developmental processes is not new (Mehler & Gokhan, 2000; Nguyen, Gokhan, Molero, & Mehler, 2013) and huntingtin has been found to regulate cortical neurogenesis (Godin et al., 2010). Thus, further study should be directed toward exploring the contribution of neurodevelopmental processes in HD.

### *Selective effect of anaesthesia in $Hdh^{Q150/Q150}$ mice*

In terms of survival, there was no difference in the lifespan of the $Hdh^{Q150/Q150}$ mice compared to $Hdh^{+/+}$ mice up until 19 months of age, which was expected as the HdhQ150 model has a normal lifespan (Lin, et al., 2001). However, it was found that $Hdh^{Q150/Q150}$ mice were less tolerant of anaesthesia required for the MRI acquisition at 19-months old, and the mortality rate was significantly higher in $Hdh^{Q150/Q150}$ mice compared to $Hdh^{+/+}$ mice, with more mice not recovering from anaesthesia. This could be explained by a number of factors, such as a difference in metabolic rate in the aged Hdh$^{Q150/Q150}$ mice, a change in oxygen consumption rate affecting the survival rate for hypoxemia, a difference in thermoregulatory efficiency, or differential hepatic glycogen reserves in the two groups of animals with the Hdh$^{Q150/Q150}$ mice more at risk of hypoglycaemia. As mutant HTT is expressed throughout the entire body, it is likely that deficits in hepatic, renal and/or cardiac systems affected the response to anaesthesia in the Hdh$^{Q150/Q150}$ mice; cardiac abnormalities have recently been shown in Hdh$^{Q150/Q150}$ mice (Mielcarek et al., 2014), and hepatic dysfunction is an area of recent research attention in HD (Chiang, Chern, & Juo, 2011; Hoffmann et al., 2014; Stüwe et al., 2013). This highlights that the suitability of an anaesthetic procedure is dependent on the strain, age and weight of the mouse (Gargiulo et al., 2012), which is problematic in longitudinal studies where these factors are not fixed. Further work is required to examine the effects of different anaesthetic procedures on the measures under examination (diffusion properties, tissue volume) in order to determine the effect of altering anaesthetic procedures throughout the course of an experiment to adapt to the change in age and/or weight of the animal.

### *Methodological considerations*

A strength of this study was the longitudinal design, allowing for the examination of disease progression and neuropathology over time. However, the lack of histological validation available at the pre-symptomatic, 7-month time-point is a limit of the study. The study was planned so that 5 Hdh$^{Q150/Q150}$ mice and 5 Hdh$^{+/+}$ mice would be humanely sacrificed at 7 months in order to validate the MRI findings with histology, however the unexpectedly high rate of mice failing to recover from the anaesthesia during MRI affected the sample size. The reduced sample size meant that it was necessary to retain all mice in the study in order to achieve sufficient power for the second time-point. This unexpected effect also resulted in a change in anaesthetic procedure which was not ideal for experimental consistency across time-points, but was necessary for animal welfare and to be able to acquire longer diffusion sequences. Pilot studies were conducted using the original anaesthetic protocol, however only with C57BL6/J mice and not with knock-in mice. This suggests that the reaction to the anaesthesia is strain and genotype specific, and future studies would pilot the anaesthesia with the specific strain under examination.

It was not possible to achieve sufficient neuronal counts from the immunohistochemistry conducted in this study. This was because some of the steps in the protocol were specifically used to optimise MRI acquisition, which may have been detrimental to the immunohistochemistry. For the ex vivo imaging, this included the extensive washing procedure before scanning, and retaining the brains in the skull to reduce motion, both of which were found to improve the image quality during piloting. However, the transfer of brains from sucrose to buffer for washing prior to MRI may explain the issues with tissue contamination experienced, and retaining the brains in the skulls meant that the 24-hour post-fixation period may not have been sufficient. Future work is required to achieve an optimal protocol for both MRI and histology combined, with a shorter wash duration and longer fixation period.

The effect of correcting for free water contamination on the statistical outcome of the results showed that partial volume was an issue in the mouse brain and efforts should be made to correct for this. The relationship between free water fraction and rearing behaviour in Hdh$^{+/+}$ mice suggest that the amount of free water may be functionally relevant, which is in agreement with the results presented in the patient cohort in chapter 4 and is a novel finding in HD.

It is normal practice in the research literature to use homozygous knock-in mice (Brooks, Higgs, Jones, et al., 2012) as was done in this study. However, this represents an important difference when translating to patient work. This is because the majority of HD patients are heterozygous with one normal Htt allele and one CAG-expanded allele and the contribution the remaining wild-type Htt gene makes to the disease is a contentious issue ((Aziz et al., 2009; Aziz, Roos, Gusella, Lee, & Macdonald, 2012; Cattaneo, Zuccato, & Tartari, 2005; Djoussé et al., 2003). Because homozygous HD patients are rare, there have been only a handful of studies comparing the disease features with heterozygous HD patients. These strudies converge to show that homozygosity for the HD mutation did not affect the age at onset of symptoms or clinical severity (Myers et al., 1989; Squitieri et al., 2003; Wexler et al., 1987), whereas the rate of disease progression was affected (Squitieri, et al., 2003).

Finally, the discrepancy between the MRI and histology based measures for cortical thickness can be explained in terms of methodology. The poor tissue quality that resulted from the immunohistochemistry processing stages may explain why the measures of cortical thickness obtained from stained sections do not show the same genotype differences as those seen with MRI measurements, with a reduced sample size due to poor quality samples being removed from the analysis. There were also differences in terms of the software used to measure cortical thickness, which are likely to differ in terms of sensitivity to detect effects. The immunohistochemistry was only conducted on one hemisphere, whereas the MRI measurements came from both hemispheres, whilst working with half hemispheres increased the damage suffered by the tissue during processing. Future work will involve analysing the second hemisphere using electron microscopy.

### *Concluding comment*

In conclusion, this longitudinal study suggests in vivo MRI has the sensitivity to detect disease-related macrostructural changes in a mouse model of Huntington's disease, with the most marked finding being a loss of total brain volume before the onset of motor signs. There was no evidence for white matter microstructural abnormalities at any time point; although future planned electron microscopy analyses will be able to validate this null result. Finally, this work highlights a number of methodological considerations for longitudinal MRI-histology studies.

# 7 In vivo MRI evidence that neuropathology is attenuated by environmental modifiers in the YAC128 Huntington's disease mouse model

## Chapter Summary

The aim of this final experimental chapter was to examine whether in vivo high-field magnetic resonance imaging (MRI) can detect a disease-modifying effect in gross tissue macrostructure and/or more subtle effects in white matter microstructure following an environmental intervention.

YAC128 transgenic and wild type mice were exposed to a high-level intervention paradigm involving both cognitive training and associated dietary restriction throughout their lifetime. The combination of interventions was designed to maximise the influence of the environmental effect rather than specifically probe the role of either cognitive training or food restriction, to determine whether such an intervention was sufficient to induce an effect. At 20-months old, mice were scanned with $T_2$-weighted and diffusion-weighted sequences. Locomotor activity level and performance on the rotarod and serial discrimination task were assessed to measure motor and cognitive function respectively. A region-of-interest (ROI) approach measured gross structural changes whereas water diffusivity indicative of tissue microstructure was assessed using tractography analysis.

Results support previous ex-vivo findings of a disease-modifying effect of environmental factors on neuropathology and show novel findings of white matter alterations following exposure to environmental modifiers.

## Introduction

There is some evidence that 'environmental' rehabilitation such as cognitive stimulation may have beneficial effects on the speed of symptom progression in HD patients (Zinzi et al., 2007). Similarly, in genetic mouse models of HD there is now a substantial body of research showing that various forms of environmental enrichment can delay symptom progression and ameliorate disease severity (Dellen, Blakemore, Deacon, York, & Hannan, 2000; Dellen, Cordery, Spires, Blakemore, & Hannan, 2008; Spires et al., 2004). Cognitive stimulation has been shown to retard symptom progression (Wood, et al., 2011), whilst enriched living conditions slowed the decline in motor performance and delayed the onset of disease-related neuropathology (Hockly, et al., 2002). Dietary restriction also slowed the progression of neuropathological, metabolic and motor abnormalities in a mouse model of HD (Duan et al., 2003). A shared potential shortcoming in these mouse studies is the use of fixed tissue and ex vivo techniques to demonstrate effects on neuropathology, as the fixing, embedding and sectioning procedures used in these techniques causes tissue shrinkage and deformation (Biedermann et al., 2012).

Learning-induced plasticity at the white matter microstructural level has been detected in rats using in vivo diffusion MRI (Sagi et al., 2012) suggesting that just as in humans, diffusion MRI may have the sensitivity necessary to detect an effect of environmental modification in the rodent brain (Sagi, et al., 2012; Scholz, Klein, Behrens, & Johansen-Berg, 2009). Nevertheless, in vivo MRI and particularly diffusion MRI is technically more challenging in the mouse brain compared to the rat brain, due to the difference is size and thus spatial resolution required. The ability to detect environmental modification effects in the mouse brain using in vivo techniques would allow for longitudinal designs which are imperative for a time-dependent disease such as HD. For this reason, in order to assess the effects of environmental modification on neuropathology at a level detectable with in vivo MRI, a high level of environmental modification was used in order to maximize the chance of detecting any amelioration in neuropathology or behavioural phenotype, with the notion of specifically targeting the role of both interventions separately in subsequent studies in the event of disease modification with the present manipulations.

A whole brain fiber tractography approach was used to compare specific white matter fiber pathways in 3-dimensions (Jones, 2008) between wild type and diseased mice, and between control and experimental groups. In order to be able to compare with results presented in the previous experimental chapters, the corpus callosum was examined. The aim of this work was to replicate the disease-modifying effects of a cognitive stimulation and dietary restriction regime previously seen in HD mice, including the effects on neuropathology seen with ex vivo techniques, using in vivo MRI.

## Methods

### *Animals*

A total of 22 YAC128 hemizygote transgene carrier mice (10 female, 12 male) and 23 wild type litter-mate mice (17 female, 6 male) were used. The YAC128 mice have 128 CAG repeats and were selected based on the HD-related phenotypic uniformity and low inter-animal variability (Slow, et al., 2003b), age-dependent striatal neurodegeneration, and longer lifespan compared to the commonly used R6 mouse lines. Genetic background, breeding, housing, and genotyping information are detailed in Chapter 2. 11 transgenic mice and 11 wild type mice were randomly allocated into the experimental group, and the remaining 11 transgenic and 12 wild type mice were randomly allocated into the control group.

### *Environmental Modification (EM) Regime*

The environmental modification (EM) regime combined dietary restriction with cognitive training using an operant learning task, giving the animals both cognitive and motor stimulation during the training periods, as well as exposure to a different environment than the home cage, in order to deliver a high level of environmental modification.  Food restriction involved providing mice with a limited number of food pellets which were adjusted based on the animals weight in order to achieve a weight loss of 10% from their non-restricted weight. Animals were weighed daily and food delivery was adjusted accordingly.

All cognitive training occurred between the hours of 08:30 and 18:00. Animals were trained 5 times a week for 30 minutes a day throughout their lifespan on a stimulus response learning task containing an implicit learning component (Jay & Dunnett, 2007),  previously shown to be sensitive to striatal dysfunction (Trueman, et al., 2005) and genotype differences in knock-in HD mice (Trueman, Brooks, Jones, & Dunnett, 2007).

For the cognitive enrichment, 16 operant 9-hole chambers (Campden Instruments, Loughborough, UK) measuring 14 cm x 13.5 cm x 13.5 cm were used in parallel. The chamber contained a horizontal array of 9 holes 11mm in diameter, placed 2mm apart and 15mm above floor level. Each hole contained an LED light and a photocell beam to detect when the nose of the mouse entered the hole. Only five of the nine holes were utilised in this experiment, with the remaining holes blocked and inaccessible.

In preparation for the delivery of the cognitive stimulation regime, mice were first trained in the operant boxes. A simple association task was used for the first 3 days to train the mice to associate the magazine light with reward delivery by presenting the reward (strawberry milkshake) into the food magazine in a non-contingent manner. Next, mice were trained to make a response for a reward (strawberry milkshake) using a continuous reinforcement task, which required the mouse to respond to a light stimulus in hole C of the array by poking their nose once into the illuminated hole in order to elicit reward delivery. This was completed daily until the mice met a performance threshold. Mice were then moved on to the 5-choice serial reaction time task whereby the stimulus light now appeared randomly in any of the 5 holes of the array and a single correct response to the lit hole resulted in reward delivery. After reaching an adequate level of performance (>40 responses), the mice were introduced to the serial implicit learning task (SILT), described in detail in Jay and Dunnett (2007). Briefly, the mouse was required to make a chained response consisting of 2 consecutive correct responses in order to receive a reward. At the start of each trial, the house lights were off and one of the five open holes was illuminated at random. The first response (S1) is the same as for the 5-choice task, but if the mouse made a correct response, the illuminated light was turned off and a second hole (S2) was lit. A successful nose-poke to S2 resulted in the simultaneous extinction of the stimulus light, illumination of the magazine light and delivery of the reward. Embedded within the random presentations of 2 light sequences, was a single predictable 2-light sequence.

Two versions of the task were employed to test the mice. In the first version the S2 was continuously illuminated until the mouse responded. The mice remained on this until their performance reached asymptote. With the second version the S2 was illuminated for 0.5 s and the mouse could make a correct response in the location where the light had been for up to 10 seconds after extinction of the light. In both versions of the task a correct response to S2 was reinforced by delivery of 5 µl of strawberry milk (Trueman, et al., 2007). Performance on the task was operationalized in a number of ways. For the S1 stimuli, accuracy (% correct responses over total number of trials initiated) was analysed by hole (A-E), whereas the S2 stimuli were calculated by step-size, the distance (number of steps/holes) between the S1 and S2 stimuli. Performance was monitored in each training block to avoid ceiling and floor effects.

At approximately 18 months of age, the performance of the transgenic mice on the more stringent second version of the SILT task began to approach a floor effect which we recognized may bias the MRI measurements (Figure 7.1). Consequently, to ensure both transgenic and wild type animals were receiving acute and comparable cognitive stimulation, all mice were moved to the less stringent 'version 1' SILT schedule whereby the S2 was continually lit and performance was monitored to ensure all animals were stimulated cognitively.

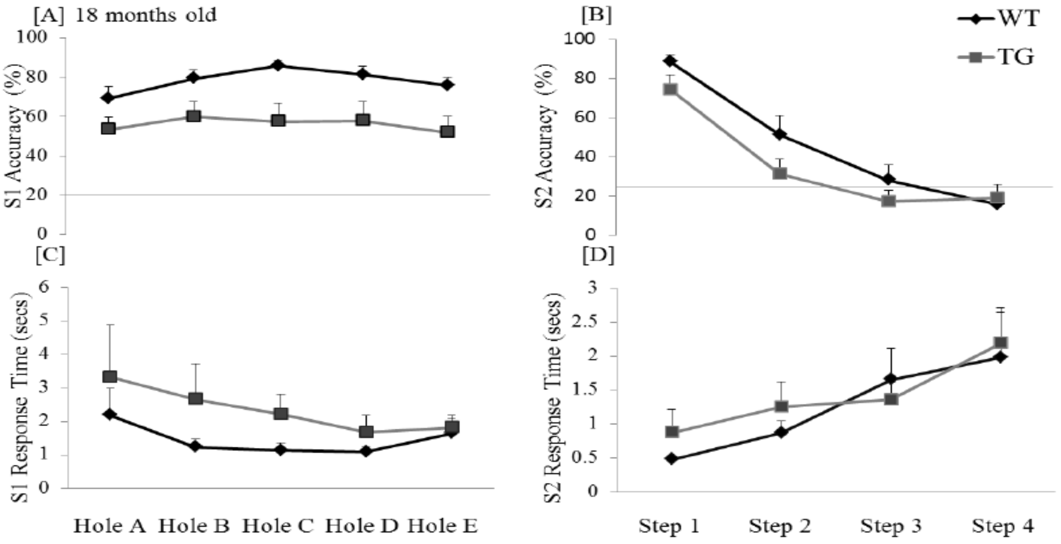

Figure 7.1 Cognitive enrichment performance at 18-months old. Response accuracy and response time to Stimulus 1 (S1; A and C) and Stimulus 2 (S2; B and D) on the Serial Implicit Learning Task (SILT; Jay and Dunnett, 2007) for wild-type (WT) and transgenic (TG) mice. Axis crossing point represents chance performance levels. Error bars show standard error of the mean.

### *Image Acquisition*

MRI acquisition and animal preparation details are described fully in Chapter 2. A transmit 1H 500 watt echo-planar imaging (EPI) volume coil was used with a mouse head receive-only surface coil. Paravision 5.0 software (Bruker Biospin) was used for data acquisition. All scans were performed in vivo, with animals anesthetised with isofluorane (5% for induction, 1.8-2.2% for maintenance) mixed with carrier gas (30% pure oxygen, 70% air) delivered at 1 litre/minute.

At 20 months old, all 44 animals underwent a 2D Rapid Acquisition with Refocused Echoes (RARE) T2-weighted scan (repetition time (TR) 4000 ms, echo time (TE) 35 ms) with a FOV of 1.54 x 1.54 cm and slice thickness of 0.40 mm, in-plane resolution of 120 x 120 um, 30 slices bandwidth 50000 Hz, RARE factor of 2, with 8 averages. A subset of animals (n=32, 16 WT [8 control, 8 trained], 16 transgenic carriers [8 control, 8 trained]) had a diffusion MRI scan in the same session. A 4-shot DTI-EPI sequence was used to investigate white matter microstructure. 27 adjacent axial slices of 320 µm in thickness were acquired with a repetition time (TR) of 14604 ms and an echo time (TE) of 20 ms. Diffusion gradients were applied for 4 ms (δ) with a 10 ms gap (Δ) between pulses. 4 averages were used to increase the signal to noise ratio. The in-plane resolution was 213 x 213 µm at a FOV of 2.24 cm x 2.24 cm and an acquisition matrix of 96 x 96. 4 dummy scans were used at the beginning of the acquisition in order to stabilise the magnetisation equilibrium. Data were acquired with a b-value of 1000 s/mm$^2$ applied over 30 diffusion-weighted directions (D. Jones & Simmons, 1999) uniformly distributed in three dimensional space with 5 b = 0 s/mm$^2$ images without diffusion weighting. Respiratory-gating was used to minimise respiratory motion artefacts using procedures provided with the Bruker Paravision 5.0 system.

### *Image processing*

Processing of the $T_2$-weighted images was carried out using Analyze 10.0 (Mayo Clinic) software, whereas diffusion MRI images were processed using ExploreDTI software (Leemans, et al., 2009). One $T_2$- and diffusion scan was corrupted and not included in the analysis. For the $T_2$-weighted images, skull-stripping was first performed using a Brain Extraction Tool (Smith, 2002), modified for rodent brains. Diffusion images were processed according to the methodology detailed in Chapter 2.

***Region of interest (ROI) analysis*** *In* order to compare with previously published data, mean volume for different ROI's were calculated for the $T_2$-weighted images based on the mouse brain histology atlas (Paxinos & Franklin, 2004) by a single rater blinded to the animal's genotype or experimental group. In order to avoid hemispheric differences due to handedness bias, all images were drawn on the hemisphere to the left of the screen, with the original and flipped image used

The striatum, lateral ventricles and cortex were determined a priori as ROI's and were manually identified according to the image contrast on the $T_2$-weighted image. In order to avoid poor reproducibility due to inconspicuous structure boundaries, 5 slices were selected at approximately Bregma 1.42, 1.10, 0.14, -0.22 and -0.58. Manual delineation was mainly performed in the coronal view on a slice-by-slice basis and refined in the axial and sagittal view to ensure the structure boundaries appeared as smooth as possible in all the three views. All slices contained clear anatomical landmarks and provided reproducible coverage of the structures being analysed. In all 5 slices, the regions of interest were drawn for the striatum, lateral ventricles, and cerebral cortex, and for reproducibility, the ventral boundary for all three ROI's was a 10° angle from the jawbone as shown in Figure 7.3. Structures were examined separately in both hemispheres. ROI's were also drawn on every brain slice for the whole brain region in order to get a measure of whole brain volume.

Reproducibility was tested using the coefficient of variation and Cronbach's alpha. The intra-rater coefficient of variation (CV) was <4.5% for volume measures from ROI's drawn on T2-weighted images, with the exception of the lateral ventricles which were more variable, with 9.54% CV. Cronbach's alpha was 0.9 for all metrics indicating excellent internal consistency, with the exception of the lateral ventricles (alpha = 0.6).

***Tractography analysis*** The methodology is the same as in Chapter 6, with whole-brain deterministic tracking conducted using ExploreDTI (Leemans, et al., 2009) and based on the constrained spherical deconvolution algorithm (Tournier, et al., 2004; Tournier, et al., 2008). Multiple waypoint ROI's which were drawn manually in native space on color-coded fiber orientation maps by a single operator blinded to the genotype and training status of the mouse. The mean FA and MD were then calculated for all reconstructed pathways by averaging the values sampled at each step along the pathways (D. Jones et al., 2005). As an extension to the segmentation presented in chapter 6, tract-specific means of FA, ADC and eigenvalues were calculated in the genu, body and splenium segments of the corpus callosum, as different segments of the callosum may differ in their susceptibility to neurodegeneration due to the different inter-hemispheric connections. As in chapter 6, an initial seed ROI was drawn on the colour-coded diffusion image (Pajevic & Pierpaoli, 2000) on the mid-sagittal slice in order to capture all the tracts passing through this ROI, which included many association fibers and fibers of the external capsule (see Figure 7.4).  The analysis was then restricted to the corpus callosum with external capsule tracts excluded through two additional 'AND' gate ROI's drawn in the sagittal plane in line with the medial cingulum in both hemispheres as visualised in the coronal plane. For the genu of the corpus callosum, the seed region was drawn from the most anterior section of the genu to the posterior boundary where the anterior commissure crosses the midline. For the body of the corpus callosum, the seed region was drawn from the anterior boundary where the anterior commissure crosses the midline, and the posterior boundary was the start of the splenium defined by the position of the lateral ventricles as seen on the MD map.

***Behavioural outcome measures***

Three outcome measures were used at 20 months of age to assess functional change due to EM. The rotarod test (B. Jones & Roberts, 1968) was used to assess overall performance in motor coordination, balance and endurance (see Chapter 2 and 6) with the average of the two runs taken as the outcome measure. Automated home-cage analysis was used to measure locomotor activity, with total number of beam breaks made in 5-minute intervals recorded over a 30-minute time period, on MED-PC® software (Vermont, USA).

The water T-maze serial discrimination task was used as a measure of procedural discrimination learning and cognitive flexibility (Brooks, Nari Janghra, et al., 2012). The arms of the maze were 30 cm high and 7 cm wide, the stem was 21.5 cm long and the two perpendicular side arms each 37 cm long. The maze was filled at 23 ± 2 °C to a depth of 22.5 cm with water whitened with milk to conceal an escape platform (6 × 6 × 21.5 cm high) positioned 1 cm below the surface at the end of one of the maze arms depending on the task. In the watermaze, testing was conducted in low light conditions; illumination came from one of two standard angle poise 40 W lamps placed over the end of each arm. Mice were placed into the water and swam toward the ‘T’ where they had to make a choice to turn either left or right. A choice was deemed to have been made when the entire body had entered an arm. A correct choice would be a turn toward the escape platform, which allowed the mouse to exit the maze. An incorrect choice led to the mouse being temporarily blocked into that arm, thus elongating the length of time in the water, before being allowed to swim to the escape platform. Briefly, the rules to learn were a simple directional discrimination (for example always go left) followed by a reversal (always go right), which was followed by a visual discrimination (for example go to light) and reversal (go to dark), which was followed by a switch to the original rule (always go left). During the directional discrimination tasks one of the two lamps was randomly illuminated for each trial, whereas during the visual discrimination tasks the platform location was randomly allocated. When mice were able to select the correct arm with 90% accuracy (maximum of 100 trials), they were assumed to have learned the rule and were progressed to the next rule.

### ***Statistical analysis***

Because gender distribution was unbalanced across groups, an analysis of variance was implemented using a regression model (SPSS 10.0) with the associated main and interaction effects with genotype, EM exposure, and gender as independent variables using the enter method. A mixed-model ANOVA was used to examine the main and interaction effects with genotype, EM exposure, and gender at 5-minute intervals in the automated home-cage analysis, with time as the within-subject variable (5-, 10-, 15-, 20-, 25-, 30-minutes). When correcting for multiple comparisons due to multiple ROI's, it was acknowledged that alterations in different ROI's may not be independent measures, resulting in the Bonferroni method being overly conservative. Thus, Type I error was controlled with the false discovery rate (FDR) at 5% ($q < 0.05$), with the q-value software (Storey, 2002).

## Results

Results are expressed as mean ± standard error of the mean (S.E.M). Unless reported, there were no interactions between gender and the two independent variables, genotype and environmental modification (EM) exposure. 1 scan (Diffusion and T2) of a transgenic enriched mouse corrupted.

### ***Survival Rate***

Genotype and exposure to EM had no effect on survival rate, both $p > 0.05$, with mice scanned prior to the end point and humanely scarified thereafter.

### *Body weight*

Genotype, EM group, and gender did not explain the variance in body weight measured on the day of scanning, F (3, 40) = .758, $p > 0.05$, $R^2 = .054$, $R^2_{Adjusted} = -.017$. Exposure to EM had no effect on body weight β = .543, t = 1.075, $p > 0.05$, and there was no difference in body weight between YAC128 and wild-type mice at 20-months old, β = .444, t = .875, $p > 0.05$, in line with previous findings (Brooks, Higgs, Janghra, Jones, & Dunnett, 2012). There was also no effect of gender on body weight, β = -.194, t= -1.118, $p > 0.05$, and no interaction effect between EM exposure and genotype, β = -.875, t = -1.260, $p > 0.05$.

### *Cognitive Training Performance*

At 20-months old, and averaged over the final 5 trial days, there was no difference between wild-type and YAC128 mouse in accuracy to respond to the S2 stimuli across the step sizes, F (1,20) = 2.04, $p \geq 0.05$. Similarly, there was no difference in response accuracy to S1, F (1,20) = .314, $p \geq 0.05$.The mice were able to detect and use the predictable stimuli to increase response accuracy (t(21) = 4.11, $p \leq 0.001$), however there was no difference between the genotypes in performance to the predictable stimuli (genotype x predict, F (1,20) = .152, $p \geq 0.05$), in line with previous work (Brooks et al., 2012).

### *Behavioural outcomes*

The contribution of genotype, environmental modification (E.M.) and gender to the regression model predicting performance on the behavioural tests is shown in Table 7.1, along with model statistics. For the home-cage analysis, activity levels were assessed at 5-minute intervals over a 30-minute time window (Figure 7.2A). Exposure to EM had a significant effect on locomotor activity ($p < 0.05$ FDR-corrected); mice exposed to EM were more active over a 30-minute time period compared to control mice, making significantly more beam breaks in the activity boxes. Genotype and gender had no effect on locomotor activity, and there was no interaction between EM exposure and genotype, p > 0.05.

On the rotarod test, it was found that genotype, EM group, and gender explained a significant amount of the variance in latency to fall (Figure 7.2B). Both exposure to EM and genotype significantly predicted latency to fall, with EM exposed mice able to stay on the rotating rod longer (mean = 84.5 ± 7.56 s) compared to mice in the control group (mean = 69.1 ± 7.57s), and transgenic mice able to stay on the rotating rod for less time (61.98 ± 6.90 s) compared to wild-type mice (90.85±7.17 s).

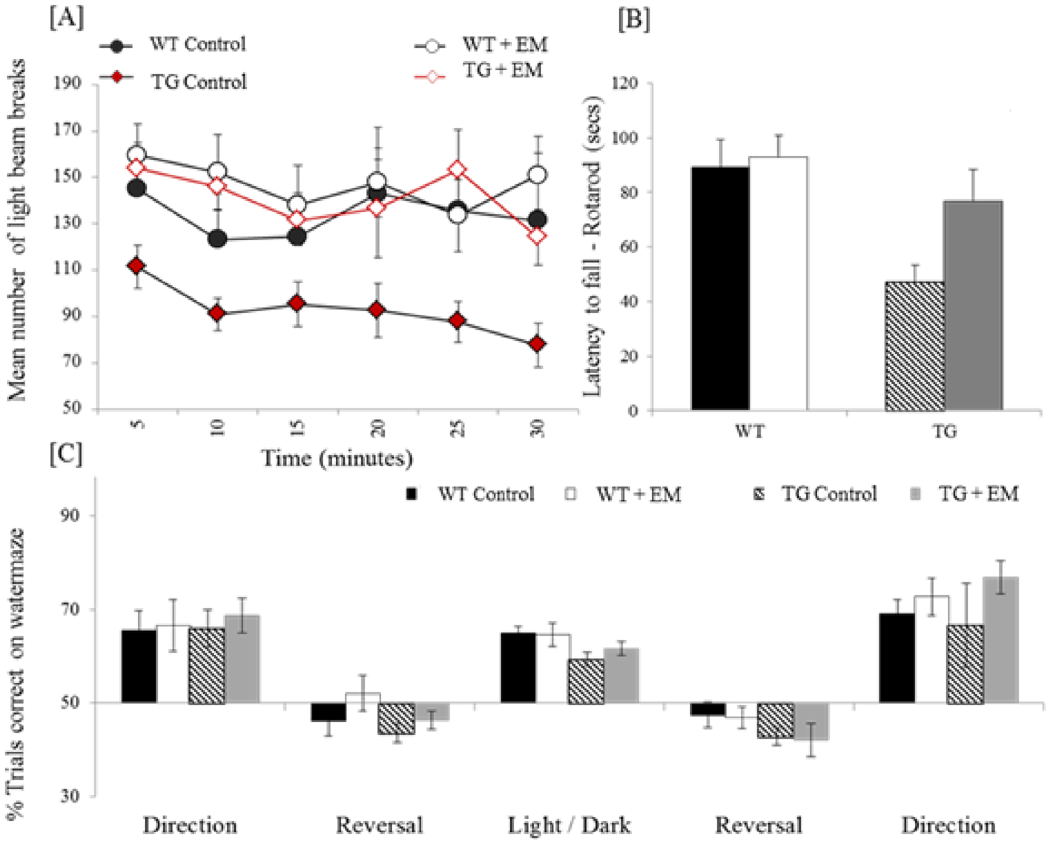

Figure 7.2 Behavioural Outcome Measures. [A] Activity levels over 30-minutes shown as the mean number of light beam breaks; EM mice made significantly more beam breaks, p <0.05. [B] Latency to fall on the rotarod test. C] Percentage of correct trials on the Water T-Maze task to the 5 rules: Direction (Left-Right), Direction Reversal, Light/Dark Discrimination, Light/Dark Rule Reversal, and Original (Direction discrimination). WT: wild type. TG: transgenic. Error bars: standard error of the mean.

Table 7.1 Multiple regression analysis for behavioural measures. E.M: environmental modification. Uncorrected p values shown.

|  |  |  |  |  | Model |  |  |  |
|---|---|---|---|---|---|---|---|---|
| Outcome variable | Predictor variable | Std Errror | Std. β | p | $R^2$ | Adj. $R^2$ | F | p |
| **Open Field Locomotion** | Genotype | 92.25 | -0.18 | .245 |  |  |  |  |
|  | E.M. | 92.09 | 0.38 | **.018** | 0.21 | 0.14 | 3.31 | **0.03** |
|  | Gender | 99.17 | 0.26 | .112 |  |  |  |  |
| **Rotarod** | Genotype | 10.24 | -0.35 | **.027** |  |  |  |  |
|  | E.M. | 9.70 | 0.29 | **.048** | 0.29 | 0.24 | 5.00 | **0.01** |
|  | Gender | 11.13 | 0.25 | 0.12 |  |  |  |  |
| **Watermaze Discrimination** |  |  |  |  |  |  |  |  |
| Left/ Right | Genotype | 4.57 | -0.05 | 0.74 |  |  |  |  |
|  | E.M. | 4.34 | 0.01 | 0.93 | 0.07 | -0.003 | 0.95 | 0.43 |
|  | Gender | 4.87 | -0.27 | 0.12 |  |  |  |  |
| Reversal Left/Right | Genotype | 3.02 | -0.24 | 0.15 |  |  |  |  |
|  | E.M. | 2.87 | 0.22 | 0.15 | 0.10 | 0.03 | 1.51 | 0.23 |
|  | Gender | 3.22 | -0.06 | 0.72 |  |  |  |  |
| Light/Dark | Genotype | 1.86 | -0.40 | .014 |  |  |  |  |
|  | E.M. | 1.77 | 0.06 | 0.68 | 0.15 | 0.08 | 2.32 | 0.09 |
|  | Gender | 1.98 | -0.09 | 0.57 |  |  |  |  |
| Reversal Light/Dark | Genotype | 2.84 | -0.19 | 0.25 |  |  |  |  |
|  | E.M. | 2.75 | 0.01 | 0.94 | 0.12 | 0.05 | 1.73 | 0.18 |
|  | Gender | 3.09 | 0.23 | 0.17 |  |  |  |  |

Gender did not significantly predict rotarod performance. There was no interaction between genotype and EM exposure for latency to fall, suggesting wild type mice and transgenic mice benefited from EM in a similar manner.

On the watermaze task, genotype, EM group, and gender did not explain a significant amount of the variance on any discrimination trial, all $p > 0.05$. EM exposure did not have an effect on performance accuracy on the water–maze serial discrimination task, $p > 0.05$ (Figure 7.2C). Genotype significantly predicted the ability to discriminate between light and dark, with YAC128 mice making fewer correct choices in the light- dark discrimination stage, , with a performance accuracy of 60.52 ± 1.07% compared to 65.04±1.43% in wild types, however this did not survive correction for multiple corrections, FDR-adjusted $p = 0.056$.

There were no differences between transgenic and wild type mice on the reversal stages of the T-maze task, possibly because all mice were performing at chance level. There was no interaction between EM and genotype for performance accuracy of the water T-maze, suggesting a beneficial effect of EM specifically in the motor domain.

***Tissue Macrostructure***

As shown in Figure 7.3, mean whole brain volume was 437.72 ± 3.36 $mm^3$ for wild-type mice, and 432.99 ± 2.68 $mm^3$ for YAC128 mice. Genotype, EM group, and gender did not explain a significant amount of the variance in whole brain volume; neither EM exposure or genotype predicted whole brain volume, all $p > 0.05$. Whole brain volume was not significantly correlated with volume in the left and right caudate in wild-type mice, $r = -.220$ and .330 respectively, $p > 0.05$, or in YAC128 mice, $r = -.348$ and -.286 respectively, $p > 0.05$. Similarly, whole brain volume was not significantly correlated with cortical volume in the left and right hemisphere in wild-type mice, $r = .131$ and -.108 respectively, $p > 0.05$, or in YAC128 mice, $r = .343$ and .022 respectively, $p > 0.05$.

There was also no relationship between whole brain volume and lateral ventricular volume in wild-type mice, $r =.268$, $p > 0.05$, and YAC128 mice, $r = .153$, $p > 0.05$. Thus, it was not necessary to include whole brain volume as a covariate in the subsequent analyses.

Genotype, EM group, and gender explained a significant amount of the variance in the absolute caudate-putamen volume in the left and right hemisphere, both $p < 0.05$ FDR-corrected. EM exposure did not predict the raw volume in the left or the right caudate-putamen, $p > 0.05$. In contrast, genotype significantly predicted volume in the left and right hemisphere, $p < 0.01$ FR-corrected, with caudate-putamen volume being reduced by 15.57 % in the left hemisphere and 17.81% in the right hemisphere in YAC128 mice compared to controls.

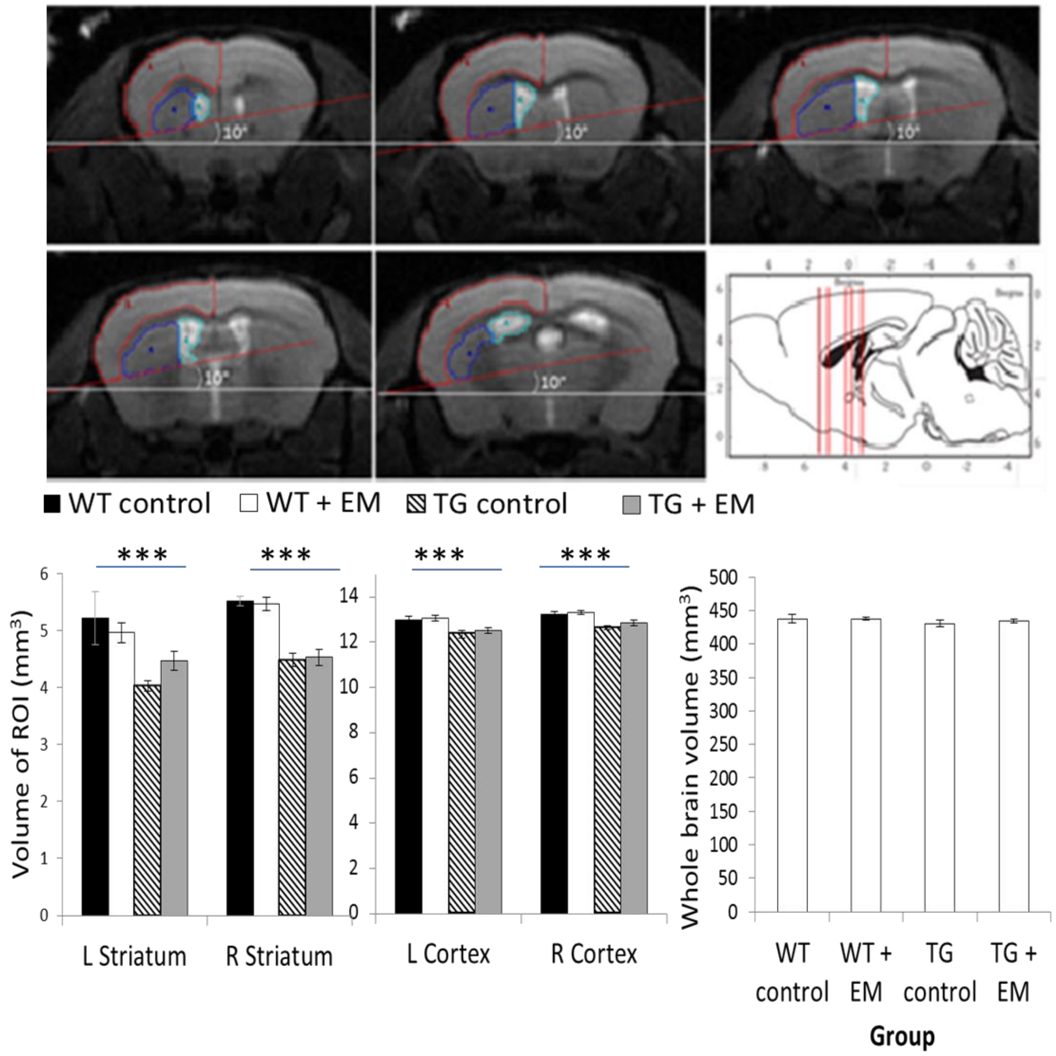

Figure 7.3 Top. Manual segmentation of ROI's on the T2-weighted image with approximate Bregma positions. Bottom. Mean raw volume (mm$^3$) showing a main effect of genotype. Error bars represent standard error of the mean. TG: transgenic, WT: wild-type. EM: environmental modification. *** $p < 0.001$ uncorrected.

Table 7.2 Multiple regression analysis for macrostructural measures from the $T_2$-weighted image. Uncorrected p values shown.

| | | | | | Model | | | |
|---|---|---|---|---|---|---|---|---|
| ***Outcome variable*** | ***Predictor variable*** | ***Std Errror*** | ***Std. β*** | ***p*** | ***$R^2$*** | ***Adj. $R^2$*** | ***F*** | ***p*** |
| **Total Brain Volume (µm)** | Genotype | 4800.76 | -0.14 | 0.45 | | | | |
| | E.M. | 4522.44 | 0.09 | 0.58 | 0.05 | -0.031 | 0.62 | 0.60 |
| | Gender | 5188.00 | 0.13 | 0.48 | | | | |
| **Caudate-Putamen (µm)** | | | | | | | | |
| *Left hemisphere* | Genotype | 182.72 | -0.63 | **.000** | | | | |
| | E.M. | 172.12 | 0.05 | 0.70 | 0.4 | 0.342 | 7.4 | **0.001** |
| | Gender | 197.46 | 0.01 | 0.95 | | | | |
| *Right hemisphere* | Genotype | 130.44 | -0.81 | **0.000** | | | | |
| | E.M. | 122.87 | -0.001 | .993 | 0.66 | 0.629 | 21.9 | **0** |
| | Gender | 140.96 | .007 | .948 | | | | |
| **Cerebral Cortex (µm)** | | | | | | | | |
| *Left hemisphere* | Genotype | 153.07 | -0.50 | **0.002** | | | | |
| | E.M. | 139.58 | 0.11 | 0.43 | 0.37 | 0.313 | 6.63 | **0.001** |
| | Gender | 160.76 | 0.20 | 0.2 | | | | |
| *Right hemisphere* | Genotype | 136.06 | -0.51 | **.002** | | | | |
| | E.M. | 124.08 | 0.17 | 0.22 | 0.35 | 0.296 | 6.19 | **0.002** |
| | Gender | 142.90 | 0.14 | 0.36 | | | | |
| **Lateral Ventricles (µm)** | Genotype | 265.66 | .326 | 0.12 | | | | |
| | E.M. | 264.07 | .105 | 0.60 | 0.19 | 0.104 | 2.2 | 0.11 |
| | Gender | 215.43 | .366 | **.041** | | | | |

When the interaction term (Genotype * EM exposure) was added, the model remained significant with an increase in the amount of variance explained in the left hemisphere, F (4, 33) = 7.388, $p < 0.001$, $R^2 = .471$, $R^2_{\text{Adjusted}} = .407$, and in the right hemisphere, F (4, 33) = 16.056, $p < 0.001$, $R^2 = .661$, $R^2_{\text{Adjusted}} = .619$. The interaction between genotype and EM exposure had a significant effect on left caudate-putamen volume, β = 1.323, t = 2.173, $p < 0.05$ but not on right caudate-putamen volume, β = .184, t = .378, $p > 0.05$. Post-hoc analyses in the left hemisphere for YAC128 and wild-type mice separately found that EM exposure significantly predicted left caudate-putamen volume in transgenic mice, β= .486, t = 2.310, $p < 0.05$, but not in wild-type mice, β = -.097, t =-.398, $p > 0.05$, suggesting that EM exposure has a selective effect on left caudate-putamen volume in YAC128 mice, reducing the degree of disease-related atrophy. A Post-hoc t-test comparing wild-type control mice with YAC128 mice exposed to EM found that volume in the left caudate putamen in EM-exposed YAC128 mice was significantly smaller than wild-type control mice, t (10) - -2.972, $p < 0.05$, suggesting that EM exposure reduced disease-related atrophy in the left caudate-putamen, but does not ameliorate it.

Genotype, EM group, and gender explained a significant amount of the variance in raw cortical volume in the left and right hemisphere, both $p < 0.05$ FDR-corrected. EM exposure did not predict the raw volume in the left or right cortex, $p > 0.05$. In contrast, genotype significantly predicted volume in the left and right hemisphere, $p < 0.01$ FDR-corrected, with cortical volume reduced by 4.45% in the left hemisphere and 3.73% in the right hemisphere in YAC128 mice compared to wild-type mice. The interaction between genotype and EM exposure had no effect on volume in the left and right cortex, $\beta = -.046$ and .179, SE= 299.82 and 266.25 µm, t= -.067 and .260, both $p > 0.05$.

Genotype, EM group, and gender did not explain a significant amount of the variance in the lateral ventricle volume, both $p > 0.05$, and genotype and EM exposure did not predict ventricular volume. Gender was found to predict ventricular volume, however the interaction between gender and genotype, and between gender and EM exposure, did not predict lateral ventricle volume, both $p > 0.05$.

### ***Tissue Microstructure***

For the tractography based analysis of the corpus callosal reconstructions, FA values in the genu segments were predicted by exposure to environmental modifiers, $p < 0.05$ uncorrected, as shown in Table 7.3. The interaction between genotype and exposure to environmental modifiers was not a significant predictor of FA values in the genu segment, $\beta = -1.522$, SE = .033, t = -1.830, $p > 0.05$.

In the body of the corpus callosum, both genotype ($p < 0.05$ FDR-corrected) and exposure to environmental modifiers ($p< 0.001$ uncorrected) significantly predicted FA values. The interaction between genotype and exposure to environmental modifiers was also a significant predictor of FA values, $\beta = -2.059$, SE = 0.028, $t = -2.64$, $p < 0.05$. Post-hoc analyses found that exposure to environmental modifier was a significant predictor of FA values for wild-type mice, $\beta = .694$, SE = 0.027, $t = 2.61$, $p < 0.05$ uncorrected, with the average FA value in the body of the corpus callosum 11.03% higher for wild-type mice exposed to environmental modifiers, compared to control wild-type mice. However, exposure to environmental modifier did not predict FA values forYAC128 mice, $\beta = .015$, SE = .020, $t = 0.052$, $p > 0.05$.

In the splenium portion of the corpus callosum, gender significantly predicted FA values, $p < 0.05$ uncorrected, with no effect of genotype or environmental modification. The interaction between gender and genotype, and gender and EM group did not significantly predict FA values in the splenium, both $p > 0.05$.

The interaction between genotype and exposure to environmental modifiers did not significantly predict MD values in any callosal segment, all $p > 0.05$, and did not predict FA values in the genu or splenium segment of the corpus callosum, $p > 0.05$.

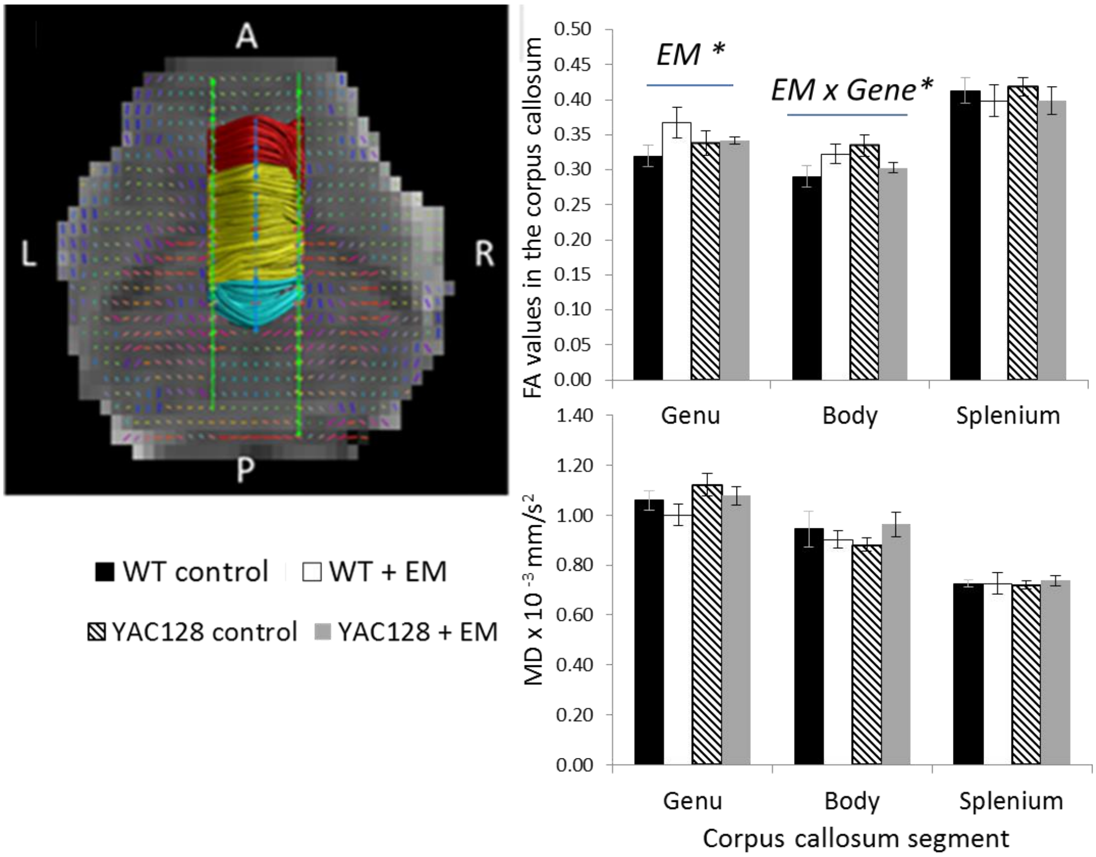

Figure 7.4. Reconstructed pathways and statistics in the corpus callosum shown in the axial plane on a MD map with principal diffusion vectors. The genu (red), body (yellow) and splenium (blue) were reconstructed using a single ROI drawn on the mid-sagittal slice, with two AND gates to remove external capsule fibers. WT: Wild type, EM: environmental modification. * $p < 0.05$ uncorrected.

Table 7.3 Multiple regression analysis for microstructural measures from the diffusion MRI image. CC: corpus callosum. FA: fractional anisotropy. MD: mean diffusivity. Uncorrected p values shown.

| | | | | | Model | | | |
|---|---|---|---|---|---|---|---|---|
| ***Outcome variable*** | ***Predictor variable*** | ***Std Errror*** | ***Std. β*** | ***p*** | ***$R^2$*** | ***Adj. $R^2$*** | ***F*** | ***p*** |
| FA Genu CC | Genotype | .053 | 1.18 | .071 | 0.23 | 0.097 | 1.76 | 0.171 |
| | E.M. | .052 | 1.36 | **.034** | | | | |
| | Gender | .019 | 0.35 | 0.13 | | | | |
| FA Body CC | Genotype | .047 | 1.71 | **.007** | 0.25 | 0.132 | 2.14 | 0.105 |
| | E.M. | .045 | 1.42 | **.018** | | | | |
| | Gender | .017 | 0.30 | 0.17 | | | | |
| FA Splenium CC | Genotype | .058 | 0.78 | .214 | 0.22 | 0.099 | 1.8 | 0.16 |
| | E.M. | .057 | 0.34 | **.577** | | | | |
| | Gender | .021 | 0.54 | **0.021** | | | | |
| MD Genu CC x $10^{-3}$ $mm/s^2$ | Genotype | .144 | -0.19 | 0.76 | 0.21 | 0.072 | 1.55 | 0.221 |
| | E.M. | .141 | -0.59 | 0.35 | | | | |
| | Gender | .052 | -0.32 | 0.17 | | | | |
| MD Body CC x $10^{-3}$ $mm/s^2$ | Genotype | .174 | -0.81 | 0.23 | 0.07 | -0.078 | 0.46 | 0.765 |
| | E.M. | .167 | -0.69 | 0.28 | | | | |
| | Gender | .064 | -0.09 | 0.71 | | | | |
| MD Splenium CC x $10^{-3}$ $mm/s^2$ | Genotype | .079 | -0.67 | 0.32 | 0.1 | -0.04 | 0.72 | 0.584 |
| | E.M. | .078 | -0.45 | 0.49 | | | | |
| | Gender | .029 | -0.38 | 0.12 | | | | |

## Discussion

In this chapter, in vivo MRI was used for the first time in a mouse model of HD to examine the effects of an environmental intervention on neuropathology. The environmental intervention regime involved both cognitive enrichment and dietary restriction and was found to have disease-modifying effects in the YAC128 mouse model of HD. Changes were observed in both tissue macrostructure and tissue microstructure as well as motor function, replicating previous ex vivo work and providing additional information on the role of white matter in the neural response to environmental modifiers. These findings provide the initial data with which to base subsequent and more detailed study in order to dissect the effects of cognitive training and food restriction.

### *Genotype Differences*

Transgenic YAC128 mice displayed motor deficits on the rotarod test and more subtle cognitive deficits on the Water T-maze serial discrimination task, in line with previous findings (Brooks, Higgs, Janghra, et al., 2012; Slow, et al., 2003b) although there was no difference on the reversal stage of the Water T-maze as previously shown (Brooks, Janghra, et al., 2012). A floor effect was seen in both wild type and transgenic mice on the reversal tasks, suggesting that age-related decline in the wild type mice masked any genotype differences. Using in vivo $T_2$-weighted MRI, a reduction in striatal and cortical volume was found in the YAC128 mice compared to wild type mice, in line with previous ex vivo MRI and histological work using the same mouse line (Lerch, Carroll, Spring, et al., 2008; Slow, et al., 2003b) and replicating human imaging findings (Aylward et al., 2012; Nopoulos, et al., 2010; Paulsen, et al., 2010).

### *Environmental Modifier Effects*

Exposure to environmental modifiers (EM) increased both locomotor activity levels and latency to fall on the rotarod test irrespective of genotype but did not have an effect on performance on the watermaze task, suggesting a specific beneficial effect in the motor domain. This dissociation effect is the reverse of that seen previously in HD mice following exposure to exercise, where exercise improved cognitive more than motor performance (Harrison, et al., 2013) and suggests different environmental modifiers may have differential functional effects despite similar effects on neuropathology. In this study, the effect of environmental modifiers on brain structure interacted with genotype. Transgenic mice exposed to EM had reduced striatal atrophy compared to control transgenic mice, detectable on the $T_2$-weighted MRI images. Post-hoc analyses showed that wild type control mice had significantly larger striatal volumes compared to transgenic mice exposed to EM, suggesting that long-term exposure to environmental modifiers reduces neuropathology in transgenic HD mice, but does not ameliorate it altogether. This replicates previous ex vivo findings of a selective benefit in HD mice (Dellen, et al., 2000; Hockly, et al., 2002).

A novel finding is the change in tissue microstructure in the corpus callosum following environmental modification (EM). Tractography analysis (Jeurissen, et al., 2011; Tournier, et al., 2004) was used to examine tract-specific measures in the corpus callosum. The corpus callosum was segmented into 3 parts; exposure to environmental modification was shown to predict fractional anisotropy (FA) values in the genu and body of the corpus callosum, with FA values higher in mice exposed to EM. This suggests that white matter microstructure is altered by environmental modification in wild-type and YAC128 mice alike. The increase in FA values found following long-term dietary restriction combined with cognitive enrichment is in line with previous findings; postmortem diffusion MRI revealed higher FA in the forelimb motor cortex in rats exposed to motor learning (Sampaio-Baptista et al., 2013), and in vivo diffusion MRI revealed higher FA in the corpus callosum in rats exposed to a spatial navigation task (Blumenfeld-Katzir, Pasternak, Dagan, & Assaf, 2011). The current study adds to this, providing evidence of experience-dependent white matter plasticity after a striatal learning paradigm, during which neurogenesis is unlikely to occur. Taken together with previous work showing an increase in myelin staining after a cortical learning intervention (Sampaio-Baptista, et al., 2013), this study adds weight to the idea that white matter structural plasticity, and growth of new myelin, can occur without the generation of new neurons.

Whereas previous rodent work has demonstrated experience-dependent plasticity with diffusion MRI in rats, the current study is the first to examine experience-dependent plasticity with diffusion MRI in a genetic mouse model of HD. Using In vivo diffusion MRI and tractography analysis, this study showed for the first time a significant interaction between genotype and exposure to environmental modifiers for fractional anisotropy (FA) values in the body of the corpus callosum. Unlike the interaction seen in caudate-putamen volume, exposure to EM had a specific effect on white matter microstructure in wild-type animals, with wild-type mice exposed to EM having increased FA values in the callosal body compared to control wild-type mice. Thus, it appears that the benefits of exposure to environmental modifiers may be different in the HD brain, with the disease possibly reducing the propensity for environmentally-induced white matter plasticity. However, the beneficial effect of environmental modifiers on motor performance and a reduction in disease-related atrophy suggests that the YAC128 do undergo experience-dependent plasticity, and again highlights the multiple mechanisms involved in neural plasticity. It cannot be determined from this study whether the lack of changes to white matter microstructure in YAC128 mice is due to the effects of mutant Huntingtin or due to the degree of atrophy in the brain at this stage in the disease. Future work is required to examine the effects of environmental interventions at multiple time points, including early time points before neuropathology is evident.

This study provides proof of principle that $T_2$-weighted MRI has the sensitivity required to replicate findings from previous ex vivo work. This study does not aim to dissociate the specific effects of cognitive stimulation and dietary restriction on neuropathology, although previous work has shown ameliorative effects of both (Duan, et al., 2003; Wood, et al., 2011). However, considering the high cost associated with pre-clinical MRI compared to traditional histological methods, this study provides a basis for future research focused on dissociating these effects with MRI as an outcome measure.

The purpose of the study was to assess whether environmental modifiers produced structural brain changes that were detectable with in vivo MRI, thus a high level of modification was used to maximise the likelihood of detecting an effect. There are a number of factors associated with the delivery of the modification regime used in this study which would need to be controlled for in future studies aiming to dissociate the effects of specific modifiers. Alongside cognitive stimulation and dietary restriction, increased handling, increased sensory stimulation, and increased motor activity during the cognitive task may have acted as modifiers, as well as the effect of fluid intake due to dietary restriction (i.e. increased hydration). In addition, the potentially confounding effects of anaesthesia on cognitive performance have recently been suggested (Shen et al., 2013) and should be addressed in future studies where cognitive performance is an outcome measure. Further research is necessary to dissect out the contribution of each element and examine the possibility of interactive effects.

This original finding of environmentally induced changes in tissue microstructure detected using a diffusion MRI sequence combined with the changes found in tissue macrostructure with $T_2$-weighted MRI suggest a multi-modal in vivo imaging approach is valuable for evaluating intervention outcomes in mouse models of disease. The fact that this in vivo data replicates previous ex vivo studies increases confidence in the use of longitudinal designs in the future to assess how different enrichment regimes interact with ageing and disease progression, and help ascertain the temporal contingency between learning and effects on neuropathology, with clear clinical relevance.

## Acknowledgment of financial support

The work presented in this chapter was dual funded by the European Huntington's Disease Network (EHDN) [Project 0369] and The Wellcome Trust.

# 8 General Discussion

The known single genetic mutation that causes Huntington's disease (HD) means that the disease is an important model for studying the associations between gene and brain function. Based on this, the primary aim of this thesis was to characterise the structural changes that occur in the HD brain at different disease stages, using a variety of MRI techniques in both a patient cohort and animal models. The purpose of using two species was to allow for bi-directional translation, with improved insights in human neuropathology providing the basis for translational research in mouse models, and increased biological specificity from work in animal models informing knowledge and research in the human condition, in order to improve our understanding of the relationship between neuropathology, phenotype and genetics. A summary of findings is presented, following by a discussion on the translation of findings between patients and mouse models, methodological issues that arose, and finally future directions and planned work.

## White matter microstructure in HD

White matter microstructure was examined in both the patient cohort and in two different mouse models of HD using diffusion tractography analysis. The work in this thesis sought to rectify the reliance on the diffusion tensor model for tractography analysis in the HD literature (Bohanna, Georgiou-Karistianis, & Egan, 2011; O. Phillips, et al., 2013; O. Phillips, et al., 2014), applying more advanced tractography based on spherical deconvolution approaches capable of resolving multiple fiber orientations within an imaging voxel. In the patient cohort (chapter 4), a reduction in fractional anisotropy (FA) and an increase in mean diffusivity (MD) values was found in the corpus callosum in HD participants, indicative of white matter degeneration. An increase in MD values and a reduction in restricted volume fraction, a proxy measure of axon density, were found in the subgenual subdivision of the cingulum bundle specifically in HD participants, again suggestive of microstructural degeneration. In contrast, in the HdhQ150 knock-in mouse model (chapter 6), differences in DTI indices were only found in mice at the later time point, when motor signs were evident, and only on data uncorrected for free water contamination. After correcting for free water contamination, there was no genotype effect on DTI indices in the corpus callosum, although an effect of ageing was detected, with FA decreasing over time in both $Hdh^{+/+}$ and $Hdh^{Q150/Q150}$ mice. This raises issues for previous studies which do not account for free water in the diffusion signal, as atrophy based artefacts cannot be disentangled from changes in white matter microstructure.

In the YAC128 transgenic mouse model (chapter 7), white matter microstructural differences were evident in the corpus callosum between transgenic and wild-type mice. An effect of genotype was only evident in the body of the corpus callosum, with increased FA and no difference in MD in YAC128 mice compared to controls, assessed at a time point late in the disease course, when motor signs were evident. Due to the inherent limitations in interpreting a change in FA, it is not clear whether the change seen in both the mouse model and patient cohort represents a convergence or divergence of results, given that FA values differ from controls but in opposite directions. Nevertheless, they both suggest that white matter microstructure is affected in HD in the corpus callosum. FA as a metric is highly sensitive to microstructural changes (A. Alexander, Lee, Lazar, & Field, 2007) but lacks specificity to different sub-components of white matter microstructure, for example, changes in axonal membranes, axon morphology, axon density, myelination (Beaulieu, 2002), fiber architecture and the orientational dispersion of fibers in the voxel (Budde & Annese, 2013; Pierpaoli, Jezzard, Basser, Barnett, & Chiro, 1996) can all modulate FA. Thus the interpretation of an increase versus a decrease in FA values in HD patients or a HD mouse model in terms of a specific biophysical process is not possible from diffusion MR data alone.

Additional white matter pathways were investigated in the patient cohort. Despite the corticospinal tract being the main motor output pathway in the human brain, there were no statistically significant differences between HD participants and healthy controls in any microstructural indices in the corticospinal tract, although there was a trend for an increase in MD values, a reduction in myelin water fraction obtained from multi-component relaxometry, and a reduction in restricted volume fraction obtained from the CHARMED acquisition. In the cingulum bundle, which has not previously been examined as a distinct white matter pathway in HD, differences between HD and control participants were evident selectively in the subgenual subdivision of the cingulum, suggesting that specific white matter fiber populations are affected in HD early in the disease course.

Myelin water fraction and restricted volume fraction are both non-tensor based white matter microstructural indices that have never been examined previously in HD. They potentially provide increased biological specificity compared to traditional DTI indices, such as FA and MD, and thus may be useful in understanding which white matter sub-components are affected in HD. In chapter 4, there was a trend for a reduction in both myelin water fraction and restricted volume fraction in HD participants in the corpus callosum, corticospinal tract, and cingulum bundle; the magnitude of differences between HD and control participants was larger for these indices (tract and algorithm specific, commonly > 10% difference) compared to the DTI indices (commonly < 5% difference), however the difference between groups was not statistically significant after correcting for multiple comparisons, with the exception of restricted volume fraction in the subgenual cingulum. This is likely due to an insufficient sample size to detect a group difference; the sample size required has been found to vary depending on the microstructural metric and the white matter tract under investigation. Diffusion tensor derived indices (FA and MD) have been shown to require smaller sample sizes to detect the same effect size compared to the more advanced, biological specific metrics, such as myelin water fraction and restricted volume fraction (De Santis, Drakesmith, Bells, Assaf, & Jones, 2014). However, this must be qualified by the observation that the same biological effect can have different effect sizes in different metrics (Tavor, Hofstetter, & Assaf, 2013). Despite this, a relationship was found in chapter 4 between restricted volume fraction, a proxy for 'axon density', and disease burden in HD, suggesting that non-tensor metrics may be clinically useful in characterising HD.

Taken together, the results presented in this thesis suggest that white matter microstructure is affected early in HD, and evidence has been provided to implicate multiple fiber populations. Work in this thesis also highlights that different mouse models of HD produce different neuropathology and further in vitro validation is required. The clinical relevance of these microstructural changes will be discussed later in this chapter.

## Changes in tissue macrostructure in HD

Changes in tissue macrostructure were explored in both the patient cohort and in two different mouse models of HD using $T_1$ and $T_2$ weighted MRI, along with immunohistochemistry in the mouse brain. Surprising consistencies across the patient and mouse studies were found, although there are also disparities, both across species, and across different mouse models. In the pre-symptomatic and early HD patient cohort (chapter 5), no difference was found in intracranial volume, whereas total brain volume was found to be reduced by approximately 5.8%. In the HdhQ150 knock-in mouse model in chapter 6, total brain volume was reduced to a similar degree (5.6%) at the early time point prior to the onset of motor symptoms, whereas at the later time point, brain volume was reduced by 11.6%. On the contrary, in the transgenic YAC128 mice in chapter 7, no difference was observed in total brain volume, despite MRI being acquired at a later stage in the disease when motor signs were present. This discrepancy is likely due to methodological issues; in chapter 6 an automated and optimised method was used for brain extraction which included dilating a mask image to enhance the contrast between brain tissue and CSF, and only the brain tissue was included in the total brain volume measure. In contrast, in chapter 7, whole brain volume was determined using manual segmentation, which is likely to be more variable and less accurate across subjects.

In terms of sub-cortical atrophy, volume loss was consistently found in the striatum in patients and both mouse models of HD. The magnitude of atrophy was higher in patients (15-25% for caudate and putamen separately) compared to $\mathrm{Hdh}^{Q150/Q150}$ mice at the early time point before motor signs (7%), whereas the later time point in both mouse models revealed a similar degree of atrophy in the caudate-putamen (~19% in $\mathrm{Hdh}^{Q150/Q150}$, ~ 15-18% in YAC128 mice).

The cerebellum and the cerebral cortex were found to be relatively spared in both the patient cohort and the HdhQ150 mouse model, although cortical thinning was evident at the later time point in the HdhQ150 mouse model. Cortical atrophy was evident in the YAC128 mouse, although the magnitude of atrophy (< 5%) was less than that in the caudate-putamen. Taken together, this suggests that cortical atrophy occur later in the disease time course, in line with previous work (P. Nopoulos, et al., 2010). The hippocampus and amygdala were also found to be spared in the patient work, suggesting that despite a global reduction in brain volume, localised volume loss is a feature of HD even at an early stage in the disease.

Atrophy was not restricted to the grey matter; white matter atrophy was also evident, and the volume of the corpus callosum was found to be reduced in the patient cohort, in line with previous findings (Crawford et al., 2013). The similarities found in neuropathology seen across patient and mouse studies, particularly in the

HdhQ150 mouse model suggest that in vivo pre-clinical MR has the sensitivity to detect changes in tissue macrostructure that are representative of that seen in early stage disease in patients. Finally, work presented in chapter 7 suggests that in vivo MRI is sensitive to the effects of environmental modification in the caudate-putamen selectively in transgenic HD mice, implicating a mechanism mediated by the striatum and providing additional support to work suggesting that HD may be amenable to environmental, non-pharmaceutic based therapeutics.

## Neural correlates of clinical performance

In chapter 3, HD participants were found to have selective cognitive deficits in memory and specific executive functions, with fewer disturbances seen in tasks requiring attentional processing. A composite cognitive score was formed in order to reduce the number of comparisons required and examine the relationship between brain structure and cognitive function. Patients were found to have significant motor and psychomotor slowing, but there was no significant difference in the composite score compared to healthy matched controls. In both controls and HD participants, composite cognitive function correlated with total white matter and total grey matter volume, suggesting that the battery of tests used were sensitive to individual variations in global tissue macrostructure.

In HD participants specifically, motor slowing was highly correlated with free water fraction in the cingulum and corpus callosum, as well as with sub-cortical atrophy. Cognitive functioning also correlated with sub-cortical atrophy and tissue microstructure abnormalities in the corpus callosum and subgenual cingulum, with worse cognitive performance associated with a higher degree of atrophy, increased MD values in the corpus callosum, and reduced restricted volume fraction (‘axon density’) in the subgenual cingulum. A genetic marker of disease severity, the Disease Burden Index (Penney, et al., 1997) was found to be related to sub-cortical atrophy, cortical thickness and tissue microstructural measures in the corticospinal tract, corpus callosum and cingulum bundle. This suggests that changes in both tissue macrostructure and tissue microstructure are clinical relevant and serve as biomarkers of genetically-determined disease severity. Similarly, a non-genetic index of disease severity, the Total Functional Capacity scale, was correlated with tissue microstructural measure in the corticospinal tract and corpus callosum, again highlighting the clinical significance of white matter abnormalities in HD. In chapter 4 and 5 respectively, disease burden was sensitive to variations in free water fraction in the whole cingulum as well as in the subpopulation of fibers in the subgenual subdivision of the cingulum, and to variations in cortical thickness in the isthmus cingulate gyrus. Taken together with the microstructural abnormalities found in the subgenual cingulum in HD participants, this suggests that the cingulum and cingulate gyrus are sensitive to disease progression in the pre-symptomatic and early stages of HD. This is particularly noteworthy, as previous studies in prodromal HD have found an increase in volume and thickness of the rostral anterior cingulate in prodromal HD subjects (P. C. Nopoulos, et al., 2010; H. D. Rosas et al., 2005; Tabrizi, et al., 2009), thus it appears that specific regions of the cingulate and specific fiber populations of the cingulum may respond to neurodegeneration differently.

Similar associations between functional performance and MRI measures were found in a mouse model of HD in chapter 6. In the Hdh$^{Q150/Q150}$ mice, selective motor deficits were observed on the rotarod test and in locomotor activity. A counter-intuitive positive association was found between atrophy in the thalamus and performance on the rotarod test, suggesting that atrophy to the thalamus is functionally relevant for motor performance. In agreement with the patient work in the corpus callosum, free water fraction, a relatively under-explored metric of tissue microstructure, was correlated with locomotor velocity in Hdh$^{Q150/Q150}$ mice selectively. This thesis represents the first application of free water fraction as a distinct white matter metric. The convergence across species showing the functional and clinical relevance of free water fraction demonstrates that it provides added value as a biomarker of disease severity, and should be adopted as a metric alongside tensor metrics in diffusion MRI studies of neurodegenerative diseases.

## Translation of findings

It is useful to examine consistencies across species in terms of the effects of mutant Huntingtin, in order to be able to probe the biophysical basis of neuroimaging results using in vitro techniques not possible in most human patient studies. However, it was not the intention of this thesis to achieve a direct translation between species for a number of reasons. Firstly, the neurological differences between humans and mice, in terms of anatomy, white matter architecture, vasculature, and metabolism, means that results seen in one species will not necessarily be evident in, or relevant in the other. Moreover, mouse models are simply models of the disease, shown by the differences in neuropathology and phenotype across different mouse models in chapters 6 and 7. Thus, the most accurate representation will be achieved in patients themselves. The reliance on anaesthesia for MRI in rodents means that the relationship between cognition and brain structure may be confounded (Eckel et al., 2012) and further investigation is required to fully understand how anaesthesia affects the MRI measures under investigation.

Despite these caveats, work using HD mouse models does have translational potential if applied intelligently, and there are many reasons why mouse models are needed, for example, in assessing therapeutics not previously tested in humans. Mouse models are also helpful in characterising neuropathology at later disease stages; chorea is a relatively common motor symptom at later disease stages which is problematic for acquiring sufficient quality MRI images without the use of sedation. Therefore, it is important to understand the points of similarity and difference between species in order to translate findings in both directions and improve the interpretability of any results.

As shown in the above sections, a number of common findings emerged in both patients and mouse models, which support the interpretation that the mutant huntingtin gene affects both tissue macrostructure and white matter microstructure in the brain at different stages in the disease course. Further work is planned in the mouse models using in vitro techniques to validate the MRI results and increase the biophysical specificity of the findings, as discussed in more detail below.

## Methodological considerations

In the patient work, great effort was taken to achieve education matching, along with age and gender for the control group, which is a key strength of the work presented. Previous studies which have applied deterministic tractography in HD have not matched groups for years of education (Bohanna, Georgiou-Karistianis, & Egan, 2011; Phillips, et al., 2013; Phillips, et al., 2014; Poudel, et al., 2014) , despite it being a well-known confound when measuring both brain structure (Gönül et al., 2009) and cognitive performance (Steffener et al., 2014), and has been found to mitigate the clinical impact of other neurodegenerative diseases such as Alzheimer’s disease (Amieva et al., 2014; Shpanskaya et al., 2014) and Parkinson’s disease (Armstrong et al., 2012; Hindle, Martyr, & Clare, 2014).

An inherent limitation with the patient work that is common to the literature is a bias in terms of symptom profile, with the healthier, less apathetic and more motivated gene carriers more likely to consent to being part of research, and more likely to turn up to scheduled appointments. Thus, the most psychiatrically and cognitively unwell participants are not captured in research studies, which may mean an important pathological feature of the disease which results in more severe psychiatric and cognitive symptoms is missed. Efforts were made to recruit apathetic participants as well as those with executive deficits which affect the ability to present for scheduled appointments; reminder letters and phone calls on the day before were helpful, as were the provision of taxis to transport participants to the research centre. A second limitation is that it was not possible to stratify the patient group into pre-symptomatic and early-stage HD due to the small sample size. Philosophically, this is not a big problem because disease progression in HD does not occur in a non-continuous way, and thus the functional and neuropathological profile of a participant approaching symptom onset and an early-manifest participant is not likely to be different. However, in terms of being able to compare results with previous studies and add new results to the literature, this is a limitation.

Finally, a limitation of the animal work, which will be referred to in the next section, was the lack of in vitro validation of in vivo MRI results. Measures of cortical thickness in ex vivo tissue sections revealed significantly smaller group differences compared to measurements made on MRI images. As discussed in previous chapters, the protocol for ex vivo MRI acquisition may have been detrimental to the immunohistochemistry analyses, and further optimisation work is required to achieve an optimal protocol for both techniques. Despite this, preliminary pilot results from the electron microscopy analysis are promising (Appendix 4) and should increase the biological specificity of the results presented.

## Future directions

Time did not permit a comprehensive in vitro validation of the in vivo MRI results presented in chapter 6; however electron microscopy analysis is currently being carried out in the corpus callosum to analyse the white matter changes at a greater level of detail, and achieve a quantitative measure of myelin thickness and axon diameter.

In chapters 3, 4, and 5, it is recognised that the sample size in the patient cohort was small, and recent work has shown that the sample size needed to detect differences between groups varies depending on the microstructural metric and the white matter tract under investigation (De Santis, et al., 2014). Thus, future work involves the continued recruitment of HD participants and healthy matched controls and the acquisition of multi-component relaxometry and CHARMED sequence. Furthermore, to investigate non-tensor based metrics further, CHARMED data were also acquired post mortem in the HdhQ150 mouse brains. Future work involves adapting the processing code, currently only implemented in the human and rat brain, to examine restricted volume fraction in the mouse and compare with in vitro analyses, such as the electron microscopy work detailed above.

Finally, an increased patient sample size would allow for a logistic regression analysis to be performed, which would inform on which macrostructural and/or microstructural metrics are most sensitive to HD. Achieving a sensitive and reliable biomarker in HD would be a major advancement in the field, as it would mean that intervention studies could be conducted prior to the onset of symptoms with the aim to delay or prevent the onset of symptoms, as opposed to slowing down symptom progression as is the case currently. It is likely that a combination of biomarkers may be most sensitive to disease progression in HD, and a larger sample size would allow logistic regression to determine an optimal combination of biomarkers which have adequate sensitivity and specificity required for intervention studies.

## Concluding comment

Research undertaken for this thesis has consistently shown that white matter microstructure is of clinical relevance in Huntington’s disease, with evidence showing distinct fiber populations affected, alongside more widespread macrostructural changes. In terms of white matter microstructure, a number of potential imaging biomarkers have emerged from this body of work that give more specific information about the tissue and pathology compared to tensor-derived metrics. The free water fraction, which is the fraction of the diffusion MRI signal assigned to the cerebrospinal fluid (CSF) partial volume component after removing the signal from brain tissue, was found to change linearly with both a genetic marker of disease severity and with total functional capacity in patients, and was sensitive to both motor slowing in patients and motor signs in a mouse model of HD. In addition, the restricted volume fraction, which is a proxy measure of axon density derived from the multi-shell CHARMED diffusion sequence, was found to be reduced in HD participants in the subgenual cingulum specifically, and sensitive to cognitive functioning. Moreover, in the mouse brain, sub-cortical atrophy and white matter microstructure in the corpus callosum were shown to be altered by an environmental intervention which was also found to modify motor signs. Taken together, this work puts forward evidence for potential structural neuroimaging biomarkers of disease progression in HD, with far-reaching implications in terms of removing barriers for treatment trials in pre-symptomatic HD populations, a key component in ultimately moving the field one step closer to disease-modifying treatments for HD.

# Appendix 1 Solutions

## ABC solution

5ul A (DAKO)

5 ul B (DAKO)

1ml 1 % serum in 1 x TBS

## Antifreeze

5.45g Di-sodium hydrogen orthophosphate (A)

1.57g Sodium di-hydrogen orthophosphate (B)

400ml Distilled water ( C )

A, B and C dissolved fully and pH 7.3-7.4 then add:

300ml Ethylene Glycol

300ml Glycerol

## Chemical-grade 0.1M Phosphate Buffer Saline (MRI)

950 ml Distilled water

9.5 ml Sodium Phosphate Monobasic Dihydrate 0.2 M 31.2 g / l (Sigma)

40.5 ml Sodium Phosphate Monobasic Dihydrate 0.2 M 28.4g / l (Sigma)

8.0 g Sodium Chloride (Sigma)

0.2 g Potassium Chloride (Sigma)

pH 7.4

## 10% Iron Alum

50g Ammonium iron(III) sulfate dodecahydrate (Sigma)

500 ml Distilled water

## Paraformaldehyde solution (PFA) 1 L

40g PFA (4%)

1L Prewash buffer

Heat to dissolve

pH 7.3 (orthophosphoric acid)

## Phosphate Buffer Saline

90g di-sodium hydrogen orthophosphate (Bhd)

45g Sodium Chloride (Sigma)

5000 ml Distilled water

pH 7.3

## Quench

10ml Methanol (Fisher Scientific)

10ml Hydrogen Peroxide 30% ( VWR Prolabo BHD)

80ml Distilled Water

## Solochrome cyanine

0.2 g solochrome cyanine

0.5 ml concentrated sulphuric acid ($H_2SO_4$)

10% Iron Alum (see above)

## Sucrose solution

25g sucrose (Fisher Scientific)

100 ml phosphate buffered saline (Sigma)

## TBS

12g Trizma base

9g sodium chloride

1000ml Distilled water

pH 7.4

## TNS

6g Trisma base (Sigma)

1000ml Distilled water

pH 7.4

## 0.2% Triton X-100 in TBS (TXTBS)

250 ml 1 x TBS

500 ul Triton X-100 (Sigma)

pH 7.4

# Appendix 2

# Ordinal International Standard Classification of Education (ISCED) scale

Please indicate by *ticking the box* in the right hand column, the highest education level you have achieved

| | | Please tick |
|---|---|---|
| **ISCED 0** | Pre-primary education (nursery school) | |
| **ISCED 1** | Primary school (key stage 1,2) | |
| **ISCED 2** | Comprehensive school/college (key stage 3) | |
| **ISCED 3** | Sixth form (key stage 4) | |
| **ISCED 4** | College of further education | |
| **ISCED 5** | University (further/higher education institutions) | |
| **ISCED 6** | Tertiary studies leading to an advanced research qualification (e.g. Masters, PhD ) | |

# Appendix 3

# Statistical assumptions

## Justification for including covariates

***Age as a covariate in patient cohort study*** For the work in patients, age was significantly correlated with many of the cognitive tests (see Table Appendix 3.1), however there was no significant interaction between genotype and age for the cognitive tests, Wilks' λ = 0.081, F (20, 32) = 1.57, p > 0.05, justifying the inclusion of age as a covariate in the analysis in Chapter 3.

In Chapter 4, for deterministic tracking in the corpus callosum, a bivariate correlation analysis between age and the MR measures found that Pearson's r was > 0.3, indicating moderate correlation for a number of measures. For segment I, r > 0.3 for MD estimated with DTI and CSD tracking. For segment II, r > 0.3 for MD estimated with CSD and DRL tracking. For segment III, r > 0.3 for MD measures with DTI, CSD, and DRL tracking, and for myelin water fraction and free water fraction estimated with CSD, and for FA measures estimated with DRL. For segment IV, r > 0.3 for MD measures from all tracking algorithms, and myelin water fraction and free water fraction estimated with CSD. Finally, in segment V, r > 0.3 for MD measures from all tracking algorithms, and myelin water fraction and free water fraction estimated with CSD, and for free water fraction estimated with DTI.  For restricted volume fraction,  using CSD tracking, r > 0.3 for segment II, II and IV, whereas  r > 0.3 using DRL in segment III only, and r < 0.3 in all segments using DTI tractography. For deterministic tracking in the corticospinal tract,  a bivariate correlation analysis between age and the MR measures found that Pearson's r was > 0.3 for MD and AD values obtained using CSD in the right corticospinal tract, whereas for tracking with DRL, r > 0.3 for myelin water fraction in the left corticospinal tract.  For deterministic tracking in the cingulum, a bivariate correlation analysis between age and the MR measures found that there was no significant correlation between age and any of the measures in the whole cingulum or sub-genual subdivision of the cingulum for control and HD gene positive participants, all r < 0.3, p > 0.05. For the relationship between MD values in the right retrosplenial subdivision and age, r = .325, p > 0.05.

The relationship between age and volume measures (chapter 5) can be seen in Table Appendix 3.1.

Table Appendix 3.1 Relationship between age and volume. Pearson's correlation coefficient r shown along with p value. L: left, R: right.

| | | controls | | HD | |
|---|---|---|---|---|---|
| | Hem | r | p | r | p |
| ***Freesurfer volumes*** | | | | | |
| ICV | | -.347 | .159 | .243 | .346 |
| Cerebral WM | L | -.310 | .210 | .091 | .728 |
| | R | .128 | .612 | .404 | .108 |
| Caudate | L | -.112 | .657 | -.046 | .860 |
| | R | -.188 | .454 | -.134 | .608 |
| Putamen | L | **-.455** | .058 | -.031 | .905 |
| | R | **-.498*** | .035 | -.117 | .655 |
| Pallidum | L | -.117 | .645 | -.123 | .638 |
| | R | -.259 | .299 | -.134 | .608 |
| Thalamus | L | -.436 | .070 | -.283 | .271 |
| | R | -.457 | .056 | -.385 | .127 |
| Hippocampus | L | .260 | .297 | .018 | .946 |
| | R | .012 | .963 | -.152 | .561 |
| Amydgala | L | -.252 | .312 | -.139 | .594 |
| | R | -.285 | .252 | -.262 | .310 |
| Nucleus Accumbens | L | -.208 | .408 | -.179 | .493 |
| | R | -.034 | .894 | -.269 | .297 |
| Cerebellum Cortex | L | -.217 | .387 | -.265 | .303 |
| | R | -.315 | .203 | -.237 | .361 |
| Cerebral cortex | L | -.397 | .103 | -.370 | .144 |
| | R | -.429 | .076 | -.383 | .129 |
| **FSL volumes** | | | | | |
| Total grey matter | | **-.639**** | .004 | **-.639**** | .006 |
| Total white matter | | -.232 | .354 | .197 | .448 |
| Total Brain | | **-.499*** | .035 | -.361 | .155 |
| Caudate | L | -.280 | .261 | -.096 | .713 |
| | R | -.252 | .312 | -.139 | .595 |
| Putamen | L | -.315 | .203 | .039 | .882 |
| | R | -.300 | .226 | -.037 | .888 |
| Pallidum | L | -.042 | .869 | .045 | .864 |
| | R | -.134 | .595 | .012 | .964 |
| Thalamus | L | -.367 | .134 | -.134 | .609 |
| | R | -.257 | .304 | -.254 | .326 |
| Hippocampus | L | -.252 | .312 | -.126 | .629 |
| | R | -.067 | .791 | -.446 | .073 |
| Amydgala | L | .046 | .857 | .351 | .167 |
| | R | -.329 | .183 | .098 | .709 |
| Nucleus Accumbens | L | -.126 | .618 | -.407 | .105 |
| | R | .098 | .700 | -.355 | .162 |

### *Intracranial volume as a covariate in local macrostructure analysis*

In chapter 5, intracranial volume was significantly correlated with cerebral white matter volume, cerebral cortical volume, cerebellum cortical volume, and volume in the thalamus, caudate, putamen, and globus pallidum (all $r > 0.3$, $p < 0.05$ uncorrected) in control and HD human participants alike, justifying the inclusion of ICV as a covariate.

In Chapter 6, intracranial volume (ICV) was found to significantly correlate with all sub-cortical volume measures in both Hdh$^{+/+}$ and Hdh$^{Q150/Q150}$ mice, $r > 0.3$ for volume of the thalamus, globus pallidum, caudate-putamen, hippocampus and neocortex.

As detailed in Chapter 7, whole brain volume was not significantly correlated with caudate volume, cerebral cortical volume or lateral ventricular volume in wild-type mice or transgenic mice, all $p > 0.05$, thus, it was not necessary to include whole brain volume as a covariate in the subsequent analyses.

Table Appendix 3.2 Pearson's correlation coefficient for relationship between cognitive tests and age. For all coefficients > 0.3, or < -0.3, age was added as a covariate in the analysis. *PAL: Paired Associate Learning. IGT: Iowa Gambling Task, RT: reaction time. ID: Intra-dimensional. ED: Extra-dimensional.*

| | | | | Go / No-Go | | | | ID / ED Task | | | | | | | |
|---|---|---|---|---|---|---|---|---|---|---|---|---|---|---|---|
| | Digit Span | PAL | IGT | Go accuracy | No-Go accuracy | Go RT (ms) | No-Go RT (ms) | ID shift | ED shift | Spatial Planning | Stroop | Verbal Reasoning | Feature Match | Spatial Rotation | Finger Tap Speed |
| **Controls ( n = 13)** | 0.037 | **-0.31** | 0.27 | **0.46** | 0.14 | **0.38** | **0.34** | -0.052 | **-0.36** | **-0.39** | **-0.46** | -0.13 | **-0.42** | 0.11 | -0.21 |
| **HD ( n = 15)** | **-0.32** | -0.19 | -0.11 | -0.23 | -0.22 | -.018 | **-0.48** | **-0.53** | .023 | **-0.49** | 0.12 | **-0.30** | -0.29 | 0.29 | -0.22 |

## Removal of outliers

Outliers were first identified by examining box-and-whisker plots for each dependent variable, for controls/wild-type and HD patients/genetic mice separately. Outliers that were ± 3 standard deviations from the mean were removed. For diffusion MRI analysis, outliers that were both ≥ 2 standard deviations from the mean with low FA values (< 0.2) not expected in white matter were also removed.

In chapter 4, for DTI, CSD AND DRL tracking of the corpus callosum, the same 2 outliers (1 control, 1 HD) were removed, with extreme low FA values and/or extreme high MD values. 1 outlier (control) was removed for the free water fraction measure for CSD, DRL and DTI measures with extreme high values. 1 outlier was removed for the restricted volume fraction for all tracking algorithms for both the corpus callosum and corticospinal tract reconstructions. No other outliers were identified for the corticospinal tract reconstructions.

For the automated segmentation pipeline implemented in Chapter 6, a number of segmented images were removed from the analysis after inspecting the images for data quality. The cerebellum and olfactory bulb were distorted in a number of images, so these two regions were not included in the total intracranial volume measurement for consistency across all images. 3 images were excluded from the analysis due to either image artefacts or damage to the brain.

## Test of assumptions for mixed-model ANOVA

All assumptions were tested after the removal of outliers. For human chapters, for analyses where age was a covariate in the analysis, it was not possible to test the assumptions for each level of the ANOVA. Instead, for these analyses the assumptions were tested on the residuals of the general linear model.

## *The sphericity assumption*

This assumption requires that the variance of population difference scores for any two conditions are the same as the variance of the population difference scores for any other two conditions. Mauchly's test of sphericity was used to test this assumption when there were more than 2 levels for the within-subject independent variable. Where the assumption of sphericity was violated the corrected Greenhouse-Geisser value was used when $\varepsilon < 0.75$, and the Huynh-Feldt correction when $\varepsilon > 0.75$.

***Corpus callosum tracking (Chapter 4)*** The assumption of sphericity was violated for a number of different measures for all 3 tractography algorithms. For tracking using CSD, for MD values, free water fraction, myelin water fraction and restricted volume fraction, the assumption of sphericity was violated, $\chi^2(9) =$ 25.54, 49.25, 22.89 and 27.20 respectively, $p < 0.05$ and thus the corrected Greenhouse-Geisser value was used.

For tracking using DRL, the assumption of sphericity was violated for FA, MD, free water fraction values and restricted volume fraction, $\chi^2(9) = 30.85$, 23.11, 47.77 and 29.31 respectively. For myelin water fraction, the assumed of sphericity was not violated, $\chi^2(9) = 11.67$, $p > 0.05$.

Likewise, for tracking using DTI, for MD, free water fraction and restricted volume fraction, the assumption of sphericity was violated, $\chi^2(9) = 24.50$, 36.82, and 21.55 respectively, $p < 0.05$ and thus the corrected Greenhouse-Geisser value was used.

***Corpus Callosum volume (Chapter 5)*** The assumption of sphericity was violated for volume measures in the 5 segments of the corpus callosum, $\chi^2 = 17.62$, $p < 0.05$, $\varepsilon = .799$ therefore the Huynh-Feldt correction was used.

***Longitudinal mouse study (Chapter 6)*** For cortical thickness at 20-months old, the variance of population difference scores for the different cortical sections did not differ from the variance due to genotype, , $\chi^2(5) = 0.71$, $p > 0.05$.

### *Normally distributed dependent variables*

Mixed models only requiring *approximately* normal data as the mode is quite robust to violations of normality, meaning that assumption can be a little violated and still provide valid results. The Shapiro-Wilk test was used to formally test normality at α = .001.

**Chapter 3 Cognitive Testing** For the ID/ED test, the Shapiro-Wilks (S-W) test indicated that the ID shift data was not normally distributed, S-W = .67, df =13, p < 0.001 for control participants, and S-W= .771, df = 15, p < 0.001 for HD participants. The data were transformed, however the distribution was still non-normally distributed for control participants, S-W = .692, df =13, p < 0.001. The Kruskal-Wallis non-parametic test was used to examine group based differences for this measure. For all other cognitive tests, p > 0.001.

**Chapter 4 Tracking of white matter pathways** For all measures obtained using DTI and CSD tracking of the corpus callosum, there was no violation of normality, p ≥ 0.001. Similarly, for all measures obtained using CSD and DRL tracking of the corticospinal tract, there was no violation of normality, p ≥ 0.001. Likewise, with DRL tracking in the cingulum and the distinct subdivisions, there was no violation of normality, all p ≥ 0.001.

**Chapter 5 Macrostructural measures** For all volumetric measures in cortical and sub-cortical regions, the assumption of normality was met for both healthy control and HD participants, all p ≥ 0.001.

**Chapter 6 Longitudinal mouse data** For measures of lateral ventricle volume, corpus callosum thickness, and cortical thickness from immunohistochemistry stained sections, there was no violation of normality for wild-type (df = 8) or HdhQ150 mice (df = 6), all p ≥ 0.001. Similarly, for cortical thickness measures obtained at 19-months of age from MRI images, there was no violation of normality for wild-type (df = 18) or HdhQ150 mice (df =10), all p ≥ 0.001.

For volumetric measures obtained from atlas-based segmentation, there was no violation of normality for raw volumes for Hdh$^{+/+}$ or Hdh$^{Q150/Q150}$ mice. However, when values were normalised for total intracranial volume, for many regions the data was not normally distributed. A log-transform was applied in order to transform the data to a normal distribution, all $p > 0.001$.

For diffusion tensor parameters obtained from deterministic tract reconstruction of the corpus callosum, all values were normally distributed at both time-points, before and after correction for free water contamination, all $p > 0.05$.

## Homogeneity of variances

To test that the error variance of the dependent variance is equal for each combination of the within-subjects factor and between-subjects factor, Levene's test for homogeneity of variances was used. Where Levene's test of equality of error variance was violated, data were log-transformed. If the assumption was still violated with the transformed data, a non-parametric Mann-Whitney test was used rather than an ANOVA.

***Cognitive testing (Chapter 3)*** For all of the individual cognitive tests, there was no violation of the assumption of equal error variance, all $p > 0.05$. Similarly, for the composite cognitive score formed, F (1, 25) = .121, $p > 0.05$.

***Corpus callosum tracking (Chapter 4)*** For tracking using both DTI, CSD and DRL, Levene's test of equality of error variances indicated equal variance for FA, MD, free water fraction, myelin water fraction and restricted volume fraction in all segments and both hemispheres, all $p > 0.05$.

***Corticospinal tract reconstruction (Chapter 4)*** For tracking using CSD and DRL, Levene's test of equality of error variances indicated equal variance for all metrics in both hemispheres, all $p > 0.05$.

***Cingulum tract reconstruction (Chapter 4)*** For MD values in the right subgenual subdivision of the cingulum, Levene's test was violated, F (1, 21) =

9.05, $p < 0.01$. A log(10) transformation was conducted and equal variance was found in the transformed MD values, $p > 0.05$.

***Volumetric measures (Chapter 5)*** The assumption of equality of equal variance was violated for volumes of the cerebellum white matter, cerebellum cortex, and the putamen calculated using Freesurfer, $p < 0.01$, thus a log transformation was conducted.

***Longitudinal Mouse Data (Chapter 6)*** For measurements on the immunohistochemistry stained sections, Levene's test of equality of error variances indicated equal variance for cortical thickness measurements, F (1,15) = 0.676, $p > 0.05$, and corpus callosum thickness in all 4 measured regions, F (1,11) = 1.25, 0.75, 0.023, and 0.41 for genu, anterior body, mid-body and splenium respectively $p > 0.05$. For the average lateral ventricle surface area, there was equality of error variance, F (1, 13) = 1.80, $p > 0.05$. Similarly, for cortical thickness measures at 20 months, for the left and right hemisphere respectively, there was equal variance in all 4 measured regions, F (1, 26) = 0.734, 0.068, 0.064, 0.639, 0.252, 1.33, 1.43 and 0.23 respectively, all $p > 0.05$.

For transformed, normalised volumes obtained from atlas based segmentation, Levene's test indicated equal variance at 7-, 19- and 20- months of age for all structures under investigation, $p > 0.05$ for left and right hemisphere at each time point respectively.

For the deterministic tracking of the corpus callosum, for uncorrected values, there was equal variance at 7- and 19-months for: FA (F (1, 28) = 2.94 and 0.49, $p > 0.05$)

## *Equality of Covariance*

For a multivariate ANOVA approach, it is assumed is that the vector of the dependent variables follow a multivariate normal distribution, and the variance-covariance matrices are equal across the cells formed by the between-subjects effects. Box's M test was used to test the null hypothesis that the observed covariance matrices of the dependent variables are equal across groups. The Box's M test statistic is transformed to an F statistic with df1 and df2 degrees of freedom. In line with statistical protocol (Mayers, 2013), a significant level of $\alpha = .001$ was used for this test. Where the test was violated, a log transformation was applied and the assumption tested with the transformed values.

***Chapter 4 Deterministic Tractography*** For CSD tracking in the corpus callosum, Box' test of equality of covariance was not violated for FA, MD, free water fraction, F (15, 1419.7) = 1.29, 1.37 and 1.71, respectively, $p > 0.01$, nor was the assumption violated for myelin water fraction, F (15, 645.77) = 2.4, $p > 0.001$ and restricted volume fraction, F (15, 419.53) = 2.03, $p > 0.01$. For DTI tracking in the corpus callosum, there was no violation of the assumption of equality of covariance for FA ( F (15, 1129.94) = 1.07, $p > 0.5$), MD (F (15, 2095.89) = 1.59, $p > 0.5$) free water fraction (F (15, 1199.83) = 2.04, $p > 0.01$), myelin water fraction, F (15, 1188.83) = 2.21, $p > 0.001$, or restricted volume fraction, F (15, 1948.74) = 0.84, $p > 0.05$.

As shown in Table Appendix 3.3, for DRL tracking, Box' test of equality of covariance was not violated for FA, MD or free water fraction in the corpus callosum or corticospinal tract, all $p > 0.001$. For free water fraction in the cingulum and the cingulum subdivisions, the assumption was violated and the data were transformed, $p > 0.001$. For restricted volume fraction and myelin water fraction in the corticospinal tract and cingulum bundle, $p > 0.001$.

Table Appendix 3.4 Box’s test of equality of covariance for tensor metrics sampled from DRL tracking in chapter 4, α = .001

| | df1 | df2 | Box's M | F | p | df1 | df2 | Box's M | F | p | df1 | df2 | Box's M | F | p |
|---|---|---|---|---|---|---|---|---|---|---|---|---|---|---|---|
| | FA | | | | | MD | | | | | FWF | | | | |
| Corpus callosum | 15 | 1481.5 | 36.07 | 1.73 | .040 | 15 | 2095.9 | 32.61 | 1.65 | .054 | 15 | 1741.7 | 29.51 | 1.45 | .116 |
| CST | 3 | 111064.5 | 1.01 | 0.30 | .824 | 3 | 1733837.8 | 1.65 | 0.50 | .685 | 3 | 1733837.8 | 4.75 | 1.43 | .233 |
| Cingulum | 3 | 92265.5 | 11.94 | 3.47 | .015 | 3 | 92265.5 | 8.43 | 2.45 | .061 | 3 | 92265.5 | 25.40 | 7.38 | **.000** |
| *Sub-genual* | 3 | 48185.7 | 9.27 | 2.76 | .040 | 3 | 48185.7 | 10.49 | 3.12 | .025 | 3 | 48185.7 | 23.40 | 6.97 | **.000** |
| *Retrosplenial* | 3 | 1733837.8 | 3.95 | 1.19 | .313 | 3 | 1733837.8 | 5.52 | 1.66 | .174 | 3 | 1733837.8 | 13.67 | 4.10 | **.006** |

Table Appendix 3.5 Box’s test of equality of covariance for volume metrics from automated volume segmentation in chapter 4, α = .001. WM: white matter.

| | Box's M | F | p | Box's M | F | p |
|---|---|---|---|---|---|---|
| | **Freesurfer (df [3, 221558.3])** | | | **FSL (df [ 3, 221558.3])** | | |
| Caudate | 6.04 | 1.88 | 0.131 | 7.745 | 2.412 | .065 |
| Putamen | 15.69 | 4.88 | .002 | 7.794 | 2.427 | .063 |
| Thalamus | 0.33 | 0.10 | .959 | 1.970 | .614 | .606 |
| *Globus Pallidum* | 13.27 | 4.13 | .006 | 4.855 | 1.512 | .209 |
| *Nucleus Accumbens* | 4.37 | 1.36 | .253 | 2.223 | .692 | .557 |
| Hippocampus | 1.05 | 0.33 | .805 | 1.313 | .409 | .747 |
| Amygdala | 2.54 | 0.79 | .498 | 5.866 | 1.827 | .140 |
| Cerebellum | 3.85 | 1.20 | .309 | | | |
| Cerebral Cortex | 0.61 | 0.19 | .903 | | | |
| Cerebral WM | 2.77 | 0.86 | .459 | | | |
| Cerebellum WM | 15.12 | 4.71 | .003 | | | |

***Chapter 5.*** As shown in Table Appendix 3.5, the assumption of equality of covariance was violated for putamen, globus pallidum and cerebellum white matter volumes obtained using Freesurfer. After transformation, all p > 0.001.

***Longitudinal Mouse Data (Chapter 6)*** For cortical thickness measures made from MRI images obtained at 19 months old, Box’s test of equality of covariance was not violated, F (36,1188.016) = 0.959, p > 0.05. For transformed, normalised volumes obtained from atlas based segmentation, Box’s test indicated equal covariance at 7-, 19- and 20- months of age for all structures examined, all p > 0.001.

# Appendix 4

## Preliminary electron microscopy in the HdhQ150 mouse model

Using the right hemisphere from the HdhQ150 mouse model study detailed in chapter 6, 200µm sections were cut on a sliding vibratome and sections were stored at 4° in PBS + azide for less than 1 week. Sections were then transported to the Electron Microscopy Unit (Cardiff University), where they were prepared for transmission electron microscopy (TEM). The tissue were embedded by an osmium post-fixation and epoxy resin embedding standard method and the quality of the obtained images below suggest that measures of myelin thickness and axon density will be possible with the tissue.

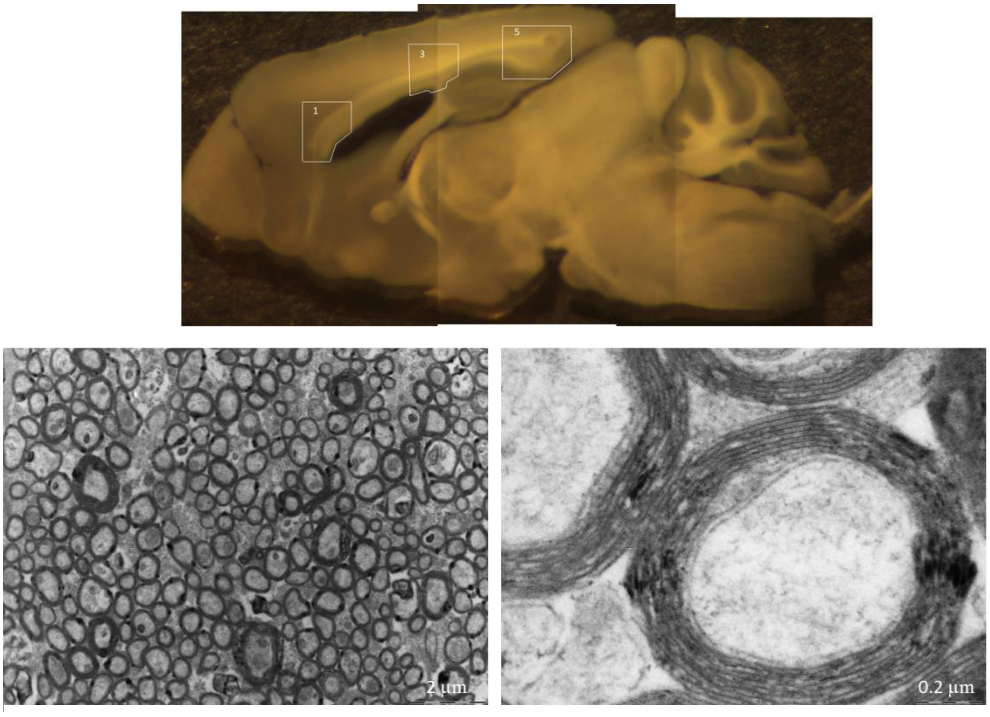

Figure Appendix 4.1 Preliminary TEM images showing the 3 sampling areas corresponding to the genu, body and splenium of the corpus callosum.

# References

Aboitiz, F., & Montiel, J. (2003). One hundred million years of interhemispheric communication: the history of the corpus callosum. *Brazilian journal of medical and biological research = Revista brasileira de pesquisas médicas e biológicas / Sociedade Brasileira de Biofísica ... [et al.], 36*(4), 409-420.

Aboitiz, F., Scheibel, A., Fisher, R., & Zaidel, E. (1992). Fiber composition of the human corpus callosum. *Brain research, 598*(1-2), 143-153.

Aggarwal, M., Duan, W., Hou, Z., Rakesh, N., Peng, Q., Ross, C., et al. (2012). Spatiotemporal mapping of brain atrophy in mouse models of Huntington's disease using longitudinal in vivo magnetic resonance imaging. *NeuroImage, 60*(4), 2086-2095.

Aggleton, J. P., & Nelson, A. J. (2014). Why do lesions in the rodent anterior thalamic nuclei cause such severe spatial deficits? *Neurosci Biobehav Rev*.

Agostinho, L., Santos, S., Alvarenga, R., & Paiva, C. (2013). A systematic review of the intergenerational aspects and the diverse genetic profiles of Huntington's disease. *Genetics and molecular research : GMR, 12*(2), 1974-1981.

Albin, R. L., Qin, Y., Young, A. B., Penney, J. B., & Chesselet, M. F. (1991). Preproenkephalin messenger RNA-containing neurons in striatum of patients with symptomatic and presymptomatic Huntington's disease: an in situ hybridization study. *Ann Neurol, 30*(4), 542-549.

Albin, R. L., Reiner, A., Anderson, K. D., Dure, L. S., Handelin, B., Balfour, R., et al. (1992). Preferential loss of striato-external pallidal projection neurons in presymptomatic Huntington's disease. *Ann Neurol, 31*(4), 425-430.

Albin, R. L., Young, A. B., Penney, J. B., Handelin, B., Balfour, R., Anderson, K. D., et al. (1990). Abnormalities of striatal projection neurons and N-methyl-D-aspartate receptors in presymptomatic Huntington's disease. *N Engl J Med, 322*(18), 1293-1298.

Alexander, A., Lee, J., Lazar, M., & Field, A. (2007). Diffusion tensor imaging of the brain. *Neurotherapeutics : the journal of the American Society for Experimental NeuroTherapeutics, 4*(3), 316-329.

Alexander, A. L., Hasan, K. M., Lazar, M., Tsuruda, J. S., & Parker, D. L. (2001). Analysis of partial volume effects in diffusion-tensor MRI. *Magn Reson Med, 45*(5), 770-780.

Alexander, D. (2005). Multiple-fiber reconstruction algorithms for diffusion MRI. *Annals of the New York Academy of Sciences, 1064*, 113-133.

Alexander, G. E., & Crutcher, M. D. (1990). Functional architecture of basal ganglia circuits: neural substrates of parallel processing. *Trends Neurosci, 13*(7), 266-271.

Alexander, G. E., Crutcher, M. D., & DeLong, M. R. (1990). Basal ganglia-thalamocortical circuits: parallel substrates for motor, oculomotor, "prefrontal" and "limbic" functions. *Prog Brain Res, 85*, 119-146.

Alvarez-Fischer, D., Henze, C., Strenzke, C., Westrich, J., Ferger, B., Höglinger, G. U., et al. (2008). Characterization of the striatal 6-OHDA model of Parkinson's disease in wild type and alpha-synuclein-deleted mice. *Exp Neurol, 210*(1), 182-193.

Amft, M., Bzdok, D., Laird, A. R., Fox, P. T., Schilbach, L., & Eickhoff, S. B. (2014). Definition and characterization of an extended social-affective default network. *Brain Struct Funct*.

Amieva, H., Mokri, H., Le Goff, M., Meillon, C., Jacqmin-Gadda, H., Foubert-Samier, A., et al. (2014). Compensatory mechanisms in higher-educated subjects with Alzheimer's disease: a study of 20 years of cognitive decline. *Brain, 137*(Pt 4), 1167-1175.

Anderson, K., Louis, E., Stern, Y., & Marder, K. (2001). Cognitive correlates of obsessive and compulsive symptoms in Huntington's disease. *The American journal of psychiatry, 158*(5), 799-801.

Ardila, A. (2013). There are two different dysexecutive syndromes (Vol. 1, pp. 114). Journal of Neurological Disorders.

Ariano, M. A., Aronin, N., Difiglia, M., Tagle, D. A., Sibley, D. R., Leavitt, B. R., et al. (2002). Striatal neurochemical changes in transgenic models of Huntington's disease. *J Neurosci Res, 68*(6), 716-729.

Armstrong, E. (1990). Limbic thalamus. In G. Paxinos (Ed.), *The human nervous system* (pp. 469–481): Academic Press, San Diego.

Armstrong, M. J., Naglie, G., Duff-Canning, S., Meaney, C., Gill, D., Eslinger, P. J., et al. (2012). Roles of Education and IQ in Cognitive Reserve in Parkinson's Disease-Mild Cognitive Impairment. *Dement Geriatr Cogn Dis Extra, 2*(1), 343-352.

Aronin, N., Chase, K., Young, C., Sapp, E., Schwarz, C., Matta, N., et al. (1995). CAG expansion affects the expression of mutant Huntingtin in the Huntington's disease brain. *Neuron, 15*(5), 1193-1201.

Arrasate, M., & Finkbeiner, S. (2012). Protein aggregates in Huntington's disease. *Exp Neurol, 238*(1), 1-11.

Arrasate, M., Mitra, S., Schweitzer, E. S., Segal, M. R., & Finkbeiner, S. (2004). Inclusion body formation reduces levels of mutant huntingtin and the risk of neuronal death. *Nature, 431*(7010), 805-810.

Ashburner, J. (2007). A fast diffeomorphic image registration algorithm. *Neuroimage, 38*(1), 95-113.

Ashburner, J., & Friston, K. J. (2000). Voxel-based morphometry--the methods. *Neuroimage, 11*(6 Pt 1), 805-821.

Ashburner, J., Hutton, C., Frackowiak, R., Johnsrude, I., Price, C., & Friston, K. (1998). Identifying global anatomical differences: deformation-based morphometry. *Hum Brain Mapp, 6*(5-6), 348-357.

Assaf, Y., & Basser, P. (2005). Composite hindered and restricted model of diffusion (CHARMED) MR imaging of the human brain. *NeuroImage, 27*(1), 48-58.

Assaf, Y., Freidlin, R., Rohde, G., & Basser, P. (2004). New modeling and experimental framework to characterize hindered and restricted water diffusion in brain white matter. *Magnetic resonance in medicine : official* *journal of the Society of Magnetic Resonance in Medicine / Society of Magnetic Resonance in Medicine, 52*(5), 965-978.

Aylward, E., Codori, A., Rosenblatt, A., Sherr, M., Brandt, J., Stine, O., et al. (2000). Rate of caudate atrophy in presymptomatic and symptomatic stages of Huntington's disease. *Movement disorders : official journal of the Movement Disorder Society, 15*(3), 552-560.

Aylward, E., Harrington, D. L., Mills, J. A., Nopoulos, P. C., Ross, C. A., Long, J. D., et al. (2013). Regional atrophy associated with cognitive and motor function in prodromal Huntington disease. *J Huntingtons Dis, 2*(4), 477-489.

Aylward, E., Liu, D., Nopoulos, P., Ross, C., Pierson, R., Mills, J., et al. (2012). Striatal volume contributes to the prediction of onset of huntington disease in incident cases. *Biological psychiatry, 71*(9), 822-828.

Aylward, E., Nopoulos, P., Ross, C., Langbehn, D., Pierson, R., Mills, J., et al. (2011). Longitudinal change in regional brain volumes in prodromal Huntington disease. *Journal of neurology, neurosurgery, and psychiatry, 82*(4), 405-410.

Aziz, N. A., Jurgens, C. K., Landwehrmeyer, G. B., van Roon-Mom, W. M., van Ommen, G. J., Stijnen, T., et al. (2009). Normal and mutant HTT interact to affect clinical severity and progression in Huntington disease. *Neurology, 73*(16), 1280-1285.

Aziz, N. A., Roos, R. A., Gusella, J. F., Lee, J. M., & Macdonald, M. E. (2012). CAG repeat expansion in Huntington disease determines age at onset in a fully dominant fashion. *Neurology, 79*(9), 952; author reply 952-953.

Bachoud-Lévi, A. C. (2009). Neural grafts in Huntington's disease: viability after 10 years. *Lancet Neurol, 8*(11), 979-981.

Bachoud-Lévi, A. C., Gaura, V., Brugières, P., Lefaucheur, J. P., Boissé, M. F., Maison, P., et al. (2006). Effect of fetal neural transplants in patients with Huntington's disease 6 years after surgery: a long-term follow-up study. *Lancet Neurol, 5*(4), 303-309.

Bachoud-Lévi, A. C., Rémy, P., Nguyen, J. P., Brugières, P., Lefaucheur, J. P., Bourdet, C., et al. (2000). Motor and cognitive improvements in patients with Huntington's disease after neural transplantation. *Lancet, 356*(9246), 1975-1979.

Baddeley, A. (1968). A three-minute reasoning test based on grammatical transformation (Vol. 10, pp. 341-342). Psychometric science.

Bamford, K., Caine, E., Kido, D., Cox, C., & Shoulson, I. (1995). A prospective evaluation of cognitive decline in early Huntington's disease: functional and radiographic correlates. *Neurology, 45*(10), 1867-1873.

Bannerman, D. M., Yee, B. K., Good, M. A., Heupel, M. J., Iversen, S. D., & Rawlins, J. N. (1999). Double dissociation of function within the hippocampus: a comparison of dorsal, ventral, and complete hippocampal cytotoxic lesions. *Behav Neurosci, 113*(6), 1170-1188.

Barker, R. A., Mason, S. L., Harrower, T. P., Swain, R. A., Ho, A. K., Sahakian, B. J., et al. (2013). The long-term safety and efficacy of bilateral transplantation of human fetal striatal tissue in patients with mild to moderate Huntington's disease. *J Neurol Neurosurg Psychiatry, 84*(6), 657-665.

Barnes, G., Duyao, M., Ambrose, C., McNeil, S., Persichetti, F., Srinidhi, J., et al. (1994). Mouse Huntington's disease gene homolog (Hdh). *Somatic cell and molecular genetics, 20*(2), 87-97.

Bartzokis, G., Lu, P. H., Tishler, T. A., & Fong, S. M. (2007). Myelin breakdown and iron changes in Huntington&#39;s disease: pathogenesis and treatment implications. *Neurochemical*.

Bartzokis, G., & Tishler, T. A. (2000). MRI evaluation of basal ganglia ferritin iron and neurotoxicity in Alzheimer's and Huntingon's disease. *Cell Mol Biol (Noisy-le-grand), 46*(4), 821-833.

Basser, P. J. (1998). Fiber-tractography via diffusion tensor MRI (DT-MRI). (pp. 1226). Proceedings of the 6th Annual Meeting ISMRM, Sydney, Australia.

Basser, P. J., Mattiello, J., & LeBihan, D. (1994). Estimation of the effective self-diffusion tensor from the NMR spin echo. *J Magn Reson B, 103*(3), 247-254.

Basser, P. J., Pajevic, S., Pierpaoli, C., Duda, J., & Aldroubi, A. (2000). In vivo fiber tractography using DT-MRI data. *Magn Reson Med, 44*(4), 625-632.

Bayram-Weston, Z., Torres, E., Jones, L., Dunnett, S., & Brooks, S. (2012). Light and electron microscopic characterization of the evolution of cellular pathology in the Hdh(CAG)150 Huntington's disease knock-in mouse. *Brain research bulletin, 88*(2-3), 189-198.

Beaulieu, C. (2002). The basis of anisotropic water diffusion in the nervous system - a technical review. *NMR in biomedicine, 15*(7-8), 435-455.

Bechara, A., Damasio, A. R., Damasio, H., & Anderson, S. W. (1994). Insensitivity to future consequences following damage to human prefrontal cortex. *Cognition, 50*(1-3), 7-15.

Beglinger, L., Nopoulos, P., Jorge, R., Langbehn, D., Mikos, A., Moser, D., et al. (2005). White matter volume and cognitive dysfunction in early Huntington's disease. *Cognitive and behavioral neurology : official journal of the Society for Behavioral and Cognitive Neurology, 18*(2), 102-107.

Ben-Amitay, S., Jones, D., & Assaf, Y. (2011). Motion correction and registration of high b-value diffusion weighted images. *Magnetic resonance in medicine : official journal of the Society of Magnetic Resonance in Medicine / Society of Magnetic Resonance in Medicine*.

Benjamini, Y., & Hochberg, Y. (1995). Controlling the false discovery rate: a practical and powerful approach to multiple testing. (pp. 289-300). Journal of the Royal Statistical Society. Series B (Methodological).

Benn, C. L., Luthi-Carter, R., Kuhn, A., Sadri-Vakili, G., Blankson, K. L., Dalai, S. C., et al. (2010). Environmental enrichment reduces neuronal intranuclear inclusion load but has no effect on messenger RNA expression in a mouse model of Huntington disease. *J Neuropathol Exp Neurol, 69*(8), 817-827.

Beste, C., Saft, C., Andrich, J., Gold, R., & Falkenstein, M. (2008). Response inhibition in Huntington's disease-a study using ERPs and sLORETA. *Neuropsychologia, 46*(5), 1290-1297.

Biedermann, S., Fuss, J., Zheng, L., Sartorius, A., Falfán-Melgoza, C., Demirakca, T., et al. (2012). In vivo voxel based morphometry: Detection of increased hippocampal volume and decreased glutamate levels in exercising mice. *NeuroImage, 61*(4), 1-7.

Birrell, J. M., & Brown, V. J. (2000). Medial frontal cortex mediates perceptual attentional set shifting in the rat. *J Neurosci, 20*(11), 4320-4324.

Björkqvist, M., Wild, E. J., Thiele, J., Silvestroni, A., Andre, R., Lahiri, N., et al. (2008). A novel pathogenic pathway of immune activation detectable before clinical onset in Huntington's disease. *J Exp Med, 205*(8), 1869-1877.

Blumenfeld-Katzir, T., Pasternak, O., Dagan, M., & Assaf, Y. (2011). Diffusion MRI of structural brain plasticity induced by a learning and memory task. *PloS one, 6*(6), e20678.

Bohanna, I., Georgiou-Karistianis, N., & Egan, G. (2011). Connectivity-based segmentation of the striatum in Huntington's disease: vulnerability of motor pathways. *Neurobiology of disease, 42*(3), 475-481.

Bohanna, I., Georgiou-Karistianis, N., Sritharan, A., Asadi, H., Johnston, L., Churchyard, A., et al. (2011). Diffusion tensor imaging in Huntington's disease reveals distinct patterns of white matter degeneration associated with motor and cognitive deficits. *Brain imaging and behavior, 5*(3), 171-180.

Bolivar, V. J., Manley, K., & Messer, A. (2003). Exploratory activity and fear conditioning abnormalities develop early in R6/2 Huntington's disease transgenic mice. *Behav Neurosci, 117*(6), 1233-1242.

Borlongan, C. V., Koutouzis, T. K., & Sanberg, P. R. (1997). 3-Nitropropionic acid animal model and Huntington's disease. *Neurosci Biobehav Rev, 21*(3), 289-293.

Brooks, S., Betteridge, H., Trueman, R., Jones, L., & Dunnett, S. (2006). Selective extra-dimensional set shifting deficit in a knock-in mouse model of Huntington's disease. *Brain research bulletin, 69*(4), 452-457.

Brooks, S., & Dunnett, S. B. (2009). Tests to assess motor phenotype in mice: a user's guide. *Nat Rev Neurosci, 10*(7), 519-529.

Brooks, S., Higgs, G., Janghra, N., Jones, L., & Dunnett, S. (2012). Longitudinal analysis of the behavioural phenotype in YAC128 (C57BL/6J) Huntington's disease transgenic mice. *Brain research bulletin, 88*(2-3), 1-8.

Brooks, S., Higgs, G., Jones, L., & Dunnett, S. (2012). Longitudinal analysis of the behavioural phenotype in Hdh(CAG)150 Huntington's disease knock-in mice. *Brain research bulletin, 88*(2-3), 182-188.

Brooks, S., Janghra, N., Higgs, G., Bayram-Weston, Z., Heuer, A., Jones, L., et al. (2012). Selective cognitive impairment in the YAC128 Huntington's disease mouse. *Brain research bulletin, 88*(2-3), 121-129.

Brooks, S., Jones, L., & Dunnett, S. (2012). Comparative analysis of pathology and behavioural phenotypes in mouse models of Huntington's disease. *Brain research bulletin, 88*(2-3), 81-93.

Brooks, S., Jones, L., & Dunnett, S. (2012). Longitudinal analyses of operant performance on the serial implicit learning task (SILT) in the YAC128 Huntington's disease mouse line. *Brain research bulletin, 88*(2-3), 130-136.

Brouillet, E., Jenkins, B. G., Hyman, B. T., Ferrante, R. J., Kowall, N. W., Srivastava, R., et al. (1993). Age-dependent vulnerability of the striatum to the mitochondrial toxin 3-nitropropionic acid. *J Neurochem, 60*(1), 356-359.

Budde, M. D., & Annese, J. (2013). Quantification of anisotropy and fiber orientation in human brain histological sections. *Front Integr Neurosci, 7*, 3.

Busse, M., Quinn, L., Debono, K., Jones, K., Collett, J., Playle, R., et al. (2013). A randomized feasibility study of a 12-week community-based exercise program for people with Huntington's disease. *J Neurol Phys Ther, 37*(4), 149-158.

Butters, N., Wolfe, J., Martone, M., Granholm, E., & Cermak, L. (1985). Memory disorders associated with Huntington's disease: verbal recall, verbal recognition and procedural memory. *Neuropsychologia, 23*(6), 729-743.

Bäckman, L., Robins-Wahlin, T. B., Lundin, A., Ginovart, N., & Farde, L. (1997). Cognitive deficits in Huntington's disease are predicted by dopaminergic PET markers and brain volumes. *Brain, 120 ( Pt 12)*, 2207-2217.

Bürgel, U., Amunts, K., Hoemke, L., Mohlberg, H., Gilsbach, J. M., & Zilles, K. (2006). White matter fiber tracts of the human brain: three-dimensional mapping at microscopic resolution, topography and intersubject variability. *Neuroimage, 29*(4), 1092-1105.

Calamante, F., Tournier, J. D., Kurniawan, N. D., Yang, Z., Gyengesi, E., Galloway, G. J., et al. (2012). Super-resolution track-density imaging studies of mouse brain: comparison to histology. *Neuroimage, 59*(1), 286-296.

Calder, A. J., Lawrence, A. D., & Young, A. W. (2001). Neuropsychology of fear and loathing. *Nat Rev Neurosci, 2*(5), 352-363.

Cammarata, S., Caponnetto, C., & Tabaton, M. (1993). Ubiquitin-reactive neurites in cerebral cortex of subjects with Huntington's chorea: a pathological correlate of dementia? *Neurosci Lett, 156*(1-2), 96-98.

Campbell, K., Kalén, P., Wictorin, K., Lundberg, C., Mandel, R. J., & Björklund, A. (1993). Characterization of GABA release from intrastriatal striatal transplants: dependence on host-derived afferents. *Neuroscience, 53*(2), 403-415.

Campbell, M. C., Stout, J. C., & Finn, P. R. (2004). Reduced autonomic responsiveness to gambling task losses in Huntington's disease. *J Int Neuropsychol Soc, 10*(2), 239-245.

Carroll, J. B., Lerch, J. P., Franciosi, S., & Spreeuw, A. (2011). Natural history of disease in the YAC128 mouse reveals a discrete signature of pathology in Huntington disease. *Neurobiology of*.

Carter, R., Lione, L., Humby, T., Mangiarini, L., Mahal, A., Bates, G., et al. (1999). Characterization of progressive motor deficits in mice transgenic for the human Huntington's disease mutation. *The Journal of neuroscience : the official journal of the Society for Neuroscience, 19*(8), 3248-3257.

Catani, M., Howard, R. J., Pajevic, S., & Jones, D. K. (2002). Virtual in vivo interactive dissection of white matter fasciculi in the human brain. *Neuroimage, 17*(1), 77-94.

Catani, M., & Thiebaut de Schotten, M. (2008). A diffusion tensor imaging tractography atlas for virtual in vivo dissections. *Cortex, 44*(8), 1105-1132.

Cattaneo, E., Zuccato, C., & Tartari, M. (2005). Normal huntingtin function: an alternative approach to Huntington's disease. *Nat Rev Neurosci, 6*(12), 919-930.

Cepeda-Prado, E., Popp, S., Khan, U., Stefanov, D., Rodríguez, J., Menalled, L. B., et al. (2012). R6/2 Huntington's disease mice develop early and progressive abnormal brain metabolism and seizures. *J Neurosci, 32*(19), 6456-6467.

Chang, L.-C., Jones, D. K., & Pierpaoli, C. (2005). RESTORE: Robust estimation of tensors by outlier rejection. *Magnetic Resonance in Medicine, 53*(5), 1088-1095.

Chang, Y. L., Chen, T. F., Shih, Y. C., Chiu, M. J., Yan, S. H., & Tseng, W. Y. (2014). Regional Cingulum Disruption, Not Gray Matter Atrophy, Detects Cognitive Changes in Amnestic Mild Cognitive Impairment Subtypes. *J Alzheimers Dis*.

Chiang, M. C., Chern, Y., & Juo, C. G. (2011). The dysfunction of hepatic transcriptional factors in mice with Huntington's Disease. *Biochim Biophys Acta, 1812*(9), 1111-1120.

Ciammola, A., Sassone, J., Cannella, M., Calza, S., Poletti, B., Frati, L., et al. (2007). Low brain-derived neurotrophic factor (BDNF) levels in serum of Huntington's disease patients. *Am J Med Genet B Neuropsychiatr Genet, 144B*(4), 574-577.

Ciarmiello, A., Cannella, M., Lastoria, S., Simonelli, M., Frati, L., Rubinsztein, D., et al. (2006). Brain white-matter volume loss and glucose hypometabolism precede the clinical symptoms of Huntington's disease. *Journal of nuclear medicine : official publication, Society of Nuclear Medicine, 47*(2), 215-222.

Cohen, Y., & Assaf, Y. (2002). High b-value q-space analyzed diffusion-weighted MRS and MRI in neuronal tissues - a technical review. *NMR Biomed, 15*(7-8), 516-542.

Conforti, P., Ramos, C., Apostol, B. L., Simmons, D. A., Nguyen, H. P., Riess, O., et al. (2008). Blood level of brain-derived neurotrophic factor mRNA is progressively reduced in rodent models of Huntington's disease: restoration by the neuroprotective compound CEP-1347. *Mol Cell Neurosci, 39*(1), 1-7.

Consortium, H. i. (2012). Induced pluripotent stem cells from patients with Huntington's disease show CAG-repeat-expansion-associated phenotypes. *Cell Stem Cell, 11*(2), 264-278.

Cook, P. A., Bai, Y., Nedjati-Gilani, S., Seunarine, K. K., Hall, M. G., Parker, G. J., et al. (2006). Camino: Open-Source Diffusion-MRI Reconstruction and Processing. 14th Scientific Meeting of the International Society for Magnetic Resonance in Medicine, Seattle, WA, USA.

Cook, P. A., Symms, M., Boulby, P. A., & Alexander, D. C. (2007). Optimal acquisition orders of diffusion-weighted MRI measurements. *Journal of Magnetic Resonance Imaging, 25*(5), 1051-1058.

Correll, C. U., Leucht, S., & Kane, J. M. (2004). Lower risk for tardive dyskinesia associated with second-generation antipsychotics: a systematic review of 1-year studies. *Am J Psychiatry, 161*(3), 414-425.

Craufurd, D., & Snowden, J. (2002). Neuropsychological and neuropsychiatric aspects of Huntington's disease. In G. P. Bates, P. S. Harper & L. e. Jones (Eds.), *Huntingn's Disease<div data-angle="0" data-canvas-width="117.31968571666667" data-font-name="g_font_7" style="position: absolute; left: 203.717px; top: 831.663px; font-size: 12.4998px; font-family: sans-serif; transform: rotate(0deg) scale(0.953819, 1); transform-origin: 0% 0% 0px;"><div data-angle="0" data-canvas-width="117.31968571666667" data-font-name="g_font_7" style="position: absolute; left: 203.717px; top: 831.663px; font-size: 12.4998px; font-family: sans-serif; transform: rotate(0deg) scale(0.953819, 1); transform-origin: 0% 0% 0px;">Huntington's Disease.* (pp. 62-94): Oxford, UK: Oxford University Press.

Craufurd, D., & Snowden, J. S. (2002). Neuropsychological and neuropsychiatric aspects of Huntington's disease. In G. P. Bates, P. S. Harper & L. e. Jones (Eds.), *Huntington's Disease*. Oxford, UK: Oxford University Press.

Craufurd, D., Thompson, J., & Snowden, J. (2001). Behavioral changes in Huntington Disease. *Neuropsychiatry, neuropsychology, and behavioral neurology, 14*(4), 219-226.

Crawford, H. E., Hobbs, N. Z., Keogh, R., Langbehn, D. R., Frost, C., Johnson, H., et al. (2013). Corpus callosal atrophy in premanifest and early Huntington's disease. *J Huntingtons Dis, 2*(4), 517-526.

Crook, Z. R., & Housman, D. E. (2012). Dysregulation of dopamine receptor D2 as a sensitive measure for Huntington disease pathology in model mice. *Proc Natl Acad Sci U S A, 109*(19), 7487-7492.

Crooks, L. E., Arakawa, M., Hylton, N. M., Avram, H., Hoenninger, J. C., Watts, J. C., et al. (1988). Echo-planar pediatric imager. *Radiology, 166*(1 Pt 1), 157-163.

Cudkowicz, M., & Kowall, N. W. (1990). Degeneration of pyramidal projection neurons in Huntington's disease cortex. *Ann Neurol, 27*(2), 200-204.

Cui, L., Jeong, H., Borovecki, F., Parkhurst, C. N., Tanese, N., & Krainc, D. (2006). Transcriptional repression of PGC-1alpha by mutant huntingtin leads to mitochondrial dysfunction and neurodegeneration. *Cell, 127*(1), 59-69.

Dale, A. M., Fischl, B., & Sereno, M. I. (1999). Cortical surface-based analysis. I. Segmentation and surface reconstruction. *Neuroimage, 9*(2), 179-194.

Dalrymple, A., Wild, E. J., Joubert, R., Sathasivam, K., Björkqvist, M., Petersén, A., et al. (2007). Proteomic profiling of plasma in Huntington's disease reveals neuroinflammatory activation and biomarker candidates. *J Proteome Res, 6*(7), 2833-2840.

Damiano, M., Diguet, E., Malgorn, C., D'Aurelio, M., Galvan, L., Petit, F., et al. (2013). A role of mitochondrial complex II defects in genetic models of Huntington's disease expressing N-terminal fragments of mutant huntingtin. *Hum Mol Genet, 22*(19), 3869-3882.

Davies, S. W., Turmaine, M., Cozens, B. A., DiFiglia, M., Sharp, A. H., Ross, C. A., et al. (1997). Formation of neuronal intranuclear inclusions underlies the neurological dysfunction in mice transgenic for the HD mutation. *Cell, 90*(3), 537-548.

Davies, S. W., Turmaine, M., Cozens, B. A., Raza, A. S., Mahal, A., Mangiarini, L., et al. (1999). From neuronal inclusions to neurodegeneration: neuropathological investigation of a transgenic mouse model of Huntington's disease. *Philos Trans R Soc Lond B Biol Sci, 354*(1386), 981-989.

de la Monte, S. M., Vonsattel, J. P., & Richardson, E. P. (1988). Morphometric demonstration of atrophic changes in the cerebral cortex, white matter, and neostriatum in Huntington's disease. *J Neuropathol Exp Neurol, 47*(5), 516-525.

De Rooij, K. E., De Koning Gans, P. A., Roos, R. A., Van Ommen, G. J., & Den Dunnen, J. T. (1995). Somatic expansion of the (CAG)n repeat in Huntington disease brains. *Hum Genet, 95*(3), 270-274.

De Santis, S. (2013). Diffusion MR imaging: How to get the maximum from the experimental time (Vol. 4, pp. 59-65). *Translational Neuroscience*.

De Santis, S., Drakesmith, M., Bells, S., Assaf, Y., & Jones, D. K. (2014). Why diffusion tensor MRI does well only some of the time: variance and covariance of white matter tissue microstructure attributes in the living human brain. *Neuroimage, 89*, 35-44.

de Visser, L., van den Bos, R., Kuurman, W. W., Kas, M. J., & Spruijt, B. M. (2006). Novel approach to the behavioural characterization of inbred mice: automated home cage observations. *Genes Brain Behav, 5*(6), 458-466.

Deacon, R. M., & Rawlins, J. N. (2006). T-maze alternation in the rodent. *Nat Protoc, 1*(1), 7-12.

Dell'Acqua, F., Rizzo, G., Scifo, P., Clarke, R., Scotti, G., & Fazio, F. (2007). A model-based deconvolution approach to solve fiber crossing in diffusion-weighted MR imaging. *IEEE transactions on bio-medical engineering, 54*(3), 462-472.

Dell'acqua, F., Scifo, P., Rizzo, G., Catani, M., Simmons, A., Scotti, G., et al. (2010). A modified damped Richardson-Lucy algorithm to reduce isotropic background effects in spherical deconvolution. *NeuroImage, 49*(2), 1446-1458.

Della Nave, R., Ginestroni, A., Tessa, C., Giannelli, M., Piacentini, S., Filippi, M., et al. (2010). Regional distribution and clinical correlates of white matter structural damage in Huntington disease: a tract-based spatial statistics study. *AJNR Am J Neuroradiol, 31*(9), 1675-1681.

Dellen, A., Blakemore, C., Deacon, R., York, D., & Hannan, A. (2000). Delaying the onset of Huntington's in mice. *Nature, 404*(6779), 721-722.

Dellen, A., Cordery, P., Spires, T., Blakemore, C., & Hannan, A. (2008). Wheel running from a juvenile age delays onset of specific motor deficits but does not alter protein aggregate density in a mouse model of Huntington's disease. *BMC neuroscience, 9*, 34.

Dember, W. N., & Richman, C. L. (1989). Spontaneous Alternation Behavior. Springer, New York.

Deng, Y. P., Albin, R. L., Penney, J. B., Young, A. B., Anderson, K. D., & Reiner, A. (2004). Differential loss of striatal projection systems in Huntington's disease: a quantitative immunohistochemical study. *J Chem Neuroanat, 27*(3), 143-164.

Deoni, S., Rutt, B., Arun, T., Pierpaoli, C., & Jones, D. (2008a). Gleaning multicomponent T1 and T2 information from steady-state imaging data. *Magnetic resonance in medicine : official journal of the Society of Magnetic Resonance in Medicine / Society of Magnetic Resonance in Medicine, 60*(6), 1372-1387.

Deoni, S., Rutt, B., Arun, T., Pierpaoli, C., & Jones, D. K. (2008b). Gleaning multicomponent T1 and T2 information from steady-state imaging data. *Magnetic resonance in medicine : official journal of the Society of Magnetic Resonance in Medicine / Society of Magnetic Resonance in Medicine, 60*(6), 1372-1387.

Deoni, S. C., Matthews, L., & Kolind, S. H. (2013). One component? Two components? Three? The effect of including a nonexchanging "free" water component in multicomponent driven equilibrium single pulse observation of T1 and T2. *Magn Reson Med, 70*(1), 147-154.

Dey, N. D., Bombard, M. C., Roland, B. P., Davidson, S., Lu, M., Rossignol, J., et al. (2010). Genetically engineered mesenchymal stem cells reduce behavioral deficits in the YAC 128 mouse model of Huntington's disease. *Behav Brain Res, 214*(2), 193-200.

Di Paola, M., Luders, E., Cherubini, A., Sanchez-Castaneda, C., Thompson, P. M., Toga, A. W., et al. (2012). Multimodal MRI analysis of the corpus callosum reveals white matter differences in presymptomatic and early Huntington's disease. *Cereb Cortex, 22*(12), 2858-2866.

Di Paola, M., Phillips, O. R., Sanchez-Castaneda, C., Di Pardo, A., Maglione, V., Caltagirone, C., et al. (2014). MRI measures of corpus callosum iron and myelin in early Huntington's disease. *Hum Brain Mapp, 35*(7), 3143-3151.

Dietschy, J. M., & Turley, S. D. (2004). Thematic review series: brain Lipids. Cholesterol metabolism in the central nervous system during early development and in the mature animal. *J Lipid Res, 45*(8), 1375-1397.

DiFiglia, M., Sapp, E., Chase, K., Schwarz, C., Meloni, A., Young, C., et al. (1995). Huntingtin is a cytoplasmic protein associated with vesicles in human and rat brain neurons. *Neuron, 14*(5), 1075-1081.

DiFiglia, M., Sapp, E., Chase, K. O., Davies, S. W., Bates, G. P., Vonsattel, J. P., et al. (1997). Aggregation of huntingtin in neuronal intranuclear inclusions and dystrophic neurites in brain. *Science, 277*(5334), 1990-1993.

Divac, I., Rosvold, H. E., & Szwarcbart, M. K. (1967). Behavioral effects of selective ablation of the caudate nucleus. *J Comp Physiol Psychol, 63*(2), 184-190.

Djoussé, L., Knowlton, B., Hayden, M., Almqvist, E. W., Brinkman, R., Ross, C., et al. (2003). Interaction of normal and expanded CAG repeat sizes influences age at onset of Huntington disease. *Am J Med Genet A, 119A*(3), 279-282.

Dogan, I., Saß, C., Mirzazade, S., Kleiman, A., Werner, C. J., Pohl, A., et al. (2014). Neural correlates of impaired emotion processing in manifest Huntington's disease. *Soc Cogn Affect Neurosci, 9*(5), 671-680.

Domínguez, D. J., Egan, G. F., Gray, M. A., Poudel, G. R., Churchyard, A., Chu, a. P., et al. (2013). Multi-modal neuroimaging in premanifest and early Huntington's disease: 18 month longitudinal data from the IMAGE-HD study. (Vol. 8). PLoS ONE.

Dorner, J. L., Miller, B. R., Barton, S. J., Brock, T. J., & Rebec, G. V. (2007). Sex differences in behavior and striatal ascorbate release in the 140 CAG knock-in mouse model of Huntington's disease. *Behav Brain Res, 178*(1), 90-97.

Dougherty, S., Reeves, J., Lesort, M., Detloff, P., & Cowell, R. (2013). Purkinje cell dysfunction and loss in a knock-in mouse model of Huntington disease. *Experimental neurology, 240*, 96-102.

Downes, J. J., Roberts, A. C., Sahakian, B. J., Evenden, J. L., Morris, R. G., & Robbins, T. W. (1989). Impaired extra-dimensional shift performance in medicated and unmedicated Parkinson's disease: evidence for a specific attentional dysfunction. *Neuropsychologia, 27*(11-12), 1329-1343.

Duan, W., Guo, Z., Jiang, H., Ware, M., Li, X.-J., & Mattson, M. (2003). Dietary restriction normalizes glucose metabolism and BDNF levels, slows disease progression, and increases survival in huntingtin mutant mice. *Proceedings of the National Academy of Sciences of the United States of America, 100*(5), 2911-2916.

Duff, K., Paulsen, J., Beglinger, L. J., Langbehn, D. R., Stout, J. C., & Group, P.-H. I. o. t. H. S. (2007). Psychiatric symptoms in Huntington's disease before diagnosis: the predict-HD study. *Biol Psychiatry, 62*(12), 1341-1346.

Duff, K., Paulsen, J., Mills, J., Beglinger, L., Moser, D., Smith, M., et al. (2010). Mild cognitive impairment in prediagnosed Huntington disease. *Neurology, 75*(6), 500-507.

Duijn, E., Reedeker, N., Giltay, E., Roos, R., & Mast, R. (2010). Correlates of apathy in Huntington's disease. *The Journal of neuropsychiatry and clinical neurosciences, 22*(3), 287-294.

Dumas, E., Bogaard, S., Ruber, M., Reilman, R., Stout, J., Craufurd, D., et al. (2012). Early changes in white matter pathways of the sensorimotor cortex in premanifest Huntington's disease. *Human brain mapping, 33*(1), 203-212.

Dumas, E. M., van den Bogaard, S. J., Middelkoop, H. A., & Roos, R. A. (2013). A review of cognition in Huntington's disease. *Front Biosci (Schol Ed), 5*, 1-18.

Duncan, J., Seitz, R. J., Kolodny, J., Bor, D., Herzog, H., Ahmed, A., et al. (2000). A neural basis for general intelligence. *Science, 289*(5478), 457-460.

Dunnett, S. B., Nathwani, F., & Björklund, A. (2000). The integration and function of striatal grafts. *Prog Brain Res, 127*, 345-380.

Dunnett, S. B., & Rosser, A. E. (2004). Cell therapy in Huntington's disease. *NeuroRx, 1*(4), 394-405.

Dunnett, S. B., & Rosser, A. E. (2014). Challenges for taking primary and stem cells into clinical neurotransplantation trials for neurodegenerative disease. *Neurobiol Dis, 61*, 79-89.

Duyao, M. P., Auerbach, A. B., Ryan, A., Persichetti, F., Barnes, G. T., McNeil, S. M., et al. (1995). Inactivation of the mouse Huntington's disease gene homolog Hdh. *Science, 269*(5222), 407-410.

Döbrössy, M. D., & Dunnett, S. B. (1998). Striatal grafts alleviate deficits in response execution in a lateralised reaction time task. *Brain Res Bull, 47*(6), 585-593.

Eckel, B., Ohl, F., Starker, L., Rammes, G., Bogdanski, R., Kochs, E., et al. (2012). Effects of isoflurane-induced anaesthesia on cognitive performance in a mouse model of Alzheimer's disease: a randomised trial in transgenic APP23 mice. *Eur J Anaesthesiol*.

Engel, A. K., König, P., Kreiter, A. K., & Singer, W. (1991). Interhemispheric synchronization of oscillatory neuronal responses in cat visual cortex. *Science, 252*(5009), 1177-1179.

Epping, E., Mills, J., Beglinger, L., Fiedorowicz, J., Craufurd, D., Smith, M., et al. (2013). Characterization of depression in prodromal Huntington disease in the neurobiological predictors of HD (PREDICT-HD) study. *Journal of psychiatric research, 47*(10), 1423-1431.

Evans, S., Douglas, I., Rawlins, M., Wexler, N., Tabrizi, S., et al. (2013). Prevalence of adult Huntington's disease in the UK based on diagnoses recorded in general practice records. *Journal of neurology, neurosurgery, and psychiatry* vol. 84 (10) p. 1156-60

Faber, P. W., Voisine, C., King, D. C., Bates, E. A., & Hart, A. C. (2002). Glutamine/proline-rich PQE-1 proteins protect Caenorhabditis elegans neurons from huntingtin polyglutamine neurotoxicity. *Proc Natl Acad Sci U S A, 99*(26), 17131-17136.

Fallon, S. J., Williams-Gray, C. H., Barker, R. A., Owen, A. M., & Hampshire, A. (2013). Prefrontal dopamine levels determine the balance between cognitive stability and flexibility. *Cereb Cortex, 23*(2), 361-369.

Farquharson, S., Tournier, J. D., Calamante, F., Fabinyi, G., Schneider-Kolsky, M., Jackson, G. D., et al. (2013). White matter fiber tractography: why we need to move beyond DTI. *J Neurosurg, 118*(6), 1367-1377.

Farrar, A. M., Murphy, C. A., Paterson, N. E., Oakeshott, S., He, D., Alosio, W., et al. (2014). Cognitive deficits in transgenic and knock-in HTT mice parallel those in Huntington's disease. *J Huntingtons Dis, 3*(2), 145-158.

Fennema-Notestine, C., Archibald, S. L., Jacobson, M. W., Corey-Bloom, J., Paulsen, J. S., Peavy, G. M., et al. (2004). In vivo evidence of cerebellar atrophy and cerebral white matter loss in Huntington disease. *Neurology, 63*(6), 989-995.

Fiedorowicz, J., Mills, J., Ruggle, A., Langbehn, D., & Paulsen, J. (2011). Suicidal behavior in prodromal Huntington disease. *Neuro-degenerative diseases, 8*(6), 483-490.

Fischl, B., & Dale, A. M. (2000). Measuring the thickness of the human cerebral cortex from magnetic resonance images. *Proc Natl Acad Sci U S A, 97*(20), 11050-11055.

Fischl, B., Salat, D. H., Busa, E., Albert, M., Dieterich, M., Haselgrove, C., et al. (2002). Whole brain segmentation: automated labeling of neuroanatomical structures in the human brain. *Neuron, 33*(3), 341-355.

Fischl, B., Sereno, M. I., & Dale, A. M. (1999). Cortical surface-based analysis. II: Inflation, flattening, and a surface-based coordinate system. *Neuroimage, 9*(2), 195-207.

Fitzsimmons, J., Hamoda, H. M., Swisher, T., Terry, D., Rosenberger, G., Seidman, L. J., et al. (2014). Diffusion tensor imaging study of the fornix in first episode schizophrenia and in healthy controls. *Schizophr Res, 156*(2-3), 157-160.

Fitzsimmons, J., Schneiderman, J. S., Whitford, T. J., Swisher, T., Niznikiewicz, M. A., Pelavin, P. E., et al. (2014). Cingulum bundle diffusivity and delusions of reference in first episode and chronic schizophrenia. *Psychiatry Res, 224*(2), 124-132.

Folstein, S. E. (1989). Huntingtons disease: a disorder of families.

Franciosi, S., Shim, Y., Lau, M., Hayden, M. R., & Leavitt, B. R. (2013). A systematic review and meta-analysis of clinical variables used in Huntington disease research. *Mov Disord, 28*(14), 1987-1994.

Frank, L. (2002). Characterization of anisotropy in high angular resolution diffusion-weighted MRI. *Magnetic resonance in medicine : official journal of the Society of Magnetic Resonance in Medicine / Society of Magnetic Resonance in Medicine, 47*(6), 1083-1099.

Fray, P. J., & Robbins, T. W. (1996). CANTAB battery: proposed utility in neurotoxicology. *Neurotoxicol Teratol, 18*(4), 499-504.

Gaj, T., Gersbach, C. A., & Barbas, C. F. (2013). ZFN, TALEN, and CRISPR/Cas-based methods for genome engineering. *Trends Biotechnol, 31*(7), 397-405.

Gaj, T., Guo, J., Kato, Y., Sirk, S. J., & Barbas, C. F. (2012). Targeted gene knockout by direct delivery of zinc-finger nuclease proteins. *Nat Methods, 9*(8), 805-807.

Gargiulo, S., Greco, A., Gramanzini, M., Esposito, S., Affuso, A., Brunetti, A., et al. (2012). Mice anesthesia, analgesia, and care, Part I: anesthetic considerations in preclinical research. *ILAR J, 53*(1), E55-69.

Gavazzi, C., Nave, R. D., Petralli, R., Rocca, M. A., Guerrini, L., Tessa, C., et al. (2007). Combining functional and structural brain magnetic resonance imaging in Huntington disease. *J Comput Assist Tomogr, 31*(4), 574-580.

Georgiou-Karistianis, N., Poudel, G. R., Domínguez D, J. F., Langmaid, R., Gray, M. A., Churchyard, A., et al. (2013). Functional and connectivity changes during working memory in Huntington's disease: 18 month longitudinal data from the IMAGE-HD study. *Brain Cogn, 83*(1), 80-91.

Georgiou-Karistianis, N., Stout, J., D, J., Carron, S., Ando, A., Churchyard, A., et al. (2013). Functional magnetic resonance imaging of working memory in Huntington's disease: Cross-sectional data from the IMAGE-HD study. *Human brain mapping*.

Gil, J. M., & Rego, A. C. (2008). Mechanisms of neurodegeneration in Huntington's disease. *Eur J Neurosci, 27*(11), 2803-2820.

Giralt, A., Puigdellívol, M., Carretón, O., Paoletti, P., Valero, J., Parra-Damas, A., et al. (2012). Long-term memory deficits in Huntington's disease are associated with reduced CBP histone acetylase activity. *Hum Mol Genet, 21*(6), 1203-1216.

Girotti, F., Marano, R., Soliveri, P., & Geminiani, G. (1988). Relationship between motor and cognitive disorders in Huntington&#39;s disease. *Journal of*.

Godin, J. D., Colombo, K., Molina-Calavita, M., Keryer, G., Zala, D., Charrin, B. C., et al. (2010). Huntingtin is required for mitotic spindle orientation and mammalian neurogenesis. *Neuron, 67*(3), 392-406.

Gonitel, R., Moffitt, H., Sathasivam, K., Woodman, B., Detloff, P. J., Faull, R. L., et al. (2008). DNA instability in postmitotic neurons. *Proc Natl Acad Sci U S A, 105*(9), 3467-3472.

Gould, R. L., Brown, R. G., Owen, A. M., Bullmore, E. T., Williams, S. C., & Howard, R. J. (2005). Functional neuroanatomy of successful paired associate learning in Alzheimer's disease. *Am J Psychiatry, 162*(11), 2049-2060.

Graveland, G. A., Williams, R. S., & DiFiglia, M. (1985). Evidence for degenerative and regenerative changes in neostriatal spiny neurons in Huntington's disease. *Science, 227*(4688), 770-773.

Gray, M., Shirasaki, D. I., Cepeda, C., André, V. M., Wilburn, B., Lu, X. H., et al. (2008). Full-length human mutant huntingtin with a stable polyglutamine repeat can elicit progressive and selective neuropathogenesis in BACHD mice. *J Neurosci, 28*(24), 6182-6195.

Gray, M. A., Egan, G. F., Ando, A., Churchyard, A., Chua, P., Stout, J. C., et al. (2013). Prefrontal activity in Huntington's disease reflects cognitive and neuropsychiatric disturbances: the IMAGE-HD study. *Exp Neurol, 239*, 218-228.

Greenhouse, S. W., & Geisser, S. (1959). On methods in the analysis of profile data (Vol. 24, pp. 95-112.). *Psychometrika*.

Group, H. S. (1996). Unified Huntington's Disease Rating Scale: reliability and consistency. *Mov Disord, 11*(2), 136-142.

Group, T. (1993). A novel gene containing a trinucleotide repeat that is expanded and unstable on Huntington's disease chromosomes. *Cell, 72*(6), 971-983.

Gutekunst, C., Levey, A., Heilman, C., Whaley, W., Yi, H., Nash, N., et al. (1995). Identification and localization of huntingtin in brain and human lymphoblastoid cell lines with anti-fusion protein antibodies. *Proceedings of the National Academy of Sciences of the United States of America, 92*(19), 8710-8714.

Gutekunst, C., Li, S. H., Yi, H., Mulroy, J. S., Kuemmerle, S., Jones, R., et al. (1999). Nuclear and neuropil aggregates in Huntington's disease: relationship to neuropathology. *J Neurosci, 19*(7), 2522-2534.

Gönül, A., Demirel, O., Kitis, O., Eker, Ç., Eker, Ö., & Ozan, E. (2009). The effects of the duration of formal education on adult brain: a voxel-based morphometry - (diffeomorphic anatomical registration using exponentiated lie algebra) DARTEL Study (Vol. 19, pp. **221-226**). Bulletin of Clinical Psychopharmacology.

Hamilton, J., Salmon, D., Corey-Bloom, J., Gamst, A., Paulsen, J., Jerkins, S., et al. (2003). Behavioural abnormalities contribute to functional decline in Huntington's disease. *Journal of neurology, neurosurgery, and psychiatry, 74*(1), 120-122.

Hampshire, A., Highfield, R. R., Parkin, B. L., & Owen, A. M. (2012). Fractionating human intelligence. *Neuron, 76*(6), 1225-1237.

Harper, P. S. (1992). The epidemiology of Huntington's disease. *Hum Genet, 89*(4), 365-376.

Harrington, D. L., Smith, M. M., Zhang, Y., Carlozzi, N. E., Paulsen, J. S., & Group, P.-H. I. o. t. H. S. (2012). Cognitive domains that predict time to diagnosis in prodromal Huntington disease. *J Neurol Neurosurg Psychiatry, 83*(6), 612-619.

Harris, G. J., Pearlson, G. D., Peyser, C. E., Aylward, E. H., Roberts, J., Barta, P. E., et al. (1992). Putamen volume reduction on magnetic resonance imaging exceeds caudate changes in mild Huntington's disease. *Ann Neurol, 31*(1), 69-75.

Harrison, D. J., Busse, M., Openshaw, R., Rosser, A. E., Dunnett, S. B., & Brooks, S. P. (2013). Exercise attenuates neuropathology and has greater benefit on cognitive than motor deficits in the R6/1 Huntington's disease mouse model. *Exp Neurol, 248*, 457-469.

Hart, E. P. (2013). Cognition in Huntington's disease : the influence of motor behaviour and time. Unpublished doctoral dissertation: Leiden University : The Netherlands.

Hart, E. P., Dumas, E. M., Reijntjes, R. H., van der Hiele, K., van den Bogaard, S. J., Middelkoop, H. A., et al. (2012). Deficient sustained attention to response task and P300 characteristics in early Huntington's disease. *J Neurol, 259*(6), 1191-1198.

Hart, E. P., Dumas, E. M., Schoonderbeek, A., Wolthuis, S. C., van Zwet, E. W., & Roos, R. A. (2014). Motor dysfunction influence on executive functioning in manifest and premanifest Huntington's disease. *Mov Disord, 29*(3), 320-326.

Hart, E. P., Dumas, E. M., van Zwet, E. W., van der Hiele, K., Jurgens, C. K., Middelkoop, H. A., et al. (2013). Longitudinal pilot-study of Sustained attention to response task and P300 in manifest and pre-manifest Huntington's disease. *J Neuropsychol*.

Haselgrove, J. C., & Moore, J. R. (1996). Correction for distortion of echo-planar images used to calculate the apparent diffusion coefficient. *Magn Reson Med, 36*(6), 960-964.

Hayden, M. (1980). Huntington's chorea.

Hedreen, J. C., Peyser, C. E., Folstein, S. E., & Ross, C. A. (1991). Neuronal loss in layers V and VI of cerebral cortex in Huntington's disease. *Neurosci Lett, 133*(2), 257-261.

Heikkinen, T., Lehtimäki, K., Vartiainen, N., Puoliväli, J., Hendricks, S. J., Glaser, J. R., et al. (2012). Characterization of neurophysiological and behavioral changes, MRI brain volumetry and 1H MRS in zQ175 knock-in mouse model of Huntington's disease. *PLoS One, 7*(12), e50717.

Heng, M., Tallaksen-Greene, S., Detloff, P., & Albin, R. (2007). Longitudinal evaluation of the Hdh(CAG)150 knock-in murine model of Huntington's disease. *The Journal of neuroscience : the official journal of the Society for Neuroscience, 27*(34), 8989-8998.

Heng, M. Y., Detloff, P. J., Wang, P. L., Tsien, J. Z., & Albin, R. L. (2009). In vivo evidence for NMDA receptor-mediated excitotoxicity in a murine genetic model of Huntington disease. *J Neurosci, 29*(10), 3200-3205.

Henley, S., Ridgway, G., Scahill, R., Klöppel, S., Tabrizi, S., Fox, N., et al. (2010). Pitfalls in the use of voxel-based morphometry as a biomarker: examples from huntington disease. *AJNR. American journal of neuroradiology, 31*(4), 711-719.

Hennenlotter, A., Schroeder, U., Erhard, P., Haslinger, B., Stahl, R., Weindl, A., et al. (2004). Neural correlates associated with impaired disgust processing in pre-symptomatic Huntington's disease. *Brain : a journal of neurology, 127*(Pt 6), 1446-1453.

Henry, J. D., Crawford, J. R., & Phillips, L. H. (2005). A meta-analytic review of verbal fluency deficits in Huntington's disease. *Neuropsychology, 19*(2), 243-252.

Hickey, M., Gallant, K., Gross, G., Levine, M., & Chesselet, M.-F. (2005). Early behavioral deficits in R6/2 mice suitable for use in preclinical drug testing. *Neurobiology of disease, 20*(1), 1-11.

Hickey, M., Kosmalska, A., Enayati, J., Cohen, R., Zeitlin, S., Levine, M., et al. (2008). Extensive early motor and non-motor behavioral deficits are followed by striatal neuronal loss in knock-in Huntington's disease mice. *Neuroscience, 157*(1), 280-295.

Hickie, I., Ward, P., Scott, E., Haindl, W., Walker, B., Dixon, J., et al. (1999). Neo-striatal rCBF correlates of psychomotor slowing in patients with major depression. *Psychiatry research, 92*(2-3), 75-81.

Hindle, J. V., Martyr, A., & Clare, L. (2014). Cognitive reserve in Parkinson's disease: a systematic review and meta-analysis. *Parkinsonism Relat Disord, 20*(1), 1-7.

Ho, A., Sahakian, B., Brown, R., Barker, R., Hodges, J., Ané, M. N., et al. (2003). Profile of cognitive progression in early Huntington's disease. *Neurology, 61*(12), 1702-1706.

Hobbs, N., Henley, S., Ridgway, G., Wild, E., Barker, R., Scahill, R., et al. (2010). The progression of regional atrophy in premanifest and early Huntington's disease: a longitudinal voxel-based morphometry study. *Journal of neurology, neurosurgery, and psychiatry, 81*(7), 756-763.

Hockly, E., Cordery, P., Woodman, B., Mahal, A., Dellen, A., Blakemore, C., et al. (2002). Environmental enrichment slows disease progression in R6/2 Huntington's disease mice. *Annals of neurology, 51*(2), 235-242.

Hodges, A., Hughes, G., Brooks, S., Elliston, L., Holmans, P., Dunnett, S. B., et al. (2008). Brain gene expression correlates with changes in behavior in the R6/1 mouse model of Huntington's disease. *Genes Brain Behav, 7*(3), 288-299.

Hodgson, J. G., Agopyan, N., Gutekunst, C., Leavitt, B. R., LePiane, F., Singaraja, R., et al. (1999a). A YAC mouse model for Huntington's disease with full-length mutant huntingtin, cytoplasmic toxicity, and selective striatal neurodegeneration. *Neuron, 23*(1), 181-192.

Hodgson, J. G., Agopyan, N., Gutekunst, C. A., Leavitt, B. R., LePiane, F., Singaraja, R., et al. (1999b). A YAC mouse model for Huntington's disease with full-length mutant huntingtin, cytoplasmic toxicity, and selective striatal neurodegeneration. *Neuron, 23*(1), 181-192.

Hofer, S., & Frahm, J. (2006). Topography of the human corpus callosum revisited--comprehensive fiber tractography using diffusion tensor magnetic resonance imaging. *Neuroimage, 32*(3), 989-994.

Hoffmann, R., Stüwe, S. H., Goetze, O., Banasch, M., Klotz, P., Lukas, C., et al. (2014). Progressive hepatic mitochondrial dysfunction in premanifest Huntington's disease. *Mov Disord, 29*(6), 831-834.

Holl, A., Wilkinson, L., Tabrizi, S., Painold, A., & Jahanshahi, M. (2013). Selective executive dysfunction but intact risky decision-making in early Huntington's disease. *Movement disorders : official journal of the Movement Disorder Society, 28*(8), 1104-1109.

Hosmer, D. W., & Lemeshow, S. (2000). Applied Logistic Regression, 2nd Edition, *Wiley Series in Probability and Statistics - Applied Probability and Statistics Section*: Wiley-Blackwell.

Humby, T., Laird, F. M., Davies, W., & Wilkinson, L. S. (1999). Visuospatial attentional functioning in mice: interactions between cholinergic manipulations and genotype. *Eur J Neurosci, 11*(8), 2813-2823.

Huntington, G. (1967). ON CHOREA. *Archives of neurology, 17*(3), 332-333.

Ide, K., Nukina, N., Masuda, N., Goto, J., & Kanazawa, I. (1995). Abnormal gene product identified in Huntington's disease lymphocytes and brain. *Biochemical and biophysical research communications, 209*(3), 1119-1125.

Im, K., Lee, J. M., Lyttelton, O., Kim, S. H., Evans, A. C., & Kim, S. I. (2008). Brain size and cortical structure in the adult human brain. *Cereb Cortex, 18*(9), 2181-2191.

Im, K., Pienaar, R., Lee, J. M., Seong, J. K., Choi, Y. Y., Lee, K. H., et al. (2011). Quantitative comparison and analysis of sulcal patterns using sulcal graph matching: a twin study. *Neuroimage, 57*(3), 1077-1086.

Imarisio, S., Carmichael, J., Korolchuk, V., Chen, C. W., Saiki, S., Rose, C., et al. (2008). Huntington's disease: from pathology and genetics to potential therapies. *Biochem J, 412*(2), 191-209.

Ishiguro, H., Yamada, K., Sawada, H., Nishii, K., Ichino, N., Sawada, M., et al. (2001). Age-dependent and tissue-specific CAG repeat instability occurs in mouse knock-in for a mutant Huntington's disease gene. *Journal of neuroscience research, 65*(4), 289-297.

Jacobsen, J. C., Bawden, C. S., Rudiger, S. R., McLaughlan, C. J., Reid, S. J., Waldvogel, H. J., et al. (2010). An ovine transgenic Huntington's disease model. *Hum Mol Genet, 19*(10), 1873-1882.

Jason, G. W., Pajurkova, E. M., Suchowersky, O., Hewitt, J., Hilbert, C., Reed, J., et al. (1988). Presymptomatic neuropsychological impairment in Huntington's disease. *Arch Neurol, 45*(7), 769-773.

Jay, J., & Dunnett, S. (2007). An operant serial implicit learning task (SILT) in rats: task acquisition, performance and the effects of striatal lesions. *Journal of neuroscience methods, 163*(2), 235-244.

Jech, R., Klempír, J., Vymazal, J., Zidovská, J., Klempírová, O., Růzicka, E., et al. (2007). Variation of selective gray and white matter atrophy in Huntington's disease. *Mov Disord, 22*(12), 1783-1789.

Jenkinson, M., & Smith, S. (2001). A global optimisation method for robust affine registration of brain images. *Med Image Anal, 5*(2), 143-156.

Jeurissen, Leemans, A., Jones, D., Tournier, J.-D., & Sijbers, J. (2011). Probabilistic fiber tracking using the residual bootstrap with constrained spherical deconvolution. *Human brain mapping, 32*(3), 461-479.

Jeurissen, B., Leemans, A., & Tournier, J. D. (2010). Estimating the number of fiber orientations in diffusion MRI voxels: a constrained spherical deconvolution study. *Proceedings of the*.

Jeurissen, B., Leemans, A., Tournier, J. D., Jones, D. K., & Sijbers, J. (2012). Investigating the prevalence of complex fiber configurations in white matter tissue with diffusion magnetic resonance imaging. *Human brain mapping*.

Johann, V., Schiefer, J., Sass, C., Mey, J., Brook, G., Krüttgen, A., et al. (2007). Time of transplantation and cell preparation determine neural stem cell survival in a mouse model of Huntington's disease. *Exp Brain Res, 177*(4), 458-470.

Jones, B., & Roberts, D. (1968). The quantiative measurement of motor inco-ordination in naive mice using an acelerating rotarod. *The Journal of pharmacy and pharmacology, 20*(4), 302-304.

Jones, D. (2008). Studying connections in the living human brain with diffusion MRI. *Cortex; a journal devoted to the study of the nervous system and behavior, 44*(8), 936-952.

Jones, D., Catani, M., Pierpaoli, C., Reeves, S., Shergill, S., O'Sullivan, M., et al. (2005). A diffusion tensor magnetic resonance imaging study of frontal cortex connections in very-late-onset schizophrenia-like psychosis. *The American journal of geriatric psychiatry : official journal of the American Association for Geriatric Psychiatry, 13*(12), 1092-1099.

Jones, D., & Simmons, M. (1999). Optimal strategies for measuring diffusion in anisotropic systems by magnetic resonance imaging. *Magnetic Resonance in Medicine*(42), 1-11.

Jones, D., Symms, M. R., Cercignani, M., & Howard, R. J. (2005). The effect of filter size on VBM analyses of DT-MRI data. *Neuroimage, 26*(2), 546-554.

Jones, D. K. (2008). Studying connections in the living human brain with diffusion MRI. *Cortex; a journal devoted to the study of the nervous system and behavior, 44*(8), 936-952.

Jones, D. K., & Cercignani, M. (2010). Twenty-five pitfalls in the analysis of diffusion MRI data. *NMR in biomedicine, 23*(7), 803-820.

Jones, D. K., Christiansen, K. F., Chapman, R. J., & Aggleton, J. P. (2013). Distinct subdivisions of the cingulum bundle revealed by diffusion MRI fibre tracking: implications for neuropsychological investigations. *Neuropsychologia, 51*(1), 67-78.

Jones, D. K., Symms, M. R., Cercignani, M., & Howard, R. J. (2005). The effect of filter size on VBM analyses of DT-MRI data. *Neuroimage, 26*(2), 546-554.

Jorge Cardoso, M., Leung, K., Modat, M., Keihaninejad, S., Cash, D., Barnes, J., et al. (2013). STEPS: Similarity and Truth Estimation for Propagated Segmentations and its application to hippocampal segmentation and brain parcelation. *Med Image Anal, 17*(6), 671-684.

Kandel, E., Schwartz, J., & TM, J. (2000). Principles of neural science, 5th ed: New York: McGraw-Hill.

Kassubek, J., Juengling, F. D., Kioschies, T., Henkel, K., Karitzky, J., Kramer, B., et al. (2004). Topography of cerebral atrophy in early Huntington's disease: a voxel based morphometric MRI study. *J Neurol Neurosurg Psychiatry, 75*(2), 213-220.

Kaushik, D. K., & Basu, A. (2013). A Friend in Need may not be a Friend Indeed: Role of Microglia in Neurodegenerative Diseases. *CNS Neurol Disord Drug Targets*.

Kazantsev, A., Preisinger, E., Dranovsky, A., Goldgaber, D., & Housman, D. (1999). Insoluble detergent-resistant aggregates form between pathological and nonpathological lengths of polyglutamine in mammalian cells. *Proc Natl Acad Sci U S A, 96*(20), 11404-11409.

Kazantsev, A., Walker, H. A., Slepko, N., Bear, J. E., Preisinger, E., Steffan, J. S., et al. (2002). A bivalent Huntingtin binding peptide suppresses polyglutamine aggregation and pathogenesis in Drosophila. *Nat Genet, 30*(4), 367-376.

Keedwell, P. A., Chapman, R., Christiansen, K., Richardson, H., Evans, J., & Jones, D. K. (2012). Cingulum white matter in young women at risk of depression: the effect of family history and anhedonia. *Biol Psychiatry, 72*(4), 296-302.

Kennedy, L., Evans, E., Chen, C. M., Craven, L., Detloff, P. J., Ennis, M., et al. (2003). Dramatic tissue-specific mutation length increases are an early molecular event in Huntington disease pathogenesis. *Hum Mol Genet, 12*(24), 3359-3367.

Kermadi, I., & Joseph, J. P. (1995). Activity in the caudate nucleus of monkey during spatial sequencing. *J Neurophysiol, 74*(3), 911-933.

Khalil, H., Quinn, L., van Deursen, R., Dawes, H., Playle, R., Rosser, A., et al. (2013). What effect does a structured home-based exercise programme have on people with Huntington's disease? A randomized, controlled pilot study. *Clin Rehabil, 27*(7), 646-658.

Kim, E. H., Thu, D. C., Tippett, L. J., Oorschot, D. E., Hogg, V. M., Roxburgh, R., et al. (2014). Cortical interneuron loss and symptom heterogeneity in Huntington disease. *Ann Neurol*.

Kim, Y. G., Cha, J., & Chandrasegaran, S. (1996). Hybrid restriction enzymes: zinc finger fusions to Fok I cleavage domain. *Proc Natl Acad Sci U S A, 93*(3), 1156-1160.

Kincses, Z. T., Szabó, N., Tóth, E., Zádori, D., Faragó, P., Németh, D., et al. (2013). Diffusion MRI measured white matter microstructure as a biomarker of neurodegeneration in preclinical Huntington's disease. *Ideggyogy Sz, 66*(11-12), 399-405.

Kingma, E. M., van Duijn, E., Timman, R., van der Mast, R. C., & Roos, R. A. (2008). Behavioural problems in Huntington's disease using the Problem Behaviours Assessment. *Gen Hosp Psychiatry, 30*(2), 155-161.

Kirkwood, S., Siemers, E., Hodes, M., Conneally, P., Christian, J., & Foroud, T. (2000). Subtle changes among presymptomatic carriers of the Huntington's disease gene. *Journal of neurology, neurosurgery, and psychiatry, 69*(6), 773-779.

Kirkwood, S., Su, J., Conneally, P., & Foroud, T. (2001). Progression of symptoms in the early and middle stages of Huntington disease. *Archives of neurology, 58*(2), 273-278.

Klein, S., Staring, M., Murphy, K., Viergever, M. A., & Pluim, J. P. (2010). elastix: a toolbox for intensity-based medical image registration. *IEEE Trans Med Imaging, 29*(1), 196-205.

Klöppel, S., Draganski, B., Golding, C., Chu, C., Nagy, Z., Cook, P., et al. (2008). White matter connections reflect changes in voluntary-guided saccades in pre-symptomatic Huntington's disease. *Brain : a journal of neurology, 131*(Pt 1), 196-204.

Klöppel, S., Draganski, B., Golding, C. V., Chu, C., Nagy, Z., Cook, P. A., et al. (2008). White matter connections reflect changes in voluntary-guided saccades in pre-symptomatic Huntington's disease. *Brain, 131*(Pt 1), 196-204.

Klöppel, S., Draganski, B., Siebner, H., Tabrizi, S., Weiller, C., & Frackowiak, R. (2009). Functional compensation of motor function in pre-symptomatic Huntington's disease. *Brain : a journal of neurology, 132*(Pt 6), 1624-1632.

Klöppel, S., Stonnington, C., Petrovic, P., Mobbs, D., Tüscher, O., Craufurd, D., et al. (2010). Irritability in pre-clinical Huntington's disease. *Neuropsychologia, 48*(2), 549-557.

Kobal, J., Melik, Z., Cankar, K., & Strucl, M. (2014). Cognitive and autonomic dysfunction in presymptomatic and early Huntington's disease. *J Neurol, 261*(6), 1119-1125.

Kopyov, O. V., Jacques, S., Kurth, M., Philpott, L. M., Lee, A., & Patterson, M. e. a. (1998). Fetal transplantation for Huntington's disease: clinical studies. In T. B. Freeman & J. H. e. Kordower (Eds.), *Cell transplantation for neurological disorders* (pp. 95–134): Totowa, NJ: Humana Press.

Kordasiewicz, H. B., Stanek, L. M., Wancewicz, E. V., Mazur, C., McAlonis, M. M., Pytel, K. A., et al. (2012). Sustained therapeutic reversal of Huntington's disease by transient repression of huntingtin synthesis. *Neuron, 74*(6), 1031-1044.

Kulisevsky, J., Litvan, I., Berthier, M., Pascual-Sedano, B., Paulsen, J., & Cummings, J. (2001). Neuropsychiatric assessment of Gilles de la Tourette patients: comparative study with other hyperkinetic and hypokinetic movement disorders. *Movement disorders : official journal of the Movement Disorder Society, 16*(6), 1098-1104.

Kuo, Y.-T., Herlihy, A., So, P.-W., Bhakoo, K., & Bell, J. (2005). In vivo measurements of T1 relaxation times in mouse brain associated with different modes of systemic administration of manganese chloride. *Journal of magnetic resonance imaging : JMRI, 21*(4), 1-6.

Lalonde, R. (2002). The neurobiological basis of spontaneous alternation. *Neurosci Biobehav Rev, 26*(1), 91-104.

Landwehrmeyer, G. B., McNeil, S. M., Dure, L. S., Ge, P., Aizawa, H., Huang, Q., et al. (1995). Huntington's disease gene: regional and cellular expression in brain of normal and affected individuals. *Ann Neurol, 37*(2), 218-230.

Lange, H., Thörner, G., Hopf, A., & Schröder, K. F. (1976). Morphometric studies of the neuropathological changes in choreatic diseases. *J Neurol Sci, 28*(4), 401-425.

Lanska, D. (2000). George Huntington (1850-1916) and hereditary chorea. *Journal of the history of the neurosciences, 9*(1), 76-89.

Lawrence, A., Sahakian, B., Hodges, J., Rosser, A., Lange, K., & Robbins, T. (1996). Executive and mnemonic functions in early Huntington's disease. *Brain : a journal of neurology, 119 ( Pt 5)*, 1633-1645.

Lawrence, A., Sahakian, B., Rogers, R., Hodge, J., & Robbins, T. (1999). Discrimination, reversal, and shift learning in Huntington's disease: mechanisms of impaired response selection. *Neuropsychologia, 37*(12), 1359-1374.

Lawrence, A. D., Watkins, L. H., Sahakian, B. J., Hodges, J. R., & Robbins, T. W. (2000). Visual object and visuospatial cognition in Huntington's disease: implications for information processing in corticostriatal circuits. *Brain, 123 ( Pt 7)*, 1349-1364.

Laws, K. R. (1999). A meta-analytic review of Wisconsin Card Sort studies in schizophrenia: general intellectual deficit in disguise? *Cogn Neuropsychiatry, 4*(1), 1-30; discussion 31-35.

Le Bihan, D., Poupon, C., Amadon, A., & Lethimonnier, F. (2006). Artifacts and pitfalls in diffusion MRI. *J Magn Reson Imaging, 24*(3), 478-488.

Le Bé, J. V., Silberberg, G., Wang, Y., & Markram, H. (2007). Morphological, electrophysiological, and synaptic properties of corticocallosal pyramidal cells in the neonatal rat neocortex. *Cereb Cortex, 17*(9), 2204-2213.

Lee, S. T., Chu, K., Im, W. S., Yoon, H. J., Im, J. Y., & Park, J. E. (2011). Altered microRNA regulation in Huntington&#39;s disease models. *Experimental*.

Lee, S. T., Park, J. E., Lee, K., Kang, L., Chu, K., Kim, S. U., et al. (2006). Noninvasive method of immortalized neural stem-like cell transplantation in an experimental model of Huntington's disease. *J Neurosci Methods, 152*(1-2), 250-254.

Leemans, A., Jeurissen, B., & Sijbers, J. (2009). ExploreDTI: a graphical toolbox for processing, analyzing, and visualizing diffusion MR data. *Proc Intl Soc Mag Reson*.

Leemans, A., & Jones, D. (2009). The B-matrix must be rotated when correcting for subject motion in DTI data. *Magnetic resonance in medicine : official journal of the Society of Magnetic Resonance in Medicine / Society of Magnetic Resonance in Medicine, 61*(6), 1336-1349.

Leemans, A., & Jones, D. K. (2009). The B-matrix must be rotated when correcting for subject motion in DTI data. *Magnetic resonance in medicine : official journal of the Society of Magnetic Resonance in Medicine / Society of Magnetic Resonance in Medicine, 61*(6), 1336-1349.

Lemiere, J., Decruyenaere, M., Evers-Kiebooms, G., Vandenbussche, E., & Dom, R. (2004). Cognitive changes in patients with Huntington's disease (HD) and asymptomatic carriers of the HD mutation--a longitudinal follow-up study. *J Neurol, 251*(8), 935-942.

Lerch, J., Carroll, J., Dorr, A., Spring, S., Evans, A., Hayden, M., et al. (2008). Cortical thickness measured from MRI in the YAC128 mouse model of Huntington's disease. *NeuroImage, 41*(2), 243-251.

Lerch, J., Carroll, J., Spring, S., Bertram, L., Schwab, C., Hayden, M., et al. (2008). Automated deformation analysis in the YAC128 Huntington disease mouse model. *NeuroImage, 39*(1), 32-39.

Leroi, I., & Michalon, M. (1998). Treatment of the psychiatric manifestations of Huntington's disease: a review of the literature. *Canadian journal of psychiatry. Revue canadienne de psychiatrie, 43*(9), 933-940.

Leung, K. K., Barnes, J., Modat, M., Ridgway, G., Bartlett, J., Fox, N., et al. (2011). Automated brain extraction using multi-atlas propagation and segmentation (MAPS) (pp. 2053 - 2056). 8TH IEEE International symposium on Biomedical Imaging: From nano to macro.

Levine, M., Cepeda, C., Hickey, M., Fleming, S., & Chesselet, M.-F. (2004). Genetic mouse models of Huntington's and Parkinson's diseases: illuminating but imperfect. *Trends in neurosciences, 27*(11), 691-697.

Levine, M. S., Klapstein, G. J., Koppel, A., Gruen, E., Cepeda, C., Vargas, M. E., et al. (1999). Enhanced sensitivity to N-methyl-D-aspartate receptor activation in transgenic and knockin mouse models of Huntington's disease. *J Neurosci Res, 58*(4), 515-532.

Levy, M. L., Cummings, J. L., Fairbanks, L. A., Masterman, D., Miller, B. L., Craig, A. H., et al. (1998). Apathy is not depression. *J Neuropsychiatry Clin Neurosci, 10*(3), 314-319.

Lezak, M. D., Howieson, D. B., & Loring, D. W. (2004). Neuropsychological Assessment.

Fourth edition: Oxford: Oxford University Press.

Li, H., Li, S. H., Yu, Z. X., Shelbourne, P., & Li, X. J. (2001). Huntingtin aggregate-associated axonal degeneration is an early pathological event in Huntington's disease mice. *J Neurosci, 21*(21), 8473-8481.

Li, J. Y., & Conforti, L. (2013). Axonopathy in Huntington's disease. *Exp Neurol, 246*, 62-71.

Li, S. H., & Li, X. J. (2004). Huntingtin-protein interactions and the pathogenesis of Huntington's disease. *Trends Genet, 20*(3), 146-154.

Li, X. J. (1999). The early cellular pathology of Huntington's disease. *Mol Neurobiol, 20*(2-3), 111-124.

Lin, C., Tallaksen-Greene, S., Chien, W., Cearley, J., Jackson, W., Crouse, A., et al. (2001). Neurological abnormalities in a knock-in mouse model of Huntington's disease. *Human molecular genetics, 10*(2), 137-144.

Lione, L. A., Carter, R. J., Hunt, M. J., Bates, G. P., Morton, A. J., & Dunnett, S. B. (1999). Selective discrimination learning impairments in mice expressing the human Huntington's disease mutation. *J Neurosci, 19*(23), 10428-10437.

Lu, X. H., & Yang, X. W. (2012). "Huntingtin holiday": progress toward an antisense therapy for Huntington's disease. *Neuron, 74*(6), 964-966.

Ma, D., Cardoso, M. J., Modat, M., Powell, N., Wells, J., Holmes, H., et al. (2014). Automatic structural parcellation of mouse brain MRI using multi-atlas label fusion. *PLoS One, 9*(1), e86576.

Ma, L., Morton, A. J., & Nicholson, L. F. (2003). Microglia density decreases with age in a mouse model of Huntington's disease. *Glia, 43*(3), 274-280.

Ma, Y., Hof, P. R., Grant, S. C., Blackband, S. J., Bennett, R., Slatest, L., et al. (2005). A three-dimensional digital atlas database of the adult C57BL/6J mouse brain by magnetic resonance microscopy. *Neuroscience, 135*(4), 1203-1215.

Ma, Y., Smith, D., Hof, P. R., Foerster, B., Hamilton, S., Blackband, S. J., et al. (2008). In Vivo 3D Digital Atlas Database of the Adult C57BL/6J Mouse Brain by Magnetic Resonance Microscopy. *Front Neuroanat, 2*, 1.

Macdonald, V., & Halliday, G. (2002). Pyramidal cell loss in motor cortices in Huntington's disease. *Neurobiology of disease, 10*(3), 378-386.

Maddock, R. J. (1999). The retrosplenial cortex and emotion: new insights from functional neuroimaging of the human brain. *Trends Neurosci, 22*(7), 310-316.

Magnotta, V., Kim, J., Koscik, T., Beglinger, L., Espinso, D., Langbehn, D., et al. (2009). Diffusion Tensor Imaging in Preclinical Huntington's Disease. *Brain imaging and behavior, 3*(1), 77-84.

Majid, D. S., Stoffers, D., Sheldon, S., Hamza, S., Thompson, W. K., Goldstein, J., et al. (2011). Automated structural imaging analysis detects premanifest Huntington's disease neurodegeneration within 1 year. *Mov Disord, 26*(8), 1481-1488.

Malone, I. B., Leung, K. K., Clegg, S., Barnes, J., Whitwell, J. L., Ashburner, J., et al. (2014). Accurate automatic estimation of total intracranial volume: A nuisance variable with less nuisance. *Neuroimage*.

Mangiarini, L., Sathasivam, K., Seller, M., Cozens, B., Harper, A., Hetherington, C., et al. (1996). Exon 1 of the HD gene with an expanded CAG repeat is sufficient to cause a progressive neurological phenotype in transgenic mice. *Cell, 87*(3), 493-506.

Martin, E., Betuing, S., Pagès, C., Cambon, K., Auregan, G., Deglon, N., et al. (2011). Mitogen- and stress-activated protein kinase 1-induced neuroprotection in Huntington's disease: role on chromatin remodeling at the PGC-1-alpha promoter. *Hum Mol Genet, 20*(12), 2422-2434.

Mascalchi, M., Lolli, F., Della Nave, R., Tessa, C., Petralli, R., Gavazzi, C., et al. (2004). Huntington disease: volumetric, diffusion-weighted, and magnetization transfer MR imaging of brain. *Radiology, 232*(3), 867-873.

Mascalchi, M., Lolli, F., Nave, R., Tessa, C., Petralli, R., Gavazzi, C., et al. (2004). Huntington disease: volumetric, diffusion-weighted, and magnetization transfer MR imaging of brain. *Radiology, 232*(3), 867-873.

Mason, S., Wijeyekoon, R., Swain, R., Ho, A., Smith, E., Sahakian, B., et al. (2010). Cognitive follow up of a small cohort of Huntington's disease patients over a 5 year period. *PLoS currents, 2*, RRN1174.

Matsui, J., Vaidya, J., Johnson, H., Magnotta, V., Long, J., Mills, J., et al. (2013). Diffusion weighted imaging of prefrontal cortex in prodromal huntington's disease. *Human brain mapping*.

Matsuzaka, T., Ono, K., Baba, H., Matsuo, M., Tanaka, S., Kamimura, N., et al. (1999). Quantitative EEG analyses and surgical outcome after corpus callosotomy. *Epilepsia, 40*(9), 1269-1278.

Matsuzaka, T., Ono, K., Baba, H., Matsuo, M., Tanaka, S., Tsuji, Y., et al. (1993). Interhemispheric correlation analysis of EEGs before and after corpus callosotomy. *Jpn J Psychiatry Neurol, 47*(2), 329-330.

Matsuzaka, Y., Aizawa, H., & Tanji, J. (1992). A motor area rostral to the supplementary motor area (presupplementary motor area) in the monkey: neuronal activity during a learned motor task. *Journal of neurophysiology*.

Mauchly, J. W. (1940). Significance test for sphericity of a normal n-variate distribution (Vol. 11, pp. 204-209). *The Annals of Mathematical Statistics*.

Mayer, E., Brown, V. J., Dunnett, S. B., & Robbins, T. W. (1992). Striatal graft-associated recovery of a lesion-induced performance deficit in the rat requires learning to use the transplant. *Eur J Neurosci, 4*(2), 119-126.

Mayers, A. (2013). Introduction to Statistics and SPSS in Psychology: Pearson.

Mazarakis, N. K., Cybulska-Klosowicz, A., Grote, H., Pang, T., Van Dellen, A., Kossut, M., et al. (2005). Deficits in experience-dependent cortical plasticity and sensory-discrimination learning in presymptomatic Huntington's disease mice. *J Neurosci, 25*(12), 3059-3066.

Mazzocchi-Jones, D., Döbrössy, M., & Dunnett, S. B. (2009). Embryonic striatal grafts restore bi-directional synaptic plasticity in a rodent model of Huntington's disease. *Eur J Neurosci, 30*(11), 2134-2142.

Mazzocchi-Jones, D., Döbrössy, M., & Dunnett, S. B. (2011). Environmental enrichment facilitates long-term potentiation in embryonic striatal grafts. *Neurorehabil Neural Repair, 25*(6), 548-557.

McBride, J., Ramaswamy, S., Gasmi, M., Bartus, R., Herzog, C., Brandon, E., et al. (2006). Viral delivery of glial cell line-derived neurotrophic factor improves behavior and protects striatal neurons in a mouse model of Huntington's disease. *Proceedings of the National Academy of Sciences of the United States of America, 103*(24), 9345-9350.

McBride, J. L., Behrstock, S. P., Chen, E. Y., Jakel, R. J., Siegel, I., Svendsen, C. N., et al. (2004). Human neural stem cell transplants improve motor function in a rat model of Huntington's disease. *J Comp Neurol, 475*(2), 211-219.

Mehler, M. F., & Gokhan, S. (2000). Mechanisms underlying neural cell death in neurodegenerative diseases: alterations of a developmentally-mediated cellular rheostat. *Trends Neurosci, 23*(12), 599-605.

Menalled, L., & Chesselet, M.-F. (2002). Mouse models of Huntington's disease. *Trends in pharmacological sciences, 23*(1), 32-39.

Menalled, L., El-Khodor, B., Patry, M., Suárez-Fariñas, M., Orenstein, S., Zahasky, B., et al. (2009). Systematic behavioral evaluation of Huntington's disease transgenic and knock-in mouse models. *Neurobiology of disease, 35*(3), 1-18.

Menalled, L. B., Sison, J. D., Dragatsis, I., Zeitlin, S., & Chesselet, M. F. (2003). Time course of early motor and neuropathological anomalies in a knock-in mouse model of Huntington's disease with 140 CAG repeats. *J Comp Neurol, 465*(1), 11-26.

Mickes, L., Jacobson, M., Peavy, G., Wixted, J. T., Lessig, S., Goldstein, J. L., et al. (2010). A comparison of two brief screening measures of cognitive impairment in Huntington's disease. *Mov Disord, 25*(13), 2229-2233.

Mielcarek, M., Inuabasi, L., Bondulich, M. K., Muller, T., Osborne, G. F., Franklin, S. A., et al. (2014). Dysfunction of the CNS-heart axis in mouse models of Huntington's disease. *PLoS Genet, 10*(8), e1004550.

Miller, B. R., & Bezprozvanny, I. (2010). Corticostriatal circuit dysfunction in Huntington's disease: intersection of glutamate, dopamine and calcium. *Future Neurol, 5*(5), 735-756.

Miller, E. (1984). Verbal fluency as a function of a measure of verbal intelligence and in relation to different types of cerebral pathology. *Br J Clin Psychol, 23 ( Pt 1)*, 53-57.

Miller, J., Arrasate, M., Shaby, B. A., Mitra, S., Masliah, E., & Finkbeiner, S. (2010). Quantitative relationships between huntingtin levels, polyglutamine length, inclusion body formation, and neuronal death provide novel insight into huntington's disease molecular pathogenesis. *J Neurosci, 30*(31), 10541-10550.

Mittal, S. K., & Eddy, C. (2013). The role of dopamine and glutamate modulation in Huntington disease. *Behav Neurol, 26*(4), 255-263.

Miyachi, S., Lu, X., Imanishi, M., Sawada, K., Nambu, A., & Takada, M. (2006). Somatotopically arranged inputs from putamen and subthalamic nucleus to primary motor cortex. *Neurosci Res, 56*(3), 300-308.

Modat, M., Ridgway, G. R., Taylor, Z. A., Lehmann, M., Barnes, J., Hawkes, D. J., et al. (2010). Fast free-form deformation using graphics processing units. *Comput Methods Programs Biomed, 98*(3), 278-284.

Montoya, A., Pelletier, M., Menear, M., Duplessis, E., Richer, F., & Lepage, M. (2006). Episodic memory impairment in Huntington's disease: a meta-analysis. *Neuropsychologia, 44*(10), 1984-1994.

Morris, R. G., Garrud, P., Rawlins, J. N., & O'Keefe, J. (1982). Place navigation impaired in rats with hippocampal lesions. *Nature, 297*(5868), 681-683.

Morton, A., Lagan, M., Skepper, J., & Dunnett, S. (2000). Progressive formation of inclusions in the striatum and hippocampus of mice transgenic for the human Huntington's disease mutation. *Journal of neurocytology, 29*(9), 679-702.

Mufson, E. J., & Pandya, D. N. (1984). Some observations on the course and composition of the cingulum bundle in the rhesus monkey. *J Comp Neurol, 225*(1), 31-43.

Murgod, U., Saleem, Q., Anand, A., Brahmachari, S., Jain, S., & Muthane, U. (2001). A clinical study of patients with genetically confirmed Huntington's disease from India. *Journal of the Neurological Sciences, 190*(1-2), 73-78.

Mushiake, H., & Strick, P. L. (1993). Preferential activity of dentate neurons during limb movements guided by vision. *J Neurophysiol, 70*(6), 2660-2664.

Mushiake, H., & Strick, P. L. (1995). Pallidal neuron activity during sequential arm movements. *J Neurophysiol, 74*(6), 2754-2758.

Mussolino, C., Morbitzer, R., Lütge, F., Dannemann, N., Lahaye, T., & Cathomen, T. (2011). A novel TALE nuclease scaffold enables high genome editing activity in combination with low toxicity. *Nucleic Acids Res, 39*(21), 9283-9293.

Myers, R. H., Leavitt, J., Farrer, L. A., Jagadeesh, J., McFarlane, H., Mastromauro, C. A., et al. (1989). Homozygote for Huntington disease. *Am J Hum Genet, 45*(4), 615-618.

Myers, R. H., Vonsattel, J. P., Paskevich, P. A., Kiely, D. K., Stevens, T. J., Cupples, L. A., et al. (1991). Decreased neuronal and increased oligodendroglial densities in Huntington's disease caudate nucleus. *J Neuropathol Exp Neurol, 50*(6), 729-742.

Nakao, N., Ogura, M., Nakai, K., & Itakura, T. (1999). Embryonic striatal grafts restore neuronal activity of the globus pallidus in a rodent model of Huntington's disease. *Neuroscience, 88*(2), 469-477.

Nambu, A. (2011). Somatotopic organization of the primate Basal Ganglia. *Front Neuroanat, 5*, 26.

Nance, M., Mathias-Hagen, V., Breningstall, G., Wick, M., & McGlennen, R. (1999). Analysis of a very large trinucleotide repeat in a patient with juvenile Huntington's disease. *Neurology, 52*(2), 392-394.

Napoli, E., Wong, S., Hung, C., Ross-Inta, C., Bomdica, P., & Giulivi, C. (2013). Defective mitochondrial disulfide relay system, altered mitochondrial morphology and function in Huntington's disease. *Hum Mol Genet, 22*(5), 989-1004.

Nasir, J., Floresco, S. B., O'Kusky, J. R., Diewert, V. M., Richman, J. M., Zeisler, J., et al. (1995). Targeted disruption of the Huntington's disease gene results in embryonic lethality and behavioral and morphological changes in heterozygotes. *Cell, 81*(5), 811-823.

Naver, B., Stub, C., Møller, M., Fenger, K., Hansen, A., Hasholt, L., et al. (2003). Molecular and behavioral analysis of the R6/1 Huntington's disease transgenic mouse. *Neuroscience, 122*(4), 1049-1057.

Nehl, C., Paulsen, J. S., & Group, H. S. (2004). Cognitive and psychiatric aspects of Huntington disease contribute to functional capacity. *J Nerv Ment Dis, 192*(1), 72-74.

Nguyen, G. D., Gokhan, S., Molero, A. E., & Mehler, M. F. (2013). Selective roles of normal and mutant huntingtin in neural induction and early neurogenesis. *PLoS One, 8*(5), e64368.

Nithianantharajah, J., & Hannan, A. J. (2006). Enriched environments, experience-dependent plasticity and disorders of the nervous system. *Nat Rev Neurosci, 7*(9), 697-709.

Nopoulos, P., Aylward, E., Ross, C., Johnson, H., Magnotta, V., Juhl, A., et al. (2010). Cerebral cortex structure in prodromal Huntington disease. *Neurobiology of disease, 40*(3), 544-554.

Nopoulos, P., Epping, E. A., Wassink, T., Schlaggar, B. L., & Perlmutter, J. (2011). Correlation of CAG repeat length between the maternal and paternal allele of the Huntingtin gene: evidence for assortative mating. *Behav Brain Funct, 7*, 45.

Nopoulos, P., Magnotta, V., & Mikos, A. (2007). Morphology of the cerebral cortex in preclinical Huntington&#39;s disease. *American Journal of*.

Nopoulos, P. C., Aylward, E. H., Ross, C. A., Johnson, H. J., Magnotta, V. A., Juhl, A. R., et al. (2010). Cerebral cortex structure in prodromal Huntington disease. *Neurobiol Dis, 40*(3), 544-554.

Nordenskjöld, R., Malmberg, F., Larsson, E. M., Simmons, A., Brooks, S. J., Lind, L., et al. (2013). Intracranial volume estimated with commonly used methods could introduce bias in studies including brain volume measurements. *Neuroimage, 83*, 355-360.

O'Kusky, J. R., Nasir, J., Cicchetti, F., Parent, A., & Hayden, M. R. (1999). Neuronal degeneration in the basal ganglia and loss of pallido-subthalamic synapses in mice with targeted disruption of the Huntington's disease gene. *Brain Res, 818*(2), 468-479.

Olton, D. S. (1979). Mazes, maps, and memory. *Am Psychol, 34*(7), 583-596.

Olton, D. S., & Papas, B. C. (1979). Spatial memory and hippocampal function. *Neuropsychologia, 17*(6), 669-682.

Orth, M., Handley, O., Schwenke, C., Dunnett, S., Wild, E., Tabrizi, S., et al. (2011). Observing Huntington's disease: the European Huntington's Disease Network's REGISTRY. *Journal of neurology, neurosurgery, and psychiatry, 82*(12), 1409-1412.

Ourselin, S., Roche, A., Prima, S., & Ayache, N. (2000). Block matching: A general framework to improve robustness of rigid registration of medical images. (Vol. 1935, pp. 557–566). Proc MICCAI Int Conf Med Image Comput Comput Assist Interv.

Owen, A. M., Hampshire, A., Grahn, J. A., Stenton, R., Dajani, S., Burns, A. S., et al. (2010). Putting brain training to the test. *Nature, 465*(7299), 775-778.

Owen, A. M., James, M., Leigh, P. N., Summers, B. A., Marsden, C. D., Quinn, N. P., et al. (1992). Fronto-striatal cognitive deficits at different stages of Parkinson's disease. *Brain, 115 ( Pt 6)*, 1727-1751.

Owen, A. M., Roberts, A. C., Polkey, C. E., Sahakian, B. J., & Robbins, T. W. (1991). Extra-dimensional versus intra-dimensional set shifting performance following frontal lobe excisions, temporal lobe excisions or amygdalo-hippocampectomy in man. *Neuropsychologia, 29*(10), 993-1006.

Paganini, M., Biggeri, A., Romoli, A. M., Mechi, C., Ghelli, E., Berti, V., et al. (2013). Foetal striatal grafting slows motor and cognitive decline in Huntington disease. J Neurol Neurosurg Psychiatry.

Pajevic, S., & Pierpaoli, C. (2000). Color schemes to represent the orientation of anisotropic tissues from diffusion tensor data: application to white matter fiber tract mapping in the human brain. *Magn Reson Med, 43*(6), 921.

Pakkenberg, B., & Gundersen, H. J. (1997). Neocortical neuron number in humans: effect of sex and age. *J Comp Neurol, 384*(2), 312-320.

Panov, A. V., Gutekunst, C., Leavitt, B. R., Hayden, M. R., Burke, J. R., Strittmatter, W. J., et al. (2002). Early mitochondrial calcium defects in Huntington's disease are a direct effect of polyglutamines. *Nat Neurosci, 5*(8), 731-736.

Paola, M., Luders, E., Cherubini, A., Sanchez-Castaneda, C., Thompson, P., Toga, A., et al. (2012). Multimodal MRI Analysis of the Corpus Callosum Reveals White Matter Differences in Presymptomatic and Early Huntington's Disease. *Cerebral cortex (New York, N.Y. : 1991)*.

Papoutsi, M., Labuschagne, I., Tabrizi, S. J., & Stout, J. C. (2014). The cognitive burden in Huntington's disease: pathology, phenotype, and mechanisms of compensation. *Mov Disord, 29*(5), 673-683.

Papp, K., Kaplan, R., & Snyder, P. (2011). Biological markers of cognition in prodromal Huntington's disease: a review. *Brain and cognition, 77*(2), 280-291.

Papp, K., Snyder, P., Mills, J., Duff, K., Westervelt, H., Long, J., et al. (2013). Measuring executive dysfunction longitudinally and in relation to genetic burden, brain volumetrics, and depression in prodromal Huntington disease. *Archives of clinical neuropsychology : the official journal of the National Academy of Neuropsychologists, 28*(2), 156-168.

Parker, G. J. (2004). Analysis of MR diffusion weighted images. *Br J Radiol, 77 Spec No 2*, S176-185.

Passingham, R. (1994). The Frontal Lobes and Voluntary Action.

Pasternak, O., Sochen, N., Gur, Y., Intrator, N., & Assaf, Y. (2009). Free water elimination and mapping from diffusion MRI. *Magnetic resonance in medicine : official journal of the Society of Magnetic Resonance in Medicine / Society of Magnetic Resonance in Medicine, 62*(3), 717-730.

Patel, S. S., Jankovic, J., Hood, A. J., Jeter, C. B., & Sereno, A. B. (2012). Reflexive and volitional saccades: biomarkers of Huntington disease severity and progression. *J Neurol Sci, 313*(1-2), 35-41.

Paulsen, J. (2011). Cognitive impairment in Huntington disease: diagnosis and treatment. *Current neurology and neuroscience reports, 11*(5), 474-483.

Paulsen, J., Hayden, M., Stout, J., Langbehn, D., Aylward, E., Ross, C., et al. (2006). Preparing for Preventive Clinical Trials<subtitle>The Predict-HD Study</subtitle>. *Archives of neurology, 63*(6), 883.

Paulsen, J., Langbehn, D., Stout, J., Aylward, E., Ross, C., Nance, M., et al. (2008). Detection of Huntington's disease decades before diagnosis: the Predict-HD study. *Journal of neurology, neurosurgery, and psychiatry, 79*(8), 874-880.

Paulsen, J., Nehl, C., Hoth, K., Kanz, J., Benjamin, M., Conybeare, R., et al. (2005). Depression and stages of Huntington's disease. *The Journal of neuropsychiatry and clinical neurosciences, 17*(4), 496-502.

Paulsen, J., Nopoulos, P., Aylward, E., Ross, C., Johnson, H., Magnotta, V., et al. (2010). Striatal and white matter predictors of estimated diagnosis for Huntington disease. *Brain research bulletin, 82*(3-4), 201-207.

Paulsen, J., Ready, R., Hamilton, J., Mega, M., & Cummings, J. (2001). Neuropsychiatric aspects of Huntington's disease. *Journal of neurology, neurosurgery, and psychiatry, 71*(3), 310-314.

Paulsen, J. S., Smith, M. M., Long, J. D., & Group, P. H. i. a. C. o. t. H. S. (2013). Cognitive decline in prodromal Huntington Disease: implications for clinical trials. *J Neurol Neurosurg Psychiatry, 84*(11), 1233-1239.

Paxinos, G., & Franklin, K. B. J. (2004). The mouse brain in stereotaxic coordinates.

Pearson, C. E. (2003). Slipping while sleeping? Trinucleotide repeat expansions in germ cells. *Trends Mol Med, 9*(11), 490-495.

Peavy, G., Jacobson, M., Goldstein, J., Hamilton, J., Kane, A., Gamst, A., et al. (2010). Cognitive and functional decline in Huntington's disease: dementia criteria revisited. *Movement disorders : official journal of the Movement Disorder Society, 25*(9), 1163-1169.

Pengas, G., Pereira, J. M., Williams, G. B., & Nestor, P. J. (2009). Comparative reliability of total intracranial volume estimation methods and the influence of atrophy in a longitudinal semantic dementia cohort. *J Neuroimaging, 19*(1), 37-46.

Penney, J. B., Vonsattel, J. P., MacDonald, M. E., Gusella, J. F., & Myers, R. H. (1997). CAG repeat number governs the development rate of pathology in Huntington's disease. *Ann Neurol, 41*(5), 689-692.

Penney, J. B., Young, A. B., Shoulson, I., Starosta-Rubenstein, S., Snodgrass, S. R., Sanchez-Ramos, J., et al. (1990). Huntington's disease in Venezuela: 7 years of follow-up on symptomatic and asymptomatic individuals. *Mov Disord, 5*(2), 93-99.

Perry, T. A., Torres, E. M., Czech, C., Beyreuther, K., Richards, S., & Dunnett, S. B. (1995). Cognitive and motor function in transgenic mice carrying excess copies of the 695 and 751 amino acid isoforms of the amyloid precursor protein gene (Vol. 1, pp. 5-14). Alzheimer’s Research.

Persichetti, F., Ambrose, C., Ge, P., McNeil, S., Srinidhi, J., Anderson, M., et al. (1995). Normal and expanded Huntington's disease gene alleles produce distinguishable proteins due to translation across the CAG repeat. *Molecular medicine (Cambridge, Mass.), 1*(4), 374-383.

Persichetti, F., Carlee, L., Faber, P., McNeil, S., Ambrose, C., Srinidhi, J., et al. (1996). Differential expression of normal and mutant Huntington's disease gene alleles. *Neurobiology of disease, 3*(3), 183-190.

Petiet, A., Delatour, B., & Dhenain, M. (2011). Models of neurodegenerative disease - Alzheimer's anatomical and amyloid plaque imaging. *Methods Mol Biol, 771*, 293-308.

Phillips, J. G., Bradshaw, J. L., & Chiu, E. (1994). Characteristics of handwriting of patients with Huntington&#39;s disease. *Movement*.

Phillips, O., Sanchez-Castaneda, C., Elifani, F., Maglione, V., Di Pardo, A., Caltagirone, C., et al. (2013). Tractography of the corpus callosum in Huntington's disease. *PLoS One, 8*(9), e73280.

Phillips, O., Squitieri, F., Sanchez-Castaneda, C., Elifani, F., Griguoli, A., Maglione, V., et al. (2014). The Corticospinal Tract in Huntington's Disease. *Cereb Cortex*.

Philpott, L. M., Kopyov, O. V., Lee, A. J., Jacques, S., Duma, C. M., Caine, S., et al. (1997). Neuropsychological functioning following fetal striatal transplantation in Huntington's chorea: three case presentations. *Cell Transplant, 6*(3), 203-212.

Pierpaoli, C., Jezzard, P., Basser, P., Barnett, A., & Chiro, G. (1996). Diffusion tensor MR imaging of the human brain. *Radiology, 201*(3), 637-648.

Politis, M., Pavese, N., Tai, Y., Kiferle, L., Mason, S., Brooks, D., et al. (2011). Microglial activation in regions related to cognitive function predicts disease onset in Huntington's disease: a multimodal imaging study. *Human brain mapping, 32*(2), 258-270.

Porsolt, R. D., Bertin, A., & Jalfre, M. (1978). "Behavioural despair" in rats and mice: strain differences and the effects of imipramine. *Eur J Pharmacol, 51*(3), 291-294.

Poudel, G. R., Stout, J. C., Domínguez D, J. F., Salmon, L., Churchyard, A., Chua, P., et al. (2014). White matter connectivity reflects clinical and cognitive status in Huntington's disease. *Neurobiol Dis, 65*, 180-187.

Pouladi, M., Graham, R., Karasinska, J., Xie, Y., Santos, R., Petersén, A., et al. (2009). Prevention of depressive behaviour in the YAC128 mouse model of Huntington disease by mutation at residue 586 of huntingtin. *Brain : a journal of neurology, 132*(Pt 4), 919-932.

Qazi, A. A., Radmanesh, A., O'Donnell, L., Kindlmann, G., Peled, S., Whalen, S., et al. (2009). Resolving crossings in the corticospinal tract by two-tensor streamline tractography: Method and clinical assessment using fMRI. *Neuroimage, 47 Suppl 2*, T98-106.

Qiu, L., Lui, S., Kuang, W., Huang, X., Li, J., Zhang, J., et al. (2014). Regional increases of cortical thickness in untreated, first-episode major depressive disorder. *Transl Psychiatry, 4*, e378.

Quarrell, O. W. (2014). Juvenile Huntington’s disease. In G. Bates, L. Jones & S. e. Tabrizi (Eds.): Oxford University Press; NY, USA.

Ramaswamy, S., Goings, G., Soderstrom, K., Szele, F., & Kozlowski, D. (2005). Cellular proliferation and migration following a controlled cortical impact in the mouse. *Brain research, 1053*(1-2), 38-53.

Ramaswamy, S., & Kordower, J. H. (2012). Gene therapy for Huntington's disease. *Neurobiol Dis, 48*(2), 243-254.

Rattray, I., Smith, E., Gale, R., Matsumoto, K., Bates, G. P., & Modo, M. (2013). Correlations of behavioral deficits with brain pathology assessed through longitudinal MRI and histopathology in the R6/2 mouse model of HD. *PLoS One, 8*(4), e60012.

Reading, S., Yassa, M., Bakker, A., Dziorny, A., Gourley, L., Yallapragada, V., et al. (2005). Regional white matter change in pre-symptomatic Huntington's disease: a diffusion tensor imaging study. *Psychiatry research, 140*(1), 55-62.

Reiner, A., Albin, R. L., Anderson, K. D., D'Amato, C. J., Penney, J. B., & Young, A. B. (1988). Differential loss of striatal projection neurons in Huntington disease. *Proc Natl Acad Sci U S A, 85*(15), 5733-5737.

Reitan, R. M. (1979). Manual for administration and scoring of the Halstead–Reitan of neuropsychological test battery for adults and children: Tucson: Neuropsychology Press.

Rigamonti, D., Bauer, J. H., De-Fraja, C., Conti, L., Sipione, S., Sciorati, C., et al. (2000). Wild-type huntingtin protects from apoptosis upstream of caspase-3. *J Neurosci, 20*(10), 3705-3713.

Rinaldi, C., Salvatore, E., Giordano, I., Matteis, S., Tucci, T., Cinzia, V., et al. (2012). Predictors of survival in a Huntington's disease population from southern Italy. *The Canadian journal of neurological sciences. Le journal canadien des sciences neurologiques, 39*(1), 48-51.

Robbins, T. W., & Brown, V. J. (1990). The role of the striatum in the mental chronometry of action: a theoretical review. *Rev Neurosci, 2*(4), 181-214.

Roberts, T. J., Price, J., Williams, S. C., & Modo, M. (2006). Preservation of striatal tissue and behavioral function after neural stem cell transplantation in a rat model of Huntington's disease. *Neuroscience, 139*(4), 1187-1199.

Rohrer, D., Salmon, D., Wixted, J., & Paulsen, J. (1999). The disparate effects of Alzheimer's disease and Huntington's disease on semantic memory. *Neuropsychology, 13*(3), 381-388.

Roos, R. (2010). Huntington's disease: a clinical review. *Orphanet journal of rare diseases, 5*(1), 40.

Rosas, H., Lee, S., Bender, A., Zaleta, A., Vangel, M., Yu, P., et al. (2010). Altered white matter microstructure in the corpus callosum in Huntington's disease: implications for cortical "disconnection". *NeuroImage, 49*(4), 2995-3004.

Rosas, H., Tuch, D., Hevelone, N., Zaleta, A., Vangel, M., Hersch, S., et al. (2006). Diffusion tensor imaging in presymptomatic and early Huntington's disease: Selective white matter pathology and its relationship to clinical measures. *Movement disorders : official journal of the Movement Disorder Society, 21*(9), 1-9.

Rosas, H. D., Hevelone, N. D., Zaleta, A. K., Greve, D. N., Salat, D. H., & Fischl, B. (2005). Regional cortical thinning in preclinical Huntington disease and its relationship to cognition. *Neurology, 65*(5), 745-747.

Rosas, H. D., Liu, A. K., Hersch, S., Glessner, M., Ferrante, R. J., Salat, D. H., et al. (2002). Regional and progressive thinning of the cortical ribbon in Huntington's disease. *Neurology, 58*(5), 695-701.

Rosenstock, T. R., Bertoncini, C. R., Teles, A. V., Hirata, H., Fernandes, M. J., & Smaili, S. S. (2010). Glutamate-induced alterations in Ca2+ signaling are modulated by mitochondrial Ca2+ handling capacity in brain slices of R6/1 transgenic mice. *Eur J Neurosci, 32*(1), 60-70.

Rothlind, J., Brandt, J., Zee, D., Codori, A., & Folstein, S. (1993). Unimpaired verbal memory and oculomotor control in asymptomatic adults with the genetic marker for Huntington's disease. *Archives of neurology, 50*(8), 799-802.

Rowe, K. C., Paulsen, J. S., Langbehn, D. R., Duff, K., Beglinger, L. J., Wang, C., et al. (2010). Self-paced timing detects and tracks change in prodromal Huntington disease. *Neuropsychology, 24*(4), 435-442.

Ruocco, H. H., Bonilha, L., Li, L. M., Lopes-Cendes, I., & Cendes, F. (2008). Longitudinal analysis of regional grey matter loss in Huntington disease: effects of the length of the expanded CAG repeat. *J Neurol Neurosurg Psychiatry, 79*(2), 130-135.

Ryu, J. K., Kim, J., Cho, S. J., Hatori, K., Nagai, A., Choi, H. B., et al. (2004). Proactive transplantation of human neural stem cells prevents degeneration of striatal neurons in a rat model of Huntington disease. *Neurobiol Dis, 16*(1), 68-77.

Sach, M., Winkler, G., Glauche, V., Liepert, J., Heimbach, B., Koch, M. A., et al. (2004). Diffusion tensor MRI of early upper motor neuron involvement in amyotrophic lateral sclerosis. *Brain, 127*(Pt 2), 340-350.

Sadan, O., Melamed, E., & Offen, D. (2012). Intrastriatal transplantation of neurotrophic factor-secreting human mesenchymal stem cells improves motor function and extends survival in R6/2 transgenic mouse model for Huntington's disease. *PLoS Curr, 4*, e4f7f6dc013d014e.

Sagi, Y., Tavor, I., Hofstetter, S., Tzur-Moryosef, S., Blumenfeld-Katzir, T., & Assaf, Y. (2012). Learning in the fast lane: new insights into neuroplasticity. *Neuron, 73*(6), 1195-1203.

Saher, G., Brügger, B., Lappe-Siefke, C., Möbius, W., Tozawa, R., Wehr, M. C., et al. (2005). High cholesterol level is essential for myelin membrane growth. *Nat Neurosci, 8*(4), 468-475.

Sampaio-Baptista, C., Khrapitchev, A. A., Foxley, S., Schlagheck, T., Scholz, J., Jbabdi, S., et al. (2013). Motor skill learning induces changes in white matter microstructure and myelination. *J Neurosci, 33*(50), 19499-19503.

Sapp, E., Kegel, K. B., Aronin, N., Hashikawa, T., Uchiyama, Y., Tohyama, K., et al. (2001). Early and progressive accumulation of reactive microglia in the Huntington disease brain. *J Neuropathol Exp Neurol, 60*(2), 161-172.

Sathasivam, K., Woodman, B., Mahal, A., Bertaux, F., Wanker, E. E., Shima, D. T., et al. (2001). Centrosome disorganization in fibroblast cultures derived from R6/2 Huntington's disease (HD) transgenic mice and HD patients. *Hum Mol Genet, 10*(21), 2425-2435.

Sawiak, S., Wood, N., Williams, G., Morton, A., & Carpenter, T. (2009). Voxel-based morphometry in the R6/2 transgenic mouse reveals differences between genotypes not seen with manual 2D morphometry. *Neurobiology of disease, 33*(1), 20-27.

Sawiak, S., Wood, N., Williams, G., Morton, J., Carpenter, T., absolute, l. d. d.-a. q. q. d.-c.-w. q. q. d.-f.-n. q. T. q. s. q. p., et al. (2009). SPMMouse: A new toolbox for SPM in the animal brain (pp. 1086). Proc Int'l Soc Mag Res Med.

Scahill, R., Hobbs, N., Say, M., Bechtel, N., Henley, S., Hyare, H., et al. (2013). Clinical impairment in premanifest and early Huntington's disease is associated with regionally specific atrophy. *Human brain mapping, 34*(3), 519-529.

Schallert, T., Fleming, S. M., Leasure, J. L., Tillerson, J. L., & Bland, S. T. (2000). CNS plasticity and assessment of forelimb sensorimotor outcome in unilateral rat models of stroke, cortical ablation, parkinsonism and spinal cord injury. *Neuropharmacology, 39*(5), 777-787.

Scheibe, K. E., Shaver, P. R., & Carrier, S. C. (1967). Color association values and response interference on variants of the Stroop test. *Acta Psychologica*.

Schiffer, N. W., Broadley, S. A., Hirschberger, T., Tavan, P., Kretzschmar, H. A., Giese, A., et al. (2007). Identification of anti-prion compounds as efficient inhibitors of polyglutamine protein aggregation in a zebrafish model. *J Biol Chem, 282*(12), 9195-9203.

Schilling, G., Jinnah, H., Gonzales, V., Coonfield, M., Kim, Y., Wood, J., et al. (2001). Distinct behavioral and neuropathological abnormalities in transgenic mouse models of HD and DRPLA. *Neurobiology of disease, 8*(3), 405-418.

Schilling, G., Sharp, A., Loev, S., Wagster, M., Li, S., Stine, O., et al. (1995). Expression of the Huntington's disease (IT15) protein product in HD patients. *Human molecular genetics, 4*(8), 1365-1371.

Schilling, G., Wood, J. D., Duan, K., Slunt, H. H., Gonzales, V., Yamada, M., et al. (1999). Nuclear accumulation of truncated atrophin-1 fragments in a transgenic mouse model of DRPLA. *Neuron, 24*(1), 275-286.

Schmahmann, J. D., Pandya, D. N., Wang, R., Dai, G., D'Arceuil, H. E., de Crespigny, A. J., et al. (2007). Association fibre pathways of the brain: parallel observations from diffusion spectrum imaging and autoradiography. *Brain, 130*(Pt 3), 630-653.

Scholz, J., Klein, M., Behrens, T., & Johansen-Berg, H. (2009). Training induces changes in white-matter architecture. *Nature neuroscience, 12*(11), 1370-1371.

Schulte, J., & Littleton, J. T. (2011). The biological function of the Huntingtin protein and its relevance to Huntington's Disease pathology. *Curr Trends Neurol, 5*, 65-78.

Schultz, S. K. (2001). Principles of neural science, 4th ed. (Vol. 158, pp. 662). American Journal of Psychiatry.

Schwarcz, R., Whetsell, W. O., & Mangano, R. M. (1983). Quinolinic acid: an endogenous metabolite that produces axon-sparing lesions in rat brain. *Science, 219*(4582), 316-318.

Selemon, L. D., Rajkowska, G., & Goldman-Rakic, P. S. (2004). Evidence for progression in frontal cortical pathology in late-stage Huntington's disease. *J Comp Neurol, 468*(2), 190-204.

Seunarine, K. K., & Alexander, D. C. (2009). Multiple fibers: beyond the diffusion tensor. In H. Johansen-Berg, T. Behrens & (Eds.) (Eds.), *Diffusion MRI: From Quantitative Measurement to In vivo Neuroanatomy* (pp. 55-72). Elsevier.

Shamonin, D. P., Bron, E. E., Lelieveldt, B. P., Smits, M., Klein, S., Staring, M., et al. (2013). Fast parallel image registration on CPU and GPU for diagnostic classification of Alzheimer's disease. *Front Neuroinform, 7*, 50.

Sharp, A., Loev, S., Schilling, G., Li, S., Li, X., Bao, J., et al. (1995). Widespread expression of Huntington's disease gene (IT15) protein product. *Neuron, 14*(5), 1065-1074.

Shelbourne, P., Killeen, N., Hevner, R., Johnston, H., Tecott, L., Lewandoski, M., et al. (1999). A Huntington's disease CAG expansion at the murine Hdh locus is unstable and associated with behavioural abnormalities in mice. *Human molecular genetics, 8*(5), 763-774.

Shelbourne, P. F., Keller-McGandy, C., Bi, W. L., Yoon, S. R., Dubeau, L., Veitch, N. J., et al. (2007). Triplet repeat mutation length gains correlate with cell-type specific vulnerability in Huntington disease brain. *Hum Mol Genet, 16*(10), 1133-1142.

Shen, X., Dong, Y., Xu, Z., Wang, H., Miao, C., Soriano, S. G., et al. (2013). Selective anesthesia-induced neuroinflammation in developing mouse brain and cognitive impairment. *Anesthesiology, 118*(3), 502-515.

Shepard, R. N., & Metzler, J. (1971). Mental rotation of three-dimensional objects. *Science, 171*(3972), 701-703.

Shin, J. Y., Fang, Z. H., Yu, Z. X., Wang, C. E., Li, S. H., & Li, X. J. (2005). Expression of mutant huntingtin in glial cells contributes to neuronal excitotoxicity. *J Cell Biol, 171*(6), 1001-1012.

Shoulson, I., & Fahn, S. (1979). Huntington disease: clinical care and evaluation. *Neurology, 29*(1), 1-3.

Shpanskaya, K. S., Choudhury, K. R., Hostage, C., Murphy, K. R., Petrella, J. R., Doraiswamy, P. M., et al. (2014). Educational attainment and hippocampal atrophy in the Alzheimer's disease neuroimaging initiative cohort. *J Neuroradiol*.

Silajdžić, E., Rezeli, M., Végvári, Á., Lahiri, N., Andre, R., Magnusson-Lind, A., et al. (2013). A critical evaluation of inflammatory markers in Huntington's Disease plasma. *J Huntingtons Dis, 2*(1), 125-134.

Silverman, I., Choi, J., Mackewn, A., Fisher, M., Moro, J., & Olshansky, E. (2000). Evolved mechanisms underlying wayfinding. further studies on the hunter-gatherer theory of spatial sex differences. *Evol Hum Behav, 21*(3), 201-213.

Simmons, D. A., Casale, M., Alcon, B., Pham, N., Narayan, N., & Lynch, G. (2007). Ferritin accumulation in dystrophic microglia is an early event in the development of Huntington's disease. *Glia, 55*(10), 1074-1084.

Sinadinos, C., Burbidge-King, T., Soh, D., Thompson, L. M., Marsh, J. L., Wyttenbach, A., et al. (2009). Live axonal transport disruption by mutant huntingtin fragments in Drosophila motor neuron axons. *Neurobiol Dis, 34*(2), 389-395.

Sipione, S., & Cattaneo, E. (2001). Modeling Huntington's disease in cells, flies, and mice. *Mol Neurobiol, 23*(1), 21-51.

Sirinathsinghji, D. J., Dunnett, S. B., Isacson, O., Clarke, D. J., Kendrick, K., & Björklund, A. (1988). Striatal grafts in rats with unilateral neostriatal lesions--II. In vivo monitoring of GABA release in globus pallidus and substantia nigra. *Neuroscience, 24*(3), 803-811.

Sirinathsinghji, D. J., Heavens, R. P., Torres, E. M., & Dunnett, S. B. (1993). Cholecystokinin-dependent regulation of host dopamine inputs to striatal grafts. *Neuroscience, 53*(3), 651-663.

Sled, J. G., Zijdenbos, A. P., & Evans, A. C. (1998). A nonparametric method for automatic correction of intensity nonuniformity in MRI data. *IEEE Trans Med Imaging, 17*(1), 87-97.

Slow, E., Raamsdonk, J., Rogers, D., Coleman, S., Graham, R., Deng, Y., et al. (2003a). Selective striatal neuronal loss in a YAC128 mouse model of Huntington disease. *Human molecular genetics, 12*(13), 1-13.

Slow, E., Raamsdonk, J., Rogers, D., Coleman, S., Graham, R., Deng, Y., et al. (2003b). Selective striatal neuronal loss in a YAC128 mouse model of Huntington disease. *Human molecular genetics, 12*(13), 1-13.

Smith, M., Mills, J., Epping, E., Westervelt, H., & Paulsen, J. (2012). Depressive symptom severity is related to poorer cognitive performance in prodromal Huntington disease. *Neuropsychology, 26*(5), 664-669.

Smith, M. A., Brandt, J., & Shadmehr, R. (2000). Motor disorder in Huntington's disease begins as a dysfunction in error feedback control. *Nature, 403*(6769), 544-549.

Smith, R., Bacos, K., Fedele, V., Soulet, D., Walz, H. A., Obermüller, S., et al. (2009). Mutant huntingtin interacts with {beta}-tubulin and disrupts vesicular transport and insulin secretion. *Hum Mol Genet, 18*(20), 3942-3954.

Smith, S. M., Jenkinson, M., Johansen-Berg, H., Rueckert, D., Nichols, T. E., Mackay, C. E., et al. (2006). Tract-based spatial statistics: voxelwise analysis of multi-subject diffusion data. *Neuroimage, 31*(4), 1487-1505.

Smith, S. M., Jenkinson, M., Woolrich, M. W., Beckmann, C. F., Behrens, T. E., Johansen-Berg, H., et al. (2004). Advances in functional and structural MR image analysis and implementation as FSL. *Neuroimage, 23 Suppl 1*, S208-219.

Smith, S. M., Zhang, Y., Jenkinson, M., Chen, J., Matthews, P. M., Federico, A., et al. (2002). Accurate, robust, and automated longitudinal and cross-sectional brain change analysis. *Neuroimage, 17*(1), 479-489.

Snell, R. G., MacMillan, J. C., Cheadle, J. P., & Fenton, I. (1993). Relationship between trinucleotide repeat expansion and phenotypic variation in Huntington&#39;s disease. *Nature*.

Snowden, J., Craufurd, D., Thompson, J., & Neary, D. (2002). Psychomotor, executive, and memory function in preclinical Huntington's disease. *Journal of clinical and experimental neuropsychology, 24*(2), 133-145.

Song, J., Lee, S. T., Kang, W., Park, J. E., Chu, K., Lee, S. E., et al. (2007). Human embryonic stem cell-derived neural precursor transplants attenuate apomorphine-induced rotational behavior in rats with unilateral quinolinic acid lesions. *Neurosci Lett, 423*(1), 58-61.

Song, S.-K., Sun, S.-W., Ju, W.-K., Lin, S.-J., Cross, A., & Neufeld, A. (2003). Diffusion tensor imaging detects and differentiates axon and myelin degeneration in mouse optic nerve after retinal ischemia. *NeuroImage, 20*(3), 1714-1722.

Song, S.-K., Sun, S.-W., Ramsbottom, M., Chang, C., Russell, J., & Cross, A. (2002). Dysmyelination revealed through MRI as increased radial (but unchanged axial) diffusion of water. *NeuroImage, 17*(3), 1429-1436.

Song, S.-K., Yoshino, J., Q, T., Lin, S.-J., Sun, S.-W., Cross, A., et al. (2005). Demyelination increases radial diffusivity in corpus callosum of mouse brain. *NeuroImage, 26*(1), 132-140.

Sotrel, A., Paskevich, P. A., Kiely, D. K., Bird, E. D., Williams, R. S., & Myers, R. H. (1991). Morphometric analysis of the prefrontal cortex in Huntington's disease. *Neurology, 41*(7), 1117-1123.

Spader, H. S., Ellermeier, A., O'Muircheartaigh, J., Dean, D. C., Dirks, H., Boxerman, J. L., et al. (2013). Advances in myelin imaging with potential clinical application to pediatric imaging. *Neurosurg Focus, 34*(4), E9.

Spires, T., Grote, H., Varshney, N., Cordery, P., Dellen, A., Blakemore, C., et al. (2004). Environmental enrichment rescues protein deficits in a mouse model of Huntington's disease, indicating a possible disease mechanism. *The Journal of neuroscience : the official journal of the Society for Neuroscience, 24*(9), 2270-2276.

Spires, T. L., Grote, H. E., Varshney, N. K., Cordery, P. M., van Dellen, A., Blakemore, C., et al. (2004). Environmental enrichment rescues protein deficits in a mouse model of Huntington's disease, indicating a possible disease mechanism. *J Neurosci, 24*(9), 2270-2276.

Squitieri, F., Gellera, C., Cannella, M., Mariotti, C., Cislaghi, G., Rubinsztein, D. C., et al. (2003). Homozygosity for CAG mutation in Huntington disease is associated with a more severe clinical course. *Brain, 126*(Pt 4), 946-955.

Steffan, J. S., Kazantsev, A., Spasic-Boskovic, O., Greenwald, M., Zhu, Y. Z., Gohler, H., et al. (2000). The Huntington's disease protein interacts with p53 and CREB-binding protein and represses transcription. *Proc Natl Acad Sci U S A, 97*(12), 6763-6768.

Steffener, J., Barulli, D., Habeck, C., O'Shea, D., Razlighi, Q., & Stern, Y. (2014). The role of education and verbal abilities in altering the effect of age-related gray matter differences on cognition. *PLoS One, 9*(3), e91196.

Stern, Y. (2009). Cognitive reserve. *Neuropsychologia, 47*(10), 2015-2028.

Stout, J., Paulsen, J., Queller, S., Solomon, A., Whitlock, K., Campbell, J., et al. (2011). Neurocognitive signs in prodromal Huntington disease. *Neuropsychology, 25*(1), 1-14.

Stout, J. C., Jones, R., Labuschagne, I., O'Regan, A. M., Say, M. J., Dumas, E. M., et al. (2012). Evaluation of longitudinal 12 and 24 month cognitive outcomes in premanifest and early Huntington's disease. *J Neurol Neurosurg Psychiatry, 83*(7), 687-694.

Stout, J. C., Rodawalt, W. C., & Siemers, E. R. (2001). Risky decision making in Huntington's disease. *J Int Neuropsychol Soc, 7*(1), 92-101.

Strong, T., Tagle, D., Valdes, J., Elmer, L., Boehm, K., Swaroop, M., et al. (1993). Widespread expression of the human and rat Huntington's disease gene in brain and nonneural tissues. *Nature genetics, 5*(3), 259-265.

Stroop, J. R. (1935). Studies of interference in serial verbal reactions. *Journal of experimental psychology*.

Stüwe, S. H., Goetze, O., Lukas, C., Klotz, P., Hoffmann, R., Banasch, M., et al. (2013). Hepatic mitochondrial dysfunction in manifest and premanifest Huntington disease. *Neurology, 80*(8), 743-746.

Sutherland, N. S., & Mackintosh, N. J. (1971). Mechanisms of animal discrimination learning: Academic Press: New York, USA.

Szeszko, P. R., Ardekani, B. A., Ashtari, M., Malhotra, A. K., Robinson, D. G., Bilder, R. M., et al. (2005). White matter abnormalities in obsessive-compulsive disorder: a diffusion tensor imaging study. *Arch Gen Psychiatry, 62*(7), 782-790.

Sánchez-Pernaute, R., Künig, G., Alba, A., Yébenes, J., Vontobel, P., & Leenders, K. (2000). Bradykinesia in early Huntington's disease. *Neurology, 54*(1), 119-125.

Tabrizi, S., Langbehn, D., Leavitt, B., Roos, R., Durr, A., Craufurd, D., et al. (2009). Biological and clinical manifestations of Huntington's disease in the longitudinal TRACK-HD study: cross-sectional analysis of baseline data. *Lancet neurology, 8*(9), 791-801.

Tabrizi, S., Reilmann, R., Roos, R., Durr, A., Leavitt, B., Owen, G., et al. (2012). Potential endpoints for clinical trials in premanifest and early Huntington's disease in the TRACK-HD study: analysis of 24 month observational data. *The Lancet Neurology, 11*(1), 42-53.

Tabrizi, S., Scahill, R., Durr, A., Roos, R., Leavitt, B., Jones, R., et al. (2011). Biological and clinical changes in premanifest and early stage Huntington's disease in the TRACK-HD study: the 12-month longitudinal analysis. *Lancet neurology, 10*(1), 31-42.

Tabrizi, S., Scahill, R., Owen, G., Durr, A., Leavitt, B., Roos, R., et al. (2013). Predictors of phenotypic progression and disease onset in premanifest and early-stage Huntington's disease in the TRACK-HD study: analysis of 36-month observational data. *Lancet neurology, 12*(7), 637-649.

Tai, Y. F., Pavese, N., Gerhard, A., Tabrizi, S. J., Barker, R. A., Brooks, D. J., et al. (2007a). Imaging microglial activation in Huntington's disease. *Brain Res Bull, 72*(2-3), 148-151.

Tai, Y. F., Pavese, N., Gerhard, A., Tabrizi, S. J., Barker, R. A., Brooks, D. J., et al. (2007b). Microglial activation in presymptomatic Huntington's disease gene carriers. *Brain, 130*(Pt 7), 1759-1766.

Takahashi, K., Okita, K., Nakagawa, M., & Yamanaka, S. (2007). Induction of pluripotent stem cells from fibroblast cultures. *Nat Protoc, 2*(12), 3081-3089.

Tallaksen-Greene, S. J., Janiszewska, A., Benton, K., Ruprecht, L., & Albin, R. L. (2010). Lack of efficacy of NMDA receptor-NR2B selective antagonists in the R6/2 model of Huntington disease. *Exp Neurol, 225*(2), 402-407.

Tavor, I., Hofstetter, S., & Assaf, Y. (2013). Micro-structural assessment of short term plasticity dynamics. *NeuroImage*.

Taylor, H., & Hansotia, P. (1983). Neuropsychological testing of Huntington's patients. Clues to progression. *The Journal of nervous and mental disease, 171*(8), 492-496.

Thieben, M. J., Duggins, A. J., Good, C. D., Gomes, L., Mahant, N., Richards, F., et al. (2002). The distribution of structural neuropathology in pre-clinical Huntington's disease. *Brain, 125*(Pt 8), 1815-1828.

Thompson, J. C., Poliakoff, E., Sollom, A. C., Howard, E., Craufurd, D., & Snowden, J. S. (2010). Automaticity and attention in Huntington's disease: when two hands are not better than one. *Neuropsychologia, 48*(1), 171-178.

Thu, D. C., Oorschot, D. E., Tippett, L. J., Nana, A. L., Hogg, V. M., Synek, B. J., et al. (2010). Cell loss in the motor and cingulate cortex correlates with symptomatology in Huntington's disease. *Brain, 133*(Pt 4), 1094-1110.

Toh, E. A., MacAskill, M. R., Dalrymple-Alford, J. C., Myall, D. J., Livingston, L., Macleod, S. A., et al. (2014). Comparison of cognitive and UHDRS measures in monitoring disease progression in Huntington's disease: a 12-month longitudinal study. *Transl Neurodegener, 3*, 15.

Tournier, J. D., Calamante, F., & Connelly, A. (2007). Robust determination of the fibre orientation distribution in diffusion MRI: non-negativity constrained super-resolved spherical deconvolution. *Neuroimage, 35*(4), 1459-1472.

Tournier, J. D., Calamante, F., Gadian, D., & Connelly, A. (2004). Direct estimation of the fiber orientation density function from diffusion-weighted MRI data using spherical deconvolution. *NeuroImage, 23*(3), 1176-1185.

Tournier, J. D., Yeh, C.-H., Calamante, F., Cho, K.-H., Connelly, A., & Lin, C.-P. (2008). Resolving crossing fibres using constrained spherical deconvolution: validation using diffusion-weighted imaging phantom data. *NeuroImage, 42*(2), 1-9.

Treisman, A. M., & Gelade, G. (1980). A feature-integration theory of attention. *Cogn Psychol, 12*(1), 97-136.

Treuting, P. M., & Dintzis, S. M. (2012). Comparative Anatomy and Histology: A Mouse and Human Atlas. Elsevier.

Trottier, Y., Devys, D., Imbert, G., Saudou, F., An, I., Lutz, Y., et al. (1995). Cellular localization of the Huntington's disease protein and discrimination of the normal and mutated form. *Nature genetics, 10*(1), 104-110.

Trueman, R., Brooks, S., & Dunnett, S. (2005). Implicit learning in a serial choice visual discrimination task in the operant 9-hole box by intact and striatal lesioned mice. *Behavioural brain research, 159*(2), 313-322.

Trueman, R., Brooks, S., Jones, L., & Dunnett, S. (2007). The operant serial implicit learning task reveals early onset motor learning deficits in the Hdh knock-in mouse model of Huntington's disease. *The European journal of neuroscience, 25*(2), 551-558.

Trueman, R., Brooks, S., Jones, L., & Dunnett, S. (2009). Rule learning, visuospatial function and motor performance in the Hdh(Q92) knock-in mouse model of Huntington's disease. *Behavioural brain research, 203*(2), 215-222.

Trueman, R. C., Dunnett, S. B., & Brooks, S. P. (2012). Operant-based instrumental learning for analysis of genetically modified models of Huntington's disease. *Brain Res Bull, 88*(2-3), 261-275.

Tuch, D., Reese, T., Wiegell, M., Makris, N., Belliveau, J., & Wedeen, J. (2002). High angular resolution diffusion imaging reveals intravoxel white matter fiber heterogeneity. *Magnetic resonance in medicine : official journal of the Society of Magnetic Resonance in Medicine / Society of Magnetic Resonance in Medicine, 48*(4), 577-582.

Turner, R., Le Bihan, D., Maier, J., Vavrek, R., Hedges, L. K., & Pekar, J. (1990). Echo-planar imaging of intravoxel incoherent motion. *Radiology, 177*(2), 407-414.

Unified Huntington's Disease Rating Scale: reliability and consistency. Huntington Study Group. (1996). *Mov Disord, 11*(2), 136-142.

Valenza, M., Carroll, J. B., Leoni, V., Bertram, L. N., Björkhem, I., Singaraja, R. R., et al. (2007). Cholesterol biosynthesis pathway is disturbed in YAC128 mice and is modulated by huntingtin mutation. *Hum Mol Genet, 16*(18), 2187-2198.

Valenza, M., & Cattaneo, E. (2010). Neuroprotection and brain cholesterol biosynthesis in Huntington's disease. *Proc Natl Acad Sci U S A, 107*(37), E143; author reply 144.

Valenza, M., & Cattaneo, E. (2011). Emerging roles for cholesterol in Huntington's disease. *Trends Neurosci, 34*(9), 474-486.

Valenza, M., Rigamonti, D., Goffredo, D., Zuccato, C., Fenu, S., Jamot, L., et al. (2005). Dysfunction of the cholesterol biosynthetic pathway in Huntington's disease. *J Neurosci, 25*(43), 9932-9939.

van de Ven, R. C., Hogers, B., van den Maagdenberg, A. M., de Groot, H. J., Ferrari, M. D., Frants, R. R., et al. (2007). T(1) relaxation in in vivo mouse brain at ultra-high field. *Magn Reson Med, 58*(2), 390-395.

van Dellen, A., Cordery, P. M., Spires, T. L., Blakemore, C., & Hannan, A. J. (2008). Wheel running from a juvenile age delays onset of specific motor deficits but does not alter protein aggregate density in a mouse model of Huntington's disease. *BMC Neurosci, 9*, 34.

van Dellen, A., Deacon, R., York, D., Blakemore, C., & Hannan, A. J. (2001). Anterior cingulate cortical transplantation in transgenic Huntington's disease mice. *Brain Res Bull, 56*(3-4), 313-318.

van Dellen, A., Welch, J., Dixon, R. M., Cordery, P., York, D., Styles, P., et al. (2000). N-Acetylaspartate and DARPP-32 levels decrease in the corpus striatum of Huntington's disease mice. *Neuroreport, 11*(17), 3751-3757.

van den Bogaard, S. J., Dumas, E. M., Ferrarini, L., Milles, J., van Buchem, M. A., van der Grond, J., et al. (2011). Shape analysis of subcortical nuclei in Huntington's disease, global versus local atrophy--results from the TRACK-HD study. *J Neurol Sci, 307*(1-2), 60-68.

van Duijn, E., Kingma, E. M., & van der Mast, R. C. (2007). Psychopathology in verified Huntington's disease gene carriers. *J Neuropsychiatry Clin Neurosci, 19*(4), 441-448.

Vann, S. D., Aggleton, J. P., & Maguire, E. A. (2009). What does the retrosplenial cortex do? *Nat Rev Neurosci, 10*(11), 792-802.

Vazey, E. M., Chen, K., Hughes, S. M., & Connor, B. (2006). Transplanted adult neural progenitor cells survive, differentiate and reduce motor function impairment in a rodent model of Huntington's disease. *Exp Neurol, 199*(2), 384-396.

Vazey, E. M., & Connor, B. (2010). Differential fate and functional outcome of lithium chloride primed adult neural progenitor cell transplants in a rat model of Huntington disease. *Stem Cell Res Ther, 1*(5), 41.

Verbruggen, F., & Logan, G. D. (2008). Automatic and controlled response inhibition: associative learning in the go/no-go and stop-signal paradigms. *J Exp Psychol Gen, 137*(4), 649-672.

Via, E., Zalesky, A., Sánchez, I., Forcano, L., Harrison, B. J., Pujol, J., et al. (2014). Disruption of brain white matter microstructure in women with anorexia nervosa. *J Psychiatry Neurosci, 39*(6), 367-375.

Vogt, B. A., Vogt, L., & Laureys, S. (2006). Cytology and functionally correlated circuits of human posterior cingulate areas. *Neuroimage, 29*(2), 452-466.

von Hörsten, S., Schmitt, I., Nguyen, H. P., Holzmann, C., Schmidt, T., Walther, T., et al. (2003). Transgenic rat model of Huntington's disease. *Hum Mol Genet, 12*(6), 617-624.

Vonsattel, J., Myers, R., Stevens, T., Ferrante, R., Bird, E., & Richardson, E. (1985). Neuropathological classification of Huntington's disease. *Journal of neuropathology and experimental neurology, 44*(6), 559-577.

Vonsattel, J. P., & DiFiglia, M. (1998). Huntington disease. *J Neuropathol Exp Neurol, 57*(5), 369-384.

Wagster, M. V., Hedreen, J. C., Peyser, C. E., Folstein, S. E., & Ross, C. A. (1994). Selective loss of [3H]kainic acid and [3H]AMPA binding in layer VI of frontal cortex in Huntington's disease. *Exp Neurol, 127*(1), 70-75.

Wakana, S., Jiang, H., Nagae-Poetscher, L. M., van Zijl, P. C., & Mori, S. (2004). Fiber tract-based atlas of human white matter anatomy. *Radiology, 230*(1), 77-87.

Walf, A. A., & Frye, C. A. (2007). The use of the elevated plus maze as an assay of anxiety-related behavior in rodents. *Nat Protoc, 2*(2), 322-328.

Warrick, J. M., Paulson, H. L., Gray-Board, G. L., Bui, Q. T., Fischbeck, K. H., Pittman, R. N., et al. (1998). Expanded polyglutamine protein forms nuclear inclusions and causes neural degeneration in Drosophila. *Cell, 93*(6), 939-949.

Watkins, L. H., Rogers, R. D., Lawrence, A. D., Sahakian, B. J., Rosser, A. E., & Robbins, T. W. (2000). Impaired planning but intact decision making in early Huntington's disease: implications for specific fronto-striatal pathology. *Neuropsychologia, 38*(8), 1112-1125.

Weaver, K., Richards, T., Liang, O., Laurino, M., Samii, A., & Aylward, E. (2009). Longitudinal diffusion tensor imaging in Huntington's Disease. *Experimental neurology, 216*(2), 525-529.

Wechsler, D. A. (1981). *Wechsler Adult Intelligence Scale—Revised manual*.: New York: Psychological Corporation.

Wetzel, H., Gehl, C., Dellefave-Castillo, L., Schiffman, J., Shannon, K., & Paulsen, J. (2011). Suicidal ideation in Huntington disease: the role of comorbidity. *Psychiatry research, 188*(3), 372-376.

Wexler, N. S., Lorimer, J., Porter, J., Gomez, F., Moskowitz, C., Shackell, E., et al. (2004). Venezuelan kindreds reveal that genetic and environmental factors modulate Huntington's disease age of onset. *Proc Natl Acad Sci U S A, 101*(10), 3498-3503.

Wexler, N. S., Young, A. B., Tanzi, R. E., Travers, H., Starosta-Rubinstein, S., Penney, J. B., et al. (1987). Homozygotes for Huntington's disease. *Nature, 326*(6109), 194-197.

Wheeler, V., Gutekunst, C., Vrbanac, V., Lebel, L.-A., Schilling, G., Hersch, S., et al. (2002). Early phenotypes that presage late-onset neurodegenerative disease allow testing of modifiers in Hdh CAG knock-in mice. *Human molecular genetics, 11*(6), 633-640.

Wheeler, V., Persichetti, F., McNeil, S., Mysore, J., Mysore, S., MacDonald, M., et al. (2007). Factors associated with HD CAG repeat instability in Huntington disease. *Journal of Medical Genetics, 44*(11), 695-701.

Wheeler, V., White, J., Gutekunst, C., Vrbanac, V., Weaver, M., Li, X., et al. (2000). Long glutamine tracts cause nuclear localization of a novel form of huntingtin in medium spiny striatal neurons in HdhQ92 and HdhQ111 knock-in mice. *Human molecular genetics, 9*(4), 503-513.

Wheeler, V. C., Auerbach, W., White, J. K., Srinidhi, J., Auerbach, A., Ryan, A., et al. (1999). Length-dependent gametic CAG repeat instability in the Huntington's disease knock-in mouse. *Hum Mol Genet, 8*(1), 115-122.

Wheeler, V. C., Lebel, L. A., Vrbanac, V., Teed, A., te Riele, H., & MacDonald, M. E. (2003). Mismatch repair gene Msh2 modifies the timing of early disease in Hdh(Q111) striatum. *Hum Mol Genet, 12*(3), 273-281.

Wheeler-Kingshott, C. A., & Cercignani, M. (2009). About "axial" and "radial" diffusivities. *Magn Reson Med, 61*(5), 1255-1260.

Whishaw, I. Q. (1995). A comparison of rats and mice in a swimming pool place task and matching to place task: some surprising differences. *Physiol Behav, 58*(4), 687-693.

White, J. K., Auerbach, W., Duyao, M. P., Vonsattel, J. P., Gusella, J. F., Joyner, A. L., et al. (1997). Huntingtin is required for neurogenesis and is not impaired by the Huntington's disease CAG expansion. *Nat Genet, 17*(4), 404-410.

Wictorin, K. (1992). Anatomy and connectivity of intrastriatal striatal transplants. *Prog Neurobiol, 38*(6), 611-639.

Wild, E., Magnusson, A., Lahiri, N., Krus, U., Orth, M., Tabrizi, S. J., et al. (2011). Abnormal peripheral chemokine profile in Huntington's disease. *PLoS Curr, 3*, RRN1231.

Williams, J. K., Barnette, J. J., Reed, D., Sousa, V. D., Schutte, D. L., McGonigal-Kenney, M., et al. (2010). Development of the Huntington disease family concerns and strategies survey from focus group data. *J Nurs Meas, 18*(2), 83-99.

Willner, P., Towell, A., Sampson, D., Sophokleous, S., & Muscat, R. (1987). Reduction of sucrose preference by chronic unpredictable mild stress, and its restoration by a tricyclic antidepressant. *Psychopharmacology (Berl), 93*(3), 358-364.

Winkler, A. M., Kochunov, P., Blangero, J., Almasy, L., Zilles, K., Fox, P. T., et al. (2010). Cortical thickness or grey matter volume? The importance of selecting the phenotype for imaging genetics studies. *Neuroimage, 53*(3), 1135-1146.

Winkler, A. M., Ridgway, G. R., Webster, M. A., Smith, S. M., & Nichols, T. E. (2014). Permutation inference for the general linear model. *Neuroimage, 92*, 381-397.

Wolf, R., Vasic, N., Schönfeldt-Lecuona, C., Ecker, D., & Landwehrmeyer, G. (2009). Cortical dysfunction in patients with Huntington's disease during working memory performance. *Human brain mapping, 30*(1), 327-339.

Wolf, R. C., Sambataro, F., Vasic, N., Schönfeldt-Lecuona, C., Ecker, D., & Landwehrmeyer, B. (2008). Aberrant connectivity of lateral prefrontal networks in presymptomatic Huntington's disease. *Exp Neurol, 213*(1), 137-144.

Wolf, R. C., Thomann, P. A., Thomann, A. K., Vasic, N., Wolf, N. D., Landwehrmeyer, G. B., et al. (2013). Brain structure in preclinical Huntington's disease: a multi-method approach. *Neurodegener Dis, 12*(1), 13-22.

Wood, N., Glynn, D., & Morton, A. (2011). "Brain training" improves cognitive performance and survival in a transgenic mouse model of Huntington's disease. *Neurobiology of disease, 42*(3), 427-437.

Xiang, Z., Valenza, M., Cui, L., Leoni, V., Jeong, H.-K., Brilli, E., et al. (2011). Peroxisome-proliferator-activated receptor gamma coactivator 1 α contributes to dysmyelination in experimental models of Huntington's disease. *The Journal of neuroscience : the official journal of the Society for Neuroscience, 31*(26), 9544-9553.

Xu, Z. C., Wilson, C. J., & Emson, P. C. (1991). Synaptic potentials evoked in spiny neurons in rat neostriatal grafts by cortical and thalamic stimulation. *J Neurophysiol, 65*(3), 477-493.

Yang, S.-H., Cheng, P.-H., Banta, H., Piotrowska-Nitsche, K., Yang, J.-J., Cheng, E., et al. (2008). Towards a transgenic model of Huntington's disease in a non-human primate. *Nature, 453*(7197), 921-924.

Yano, H., Baranov, S. V., Baranova, O. V., Kim, J., Pan, Y., Yablonska, S., et al. (2014). Inhibition of mitochondrial protein import by mutant huntingtin. *Nat Neurosci, 17*(6), 822-831.

Younes, L., Ratnanather, J. T., Brown, T., Aylward, E., Nopoulos, P., Johnson, H., et al. (2014). Regionally selective atrophy of subcortical structures in prodromal HD as revealed by statistical shape analysis. *Hum Brain Mapp, 35*(3), 792-809.

Young, A. B., Greenamyre, J. T., Hollingsworth, Z., Albin, R., D'Amato, C., Shoulson, I., et al. (1988). NMDA receptor losses in putamen from patients with Huntington's disease. *Science, 241*(4868), 981-983.

Young, A. B., Shoulson, I., & Penney, J. B. (1986). Huntington&#39;s disease in Venezuela Neurologic features and functional decline. *Neurology*.

Zamboni, G., Huey, E., Krueger, F., Nichelli, P., & Grafman, J. (2008). Apathy and disinhibition in frontotemporal dementia: Insights into their neural correlates. *Neurology, 71*(10), 736-742.

Zeitlin, S., Liu, J. P., Chapman, D. L., Papaioannou, V. E., & Efstratiadis, A. (1995). Increased apoptosis and early embryonic lethality in mice nullizygous for the Huntington's disease gene homologue. *Nat Genet, 11*(2), 155-163.

Zhang, H., Li, Q., Graham, R. K., Slow, E., Hayden, M. R., & Bezprozvanny, I. (2008). Full length mutant huntingtin is required for altered Ca2+ signaling and apoptosis of striatal neurons in the YAC mouse model of Huntington's disease. *Neurobiol Dis, 31*(1), 80-88.

Zinzi, P., Salmaso, D., Grandis, R., Graziani, G., Maceroni, S., Bentivoglio, A., et al. (2007). Effects of an intensive rehabilitation programme on patients with Huntington's disease: a pilot study. *Clinical rehabilitation, 21*(7), 603-613.

Zuccato, C., Marullo, M., Conforti, P., MacDonald, M. E., Tartari, M., & Cattaneo, E. (2008). Systematic assessment of BDNF and its receptor levels in human cortices affected by Huntington's disease. *Brain Pathol, 18*(2), 225-238.

Zuccato, C., Marullo, M., Vitali, B., Tarditi, A., Mariotti, C., Valenza, M., et al. (2011). Brain-derived neurotrophic factor in patients with Huntington's disease. *PLoS One, 6*(8), e22966.

Zuccato, C., Valenza, M., & Cattaneo, E. (2010). Molecular mechanisms and potential therapeutical targets in Huntington's disease. *Physiol Rev, 90*(3), 905-981.